UNIVERSITY OF KWAZULU-NATAL ™

INYUVESI YAKWAZULU-NATALI

VIBRATION RESPONSE OF GRAPHENE-REINFORCED NANOCOMPOSITE PLATES USING FINITE ELEMENT ANALYSIS, OPTIMIZATION AND FUNCTIONALLY GRADED TECHNIQUES

By:

Yajur Jeawon

In fulfilment of a Doctor of Philosophy in Civil Engineering, the College of Agriculture, Engineering and Science, University of Kwa-Zulu Natal

Date:

25 June 2024

Name & Student Number:

Yajur Jeawon - 211558010

Supervisor:

Dr G. A. Drosopoulos

[redacted]

PREFACE

The candidate completed the research for this thesis while registered as a part time student at the University of KwaZulu-Natal's Howard Campus in Durban, South Africa's School of the College of Agriculture, Engineering and Science's Department of Civil Engineering.

This work's contents have not been submitted in any format to another university, and the results reported are the product of the candidate's investigations, with the exception of instances where the work of others is acknowledged in the text.

Signed:

… ……...

Dr Georgios A. Drosopoulos

……

Date:

DECLARATION 1 - PLAGIARISM

I, Yajur Jeawon, declare that:

1. The research reported in this thesis, except where otherwise indicated, is my original research.
2. This thesis has not been submitted for any degree or examination at any other university.
3. This thesis does not contain other persons' data, pictures, graphs or other information, unless specifically acknowledged as being sourced from other persons.
4. This thesis does not contain other persons' writing, unless specifically acknowledged as being sourced from other researchers. Where other written sources have been quoted, then :
   a) Their words have been re-written but the general information attributed to them has been referenced
   b) Where their exact words have been used, then their writing has been placed in italics, inside quotation marks, and referenced.
5. This thesis does not contain text, graphics or tables copied and pasted from the Internet, unless specifically acknowledged, with the source being detailed in the thesis and in the references sections.

Signed:

[redacted]

…… 25 June 2024

Yajur Jeawon ……

Date

As the candidate's supervisor, I agree to the submission of this thesis.

[redacted]

… ……

Dr Georgios A. Drosopoulos ……

Date

DECLARATION - PUBLICATION

The submission of the Doctor of Philosophy in Engineering Degree is by compilation of several peer reviewed scientific papers, published in journals which are accredited by the South African Department of Higher Education and Training (DHET). The research papers provided in Chapters 4, 5 and 6 of the thesis are the candidate's original works derived from investigation and analysis of the:

"VIBRATION RESPONSE OF GRAPHENE-REINFORCED NANOCOMPOSITE PLATES USING FINITE ELEMENT ANALYSIS, OPTIMIZATION AND FUNCTIONALLY GRADED TECHNIQUES"

Authorship contribution statements of the research articles are presented in the Appendix section of the thesis.
The publications contained herein:

1. Y. Jeawon, G.A. Drosopoulos, G. Foutsitzi, G.E. Stavroulakis, S. Adali, Optimization and analysis of frequencies of multi-scale graphene/fibre reinforced nanocomposite laminates with non-uniform distributions of reinforcements, Eng.Struct, 228, (2020) 111525.
2. Y. Jeawon, G.A. Drosopoulos, G. Foutsitzi, G.E. Stavroulakis, S. Adali, Optimization of graphene/fibre reinforced cantilever skew laminates for maximum fundamental frequency via non-uniform distribution of reinforcements, Thin-Walled Structures, 189, (2023) 110903.
3. Y. Jeawon, G.A. Drosopoulos, G. Foutsitzi, Fundamental frequency analysis of functionally graded graphene-reinforced rectangular composite plates, (Article has been submitted for publication and is currently under review.)

Signed:

25 June 2024

…… …… ……

Yajur Jeawon **Date**

Page intentionally left blank

ACKNOWLEDGEMENTS

I would like to acknowledge those who made it possible to complete this research.

Firstly I would like to thank Prof. Georgios A. Drosopoulos without whom I would have not been able to achieve this milestone. Your guidance and support was the key to my successful completion of this PhD research.

Secondly, I would like to thank Prof. Stavroulakis, Prof. Foutsitzi and Prof. Adali for providing core theories, experience, insight, and critical reviews of the research which elevated the articles to a standard worthy of publication by prestigious journals.

I would like to thank my family (Shanta, Vishum, Ayur and Santur) and my wife (Dr Ashmika Singh) for the continuous support, guidance and inspiration throughout this journey.

"Challenges are what make life interesting and overcoming them is what makes life meaningful"

- Joshua J. Marine

ABSTRACT

Industries naturally strive to improve processes, materials, and material applications in order to raise the quality of the resource under consideration. This thesis focuses on proposing a numerical scheme to optimize and maximize the natural frequency response generated in 3-phase nanocomposite laminated plates through the use of graphene nanoplatelets (GPLs) and fibre reinforcement in terms of glass and carbon fibres. Many industries are now interested in conducting research on graphene reinforcement to form superior composites with the intention that the research may lead to a number of useful present-day and future initiatives. The natural frequency of nanoreinforced composite laminated plates has been researched in published articles by using techniques such as the Halpin-Tsai model and rule of mixtures to derive micromechanical equations and the Hamiltonian approach to acquire the equations of motion which are later solved via governing equations to obtain the natural frequency of the system. The current study uses MATLAB coding techniques to implement a Finite Element Model to accurately analyse the frequency response of a nanocomposite plate, the effective material properties of which are found using the micromechanical equations that are further discussed in this study. The composite plate's kinematics are developed using the first order shear deformation theory (FSDT). By using micromechanical equations the properties of a 2-phase composite, reinforced with graphene nanoplatelets (GPLs) located in the matrix, can be calculated. After the effective material properties have been calculated for this graphene-reinforced composite, the same micromechanical equations are applied once again for the introduction of fibre reinforcement (glass or carbon fibre) thereby forming a 3-phase nanocomposite laminate reinforced with graphene and fibres.

The study builds itself around two major aspects which are the maximum generated natural frequencies and the optimized natural frequencies for a defined set of parameters including graphene content, fibre reinforcement type and content, boundary conditions, fibre orientation, number of layers in the laminate and thickness ratio. The first investigation focuses on optimizing a hybrid, multi-scale graphene/fibre reinforced composite laminate plate in order to provide an optimal design solution resulting in a superior natural frequency and ultimately reducing the probability of resonance. Resonance occurs when the natural frequency of an object aligns with the vibration frequency of the excitation source. When resonance occurs

it can lead to structural failure of the object. In this study a Sequential Quadratic Programming Algorithm is used to optimize the fundamental frequency. The Sequential Quadratic Programming Algorithm was chosen based on the extensive use and validity in numerous research studies and the successful application thereof. A Matlab function is used to implement the SQP optimization, called fmincon. In the central Matlab code this function is used, and the developed finite element analysis code calculating the natural frequencies for the composite laminate is called as a Matlab subroutine by this SQP function. No convergence problems were identified in these optimization simulations. The results of this research revealed that adding graphene nanoplatelets (GPLs) improved the fundamental frequency of the composite and that maximum GPLs content in all layers is not always the optimal solution. Every simulation produces both the optimized fundamental frequency and the design efficiency, which is represented as the ratio of the maximum fundamental frequency that corresponds to optimal design divided by the reference frequency of the laminate that results from uniform properties. The second research paper expands on the ideas of the first by altering the plate geometry to define a cantilever support condition for a 45° skew laminated composite plate. The second study formulates an optimization scheme for a skew cantilever plate subject to similar constraints applied to the rectangular plate and provides a comparison of their natural frequencies. By investigating skew plates and various boundary conditions the research data adapted to form solutions for a broad spectrum of industry wide applications. In the second study the findings showed that a more economical design, with lower fibre volume content, could be produced by distributing the graphene and fibres optimally throughout the plate's thickness. Secondly, the skew laminate's design efficiency appeared to decline despite the apparent increase in natural frequency when compared to the results for a rectangular laminate. The third study investigates the natural frequency of a rectangular laminated composite plate with functionally graded (FG) reinforcement material. Functionally graded materials are composites that have two or more constituent materials with contents that are changed gradually or continuously so as to maximize the composite’s strength properties. Five distinct graphene reinforcement distribution patterns applied along the thickness direction of the laminate were used in the functionally graded application to identify the distribution that produced the maximum natural frequency. The distribution patterns considered in this investigation are Type ‘V’, Type ‘A’,

Uniform (UD), Type ‘O’ and Type ‘X’. The analysis model was defined as in the previous studies for a rectangular laminated plate with the exception of the optimization scheme as this research was formulated to investigate the apparent maximum natural frequency of the laminated composite. In the majority of the simulations, the defined distribution pattern was assigned to each layer and investigated for variable constraints similar to the previous studies. Additionally, a simulation was done for a layerwise distribution of the FG patterns with different patterns assign in the subsequent layers. The data obtained from the analysis showed the Type ‘X’ distribution produces the maximum natural frequency when lower fibre content is used (<5 glass and <7.8% carbon) in combination with graphene as the reinforcement materials. On the other hand, the largest natural frequencies are produced by the uniform distribution when the fibre content rises above the specified levels.

This research introduces 3-phase material optimization framework and defines a design efficiency factor that quantifies the output of optimization. Results indicate that graphene nanoparticles, when introduced into the matrix of the nanocomposite, produced much higher natural frequencies as compared to conventional fibre reinforced laminates. The results also showed that carbon fibres that were utilized as reinforcement perform better in maximizing the natural frequency compared to glass fibres. It is noted that optimization results in increased reinforcement contents in the outer layers of the laminate and reduced or no reinforcement in the inner layers, indicating that this is the optimal distribution of reinforcement with respect to the observed fundamental frequency. Increasing the number of design variables also improved the fundamental frequency. In terms of the skew laminate versus the rectangular laminate, the observation was made that the fundamental frequency was larger for a skew laminate than a rectangular laminate but the design efficiency decreased compared to the rectangular laminate. The thesis also suggests optimal functionally graded distributions along the thickness, in terms of maximizing natural laminate frequencies.

Industrial applications in civil, aerospace, mechanical and energy sectors can adopt some of these outcomes, towards a cost-effective design of advanced nanocomposite materials.

TABLE OF CONTENTS

LIST OF FIGURES

Chapter 5

Chapter 6

LIST OF TABLES

Chapter 4

Chapter 5

Chapter 6

LIST OF ABBREVIATIONS

GPL	Graphene platelet
CNTs	Carbon nanotubes
TPa	Terapascal
FG	Functionally graded
FEM	Finite Element Analysis
UD	Uniformly distribution
FSDT	First Order Shear Deformation Theory
DoF	Degree of Freedom
M	Matrix
GM	Graphene-reinforced matrix
W_{GPL}	Weight of graphene
V_F	Fibre volume
V_{GPL}	Volume of graphene platelets
SQP	Sequential Quadratic Programming Algorithm
Eq.	Equation
CNTRC	Carbon Nanotube Reinforced Composite Plates

Chapter 1: Introduction

1.1 Background

A composite material consists of two or more constituent materials that are combined into a singular structure for which the properties are superior to the parent materials alone. A fibre reinforced composite consists of high strength fibres in a matrix which binds the fibres together and allows transfer loads between the internal fibre network [1]. Composite materials have become popular industry applications and are found in the construction of automobiles, aircrafts and submarines and others that utilize materials of superior strength vs. weight and weight vs. stiffness ratios [2].

One of the main objectives of the research is to determine a method to increase the fundamental frequency beyond that of the excitation frequency which is the frequency that the structure will experience during its operation. The fundamental frequency relates to the stiffness and mass distribution of the laminate which forms part of the structural integrity and stability of the composite. Higher fundamental frequency values indicate a stiffer structure and ultimately lead to a structure that is more equipped to resist vibrations and dynamic loads. Composites that have lower fundamental frequencies may give indications of reduced/lower stiffness which can lead to resonance and fatigue failure under vibration. For this reason, the fundamental frequency is studied in this research and not other vibration modes.

The addition of graphene nanoplatelets (GPLs) to the matrix of the composite as nano-reinforcement has gained popularity due to the enhanced properties and qualities of the resulting nanocomposite. Graphene is the name proposed in 1986 for an isolated sheet of carbon atoms occurring in a graphite compound in a 2-dimensional arrangement. The term “Graphene” was then used to represent, a solitary, isolated layer of carbon hexagons which are formed via sp^2-hybridized bonds [3].

In order to investigate important engineering issues such as vibration response, buckling, and ideal weight to cost ratio, the incorporation of GPLs in nanocomposite

laminated plates has been studied in [4] where results showed the optimized solution involves decreasing the fibre reinforcement and increasing the amount of graphene.

Studies regarding optimization of graphene-reinforced nanocomposites are an important step in understanding their applicability in various industries due to small amounts of graphene increasing the strength and stiffness of composites [5].

This thesis proposes methods of enhancing the vibrational response generated by a nanocomposite laminated plate strengthened with graphene nano-reinforcement through optimization analysis and maximization via functionally graded distribution of reinforcement. The design of nano-reinforced composites can include an optimization scheme, which aims to use a minimal amount of reinforcement component materials to optimize the structure's natural frequency and prevent the occurrence of resonance [6]. Once the micromechanics equations have been used to determine the effective material properties, the optimal natural frequency can be calculated using finite element analysis and the shear deformation theory [7]. In this thesis the effective material properties are obtained using micromechanical equations to generate the properties of a graphene-reinforced matrix and thereafter applying the micromechanical equations again for the graphene and fibre reinforced matrix resulting in the 3-phase graphene/fibre reinforced composite. The optimization analysis involves the use of MATLAB coding to structure the Sequential Quadratic Programming Optimization algorithm. To explore the frequency response for a selected set of constraints and variables, a finite element code is proposed in MATLAB. The purpose of this study is to identify natural frequency values and the corresponding optimal design variables.

The functionally graded model is developed to distribute the reinforcement, graphene and fibre, in each layer to a predetermined distribution pattern. The main concept of this approach is to determine the most appropriate distribution pattern that returns the maximum possible natural frequency for a set of given design variables.

1.2 Motivation for the Research

The industrial sector is advancing composite technology to meet demands of a more cost effective and sustainable solution which involves investigating methods to efficiently strengthen composite materials. Graphene is a strong filler material used

to enhance the matrix of composites and has a strong binding capability to the matrix [7]. Research relating to the use of graphene to replace carbon nanotubes (CNTs) as reinforcement in composites has been more evident each year due to the advantages of graphene compared to carbon nanotubes. Some of the main advantages of graphene over CNTs are the larger specific area and reduced twisting tendency which results in an easier dispersion in the matrix. Figure 1.1 shows the trend in the number of publications each year from 2004 to 2013 where an exponential increase in the research related to graphene is evident from year to year [8].

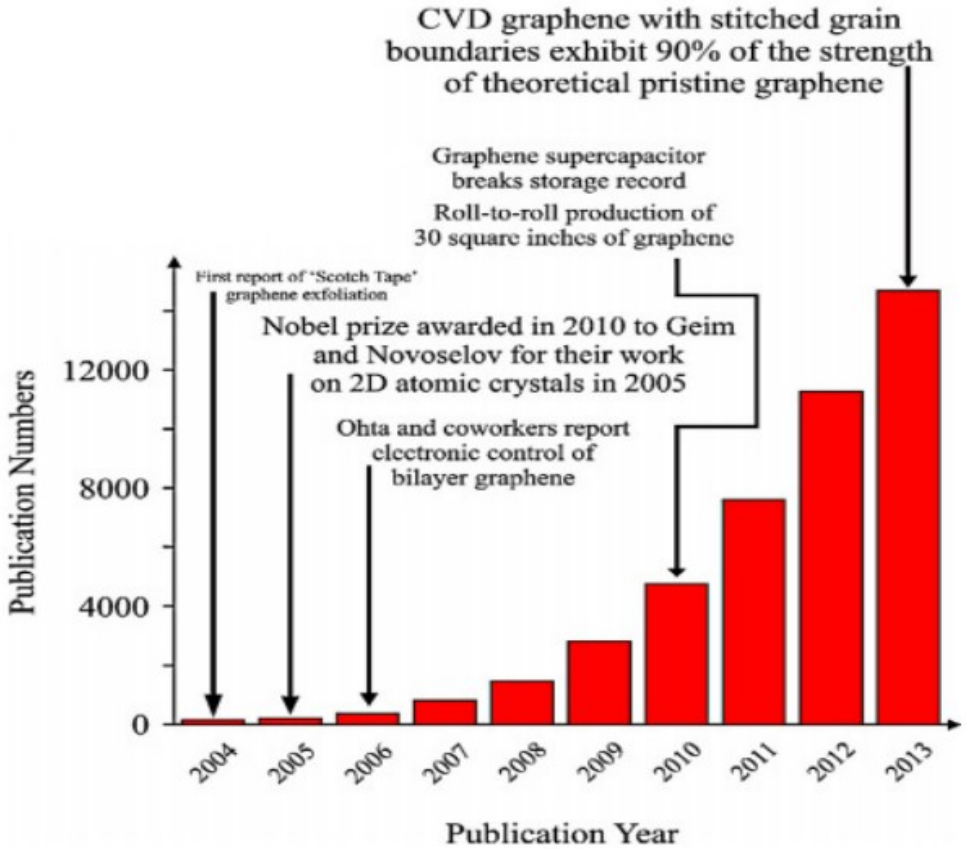

Figure 1.1: Number of research publications relating to graphene per year [6]

In [9], a study was performed to investigate the change to the natural frequency when reinforcing the matrix with minor quantities of graphene. Data on this study proved that even a small addition of graphene into the matrix of a polymer composite beam, led to a noteworthy rise in the natural frequency. In addition, the most effective method in applying the graphene particles was to disperse them in the surface layers of the composite. Variables including the graphene weight fraction,

geometry, arrangement pattern and total layer count, were examined in [10]. The findings corroborated the observation that adding graphene to the top and bottom layers of the composite increased the natural frequency.

In addition to rectangular and skew plates analysed for optimum graphene and fibre volume content, stacking sequence and boundary condition investigating functionally graded distributions gives insight into further refinements for the design of a graphene/fibre reinforced nanocomposite laminated plate. Dongying Liu studied the effect of functionally graded distributions (Figure 1.2) in [11] which resulted in the Type FG-X distribution of graphene producing the largest natural frequency compared to the others. Figure 1.2 shows each distribution pattern type where the graphene content is different in the layers. The darker layers indicate more graphene content in that layer. The 'UD' pattern shows uniform amounts of graphene in each layer. The type 'FG-X indicated larger GPL content in the outer layers and decreasing towards the inner layers. 'FG-O' indicates larger graphene content in the middle layers. 'FG-V' indicates larger graphene content in the upper layers of the laminate and decreasing towards the bottom layers. 'FG-A' is similar to 'FG-V' but reversed for more graphene content in the lower layers. As a result, a variety of graphene reinforcement distributions should be investigated, since the distribution pattern has been demonstrated to be a useful variable that may be employed to maximize and optimize the natural frequency.

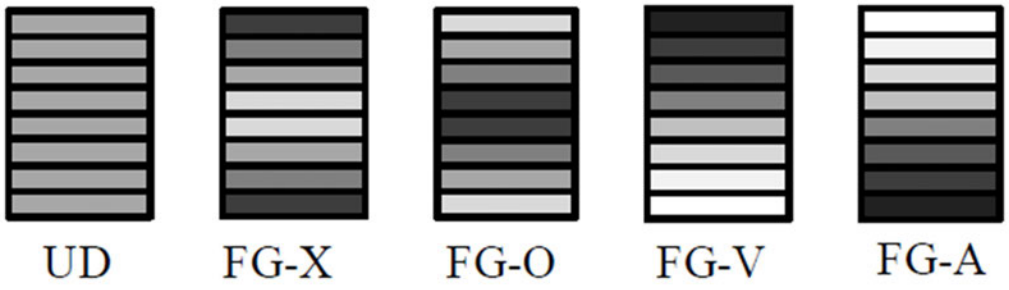

Figure 1.2: Functionally graded distribution patterns showing differing graphene content in the layers [9]

In this thesis, the natural frequency is studied for graphene/fibre reinforced nanocomposite laminated plates where a finite element model and MATLAB codes are defined by micromechanical equations, first order shear deformation theory, variable constraints and an optimization scheme. The effects on the natural frequency of variables such as, GPL content, fibre type and content, fibre stacking

sequence, boundary conditions, aspect ratio and number of layers are investigated via MATLAB models and critically analysed to determine optimum distributions of reinforcement and structure conditions relating to the most efficient methods to improve the nanocomposites natural frequency. This study is then expanded when the rectangular plate geometry is modified to a 45° skew plate under cantilever boundary conditions relating to industry applications such as aeroplane wings (aircrafts) [12]. Furthermore, the study expands on 3-phase graphene/fibre reinforced nanocomposite plates to include the analysis of functionally graded distributions of reinforcement material culminating in a holistic analysis around the improvement of the natural frequency using finite element analysis. The data presents critical information regarding core design considerations when attempting to maximize on the frequency response of nanocomposite laminated plates for industry application. The data presented in this thesis can be further expanded to improve current nanocomposite applications in various sectors.

The research contained in this document utilizes a gradient optimization algorithm which uses an iterative process to find a local minimum value of a function. This algorithm assisted in efficiently and effectively determining the optimal natural frequency for various cases. This is opposed to a global optimization algorithm that determines a point that minimized the function in totality.

1.3 Research Aims and Objectives

The aim of this research is to develop a methodology to accurately investigate the natural frequency response for a 3-phase graphene/fibre reinforced nanocomposite laminated plate and critically analyse the vibrational response data collected.

In order to achieve this, the following objectives are formulated:

- Develop a numerical, finite element analysis model to accurately simulate the vibrational response of a graphene/fibre reinforced nanocomposite plate;
- Compile data that represents the vibrational response of the composite under various constraints and variables;
- Identify the constraints and variable conditions that resulted in optimized and maximum natural frequency responses.
- Evaluate the contribution of graphene reinforcement on the vibration response
- Contribute towards cost-effective design, with optimal distribution of fibre and graphene reinforcement
- Evaluate and compare the response between rectangular and skew plates
- Investigate the impact of different functionally graded distributions on the vibration response

1.4 Contributions to Technical and Scientific Data

Research on the optimization of the natural frequency is presented in Chapters 4 and 5 and on the maximum natural frequency for functionally graded distributions in Chapter 6 by applying a finite element analysis framework.

The data obtained from the analyses give insight into the benefits of graphene nanoparticles as nano-reinforcement with the focus on improving the apparent natural frequency of a nanocomposite laminated plate. This research adds value by highlighting critical information regarding the methods and constraints that lead to the most optimized and maximized natural frequencies that can be introduced in industry applications. The methods of analysis and formulations used agree with comparative data obtained from published articles which add value in terms of verification of the model and theories used.

In Chapter 4 a model is derived for a 3-phase graphene/fibre reinforced laminated composite with an optimization scheme to accurately determine the impact of multiple variables on the natural frequency. In this chapter details regarding optimal placements of reinforcement material and superior material types are analysed and discussed. The research adds value by presenting data for superior reinforcement schemes and the design efficiency rating of each simulation thereby highlighting the most effective and efficient design and providing information regarding diminishing returns in the natural frequency as the amount of reinforcement is increased.

In Chapter 5 the previous model is expanded to add valuable insight into optimal vibration response of cantilever skew plates. Beneficial information is derived when comparisons are presented for rectangular composites vs. skew composites in terms of the effect of adding skew geometric properties to plates where rectangular plates are no longer feasible. Important information is presented regarding the shift in the magnitude of the natural frequency when the number of variable applied in one instance is increased from one to four.

In Chapter 6, data pertaining to the use of functionally graded reinforcement distributions were derived from a finite element analysis model. Valuable information is presented in terms of the effectiveness of functionally graded reinforcement distributions vs. uniform distributions. This research added value by verifying the distribution with the most potential in terms of natural frequency maximization with previous studied which investigated similar distribution patterns.

Overall this thesis contributes to the scientific field by proposing a methodology to evaluate and optimize the mechanical (vibration) response of nanocomposite laminates, adopting a hybrid reinforcement consisting of graphene nanoplatelets and conventional glass or carbon fibres, within finite element analysis. The proposed model has been verified against various results from other studies to ensure accurate and acceptable output data. This model can be adopted in further research/studies to expand the analysis into graphene nanoplatelets (GPLs) and fibre reinforcement. New theories, distribution patterns, experiments and materials can be simulated using this model to enhance the output of the experiment. The study also contributes in vibrational response analysis, highlighting optimal reinforcement distributions.

This research introduces an optimisation scheme for a 3-phase material which is not extensively studied in literature thereby providing a new concept that can be incorporated in future research to aid in optimizing structures and determining what variables are worth further research with regards to reinforcement and performance of nanocomposite structures.

A design efficiency factor was defined in this research to be the ratio of the fundamental frequency of the optimally designed laminate and the reference frequency, which is the frequency that corresponds to a laminate with uniformly distributed graphene and fibres across the thickness of the laminate, in order to verify the effectiveness of the reinforcements proposed throughout the analysis.

1.5 Research Scope and Limitations

The scope of this study is limited to the vibrational analysis of nanoreinforced composite laminated plates using graphene nano-platelets and glass/carbon fibres. This research extends to optimization of the natural frequency of rectangular and skew plates with uniform distributions of reinforcement throughout each layer of the laminate as well as a maximum natural frequency analysis involving functionally graded distributions of reinforcement in each layer for rectangular plates.

The computer resources available to perform increasingly intricate and sophisticated combinations place limitations on the study's scope. This is because higher number of variables, increased mesh density or higher layer number results in increased computational cost for the finite element analysis simulations implemented in MATLAB software. Getting more potent computer resources to shorten analysis times and boost processing capacity to handle more intricate design scenarios is one way to solve this for future study.

Data pertaining to physical testing on the 3-phase laminate are not attainable due to the cost of the material constituents and composite fabrication. Testing on real 3-phase laminated composites would yield useful information for future studies, which could be utilized to verify models and to validate the employed analysis techniques.

Because the research is being done on a part-time basis, every effort has been made to increase its breadth by conducting as many simulations and studies as possible while adhering to deadlines and milestones for the thesis submission. On the basis of the current study, future research can diversify the testing and enhance the usefulness of the research data already available.

1.6 Structure of the Thesis

The thesis consists of 6 chapters of which, two are published articles and one is an article submitted for publication. All articles are presented in their original form. The content of each chapter is provided below:

Chapter 1	an overall introduction and motivation to the presented research.
Chapter 2	literature review based on effective material properties and the vibrational response of graphene/fibre reinforced composite plates.
Chapter 3	methodology of the thesis
Chapter 4	introduces the optimization of the natural frequency for graphene/fibre reinforced composite rectangular plates (published article 1).
Chapter 5	introduces the optimization of graphene/fibre reinforced cantilever skew laminates with non-uniform distribution of reinforcements (published article 2).
Chapter 6	presents the investigation into the maximization of the fundamental frequency of functionally graded graphene-reinforced rectangular composite plates (article submitted for publication).
Chapter 7	provides a summary of the key findings and conclusions for the research. Possible future expansion and recommendations are described.

1.7 References

1. J.N. Reddy, Theory and Analysis of Laminated Composite Plate, Mechanics of Composite Materials and Structures, 361, (1999) 1–79. Available at https://doi.org/10.1007/978-94-011-4489-6_1
2. A. Lal, B. Sutaria & R. Kumar, Stress analysis of composite plate with cutout of various shape, IOP Conference Series: Materials Science and Engineering, 814, (2020) 012011. DOI 10.1088/1757-899X/814/1/012011
3. M. Inagaki, F. Kang, M. Toyoda & H. Konno, Graphene: Synthesis and Preparation. Advanced Materials Science and Engineering of Carbon, (2014) 41–65.
4. G.A. Drosopoulos, C. Gogos, G. Foutsitzi, Multi-objective optimization for maximum fundamental frequency and minimum cost of hybrid graphene/fibre-reinforced nanocomposite laminates, Structures, Volume 54, (2023) 1593-1607. Available at https://doi.org/10.1016/j.istruc.2023.05.118
5. R. Reddy, W. Karunasena, W. Lokuge, Free vibration of functionally graded-GPL reinforced composite plates with different boundary conditions, Aerospace Science and Technology, 78, (2018) 147–156. Available at https://doi.org/10.1016/j.ast.2018.04.019
6. A. Muc, Natural Frequencies of Rectangular Laminated Plates—Introduction to Optimal Design in Aeroelastic Problems. Aerospace, 5(3), (2018) 95. Available at https://doi.org/10.3390/aerospace5030095
7. T. Kuclourya, S. Mudliar, M.K. Jain & N.B. Thamba, A review on Graphene Reinforced Composites for Ballistic applications, IOP Conference DOI :10.1088/1757-899X/1123/1/012051 Series: Materials Science and Engineering, 1123(1), (2021) 012051.
8. H.G.P. Kumar & M.A. Xavior, Graphene Reinforced Metal Matrix Composite (GRMMC): A Review, Procedia Engineering, 97, (2014) 1033–1040. Available at https://doi.org/10.1016/j.proeng.2014.12.381
9. C. Feng, S. Kitipornchai & J. Yang, Nonlinear free vibration of functionally graded polymer composite beams reinforced with graphene nanoplatelets (GPLs), Engineering Structures, 140, (2017) 110–119. Available at https://doi.org/10.1016/j.engstruct.2017.02.052
10. M. Song, S. Kitipornchai & J. Yang, J., Free and forced vibrations of functionally graded polymer composite plates reinforced with graphene nanoplatelets,

Composite Structures, 159, (2017) 579–588. Available at https://doi.org/10.1016/j.compstruct.2016.09.070

11. D. Liu, Free Vibration of Functionally Graded Graphene Platelets Reinforced Magnetic Nanocomposite Beams Resting on Elastic Foundation, Nanomaterials, 10(11), (2020) 2193. Available at https://doi.org/10.3390/nano10112193
12. T. Hassan, A. Salam, A. Khan, S. U. Khan, H. Khanzada, M. Wasim, I. S. Kim, Functional nanocomposites and their potential applications: A review, Journal of Polymer Research, 28 (2021) 36. Available at https://doi.org/10.1007/s10965-021-02408-1

Chapter 2: Literature Review

Various industry use nanocomposite laminates because of their exceptional mechanical properties and wide range of applications. According to several publications [1-4], the idea of improving conventional composite structures by using cutting-edge materials with better mechanical properties has become widely accepted and has seen increased implementation and application in recent years. In order to further improve the structural response of composite materials, reinforced nanocomposite laminates are created by reinforcing them with nano-materials that have improved properties [5]. The mechanical properties of these composite materials, such as natural frequency, chemical resistance, electrical conductivity and thermal stability, can all be greatly improved by introducing nanoparticles while retaining the advantageous aspects of the base material, such as low density and high processing ability [6]. As a result, nanocomposites have found widespread use in the engineering sector for a variety of applications, such as gas pipelines, cars, aircraft, and electromagnetic shielding [7]. In [8], G.A. Drosopoulos and G.E. Stavroulakis detail several numerical methods to study composite materials emphasizing in their non-linear response and highlighting the complexity and challenges to evaluate their behaviour.

Non-uniform fibre distribution can be used to strategically increase design efficiency and lower the weight of the composite, as shown in [9–11]. In [12, 13], the Halpin-Tsai model and the rule of mixtures applied to determine the composite's effective material properties. Micromechanical equations were used in [14] to determine the resultant properties of a 2-phase fibre reinforced composite. A design which incorporated the design for reduced composite weight for a CNT/fibre reinforced composite was investigated in [15] to determine the most efficient reinforcement scheme for optimal weight design. It was determined that the distribution of the CNT reinforcement in the surface layers was the most optimal reinforcement distribution to minimize the weight. In [16, 17, 18-22] optimal design to produce the maximum fundamental frequency is studied for hybrid composite laminates. 2-phase composite analysis to improve the fundamental frequency of CNT and glass fibre composites was studied in [23]. Radebe et al. determined that the effect on the frequencies by adding more fibre reinforcement in the outermost layers depends of factors such as

the orientation of fibres and aspect ratio [24]. In [25-27], investigations showing the effects of CNTs on the fundamental frequency of composites are presented. In a study conducted by Sinha et al., increasing the total layer count in the composite improved the fundamental frequencies [28]. Similar results are seen in [29, 30].

Infusing the matrix of the composite with graphene nanoparticles as an enhancement material has been gaining positive attention and has been the topic of many research papers such as [31-33]. The term “graphene” represents a honeycomb arrangement of sp^2 hybridized carbon atoms and has been identified as an exceptional strengthening material. Graphene displays some noteworthy mechanical characteristics including 1 TPa Young’s Modulus and electrical/thermal properties similar to that of copper [34]. Other beneficial characteristics of graphene are good electrical conductivity, light weight, mechanical toughness and large surface to volume ratio resulting in an excellent bonding interface [35, 36]. [37] shows the geometric arrangement of graphene platelets has a significant effect on the design of nanocomposite curved beams.

It is evident that graphene nanoreinforcement can be significant in strengthening a structure, as demonstrated in [38], where the addition of 0.54% exfoliated graphene by volume increased the structure’s tensile strength by 10% and the elastic modulus by 25% when compared to unreinforced resin. Patra et al. tested the effect of adding GPLs to a composite in [39] where it was discovered that the mechanical strength was enhanced and smaller sized GPLs improve the dispersion compared to larger particles. Yoa et al. investigated the benefits of using GPLs enhanced woven carbon fibre/epoxy composites to improve the gas barrier and mechanical properties in the oil and gas industry in [40]. The tensile, flexural and gas permeability properties significantly improved with increased GPLs. In [41] graphene was seen to improve the buckling load when used as reinforcement in composites with woven fibres to form a hybrid laminate composite. In [42], a free vibration analysis is presented for functionally graded composite laminates reinforced with graphene. The results of the study indicated that the key factors for vibrational response were the graphene nanoplatelet volume content and boundary condition, followed by the reinforcement pattern and thickness ratio.

In [43] it was demonstrated that adding CNTs–GPL hybrids to pristine epoxy significantly improved both the mechanical properties and the effectiveness of load transfer. In [44], the biaxial buckling of 3-phase angle-ply laminates reinforced with carbon/glass fibre and graphene is examined. It was found that high fibre content lessens the graphene reinforcement matrix's contribution and that a thicker surface layer or increased thickness ratio (ratio of surface thickness to overall thickness) increased the buckling loads. Improved transfer of loads from the matrix to the reinforcement in graphene nanoplatelets (GPLs) is due to the large surface area of the particles and is one of the primary reasons for graphene's high capacity for reinforcement [45,46]. According to Guo et al. in [47], graphene-reinforced composites produced much larger natural frequencies than carbon nanotube-reinforced composites. The GPL distribution and boundary condition can also have a significant impact on the composite's natural frequency. According to research published in [48], natural frequencies for graphene/fibre reinforced hybrid polymer composites improved as graphene volume fraction increased. Additionally, natural frequency increased more under clamped conditions than under simply supported conditions.

Significant vibration actions frequently affect lightweight structures. Consequently, it is becoming more crucial to look into the best performance in order to avoid resonance through methods such as optimization [49]. Resonance is less likely to occur when the structure's natural frequency is significantly increased by an optimization scheme. In [50] Tam et al. utilized finite element analysis to study the vibration and buckling properties of GPL reinforced composite beams with functionally graded distributions. A range of techniques for enhancing the natural frequencies of nanocomposite plates have been demonstrated by numerous studies. [51] examined the natural frequencies of skew laminates that had stiffeners which increased the frequencies as the skew angle increased, according to the results. In [52] by Magdy et al., a discussion on the vibration analysis in composite wing design is discussed. It was highlighted that controlling and improving the dynamic response of structural elements in aero-elastic analysis can be done by altering the stacking sequence and ply orientation of fibres. Kalusuramanet al. compiled a study on the vibration response on fibre reinforced composites in [53]. A conclusion of the study was the importance of the fibre orientation and fibre stacking sequence in obtaining

the natural frequency of the composite. [54] studied the vibration analysis of a composite concrete/ glass fibre reinforced slab under human activities. In the study it was determined that in spite of the slabs good performance under static loading the dynamic behaviour of the slab must be considered in the slab design due to the flexibility component and slenderness of the slab.

Georgantzinos et al. investigated fibre-reinforced hybrid polymer composites where results confirmed a superior natural frequency for every mode when graphene was added to the composite matrix. Additionally, it was evident that graphene reinforcement increased the natural frequency for clamped boundaries than simply supported and the composite's mechanical characteristics were improved [55]. In [56] a study was done, in a thermal environment, on the vibrational analysis of GPL-reinforced composite plates. The results showed that the natural frequency was improved when graphene was introduced regardless of the dispersion pattern. Additionally, as the length-to-thickness ratio increases, so do the natural frequencies; the highest natural frequency is the product of greater distributions at the outermost layers and less reinforcement at the innermost layer of the plate.

The effects of adding graphene into a composite reinforced beam is studied in [57]. In the study, when the weight fraction of graphene was raised from 0% to 1%, the natural frequency of the beam increased by 170% and the beam's stiffness increased significantly, leading to a superior bending performance. The vibration analysis of a porous composite plate reinforced with graphene was investigated by Pan et al. in [58]. The findings indicated that twelve layers in the laminate was the ideal number, and that decreasing free vibration frequency was caused by a higher porosity levels in the plate. Based on the research in [59], it is possible to increase the natural frequency more effectively by increasing the quantity of square-shaped GPLs to the composite's top and bottom layers. In [60] a layerwise optimization approach was adopted in terms of stacking sequence where it was found that the layerwise approach yielded increased frequencies as compared to the reference frequencies.

Rout et al. investigated the thermo elastic free vibration of graphene-reinforced composite shells. The fundamental frequency increased when the aspect ratio increased and when the shell thickness decreased [61]. A fibre-reinforced

composite's fundamental frequency and central deflection were greatly increased by adding minimal amounts of graphene [62]. Studies on the advantages of graphene and fibre-reinforced composites can be found in [63–67], where the findings show that adding graphene to carbon-reinforced composites enhances the composite's overall properties. The fundamental frequency observed for clamped conditions is superior to that of cantilever conditions for composites with cut-outs seen in [68]. The fundamental frequency data obtained in [69] shows that higher frequencies are produced for anti-symmetric fibre orientation than for the symmetric one.

Research on the optimal vibration response has also been conducted for skew plates. In [70] the fundamental frequency was maximized for anti-symmetric and symmetric skew composite laminates by determining the optimal stacking sequence. Kiyani et al. computed the characteristics of a skew composite plate reinforced with CNTs using the modified rule of mixtures. The results showed an increase in the frequency value for increasing CNT volume content [71]. Studies relating to improving frequencies of CNT reinforced skew plates can be seen in [72-74]. The fundamental frequency improved when increasing the aspect ratio, skew angle and width-to-thickness ratio in skew isotropic plates in [75]. A study on the free vibration of laminated skew plates revealed that the frequency increased with an increase in the skew angle of the plate [76]. Similar results indicating an improved fundamental frequency for increasing skew angle is observed in [77]. In [78] Topal et al. applied the first order shear deformation theory to analyse the frequency optimization of laminated skew plates. Frequency optimization of skew composite laminates to maximize fundamental frequency was investigated via metaheuristic algorithms such as Genetic algorithms and particle swarm optimization in [79]. The study conducted in [80] examined the impact of several boundary conditions, plate geometries, graphene arrangement and weight content, and number of layers on the frequencies of a skew plate on point supports.

Amongst the research on graphene reinforcement of composite plates, studies have been extended to reinforcement over the thickness of the laminated layers to enhance the efficiency of the design as seen in [81, 82]. Functionally graded graphene or CNT reinforcement has recently been a developing approach, aiming to propose optimal distribution patterns of the reinforcement based on pre-defined

distributions, resulting in improved mechanical performance [83]. Different equations have been used in literature, to represent various nanoreinforcement distributions throughout the thickness direction and the surface of the composite.

In their study of functionally graded (FG) carbon nanotubes, Liew et al. noted that functionally graded CNT structures were typically investigated using methods such as analytical, semi-analytical, FEM, mesh-free, and differential quadrature method [84]. It was clear from [85] that the dynamic behaviour of FG graphene-reinforced composites can be modified by altering the GPL dispersion pattern. Babaei et al. studied the vibrational behaviour of thermally pre/post-buckled functionally graded CNT beams for an FG-O, UD (uniform distribution) and FG-X where the results showed that the frequency output was maximized and minimized for FG-X and FG-O distribution patterns respectively [86]. The same result can be seen in [87] where frequency was maximum for FG-X and minimum for FG-O distribution patterns.

Shen et al. studied the vibration of thermally post buckled functionally graded graphene-reinforced composite plates using the Halpin-Tsai model to determine the anisotropic and temperature-dependent material properties. It was found that the fundamental frequency of a FG graphene-reinforced composite is significantly influenced by the width-to-thickness ratio of the plate [88]. Shahrjerdi et al. [89] examined temperature dependant functionally graded graphene-reinforced nanocomposite beams. The FG-X Type produced the largest natural frequencies in all analyses, but the FG-Diamond type, uniform, FG-A type, and FG-X type distributions all showed an increase in natural frequency with increasing graphene weight percentage. The vibration of stiffened composite cylindrical panels incorporating functionally graded graphene-reinforced with FG-X, FG-A, UD and FG-O distribution types was examined by Zhou et al. [90]. The highest and lowest natural frequencies were related to FG-X and UD, respectively. According to the study, FG-X frequencies increased more when the weight fraction of GPLs was increased than when other distributions were taken into account [90].

Micromechanical models were used in [91] to produce the effective material properties for functionally graded graphene-reinforced polymer composites to effectively analyse the vibrations of the composite. The results of the analysis showed FG-X to produce larger natural frequencies followed by UD and lastly by FG-

O distribution. The non-linear vibration of functionally graded graphene-reinforced conical shells is presented in [92]. Similar to earlier research, the FG-X distribution was found to cause an increase in the system's stiffness. It was also found that the free vibration conical shell was significantly impacted by the GPL weight content and distribution, length-to-radius and radius-to-thickness ratio. A vibration analysis on FG graphene-oxide reinforced composite beams is studied in [93]. Results showed higher structural stiffness when the graphene oxide was dispersed near the top and bottom of the beam.

In [94] it was found that the GPL size and weight fraction can increase the natural frequencies for a FG graphene-reinforced composite. Non-linear vibration is examined in [95] for FG graphene-reinforced porous plates. It was discovered that while porosity distribution and GPL dispersion patterns can both have an impact on non-linear vibrations, the GPL dispersion pattern has a noticeably greater effect. Qaderi et al. investigated the vibration response of graphene-reinforced polymer composite plates. The natural frequency increases as the ratio of plate thickness to length increases, according to the results [96]. According to Wang et al.'s investigation into the static response of functionally graded graphene-reinforced plates in [97], the distribution and concentration of GPL are two factors that affect the bending behaviour of the GPL-reinforced plates. Kitipornchai et al. came to the conclusion that the boundary condition and slenderness ratio had minimal bearing on the percentage increase in the critically buckling load and fundamental frequency, with the exception of scenarios in which GPLs are asymmetrically distributed [98]. Functionally graded graphene-reinforced composites were also studied in [99-102].

Attempts were made to find articles relating to the experimental investigation into the vibration analysis of graphene/fibre reinforced nanocomposite plates but no paper was found with direct relation to the analysis contained in this thesis. This being said, future investigation into the experimental analysis of the research in this thesis can be done to further develop the analyses and provide crucial data to the field of this research.

A paper [103] was found relating to an experimental analysis of the free vibration of graphene reinforced laminated composite plates using experimental modal testing.

The analysis done in this article is close in similarity to that presented in this thesis baring some characteristic differences in the composite plate geometry. In the study a carbon fibre graphene-reinforced hybrid polymer plate, a graphene-reinforced polymer plate and a carbon fibre-reinforced polymer plate were examined. The properties of the composite are determined using the Halpin-Tsai model and the analysis done via finite element analysis for the theoretical investigation section. For the experimental testing, the impact hammer modal testing method is used to determine the plate's vibration reactions. In the experimental testing, three plates with two end conditions, clamped – free – clamped – free (CFCF) and simply supported – free – simply supported – free (SFSF) are tested. The characteristics of the carbon fibre graphene-reinforced plate are length equal to 250mm, width equal to 250 mm and thickness equal to 3mm. The plate is an eight-layered laminated composite with fibre angle [0/45/-45/90/90/-45/45/0]. The experiment, relative to the first eigenmode, showed for the SFSF plate a frequency of 87.5 Hz (experimental) and 97.4 Hz (via ANSYS analysis). This resulted in an 11.31% difference in the theoretically calculated frequency vs. the experimentally produced frequency. In terms of the CFCF boundary condition plate, a frequency of 322 Hz (experimental) and 332 Hz (via ANSYS analysis) was determined. This resulted in a 3.11% difference between the experimental and theoretically calculated data. CFCF was seen to produce higher natural frequencies than SFSF condition as the clamped condition results in larger stiffness than simply supported.

This result is a good comparison between experimental and theoretical methods that relate closely to that used in this thesis and ultimately show agreement between the experimental and theoretical data outputs. Though not directly comparable to this thesis the method used to calculate the data contained in this thesis are similar to that in the study which delivered good results.

2.1 References

1. F. Ebrahimi, Nanocomposites - New Trends and Developments, Intech, Rijeka,Croatia, 1, (2012) 1-516. Available at: http://dx.doi.org/10.5772/3389.
2. B. Reddy, Advances in Diverse Industrial Applications of Nanocomposites, Intech, Rijeka, Croatia, 1, (2011) 1-590. Available at: http://dx.doi.org/10.5772/1931.
3. F. Gao, Advances in polymer nanocomposites - Types and applications, Woodhead Publishing Limited, Cambridge, UK, 1, (2012) 1-680. Available at: https://doi.org/10.1016/B978-1-84569-940-6.50022-6.
4. S.C. Ray, Applications of Graphene and Graphene-Oxide Based Nanomaterials, William Andrew Publishing, 1, (2015) ISBN 978032337522. Available at https://doi.org/10.1016/C2014-0-02615-9.
5. C. V. Monfared, S.Ramakrishna, A.Alizadehetal., A systematic study on composite materials in civil engineering, Ain Shams Engineering Journal, 1 (2023) 2090-4479. Available at https://doi.org/10.1016/j.asej.2023.102251.
6. A. Liu, H., & Brinson, L. C. (2008). Reinforcing efficiency of nanoparticles: A simple comparison for polymer nanocomposites. Composites Science and Technology, 68(6), 1502–1512. doi:10.1016/j.compscitech.2007.10.033.
7. D. F. Tornabene, N. Fantuzzi, M. Bacciocchi, Linear static response of nanocomposite plates and shells reinforced by agglomerated carbon nanotubes, Composites Part B: Engineering, 115, (2017) 449–476.Availalbe at https://doi.org/10.1016/j.compositesb.2016.07.011.
8. G.A. Drosopoulos, G.E. Stavroulakis, (2022), “Non-linear Mechanics for Composite Heterogeneous Structures”, CRC Press, Taylor and Francis
9. Q. Liu, Exact sensitivity analysis of stresses and lightweight design of Timoshenko composite beams. Compos Struct 2016;143:272–286. https://doi.org/10.1016/j.compstruct.2016.02.028
10. S.-Y. Kuo, Thermal buckling, vibration and flutter of composite laminates containing two non-uniformly distributed fibers. J Aeronautics Astronautics Aviation 2016;48(3):173–182. Available at https://doi.org/10.6125/16-0505-888.
11. T. Vo-Duy, V. Ho-Huu, T.D. Do-Thi, H. Dang-Trung, T. Nguyen-Thoi, A global numerical approach for lightweight design optimization of laminated composite plates subjected to frequency constraints, Compos. Struct. , 159,

(2017) 646–655. Available at https://doi.org/10.1016/j.compstruct.2016.09.059.

12. Y. Huang, Z. Yang, A. Liu, J. Fu, Nonlinear buckling analysis of functionally graded graphene-reinforced composite shallow arches with elastic rotational constraints under uniform radial load, Materials 11 (6) (2018) 910. Available at https://doi.org/10.3390/ma11060910
13. J. Yang, H. Wu, S. Kitipornchai, Buckling and post-buckling of functionally graded multilayer graphene platelet-reinforced composite beams, Compos. Struct. 161 (2017) 111–118. Available at https://doi.org/10.1016/j.compstruct.2016.11.048
14. H.-S. Shen, A comparison of buckling and post-buckling behavior of FGM plates with piezoelectric fibre reinforced composite actuators, Compos. Struct. 91 (2009) 375–384. Available at https://doi.org/10.1016/j.compstruct.2009.06.005
15. S. Anashpau, G.A. Drosopoulos, S. Adali, Minimum weight design of CNT/fiber reinforced laminates subject to a frequency constraint by optimal distribution of reinforcements across the thickness, Composite Structures, 319, (2023) 117112. Available at https://doi.org/10.1016/j.compstruct.2023.117112
16. K.J. Duffy, S. Adali, Optimal fibre orientation of antisymmetric hybrid laminates for maximum fundamental frequency and frequency separation. J Sound Vib 1991;146(2):181–190. Available at https://doi.org/10.1016/0022-460X(91)90757-B
17. H. An, S. Chen, H. Huang, Multi-objective optimal design of hybrid composite laminates for minimum cost and maximum fundamental frequency and frequency gaps. Compos Struct 2019;209:268–276. Available at https://doi.org/10.1016/j.compstruct.2018.10.075
18. S. Kamarian, M. Shakeri, B. Karimi, A. Pourasghar Free vibration analysis and design optimization of nanocomposite-laminated beams using various higher order beam theories and imperialist competitive algorithm. Polym Compos 2015;37(8):2442–2451. Available at https://doi.org/10.1002/pc.23429
19. H. An, S. Chen, H. Huang Maximization of fundamental frequency and buckling load for the optimal stacking sequence design of laminated

composite structures. Proc Institution of Mechanical Engineers, Part L: J Materials: Design Appl 2018. 146442071876502. Available at https://doi.org/10.1177/1464420718765020

20. M.K. Apalak, D. Karaboga, B. Akay, The Artificial Bee Colony algorithm in layer optimization for the maximum fundamental frequency of symmetrical laminated composite plates. Eng Optim 2014;46(3):420–437. Available at https://doi.org/10.1080/0305215X.2013.776551
21. M.H. Sadr, B.H. Ghashochi Optimization of laminated composite plates for maximum fundamental frequency using Elitist-Genetic algorithm and finite strip method. J Global Optim 2011;54(4):707–728. Available at https://doi.org/10.1007/s10898-011-9787-x
22. R. Kayikci, F.O. Sonmez, Design of composite laminates for optimum frequency response. J Sound Vib 2012;331(8):1759–1776. Available at https://doi.org/10.1016/j.jsv.2011.12.020
23. S. Kamarian, M. Shakeri, M.H. Yas, Natural frequency analysis and optimal design of CNT/fiber/polymer hybrid composites plates using Mori-Tanaka approach, GDQ technique, and firefly algorithm. Polym Compos 2016;39(5):1433–1446. Available at https://doi.org/10.1002/pc.24083.
24. Radebe I.S., Drosopoulos G.A., Adali S. (2022), “Effect of non-uniform fibre distribution along thickness and non-uniform ply thicknesses on frequencies of symmetric angle-ply laminates”, Fibers and Polymers, 23, 2250–2260. Available at https://doi.org/10.1007/s12221-022-4440-5.
25. F. Ebrahimi, A. Enferadi, A. Dabbagh, Wave Dispersion Behaviors of Multi-Scale CNT/Glass Fiber/Polymer Nanocomposite Laminated Plates, Polymers , 14, (2022) 5448.
26. M. Hocaoğlu, H. Karagülle, Effect of carbon nanotube reinforcement on the natural frequencies and damping ratios of nanocomposite beams, Materials Research Express, 7, (2020) 025021. Available at https://doi.org/10.1088/2053-1591/ab721a.
27. M. Avey, F. Kadioglu, S. Ahmetolan, Mathematical modeling and solution of nonlinear vibration problem of laminated plates with CNT originating layers interacting with two-parameter elastic foundation, J Braz. Soc. Mech. Sci. Eng, 45, (2023) 185. Available at https://doi.org/10.1007/s40430-023-04016-0.

28. L. Sinha, D. Das, A. N. Nayak, S. S. Kumar, Experimental and numerical study on free vibration characteristics of laminated composite plate with/without cut-out, Composite Structures, 256, (2020) 1-54. Available at https://doi.org/10.1016/j.compstruct.2020.113051.
29. B. Wang, F. Zhao, Z. Zhao, K. Xu, Influence factors on natural frequencies of composite materials, Frontiers of Mechanical Engineering, 15(4), (2020) 571–584. Available at https://doi.org/10.1007/s11465-020-0592-4.
30. M. K. Apalak, M. Yildirim, R. Ekici, Layer optimisation for maximum fundamental frequency of laminated composite plates for different edge conditions, Composites Science and Technology, 68(2), (2008) 537-550. Available at https://doi.org/10.1016/j.compscitech.2007.06.031.
31. Mittal V. (Ed.). Polymer-Graphene Nanocomposites. The Royal Society of Chemistry 2012, Cambridge, UK. Available at https://doi.org/10.1039/9781849736794.
32. V.B. Mohan, K. Lau, D. Hui, D. Bhattacharyya, Graphene-based materials and their composites: A review on production, applications and product limitations. Compos Part B: Eng 2018;1421:200–220. Available at https://doi.org/10.1016/j.compositesb.2018.01.013.
33. A.R. Saidi, R. Bahaadini, K. Majidi-Mozafari, On vibration and stability analysis of porous plates reinforced by graphene platelets under aerodynamical loading. Compos Part B: Eng 2019;164:778–799. Available at https://doi.org/10.1016/j.compositesb.2019.01.074.
34. G. Shi, S. Araby, C.T. Gibson, Q. Meng, S. Zhu & J. Ma, Graphene Platelets and Their Polymer Composites: Fabrication, Structure, Properties, and Applications, Advanced Functional Materials, 28(19), (2018) 1706705.
35. P. Cataldi, A. Athanassiou, I. Bayer Graphene nanoplatelets-based advanced materials and recent progress in sustainable applications. Appl Sci 2018;8(9):1–35.
36. D.G. Papageorgiou, Z. Li, M. Liu, I.A. Kinloch, R.J. Young Mechanisms of mechanical reinforcement by graphene and carbon nanotubes in polymer nanocomposites. Nanoscale 2020;12:2228–2267. Available at https://doi.org/10.1039/C9NR06952F.
37. B. Anirudh, M. Ganapathi, C. Anant & O. Polit, A comprehensive analysis of porous graphene-reinforced curved beams by finite element approach using

higher-order structural theory: Bending, vibration and buckling, Composite Structures, 222, (2019) 110899. Available at https://doi.org/10.1016/j.compstruct.2019.110899.

38. J. Qiu & S. Wang, Enhancing polymer performance through graphene sheets, Journal of Applied Polymer Science, 119(6), (2010) 3670–3674. Available at https://doi.org/10.1002/app.33068.
39. S.C. Patra, S. Swain, P. Senapati, H. Sahu, R. Murmu, H. Sutar, Polypropylene and Graphene Nanocomposites: Effects of Selected 2D-Nanofiller's Plate Sizes on Fundamental Physicochemical Properties. Inventions, 8, (2023) 8. Available a https://doi.org/10.3390/inventions8010008.
40. X. Yao, T.P. Raine, M. Liu, Effect of graphene nanoplatelets on the mechanical and gas barrier properties of woven carbon fibre/epoxy composites, J. Mater. Sci., 56, (2021) 19538–19551. Available at https://doi.org/10.1007/s10853-021-06467-z
41. K. Sewnath, G.A. Drosopoulos, S. Adali, Buckling of woven fibre and graphene platelet reinforced nanocomposite laminates, Structures, 56, (2023) 104893. Available at https://doi.org/10.1016/j.istruc.2023.104893.
42. F. Pashmforoush, Statistical analysis on free vibration behavior of functionally graded nanocomposite plates reinforced by graphene platelets, Composite Structures, 213, (2019) 14-24. Available at https://doi.org/10.1016/j.compstruct.2019.01.066.
43. W. Li, A. Dichiara, J. Bai, Carbon nanotube–graphene nanoplatelet hybrids as high-performance multifunctional reinforcements in epoxy composites, Composites Science and Technology, 74, (2013) 221-227. Available at https://doi.org/10.1016/j.compscitech.2012.11.015.
44. I.S. Radebe, G.A. Drosopoulos, S. Adali, Buckling of non-uniformly distributed graphene and fibre reinforced multiscale angle-ply laminates, Meccanica, 54 (14), (2019) 2263-2279. Available at https://doi.org/10.1007/s11012-019-01067-3.
45. L.C. Tang, Y.J. Wan, D. Yan, Y.B. Pei, L. Zhao, Y.B. Li, et al. The effect of graphene dispersion on the mechanical properties of graphene/epoxy composites. Carbon 2013;60:16–27. Available at https://doi.org/10.1016/j.carbon.2013.03.050.

46. R.J. Young, M. Liu, I.A. Kinloch, S. Li, X. Zhao, C. Vallés, et al. The mechanics of reinforcement of polymers by graphene nanoplatelets. Compos Sci Technol 2018;154:110–116. Available at https://doi.org/10.1016/j.compscitech.2017.11.007.
47. H. Guo, S. Cao, T. Yang, Y. Chen Vibration of laminated composite quadrilateral plates reinforced with graphene nanoplatelets using the element-free IMLS-Ritz method. Int J Mech Sci 2018;142:610–621. Available at https://doi.org/10.1016/j.ijmecsci.2018.05.029.
48. S. K. Georgantzinos, G. I. Giannopoulos, S. I. Markolefas, Vibration Analysis of Carbon Fiber-Graphene-Reinforced Hybrid Polymer Composites Using Finite Element Techniques, Materials, 13(19), (2020) 4225. Available at https://doi.org/10.3390/ma13194225.
49. G.K. Tairidis, G. Foutsitzi, G.E. Stavroulakis, Optimal design of smart composites, Approximation and Optimization,145, (2019) 185-217. Available at http://purl.tuc.gr/dl/dias/4058B046-5FE8-40AF-AC73-FCF79634D924.
50. W. H. Liu, W. C. Chen, Vibration analysis of skew cantilever plates with stiffeners, Journal of Sound and Vibration, 159(1), (1992) 1–11. Available at https://doi.org/10.1016/0022-460X(92)90447-6.
51. M. Tam, Z. Yang, S. Zhao & J. Yang, Vibration and Buckling Characteristics of Functionally Graded Graphene Nanoplatelets Reinforced Composite Beams with Open Edge Cracks, Materials, 12(9), (2019) 1412. Available at https://doi.org/10.3390/ma12091412
52. A. Magdy, M. Kamel, M.A. Elshafei & M. Kassem, Vibration analysis of composite wing with geometric and material coupling, IOP Conf. Ser.: Mater. Sci. Eng., 1172, (2021) 012003. Available at https://doi:10.1088/1757-899X/1172/1/012003
53. G. Kalusuraman, S.T. Kumaran, K. Balamurugan, N. Sivashanmugam, P. Sivaprakasam, R. Kurniawan & V. Ezhilmaran, Vibration Studies on Fiber Reinforced Composites – a Review, Journal of Natural Fibers, 20,(2023) 2157361. Available at https://doi.org/10.1080/15440478.2022.2157361
54. P. Junges, H.L.L. Rovere, R.C. de A. Pinto, Vibration Analysis of a Composite Concrete/GFRP Slab Induced by Human Activities. Journal of Composites Science, 1(2), (2017) 11. Available at https://doi.org/10.3390/jcs1020011

55. S.K. Georgantzinos, G.I. Giannopoulos & S.I. Markolefas, Vibration Analysis of Carbon Fiber-Graphene-Reinforced Hybrid Polymer Composites Using Finite Element Techniques, Materials, 13(19), (2020) 4225. Available at https://doi.org/10.3390/ma13194225
56. S. Qaderi, F. Ebrahimi & V. Mahesh, Free Vibration Analysis of Graphene Platelets–Reinforced Composites Plates in Thermal Environment Based on Higher-Order Shear Deformation Plate Theory, International Journal of Aeronautical and Space Sciences, 20(3) , (2019) 902-912. Available at https://doi.org/10.1007/s42405-019-00184-3
57. Y. Zhang, J. Teng, J. Huang, K. Zhou, L. Huang, Free and Forced Vibration Analyses of Functionally Graded Graphene-Nanoplatelet-Reinforced Beams Based on the Finite Element Method, Materials, 15, (2022) 6135. Available at https://doi.org/10.3390/ma15176135
58. H-G. Pan, Y.S. Wu, J.N. Zhou, Y.M. Fu, X. Liang, T.Y. Zhao, Free Vibration Analysis of a Graphene-Reinforced Porous Composite Plate with Different Boundary Conditions, Materials, 14, (2021) 3879. Available at https://doi.org/10.3390/ma14143879
59. M. Song, S. Kitipornchai, J. Yang, Free and forced vibrations of functionally graded polymer composite plates reinforced with graphene nanoplatelets, Composite Structures, 159, (2017) 579–588. Available at https://doi.org/10.1016/j.compstruct.2016.09.070
60. Y. Narita, Layerwise optimization for the maximum fundamental frequency of laminated composite plates, Journal of Sound and Vibration, 263(5), (2003) 1005–1016. Available at https://doi.org/10.1016/S0022-460X(03)00270-0
61. M. Rout, S.S. Hota, A. Karmakar Thermoelastic free vibration response of graphene reinforced laminated composite shells. Eng Struct., 178, (2019) 179–190. Available at https://doi.org/10.1016/j.engstruct.2018.10.029
62. M. Rafiee, F. Nitzsche, M.R. Labrosse Modeling and mechanical analysis of multiscale fiber-reinforced graphene composites: Nonlinear bending, thermal post-buckling and large amplitude, Int. J. Non Linear. Mech., 103, (2018) 104–112. Available at https://doi.org/10.1016/j.ijnonlinmec.2018.05.004
63. X. Yang, Z. Wang, M. Xu, R. Zhao, X. Liu Dramatic mechanical and thermal increments of thermoplastic composites by multi-scale synergetic

reinforcement: Carbon fiber and graphene nanoplatelets, Mater. Des., 44 (2013)74–80. Available at https://doi.org/10.1016/j.matdes.2012.07.051

64. C.M. Hadden, D.R. Klimek-McDonald, E.J. Pineda, J.A. King, A.M. Reichanadter, I. Miskioglu, et al. Mechanical properties of graphene, nanoplatelet/carbon fiber/ epoxy hybrid composites: Multiscale modeling and experiments. Carbon, 95, (2015) 100–112. Available at https://doi.org/10.1016/j.carbon.2015.08.026
65. O. Aluko, S. Gowtham, G.M. Odegard Multiscale modeling and analysis of graphene nanoplatelet/carbon fiber/epoxy hybrid composite. Compos Part B: Eng., 131, (2017)82–90. Available at https://doi.org/10.1016/j.compositesb.2017.07.075
66. K.A. Imran, K.N. Shivakumar Graphene-modified carbon/epoxy nanocomposites: Electrical, thermal and mechanical properties. J Compos Mater., 53(1), (2019)93–106. Available at https://doi.org/10.1177/0021998318780468
67. H. Al Mahmud, M.S. Radue, S. Chinkanjanarot, W.A. Pisani, S. Gowtham, G.M. Odegard Multiscale modeling of carbon fiber-graphene nanoplatelet-epoxy hybrid composites using a reactive force field. Compos Part B: Eng., 172, (2019) 628–635. Available at https://doi.org/10.1016/j.compositesb.2019.05.035
68. S. Biswas, B. R. Lokavarapu, Fundamental frequencies of composite rectangular plates with different cut-outs, Materials Today: Proceedings, 2023, ISSN 2214-7853. Available at https://doi.org/10.1016/j.matpr.2023.03.062
69. K. Brethee, Free vibration analysis of a symmetric and anti-symmetric laminated composite plates with a cutout at the center, Al-Qadisiya Journal For Engineering Sciences Vol 2, (2009) 324-334.
70. K. Kalita, P. Dey, S. Haldar, Robust genetically-optimized skew laminates, Proceedings of the Institution of Mechanical Engineers, Part C: Journal of Mechanical Engineering Science, 233(1), (2019) 146-159. Available at https://doi.org/10.1177/09544062187569
71. Y. Kiani, Free vibration of FG-CNT reinforced composite skew plates, Aerosp. Sci. Technol., 58, (2016) 178–188. Available at https://doi.org/10.1016/j.ast.2016.08.018

72. C. Ömer, A. Mehmet, Free vibration and buckling analyses of CNT reinforced laminated non-rectangular plates by discrete singular convolution method, Eng. Comput., 38 (Suppl 1), (2022) S489–S521. Available at https://doi.org/10.1007/s00366-020-01168-8
73. E. García-Macías, R. Castro-Triguero, E. Saavedra Flores, M. Friswell, R. Gallego, Static and free vibration analysis of functionally graded carbon nanotube reinforced skew plates, Compos. Struct., 140, (2016) 473–490. Available at https://doi.org/10.1016/j.compstruct.2015.12.044
74. L.W. Zhang, On the study of the effect of in-plane forces on the frequency parameters of CNT-reinforced composite skew plates, Compos. Struct., 160, (2017) 824–837. Available at https://doi.org/10.1016/j.compstruct.2016.10.116
75. F. Gburi, L. Alansari, M. Kadhom, A. Al-Saffar, Free vibration of skew isotropic plate using ANSYS, J. Mech. Eng. Res. Dev., 43, (2020) 472–486.
76. M. Gürses, Ö. Civalek, A.K. Korkmaz, H. Ersoy, Free vibration analysis of symmetric laminated skew plates by discrete singular convolution technique based on first-order shear deformation theory, Internat. J. Numer. Methods Engrg., 79(3), (2009) 290–313. Available at https://doi.org/10.1002/nme.2553
77. T. Farsadi, D. Asadi, H. Kurtaran, Fundamental frequency optimization of variable stiffness composite skew plates, Acta Mech., 232, (2020) 555–573. Available at https://doi.org/10.1007/s00707-020-02871-9
78. U. Topal, Ü. Uzman, Frequency optimization of laminated skew plates, Mater. Des., 30, (2009) 3180–3185. Available at https://doi.org/10.1016/j.matdes.2008.11.007
79. K. Kalita, Dey P., S. Haldar, X. Gao, Optimizing frequencies of skew composite laminates with metaheuristic algorithms, Eng. Comput. 36 (2020) 741–761. Available at https://doi.org/10.1007/s00366-019-00728-x
80. Y. Kiani, K. Kamil Zur, Free vibrations of graphene platelet reinforced composite skew plates resting on point supports, Thin-Walled Struct. 176 (2022) 109363. Available at https://doi.org/10.1016/j.tws.2022.109363
81. S. S. Ahankari, K. K. Kar, Functionally Graded Composites: Processing and Applications, Composite Materials, (2016) 119–168. Available at https://doi.org/10.1007/978-3-662-49514-8_4
82. M. S. Tayebi, S. J. Salami, M. Tavakolian, Free vibration analysis of functionally graded composite rectangular plates reinforced with graphene

nanoplatelets (GPLs) using full layerwise finite element method, Proceedings of the Institution of Mechanical Engineers, Part C: Journal of Mechanical Engineering Science, 0(0), (2023). Available at https://doi.org/10.1177/09544062231166245

83. S. Zhao, Z. Zhao, Z. Yang, L. Ke, S. Kitipornchai & J. Yang, Functionally graded graphene reinforced composite structures: A review, Engineering Structures, 210, (2020) 110339. Available at https://doi.org/10.1016/j.engstruct.2020.110339
84. K. M. Liew, Z. Pan, and L.-W. Zhang, The recent progress of functionally graded CNT reinforced composites and structures, Sci. China-Phys. Mech. Astron., 63, (2020) 234601. Available at https://doi.org/10.1007/s11433-019-1457-2
85. A. Wang, Y. Pang, W. Zhang & P. Jiang, Nonlinear Dynamic Analysis of Functionally Graded Graphene Reinforced Composite Truncated Conical Shells, International Journal of Bifurcation and Chaos, 29(11), (2019) 1950148. Available at https://doi.org/10.1142/S0218127419501487
86. H. Babaei, Y. Kiani & M.R. Eslami, Vibrational behavior of thermally pre-/post-buckled FG-CNTRC beams on a nonlinear elastic foundation: a two-step perturbation technique, Acta Mechanica, 10, (2021) 3897-3915. Available at https://doi.org/10.1007/s00707-021-03027-z
87. C.H. Thai, A.J.M. Ferreira, T.D. Tran, P. Phung-Van Free vibration, buckling and bending analyses of multilayer functionally graded graphene nanoplatelets reinforced composite plates using the NURBS formulation, Compos. Struct., 220, (2019) 749–759. Available at https://doi.org/10.1016/j.compstruct.2019.03.100
88. H-S. Shen, Y. Xiang, Y. Fan, Vibration of thermally postbuckled FG-GRC laminated plates resting on elastic foundations, Journal of Vibration and Control, 25(9), (2019) 1507-1520. Available at https://doi.org/10.1177/107754631982567
89. A. Shahrjerdi & S. Yavari, Free vibration analysis of functionally graded graphene-reinforced nanocomposite beams with temperature-dependent properties, Journal of the Brazilian Society of Mechanical Sciences and Engineering, 40(1), (2018) 25. Available at https://doi.org/10.1007/s40430-017-0943-1

90. Y. Zhou, Y. Zhang, B.N. Chirukam, J. Li, C. Lu, M. Babaei, K. Asemi, Free Vibration Analyses of Stiffened Functionally Graded Graphene-Reinforced Composite Multilayer Cylindrical Panel, Mathematics, 11, (2023) 3662. Available at https://doi.org/10.3390/math11173662
91. F.A. Fazzolari, Elastic buckling and vibration analysis of FG polymer composite plates embedding graphene nanoplatelet reinforcements in thermal environment, Mechanics of Advanced Materials and Structures, 28(4), (2021) 391-404. Available at https://doi.org/10.1080/15376494.2019.1567886
92. S.W. Yang, Y.X. Hao, W. Zhang, L. Yang, & L.T. LIU, Nonlinear vibration of functionally graded graphene platelet-reinforced composite truncated conical shell using First-order shear deformation theory, Applied Mathematics and Mechanics (English Edition), 42(7), (2021) 981-998. Available at https://doi.org/10.1007/s10483-021-2747-9
93. Y. Wang, K. Xie & T. Fu, Vibration analysis of functionally graded graphene oxide-reinforced composite beams using a new Ritz-solution shape function, J Braz. Soc. Mech. Sci. Eng., 42, (2020) 180. Available at https://doi.org/10.1007/s40430-020-2258-x
94. Y. Zhou, D. Liu, J. Zhu, Vibration and Wave Analyses in the Functionally Graded Graphene-Reinforced Composite Plates Based on the First-Order Shear Deformation Plate Theory, Appl. Sci., 12, (2022) 3140. Available at https://doi.org/10.3390/app12063140 Available at https://doi.org/10.3390/app12063140
95. X. Huang, C. Wang, J. Wang, & N. Wei, Nonlinear Vibration Analysis of Functionally Graded Porous Plates Reinforced by Graphene Platelets on Nonlinear Elastic Foundations, Strojniški Vestnik - Journal of Mechanical Engineering, 68(9), (2022) 571–582. Available at https://doi.org/10.5545/sv-jme.2022.274
96. S. Qaderi, & F. Ebrahimi, Vibration analysis of polymer composite plates reinforced with graphene platelets resting on two-parameter viscoelastic foundation, Engineering with Computers, 38, (2022) 4-6. Available at https://doi.org/10.1007/s00366-020-01066-z
97. Y. Wang, C. Feng, J. Yang, D. Zhou & W. Liu, Static response of functionally graded graphene platelet–reinforced composite plate with dielectric property,

Journal of Intelligent Material Systems and Structures, 31(19), (2020) 2211-2228. Available at https://doi.org/10.1177/1045389X20943955

98. S. Kitipornchai, D. Chen & J. Yang, J. (2017). Free vibration and elastic buckling of functionally graded porous beams reinforced by graphene platelets, Materials & Design, 116, (2017) 656–665. Available at https://doi.org/10.1016/j.matdes.2016.12.061
99. Y. Kiani Isogeometric large amplitude free vibration of graphene reinforced laminated plates in thermal environment using NURBS formulation. Computer Methods Appl. Mech. Eng., 332, (2018) 86–101. Available at https://doi.org/10.1016/j.cma.2017.12.015
100. R. Gholami, R. Ansari Nonlinear harmonically excited vibration of third-order shear deformable functionally graded graphene platelet-reinforced composite rectangular plates, Eng Struct., 156, (2018) 197–209. Available at https://doi.org/10.1016/j.engstruct.2017.11.019
101. Z. Xu, Q. Huang Vibro-acoustic analysis of functionally graded graphene-reinforced nanocomposite laminated plates under thermal-mechanical loads, Eng Struct, 186, (2019) 345–355. Available at https://doi.org/10.1016/j.engstruct.2019.01.137
102. F.A. Fazzolari, Elastic buckling and vibration analysis of FG polymer composite plates embedding graphene nanoplatelet reinforcements in thermal environment, Mechanics of Advanced Materials and Structures, 28, (2019) 391-404. Available at https://doi.org/10.1080/15376494.2019.1567886
103. M. S. Koppanati, M. Naga Rani, K. Krishna Bhaskar, Free Vibration Analysis of Graphene Reinforced Laminated Composite Plates using Experimental Modal Testing, Mechanics of Advanced Composite Structures, 10, (2023), 363-374. doi: 10.22075/macs.2023.28869.1448

Chapter 3: Methodology

In Section 3.1 the proposed finite element analysis model is presented to accurately determine the free vibration of laminated composite plates. The effective material properties of the laminate for uniformly distributed and functionally graded reinforcement patterns are found using the micromechanics equations presented in Section 3.2. Section 3.3 illustrates the optimization scheme applied to the rectangular and skew composite plate.

3.1 Theoretical formulation using finite element analysis for the composite laminate and vibration response

For rectangular plates, Figure 3.1 shows the geometry profile implemented in the vibration analysis where a represents the length, b the width and h the thickness of the composite. The composite plates are formed by a combination of N number of layers with uniform thickness with θ_k representing the angle of the fibres in relation to the x-axis. The orientation of the plate is chosen so that the z-axis, which defines the direction of the plate thickness, is perpendicular to the midplane and the xy-plane is set to intersect the midplane. The k[th] layer is situated between $z = z_k$ and $z = z_{k-1}$ in the thickness direction. The composite is 3-phase due to graphene reinforcement dispersed in the matrix of the composite and fibre reinforcement introduced as traditional reinforcement. Each layer of the composite consists of the graphene/fibre reinforcement.

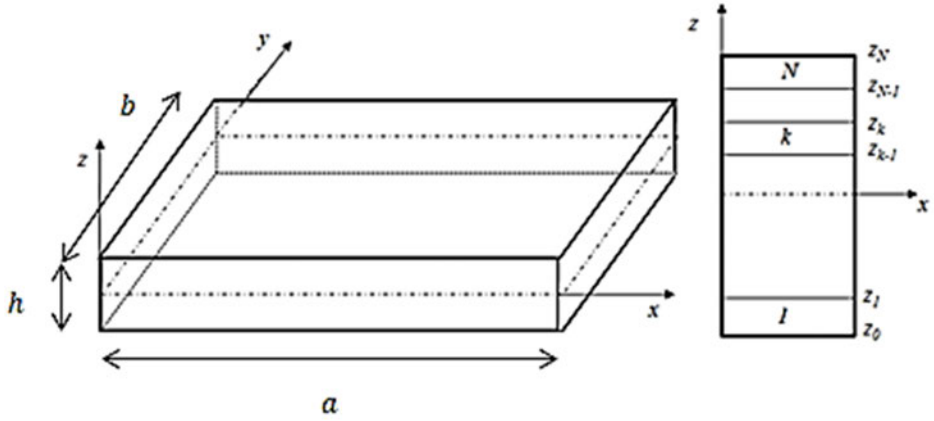

Figure 3.1: Laminated plate geometry [1]

3.1.1 Definition of Skew Plate Geometry

The geometry of the skew plate defined in the analysis is illustrated in Figure 3.2 where a, b, and D represent the plate's length, width, and thickness, respectively. The cantilever support condition is defined by implementing a clamped boundary condition on one edge of the plate with a length equal to b (Figure 3.2). The boundary conditions for the final three edges are free. The laminate is made up of N layers, with θ_k denoting the angle between the principal material direction and the coordinate x of the k^{th} lamina. As seen in Figure 3.2, the laminate is defined so that the mid-plane coincides with the xy plane with α representing the skew angle of the laminate with respect to the y axis. In the thickness direction, the coordinates of the bottom and top of the k^{th} layer are written as $z = z_k$ and $z = z_{k+1}$, respectively. Isoparametric elements, which are able to simulate arbitrary geometries, are applied due to the global axes and element edges not being parallel as seen in Figure 3.3. Then, four-noded isoparametric quadrilateral elements with each node having five degrees of freedom are used to represent the skew plate. The geometry of the plate has been selected for rectangular and skew plate arrangements which have been used extensively in different civil and aerospace engineering applications.

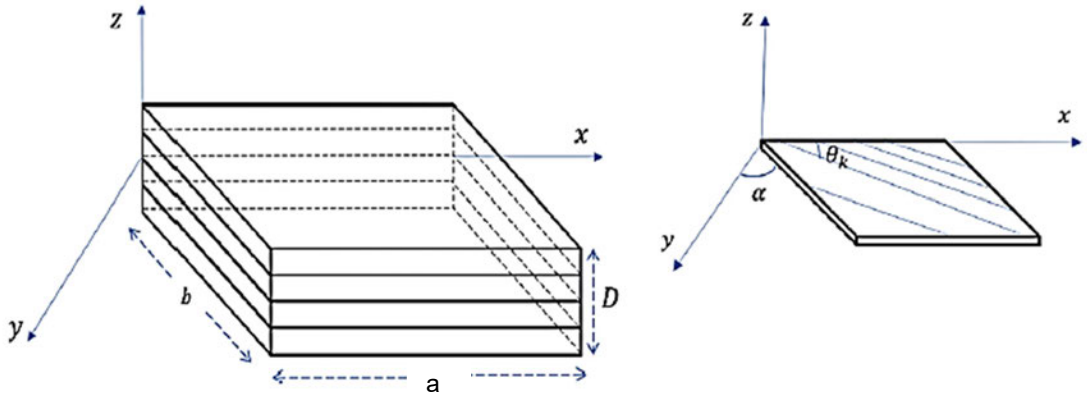

Figure 3.2: Laminated skew plate geometry [1]

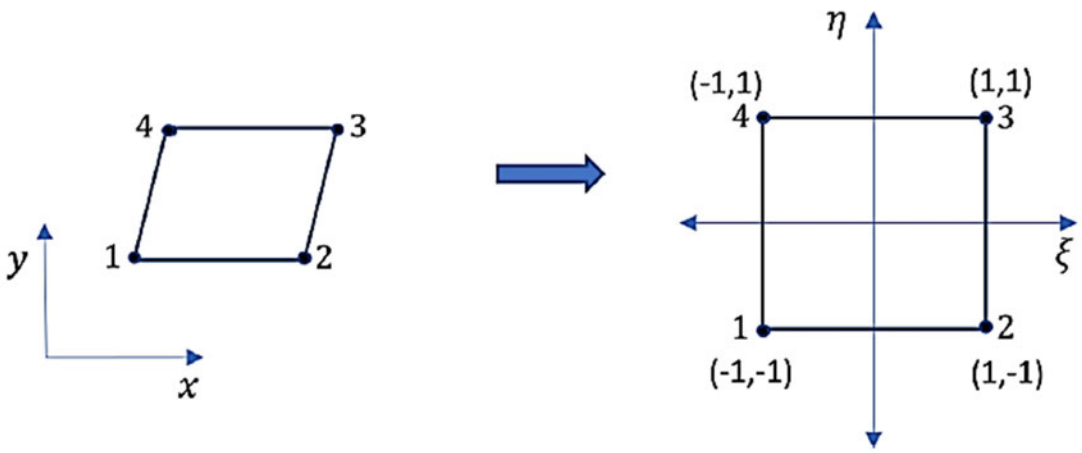

Figure 3.3: Transformation of Global Cartesian coordinates to Local Natural coordinates

3.1.2 Stresses, strains and mechanical displacement theory

To accurately ascertain the displacements of any point on the plate, the composite laminate was analysed using the first order shear deformation theory (FSDT). The following equations set the displacement field for the basis of the FSDT [1]:

$$u_1(x, y, z, t) = u(x, y, t) + z\varphi_x(x, y, t), \quad (1a)$$

$$u_2(x, y, z, t) = v(x, y, t) + z\varphi_y(x, y, t), \quad (1b)$$

$$u_3(x, y, z, t) = w(x, y, t) \quad (1c)$$

The theory is defined by the displacements (u_1, u_2, u_3) along the (x, y, z) coordinates and at any point of the plate. The constituent variables required to produce the displacement data are:

- (u, v, w) – point displacement relative to the x, y and z-axis on the laminate's mid-plane; and
- φ_x and φ_y represent the normal rotations of a point located on the midplane of the laminate about the x and y-axes, respectively.

A linear elastic strain-displacement relation is applied on the basis of the plate not being subject to plastic behaviour such as damage, large or permanent deformation. The following linear elastic strain-displacement relations are used in conjunction with the bending strain (ε_b) and the shear strain (ε_s):

$$\{\varepsilon_b\} = \{\varepsilon_{0b}\} + z\{\kappa\}, \qquad \{\varepsilon_s\} = \{\varepsilon_{0s}\} \tag{2}$$

These equations can further be defined as:

$$\{\varepsilon_b\} = \left\{\varepsilon_{xx}, \varepsilon_{yy}, \gamma_{xy}\right\}^T, \{\varepsilon_s\} = \{\gamma_{yz}, \gamma_{xz}\}^T, \quad \{\varepsilon_{0b}\} = \left\{\frac{\partial_u}{\partial_x}, \frac{\partial_v}{\partial_y}, \frac{\partial_u}{\partial_y} + \frac{\partial_v}{\partial_x}\right\}^T \tag{3a}$$

$$\{\kappa\} = \left\{-\frac{\partial \varphi_x}{\partial x}, -\frac{\partial \varphi_y}{\partial y}, -\left(\frac{\partial \varphi_x}{\partial y} + \frac{\partial \varphi_y}{\partial x}\right)\right\}^T, \quad \{\varepsilon_{0s}\} = \left\{\frac{\partial w}{\partial y} - \varphi_y, \frac{\partial w}{\partial x} - \varphi_x\right\}^T \tag{3b}$$

3.1.3 Equations to define the composite lamina

The following formulas provide the k[th] lamina in-plane stress state for a composite plate made of an orthotropic material with elastic symmetry parallel to the x-y plane:

$$\{\sigma\}_k = [Q]_k\{\varepsilon\} \tag{4}$$

Eq. (4) is defined by:

- $\{\sigma\}$ - the stress tensor;
- $[Q]$ - the *plane-stress reduced elastic stiffness* matrix; and
- $\{\varepsilon\}$ - the strain tensor.

The equation can then be expressed in terms of the bending $\{\sigma_b\}$ and shear $\{\sigma_s\}$ related variables:

$$\{\sigma_b\} = [Q_b]\{\varepsilon_b\}, \quad \{\sigma_s\} = [Q_s]\{\varepsilon_s\} \tag{5}$$

Where $\{\sigma_b\} = \{\sigma_1, \sigma_2, \sigma_6\}^T$, $\{\sigma_s\} = \{\sigma_4, \sigma_5\}^T$ and

$$[Q_b]_k = \begin{bmatrix} {Q_{11}}^{(k)} & {Q_{12}}^{(k)} & {Q_{16}}^{(k)} \\ {Q_{21}}^{(k)} & {Q_{22}}^{(k)} & {Q_{26}}^{(k)} \\ {Q_{61}}^{(k)} & {Q_{62}}^{(k)} & {Q_{66}}^{(k)} \end{bmatrix} \qquad [Q_s]_k = \begin{bmatrix} {Q_{44}}^{(k)} & {Q_{45}}^{(k)} \\ {Q_{54}}^{(k)} & {Q_{55}}^{(k)} \end{bmatrix} \tag{6}$$

Due to symmetry: $Q_{61}{}^{(k)} = Q_{16}{}^{(k)} = 0$, $Q_{12}{}^{(k)} = Q_{21}{}^{(k)}$, $Q_{26}{}^{(k)} = Q_{62}{}^{(k)} = 0$ and $Q_{54}{}^{(k)} = Q_{45}{}^{(k)} = 0$

The plane stress reduced stiffnesses of the kth lamina, $Q_{ij}^{(k)}$, in its material coordinate system (x_1, x_2, x_3), used to form Eq. (6) is given by [21].

$$Q_{11}{}^{(k)} = \frac{E_1{}^{(k)}}{(1-v_{12}{}^{(k)}v_{21}{}^{(k)})},\ Q_{12}{}^{(k)} = \frac{v_{12}{}^{(k)}E_2{}^{(k)}}{(1-v_{12}{}^{(k)}v_{21}{}^{(k)})},\ Q_{22}{}^{(k)} = \frac{E_2{}^{(k)}}{(1-v_{12}{}^{(k)}v_{21}{}^{(k)})}, \quad (7)$$

$$Q_{66}{}^{(k)} = G_{12}{}^{(k)}, \qquad Q_{44}{}^{(k)} = G_{23}{}^{(k)}, \qquad Q_{55}{}^{(k)} = G_{13}{}^{(k)}$$

The k^{th} layer properties are defined by:

- $E_1^{(k)}$ and $E_2^{(k)}$ representing the effective longitudinal and transverse moduli of elasticity;
- $v_{12}^{(k)}$ and $v_{21}^{(k)}$ representing the effective Poisson's ratios; and
- $G_{12}^{(k)}$, $G_{23}^{(k)}$ and $G_{13}^{(k)}$ are the effective shear moduli of the k^{th} layer.

Eq. (8) is produced when the reduced stiffness $Q_{ij}^{(k)}$ of the k^{th} lamina is transformed to $\overline{Q}_{ij}^{(k)}$ in the coordinate system (x, y, z):

$$[\overline{Q}]_{(k)} = ([T]^T[Q][T])_{(k)} \quad (8)$$

where $[T]$ represents a transformation matrix with $\theta(k)$ defined as the fibre angle of the k^{th} lamina [1].

3.1.4 Modelling the composite laminate with Finite Element theory

To illustrate the composite's structural response, a four-noded isoparametric quadrilateral Lagrangian element with five degrees of freedom (DoF) is used to model the laminated plate [1].

Eq (9) represents the generalized displacement vector:

$$\{\overline{u}(x, y, t)\} \equiv \{u, v, w, \varphi_x, \varphi_y\}^T = [N_u]\{d\}_e = \sum_{j=1}^{4}\left(N_j[I]_{5x5}\{d_j\}_e\right) \quad (9)$$

$\{d_j\}_e = \{u_j, v_j, w_j, \varphi_{xj}, \varphi_{yj}\}^T$ and the shape function, N_j, correspond to the j^{th} node of the element.

Eq. (10) is formed when Eq. (9) is substituted into Eq. (2)

$$\{\bar{\varepsilon}(x,y,t)\} = [B]\{d\}_e = \sum_{j=1}^{4}\left([B_j]\{d_j\}_e\right) \tag{10}$$

or equivalently

$$\{\bar{\varepsilon}\} = \begin{Bmatrix}\{\varepsilon_{b0}\}\\ \{\kappa\}\\ \{\varepsilon_{s0}\}\end{Bmatrix} = \begin{bmatrix}[B_b]\\ [B_k]\\ [B_s]\end{bmatrix}\{d\}_e = \sum_{j=1}^{4}\left(\begin{bmatrix}[B_b]_j\\ [B_k]_j\\ [B_s]_j\end{bmatrix}\{d_j\}_e\right) \tag{11}$$

where

$$[B_b]_j = \begin{bmatrix}\partial_x & 0 & 0 & 0 & 0\\ 0 & \partial_y & 0 & 0 & 0\\ \partial_y & \partial_x & 0 & 0 & 0\end{bmatrix}N_j, \quad [B_k]_j = \begin{bmatrix}0 & 0 & 0 & -\partial_x & 0\\ 0 & 0 & 0 & 0 & -\partial_y\\ 0 & 0 & 0 & -\partial_y & -\partial_x\end{bmatrix}N_j, \quad [B_s]_j = \begin{bmatrix}0 & 0 & \partial_x & -1 & 0\\ 0 & 0 & \partial_y & 0 & -1\end{bmatrix}N_j$$

and

$\partial_x = \partial/\partial x$, $\partial_y = \partial/\partial y$.

3.1.5 Calculation of the strain energy

The energy stored in a body due to its deformation is called the strain energy. The strain energy of the graphene-reinforced composite plate element is:

$$U = \frac{1}{2}\int_{V_e}\left(\{\varepsilon_{b0}\}^T[\overline{Q_b}]\{\varepsilon_{b0}\} + \{\varepsilon_{b0}\}^T z[\overline{Q_b}\{k\} + \{k\}^T z[\overline{Q_b}]\{\varepsilon_{b0}\} + \{k\}^T z^2[\overline{Q_b}]\{k\} + \{\varepsilon_{s0}\}^T[\overline{Q_s}]\{\varepsilon_{s0}\}\right)dV$$

$$= \frac{1}{2}\int_V \begin{Bmatrix}\{\varepsilon_{b0}\}\\ \{k\}\\ \{\varepsilon_{s0}\}\end{Bmatrix}^T \begin{bmatrix}[\overline{Q_b}] & z[\overline{Q_b}] & 0\\ z[\overline{Q_b}] & z^2[\overline{Q_b}] & 0\\ 0 & 0 & [\overline{Q_s}]\end{bmatrix}\begin{Bmatrix}\{\varepsilon_{b0}\}\\ \{k\}\\ \{\varepsilon_{s0}\}\end{Bmatrix}dV = \frac{1}{2}\int_V\{\bar{\varepsilon}\}^T[D(z)]\{\bar{\varepsilon}\}dV \tag{12}$$

where the element volume is represented by V. *U* can be written in terms of $\{\varepsilon_{b0}\}$, $\{\kappa\}$ and $\{\varepsilon_{s0}\}$ by substituting them into the above equation:

$$U = \frac{1}{2}\{d\}_e{}^T[K]_e\{d\}_e \tag{13}$$

where

$$[K]_e = \sum_{k=1}^{N} \left[\int_{V_k} [B\}^T [D(z)]_k [B] dV_k \right] \quad (14)$$

V_k and N represent the volume of the k^{th} layer and the number of lamina respectively.

3.1.6 Derivation of the Kinetic energy equation

To determine the kinetic energy of the graphene-reinforced composite plate the following equation is applied:

$$T = \frac{1}{2} \sum_{k=1}^{N} \left(\int_{V_k} \rho_k \left[\{\dot{u_1}\}^2 + \{\dot{u_2}\}^2 + \{\dot{u_3}\}^2 \right] dV_k \right), \quad (15)$$

Eq. (15) is a function of the density of the k^{th} layer (ρ_k). Eq. (1a-c) can be substituted into the kinetic energy equation, to represent the equation as a function of the element displacements:

$$T = \frac{1}{2} \sum_{k=1}^{N} \left(\int_{V_k} \rho_k \left[\dot{u}^2 + 2z\dot{u}\dot{\varphi}_x \dot{+} \dot{v}^2 + 2z\dot{v}\dot{\varphi}_y + \dot{w}^2 + z^2\dot{\varphi}^2 + z^2\dot{\varphi}_y^2 \right] dV_k \right)$$

$$= \frac{1}{2} \sum_{k=1}^{N} \int_{V_k} \begin{Bmatrix} u \\ v \\ w \\ \varphi_x \\ \varphi_y \end{Bmatrix}^T \rho_k \begin{bmatrix} 1 & 0 & 0 & -z & 0 \\ 0 & 1 & 0 & 0 & -z \\ 0 & 0 & 1 & 0 & 0 \\ -z & 0 & 0 & z^2 & 0 \\ 0 & -z & 0 & 0 & z^2 \end{bmatrix} \begin{Bmatrix} u \\ v \\ w \\ \varphi_x \\ \varphi_y \end{Bmatrix} dV_k = \sum_{k=1}^{N} \frac{1}{2} \int_{V_k} \left\{ \ddot{\bar{u}} \right\}^T [I(z)]_k \{\ddot{\bar{u}}\} dV_k \quad (16)$$

Substituting Eq. (9), the generalized displacement vector, in the above relation gives the equation:

$$T = \frac{1}{2} \{\dot{d}\}^T [M] \{\dot{d}\} \quad (17)$$

where

$$[M]_e = \int_{A_e} \sum_{k=1}^{N} \int_{z_{k-1}}^{z_k} [N]^T [I(z)]_k [N] dz dA \quad (18)$$

In Eq. (18), A_e represents the area of the element and the top and bottom surface of the k^{th} layer are represented by z-coordinates, z_{k-1} and z_k.

3.1.7 Calculation of mechanical force induced work done

The mechanical force induced work done is calculated using Eq. (19):

$$W = \{\overline{u}\}^T\{f_c\} + \int_{S_1} \{\overline{u}\}^T\{f_s^{(i)}\}dS + \int_V \{\overline{u}\}^T\{f_v\}dV$$

$$= \{d\}_e{}^T[N]^T\{f_c\} + \{d\}_e{}^T \int_{S_1}[N]^T\{f_s^{(i)}\}dS + \{d\}_e{}^T \int_V[N]^T\{f_v\}dV \equiv \{d\}_e{}^T\{F_m\}_e \quad (19)$$

In Eq. (19), $\{f_c\}$ represents the concentrated force vector, $\{f_s\}$ represents the surface force vector and $\{f_v\}$ represents the volume force vector. The mechanical forces are applied to the surface area, S_1 and the symbol $\{F_m\}_e$ represents the applied element mechanical forces.

3.1.8 Governing equation of the eigenvalue problem

Hamilton's principle is used to describe the governing equation for the graphene-reinforced composite with mechanical loading in Eq. (20):

$$\int_0^T(\delta T - \delta U + \delta W)\,dt = 0 \quad (20)$$

To express the global form of the final governing equation, values for *U*, *T* and *W* are substituted into Eq. (20). The expression for the global form is then:

$$[M]\{\ddot{d}\} + [K]\{d\} = \{F_m\} \quad (21)$$

where the global mass matrix, global linear stiffness matrix , global displacement matrix, and force vector are, respectively, [M], {d}, [K] and $\{F_m\}$.

The free vibration of the composite laminate can be analysed by removing the force term from Eq. (21):

$$[K]\{d\} = \lambda[M]\{d\} \quad (22)$$

for which $\lambda = \omega^2$, and ω representing the natural frequency vibration.

3.2. Application of micromechanics equations to define effective material properties

In the thesis the natural vibration is studied for a 3-phase graphene/fibre reinforced nanocomposite laminate. The nanocomposite is made up of constituent materials such as, a polymer matrix which could be resins including polyesters, vinyl esters, epoxies etc., glass or carbon fibre reinforcement and graphene nanoparticle reinforcement.

Modelling equations, which have been used in numerous published research articles, are applied to first form the effective material properties of the graphene-reinforced polymer matrix combining the material properties of the constituent graphene reinforcement and polymer matrix. The resultant material is the graphene-reinforced polymer matrix. The graphene-reinforced polymer matrix (now a 2-phase material) is then combined with glass or carbon fibre reinforcement via the ~~same~~ micromechanical modelling equations to form a 3-phase graphene/fibre reinforced nanocomposite with effective material properties derived from the properties of the fibre reinforcement and the 2-phase graphene-reinforced polymer matrix.

3.2.1 Properties of the graphene-reinforced matrix

In order to calculate the effective Shear Modulus, Poisson's ratio and Young's Modulus of the graphene-reinforced matrix micromechanical equations located in [2, 3, 4, 5] are applied. The subscripts M, GM and GPL appearing in the following equations are used to represent the Matrix, graphene-reinforced matrix and graphene nanoplatelets. Eq. (23) is used to calculate the effective Young's Modulus of the graphene-reinforced matrix and V_{GPL} is used to denote the volume content of graphene platelets:

$$E_{GM} = \left(\frac{3}{8}\frac{1+\xi_L \eta_L V_{GPL}}{1-\eta_L V_{GPL}} + \frac{5}{8}\frac{1+\xi_w \eta_w V_{GPL}}{1-\eta_w V_{GPL}}\right) \times \mathrm{E_M} \tag{23}$$

By using the dimensions of the graphene platelets in terms of width (w_{GPL}), length (l_{GPL}) and thickness (h_{GPL}), the parameters ξ_L and ξ_w can be derived from Eq. (24).

$$\xi_{\mathrm{L}} = 2\frac{l_{GPL}}{h_{GPL}}, \quad \xi_w = 2\frac{w_{GPL}}{h_{GPL}} \tag{24}$$

(E_M) and (E_{GPL}) represent the Young's moduli for the matrix and graphene nanoplatelets (GPLs) respectively and can be used to determine values for the symbols η_L and η_w used in Eq. (23).

$$\eta_L = \frac{(E_{GPL}/E_M)-1}{(E_{GPL}/E_M)+\xi_{\mathrm{L}}}, \qquad \eta_w = \frac{(E_{GPL}/E_M)-1}{(E_{GPL}/E_M)+\xi_w} \tag{25}$$

The volume content of graphene nanoplatelets (V_{GPL}) can be represented by the weight fraction (W_{GPL}) in Eq.(26):

$$V_{GPL} = \frac{W_{GPL}}{W_{GPL}+(\rho_{GPL}/\rho_M)(1-W_{GPL})} \tag{26}$$

In Eq. (26) the mass density of the polymer matrix is represented by ρ_M and the graphene nanoplatelet's mass density is represented by ρ_{GPL}. Properties of the graphene-reinforced matrix are calculated in Eq. (27 to 29).

$$v_{GM} = v_{GPL}V_{GPL} + v_M(1 - V_{GPL}) \tag{27}$$

$$G_{GM} = \frac{E_{GM}}{2(1+v_{GM})} \tag{28}$$

$$\rho_{GM} = \rho_{GPL}V_{GPL} + \rho_M(1 - V_{GPL}) \tag{29}$$

The Poisson's ratio, Shear modulus and density are defined by Eq. 27, Eq. 28 and Eq. 29 respectively.

3.2.2 Considering fibre reinforcement in the graphene/polymer matrix

The composite is further reinforced with traditional fibre reinforcement to improve its overall properties and strength. The fibres used induce directional stiffness and strength due to their unidirectional and continuous nature. The rule of mixtures can be applied in this case to determine the effective material properties of the composite due to the constituent materials used to reinforce the structure assumed to have uniform characteristics, equal fibre/particle size, fibres being parallel and continuous and reinforcement materials being perfectly bonded to the matrix [6]. Multiple studies

undertaken have successfully utilized the rule of mixtures in a similar/identical context [7,8,9,10].The micromechanical relations given in [11] are applied to determine the effective properties of the 3-phase graphene/fibre reinforced nanocomposite below where the Young's moduli, shear modulus, Poisson's ratio and composite density are given by:

$$E_{11} = E_{F1}\ V_F + E_{GM}(1 - V_F) \tag{30}$$

$$E_{22} = E_{GM}\ \left(\frac{E_{F22}+E_{GM}+(E_{F22}-E_{GM})V_F}{E_{F2}\ +E_{GM}-(E_{F22}-E_{GM})V_F}\right) \tag{31}$$

$$G_{12} = G_{GM}\ \left(\frac{G_{F12}+G_{GM}+(G_{F1}\ -G_{GM})V_F}{G_{F1}\ +G_{GM}-(G_{F12}-G_{GM})V_F}\right) \tag{32}$$

$$v_{12} = v_{F12}V_F + v_{GM}(1 - V_F) \tag{33}$$

$$\rho = \rho_F V_F + \ \rho_{GM}(1 - V_F) \tag{34}$$

In Eq. (30 to 34) the subscript GM is used to represent the graphene-reinforced matrix and F represents the fibres. In addition, V_F and ρ_F represent the fibre volume content and density respectively.

3.2.3 Properties of functionally graded materials

Functionally graded material applications were analysed in this thesis where the volume content of fibres and graphene nanoplatelets, $V_{GPL}$and V_F respectively, are selected as the parameters to be investigated. A functionally graded distribution of graphene and fibres are assumed within each layer of the laminate and through the thickness of each ply. The total graphene and fibre content (V_{GPL} and V_F) are given as:

$$V_F^{(k)} = V_F^* f^{(k)}(\bar{z}), \qquad V_{GPL}^{(k)} = V_{GPL}^* f^{(k)}(\bar{z}) \tag{35}$$

In Eq. (35), V_F^* and V_{GPL}^* represent the total volume of fibre and GPLs respectively, the component function $f^{(k)}(\bar{z})$ allocates the type of functionally graded distribution pattern applied to the graphene and fibre reinforcement and is defined by:

$$f^{(k)}(z) = \begin{cases} 1, & UD - Uniform \\ 1 + \bar{z}, & FG - \text{Type 'V'} \\ 2(1 - \bar{z}), & FG - \text{Type 'O'} \\ 2\bar{z}, & FG - \text{Type 'X'} \\ 1 - \bar{z}, & FG - \text{Type 'A'} \end{cases} \quad (36)$$

The graphene and fibre reinforcement can be applied separately in each ply resulting in layer-wise distributions therefore local coordinate systems can be set up for each ply with the mid-plane of the corresponding layer coinciding with the origin. The orthogonal component of the local system, $\bar{z}$, of the k^{th} layer is defined as:

$$\bar{z} = \frac{2z - (z_{k+1} + z_k)}{z_{k+1} - z_k} \quad (37)$$

Due to Eq. (36), the material properties $\bar{Q}_{ij}^{(k)}$ are functions of the transverse coordinates, z. The 'integral' function embedded in MATLAB has been utilized to calculate the integrals with respect to z.

3.3. Definition of the optimization framework of the composite for maximum fundamental frequency output

In order to avoid resonance, the laminate's fundamental frequency is maximized during the analysis and design of the composite plate. To achieve this an optimization framework is proposed for the composite in reference to a number of design variables including graphene weight, fibre content and stacking sequence, thickness, aspect ratio, fibre angle and boundary condition. Eq. (38) defines the optimization scheme used:

$$\max Natural\ Frequency\ f(V_F, W_{GPL}, \theta) = \Omega \quad (38a)$$

$$subject\ to\ \sum_{k=1}^{n} W_{GPL} = b \quad (38b)$$

$$c_1 \leq W_{GPL} \leq c_2 \quad (38c)$$

$$d_1 \leq V_F \leq d_2 \quad (38d)$$

$$-90^o \leq Fibre\ angle\ \theta \leq 90^o \quad (38e)$$

$$\sum_{k=1}^{n} \frac{h_k}{D} = 1 \quad (38f)$$

Eq. (38b) gives a predefined value to the total weight of the laminate, which is calculated by summing the weight of graphene (W_{GPL}) in each layer for (n) number of layers. The upper and lower bounds of the graphene weight and fibre content are specified in Eq. (38c) and (38d). Eq. (38e) describes the maximum and minimum limitations for the fibre angle and Eq. (38f) is used when the thickness of each layer becomes non-uniform. Eq. (38f) is defined as the thickness ratio of the laminate which can be further explained as the thickness of each layer divided by the laminates total thickness. The optimization problem is solved using the Sequential Quadratic Programming Algorithm (SQP). The method generates a step by step procedure for non-linearly constrained optimization by solving quadratic sub-problems [12]. Each major iteration takes into account an approximation of the Hessian of the Lagrangian function through the use of a quasi-Newton updating method. A quadratic programming sub problem is then created and solves to determine the direction of the search. Below is a brief presentation of the scheme's details.

[12] illustrates the optimization problem with non-linear equality and inequality constraints:

$$\begin{gathered} \min f(x) \\ subject\ to\ c_i(x) = 0, i \in E \\ c_i(x) \geq 0, i \in I \end{gathered} \tag{39}$$

The problem is then linearized into:

$$\begin{gathered} \min_p f_k + \nabla f_k^T p + \frac{1}{2} p^T \nabla_{xx}^2 L_k p \\ subject\ to\ \nabla c_i(x_k)^T p + c_i(x_k) = 0, i \in E \\ \nabla c_i(x_k)^T p + c_i(x_k) \geq 0, i \in I \end{gathered} \tag{40}$$

MATLAB is used to solve the given problem via optimization [13, 14]. Typically, the MATLAB algorithms previously referred to are used for minimization analysis, therefore, the following modification is applied to Eq. (38): $\min Natural\ Frequency\ f(V_F, W_{GPL}, \theta) = -\Omega$ for analysis in this research. The minimization function utilized is a MATLAB algorithm that is modified to produce the

optimized fundamental frequency under various conditions. SQP optimization is used via the MATLAB function, called fmincon. In the central Matlab code this function is used, and the developed finite element analysis code calculating the natural frequencies for the composite laminate is called as a Matlab subroutine by this SQP function.

3.4 References

1. J.N. Reddy, Mechanics of Laminated Composite Plates and Shells, 2nd ed. CRC Press, 2004. Available at https://doi.org/10.1201/b12409
2. Y. Huang,Z. Yang,A. Liu & J. Fu, Nonlinear Buckling Analysis of Functionally Graded Graphene Reinforced Composite Shallow Arches with Elastic Rotational Constraints under Uniform Radial Load, Materials, 11(6), (2018) 910. Available at https://doi.org/10.3390/ma11060910
3. M. Song, J. Yang, S. Kitipornchai & W. Zhu, Buckling and postbuckling of biaxially compressed functionally graded multilayer graphene nanoplatelet-reinforced polymer composite plates, International Journal of Mec https://doi.org/10.1016/j.ijmecsci.2017.07.017 hanical Sciences, 131-132, (2017) 345–355. Available at
4. Y. Wang, C. Feng, Z. Zhao, J. Yang, Eigenvalue buckling of functionally graded cylindrical shells reinforced with graphene platelets (gpl), Composite Structures, 202, (2018) 38-46. Available at https://doi.org/10.1016/j.compstruct.2017.10.005
5. Y. Wang, C. Feng, Z. Zhao & J. Yang, Buckling of Graphene Platelet Reinforced Composite Cylindrical Shell with Cutout, International Journal of Structural Stability and Dynamics, 18(03), (2018) 1850040:1-17. Available at https://doi.org/10.1142/S0219455418500402
6. G. Yerbolat, S. Amangeldi, M. Ali, N. Badanova, A. Ashirbeok & G. Islam, Composite Materials Property Determination by Rule of Mixture and Monte Carlo Simulation, 2018 IEEE International Conference on Advanced Manufacturing (ICAM), (2018). DOI: 10.1109/AMCON.2018.8615034
7. Y. Huang, Z. Yang, A. Liu, J. Fu, Nonlinear buckling analysis of functionally graded graphene reinforced composite shallow arches with elastic rotational constraints under uniform radial load, Materials, 11 (6), (2018) 910. Available at https://doi.org/10.3390/ma11060910
8. J. Yang, H. Wu, S. Kitipornchai, Buckling and post-buckling of functionally graded multilayer graphene platelet-reinforced composite beams, Composite Structures, 161, (2017) 111–118. Available at https://doi.org/10.1016/j.compstruct.2016.11.048

9. Y. Huang, Z. Yang, A. Liu, J. Fu, Nonlinear buckling analysis of functionally graded graphene reinforced composite shallow arches with elastic rotational constraints under uniform radial load, Materials 11 (6) (2018) 910. Available at https://doi.org/10.3390/ma11060910
10. J. Yang, H. Wu, S. Kitipornchai, Buckling and post-buckling of functionally graded multilayer graphene platelet-reinforced composite beams, Compos. Struct. 161 (2017) 111–118. Available at https://doi.org/10.1016/j.compstruct.2016.11.048
11. T. Vo-Duy, V. Ho-Huu, T. D. Do-Thi, H. Dang-Trung & T. Nguyen-Thoi, A global numerical approach for lightweight design optimization of laminated composite plates subjected to frequency constraints, Composite Structures, 159, (2017) 646–655. Available at https://doi.org/10.1016/j.compstruct.2016.09.059
12. Numerical Optimization. (2006). Springer Series in Operations Research and Financial Engineering.
13. MATLAB. (2016). version 9.0.0.341360 (R2016a). Natick, Massachusetts: The MathWorks Inc.
14. P. E. Gill, W. Murray, and M.H. Wright, Numerical Linear Algebra and Optimization, Vol. 1, Addison Wesley, 1991.

Chapter 4: Optimization and analysis of frequencies of multi-scale graphene/fibre reinforced nanocomposite laminates with non-uniform distributions of reinforcements

Engineering Structures xxx (xxxx) xxx

Contents lists available at ScienceDirect

Engineering Structures

journal homepage: www.elsevier.com/locate/engstruct

Optimization and analysis of frequencies of multi-scale graphene/fibre reinforced nanocomposite laminates with non-uniform distributions of reinforcements

Y. Jeawon [a], G.A. Drosopoulos [a,*,1], G. Foutsitzi [b], G.E. Stavroulakis [c], S. Adali [d]

[a] Discipline of Civil Engineering, University of KwaZulu-Natal, Durban, South Africa
[b] Department of Informatics and Telecommunications, University of Ioannina, Ioannina, Greece
[c] School of Production Engineering and Management, Technical University of Crete, Chania, Greece
[d] Discipline of Mechanical Engineering, University of KwaZulu-Natal, Durban, South Africa

ARTICLE INFO

Keywords:
Optimal design
Nano-structures
Graphene reinforcement
Vibration
Finite element analysis (FEA)
Laminated nanocomposite

ABSTRACT

Optimal design and analysis of three-phase graphene/fibre reinforced laminated nanocomposite plates with respect to maximizing the fundamental frequency is the subject of the present study. Optimal design solutions are given for four different sets of design parameters. First design problem determines the optimal graphene contents of individual layers, the second one both graphene and fibre contents, the third optimizes the graphene and fibre contents as well as the layer thicknesses of individual layers, and the fourth problem optimizes the graphene and fibre contents, layer thicknesses and fibre orientations. Purpose of this approach is to assess and compare different levels of optimization by means of a design efficiency index and as such to determine the effectiveness of different design parameters in maximizing the fundamental frequency. Optimization is implemented using a Sequential Quadratic Programming algorithm and the mechanical properties of graphene/fibre nanocomposite are determined via micromechanical relations. Vibration analysis is conducted by the finite element method using four-noded Mindlin plate elements. Results are obtained for simply supported (SSSS), clamped (CCCC) and simply supported-clamped boundary conditions for opposite edges (SCSC). It is observed that non-uniform distributions of graphene and fibre as well as fibre orientations are quite effective in improving the design efficiency.

1. Introduction

Nanocomposite laminates are used widely in several sectors of civil, mechanical and aerospace engineering. The concept of the enhancement of traditional composite structures by utilizing advanced materials with superior mechanical properties has gained wider acceptance, implementation and applications in the last few years as noted in a number of publications [1-3]. Recent research efforts have highlighted the idea of incorporating nano-scale reinforcements, such as carbon nanotubes (CNTs) or graphene nanoplatelets (GPLs), to improve the mechanical and physical properties of polymer composites further. The specific interest in the present study is the use of GPLs as reinforcement due to their superior properties as noted in [4,5]. Several issues concerning the reinforcement of composites by GPLs have been investigated in [6].

An important tool in the design of composite components is design optimization in order to improve their performance facilitated by the availability of several design parameters [7]. The most common way of optimizing a composite laminate is by determining the fibre orientations optimally in order to maximize (or minimize) a specific design objective. An important aspect of a design is to keep the weight of the component as low as possible. This can be achieved by placing the reinforcements mostly in the outer layers and a smaller portion of the reinforcements in the middle layers. This approach is based on the fact that reinforcements closer to the surface layers contribute more to the laminate stiffness [8]. Non-uniform fibre distribution has been implemented as a design tool in a number of studies in order to improve the design efficiency and reduce

* Corresponding author at: Structural Engineering and Computational Mechanics Group, Discipline of Civil Engineering, University of Kwazulu-Natal, Howard College, Durban, South Africa.
E-mail address: DrosopoulosG@ukzn.ac.za (G.A. Drosopoulos).
URL: http://secm.ukzn.ac.za/ (G.A. Drosopoulos).
[1] Present address: Discipline of Civil Engineering, School of Engineering, UCLan, Preston, UK.

https://doi.org/10.1016/j.engstruct.2020.111525
Received 8 May 2020; Received in revised form 25 July 2020; Accepted 1 November 2020

the weight [9-11]. In this case fibre volume fractions of layers become design parameters. In the present study the design parameters to maximize the fundamental frequencies include the volume fractions of graphene platelet and fibres in each layer, ply thicknesses and fibre orientations. In order to assess the effect of different design parameters on the design efficiency, the design parameters are introduced in four steps, namely, graphene content only of each layer, graphene and fibre contents of each layer, ply thicknesses and finally fibre orientations.

Graphene is a monolayer of sp^2 hybridized carbon atoms arranged in a honeycomb structure and is well known for its exceptional mechanical properties [12]. It also possesses additional beneficial properties such as light weight, electrical conductivity and mechanical toughness [13] and presently it is being used widely in several industrial applications [14]. It was noted that Young's modulus of graphene could approach 1000 GPa and its tensile strength 130 GPa [15]. It was also noted that 0.1% GPL added to epoxy composites can increase the Young's modulus by 31% [16]. The main reason for the high reinforcing capacity of graphene is attributed to large surface area of platelets resulting in a high level load transfer from the polymer matrix to reinforcing component as observed in [17,18]. However, the introduction of a nano-scale reinforcement into polymer matrix should also consider such effects as the diminishing returns caused by using a high amount of nano reinforcement which can lead to the nano material not dispersing in the matrix uniformly. Uniform dispersion of nano-scale reinforcements in a matrix is an important consideration as a high volume content can lead to coalescing and inadvertently affecting the stiffness and the strength of the material. Another issue is the high cost of nano materials which makes the optimal use of the nano reinforcements an important requirement to keep the material costs to a minimum. These considerations become of major importance in the design of three-phase nanocomposites (nano-scale reinforcement + fibre + matrix). Within this framework, several studies investigated the behaviour of nano-reinforced laminated structures undergoing free or forced vibrations, or subject to buckling or bending loads. One of the main areas of this research has been the study of two-phase graphene reinforced nanocomposite laminates consisting of only graphene and a matrix.

Free vibration, buckling and static bending of multi-layered and functionally graded GPL reinforced composite plates were analysed in [19]. Elastic constants of the nanocomposite were computed using the modified Halpin-Tsai micromechanical model. The results indicated that the natural frequencies and buckling loads were significantly improved with the addition of graphene. In [20], vibration damping properties of GPL reinforced NR/EPDM (Natural rubber/ethylene-propylene-diene rubber) were studied via free vibration tests. The results showed that the addition of GPLs significantly improved the damping ratio values (up to 50%) when compared to the NR/EPDM blend only.

Light weight structures are often exposed to severe vibrations and it becomes important to improve their performance by reducing the possibility of resonance. To avoid resonance, natural frequencies of the structure have to be away from the excitation frequency. One way of achieving this objective is to increase the fundamental frequency and make it higher than the excitation frequency. Another way is to increase the frequency gaps and place the excitation frequency into one of these gaps [21,22]. The first case leads to an optimal design problem to maximize the fundamental frequency. A statistical analysis is given for the free vibrations of functionally graded graphene reinforced composite plates in [23]. The study indicates that boundary conditions and volume fractions of GPLs were the most significant parameters for the vibration response, followed by thickness ratio and distribution pattern of GPLs. More recent works on the vibration of two-phase graphene reinforced nanocomposites include [19,24-32].

Recently, the research was directed towards investigating the mechanical response of three-phase multi-scale laminates. In this case, the polymer matrix is reinforced by a nano-scale material such as carbon nanotubes (CNT) or graphene as well as fibres (mostly glass or carbon) leading to a multi-scale composite involving macro (matrix), micro (fibre) and nano (CNTs or GPLs) scales. The motivation for this study emanates from the fact that the limits of improving the mechanical properties of traditional fibre reinforced composites are gradually reached [33] while the requirements for advanced material properties increase. A major reason for the high-level of reinforcement of composites by graphene platelets is the two-dimensional nature of graphene which results for the reinforcement to take place in the in-plane directions. Furthermore, graphene platelets have larger surface to volume ratios which create a larger interface for bonding [34]. In [35] it is concluded that the flexural modulus of three-phase graphene/fibre reinforced composites is 1.7, 4.5 and 6.4 times larger than those of the two-phase fibre reinforced composites, the two-phase graphene reinforced composites and the polymer host, respectively. Scanning electron microscope image analysis presented in the same article indicates that the enhancement of the mechanical properties for the three-phase composite is attributed to the synergetic effect of the fibres and the nano-reinforcement (graphene nanoplatelets) on the polymer matrix in terms of improvement of the interfacial interactions and decrease of the matrix-rich and free-volume regions. Therefore, it is expected that three-phase composites provide a further improvement over the two-phase conventional composites and two-phase nanocomposites. The advantages of a graphene and fibre reinforcement of polymer composites have also been noted in a number of publications [35-39]. Studies on the bending, buckling and vibration behaviour of multi-scale three-phase laminates are given in [40-43]. Numerical results of [40] indicated that the central deflection and fundamental frequencies were significantly improved by incorporating a small percentage of GPLs in a fibre-reinforced composite. In [43], it was observed that exceeding a certain fibre content in a three-phase laminate leads to a decrease in the buckling strength by reducing the volume fraction of graphene reinforced matrix.

Several studies were directed to the optimization of fibre composite laminates to improve the vibrations response [8,44-47]. However, a relatively small number of studies involved optimization of two-phase or three-phase nanocomposite laminates. In [48], vibration and optimization of CNT reinforced beam was investigated based on higher order theories. In [49], CNT and glass fibre reinforced composite plates were optimized for maximum frequency. Results indicated that higher CNT volume fraction does not necessarily increase the frequencies. It was observed that the stacking sequence can significantly influence the frequencies, especially in the case of simply supported boundary conditions.

Presently, there seems to be no work published on the optimization of the frequencies of three-phase, graphene/fibre reinforced composite laminates taking the graphene and fibre contents non-uniformly distributed across the thickness, taking the ply thicknesses non-uniform, combined with the optimal orientation of fibres. In the present study, this problem is studied in detail from analysis and optimization points of view to offer an insight on the vibration response of three-phase laminates. The main emphasis is on the optimal graphene distribution across the laminate thickness as well as on optimal graphene and fibre distributions across the thickness. In addition to these two design variables, optimizations with respect to layer thicknesses and fibre orientations are also studied in combination with optimal graphene and fibre distributions. To implement the analysis and optimization solutions for various boundary conditions, a finite element analysis code is developed based on the first-order shear deformation theory (FSDT) for the computation of the fundamental frequencies of the laminated composite. The code is then incorporated in an optimization scheme based on the sequential quadratic programming (SQP).

Section 2 of the paper presents the theoretical background for the finite element code developed to simulate the free vibration response of laminate plates. Section 3 is allocated to the micromechanical equations implemented to determine the effective material properties of the laminate. Section 4 presents the optimization formulation and Section 5 the verification of the proposed numerical scheme by comparing the

results to published research and also the ones obtained by commercial software. In Section 6, analysis results are given, investigating the effects of reinforcements of graphene and fibres on frequencies. Section 7 presents the optimal design results and Section 8 the conclusions of this work.

2. Theoretical formulation

The present study involves the vibrations of a laminated composite plate having length a in the x-direction, width b in the y-direction and with a total thickness of D as shown in Fig. 1. The plate consists of N layers with the principal material coordinates of the k^{th} lamina oriented at an angle θ_k to the laminate coordinate x. The $xy-$ plane coincides with the mid-plane of the plate with the z-axis being normal to the mid-plane (Fig. 1). The vertical coordinates of the top and bottom of the k^{th} layer are given by $z = z_k$ and $z = z_{k-1}$. The polymer matrix is reinforced with graphene nanoplatelets and fibres noting that their volume fractions in each lamina could be different. Furthermore, layer thicknesses could be non-uniform and could be determined optimally.

2.1. Mechanical displacements and strains

One of the most widely used displacement based theories for laminated plates is the first-order shear deformation theory (FSDT) which is based on the displacement field described by the equations:

$$\begin{aligned} u_1(x,y,z,t) &= u(x,y,t) - z\varphi_x(x,y,t) \\ u_2(x,y,z,t) &= v(x,y,t) - z\varphi_y(x,y,t) \\ u_3(x,y,z,t) &= w(x,y,t) \end{aligned} \tag{1}$$

where (u_1, u_2, u_3) are the displacements along the (x, y, z) coordinates, (u, v, w) are the displacements of a point on the mid-plane of the panel and φ_x, φ_y are the normal rotations about the $\times$ and y-axes, respectively. Using the strain–displacement relations, the bending and shear strains can be expressed as

$$\{\varepsilon_b\} = \{\varepsilon_{0b}\} + z\{\text{Đ}^o\}, \{\varepsilon_s\} = \{\varepsilon_{0s}\} \tag{2}$$

where

$$\{\varepsilon_b\} = \{\varepsilon_{xx}, \varepsilon_{yy}, \gamma_{xy}\}^T, \{\varepsilon_s\} = \{\gamma_{yz}, \gamma_{xz}\}^T, \{\varepsilon_{0b}\} = \left\{\frac{\partial u}{\partial x}, \frac{\partial v}{\partial y}, \frac{\partial u}{\partial y} + \frac{\partial v}{\partial x}\right\}^T \tag{3a}$$

$$\{\text{Đ}^o\} = \left\{-\frac{\partial \varphi_x}{\partial x}, -\frac{\partial \varphi_y}{\partial y}, -\left(\frac{\partial \varphi_x}{\partial y} + \frac{\partial \varphi_y}{\partial x}\right)\right\}^T, \{\varepsilon_{0s}\} = \left\{\frac{\partial w}{\partial y} - \varphi_y, \frac{\partial w}{\partial x} - \varphi_x\right\}^T \tag{3b}$$

2.2. Constitutive equations

For an orthotropic material possessing a plane of elastic symmetry parallel to the x-y plane, the constitutive equations for the k^{th} lamina are given by:

$$\{\sigma\}_k = [Q]_k\{\varepsilon\} \tag{4}$$

where $\{\sigma\}_k$ is the stress tensor and $\{\varepsilon\}$ is the strain tensor. $[Q]_k$ is the plane-stress reduced stiffness matrix. Bending and shear stresses for k^{th} lamina can be expressed as

$$\{\sigma_b\}_k = [Q_b]_k\{\varepsilon\}, \{\sigma_s\}_k = [Q_s]_k\{\varepsilon\} \tag{5}$$

where $\{\sigma_b\}_k = \{\sigma_1, \sigma_2, \sigma_6\}^T, \{\sigma_s\}_k = \{\sigma_4, \sigma_5\}^T$ and

$$[Q_b]_k = \begin{bmatrix} Q_{11}{}^{(k)} & Q_{12}{}^{(k)} & 0 \\ Q_{21}{}^{(k)} & Q_{22}{}^{(k)} & 0 \\ 0 & 0 & Q_{66}{}^{(k)} \end{bmatrix} \quad [Q_s]_k = \begin{bmatrix} Q_{44}{}^{(k)} & 0 \\ 0 & Q_{55}{}^{(k)} \end{bmatrix} \tag{6}$$

In Eqs. (6), $Q_{ij}^{(k)}$ are the plane stress-reduced stiffnesses of the k^{th} lamina [50]

$$Q_{11}^{(k)} = \frac{E_1^{(k)}}{(1 - \nu_{12}^{(k)}\nu_{21}^{(k)})}, Q_{12}^{(k)} = \frac{\nu_{12}{}^{(k)}E_2^{(k)}}{(1 - \nu_{12}^{(k)}\nu_{21}^{(k)})} = Q_{21}^{(k)}, Q_{22}^{(k)} = \frac{E_2^{(k)}}{(1 - \nu_{12}^{(k)}\nu_{21}^{(k)})},$$

$$Q_{66}^{(k)} = G_{12}^{(k)}, Q_{44}^{(k)} = k_s G_{23}^{(k)}, Q_{55}^{(k)} = k_s G_{13}^{(k)}$$

where $E_1^{(k)}$, $E_2^{(k)}$ are the longitudinal and transverse moduli, $\nu_{12}^{(k)}$, $\nu_{21}^{(k)}$ are the Poisson's ratios, $G_{12}^{(k)}$, $G_{23}^{(k)}$, $G_{13}^{(k)}$ are the shear moduli of the k^{th} layer and k_s is a shear correction factor taken as $\frac{5}{6}$. The reduced stiffness $Q_{ij}^{(k)}$ of the k^{th} lamina can be transformed to $\overline{Q}_{ij}^{(k)}$ as

$$\left[\overline{Q}\right]_{(k)} = \left([L]^T[Q][L]\right)_{(k)} \tag{7}$$

where $[L]$ is a transformation matrix for the fibre angle θ_k of the k^{th} lamina [50].

2.3. Finite element formulation and eigenvalue problem

In the present study, the laminated plate has been discretized using a four-noded isoparametric quadrilateral Lagrangian element with five degrees of freedom (DOF) per node. The generalized displacement vector is interpolated as:

$$\{\overline{u}(x,y,t)\} \equiv \{u, v, w, \varphi_x, \varphi_y\}^T = [N_u]\{d\}_e = \sum_{j=1}^{4}\left(N_j[I]_{5x5}\{d_j\}_e\right) \tag{8}$$

where $\{d_j\}_e = \{u_j, v_j, w_j, \varphi_{xj}, \varphi_{yj}\}^T$ corresponds to the j^{th} node of the

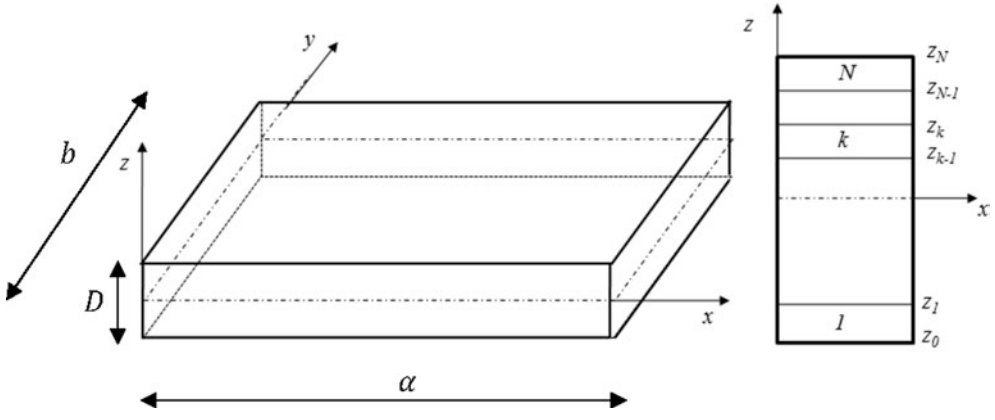

Fig. 1. Geometry of the laminated plate.

element and N_j are the shape functions. Substituting Eq. (8) into Eqs. (2) gives

$$\{\bar{\varepsilon}(x,y,t)\} = [B]\{d\}_e = \sum_{j=1}^{4}\left(\left[B_j\right]\{d_j\}_e\right) \tag{9}$$

or equivalently

$$\{\bar{\varepsilon}\} = \begin{Bmatrix}\{\varepsilon_{b0}\}\\ \{\text{Ð}^o\}\\ \{\varepsilon_{s0}\}\end{Bmatrix} = \begin{bmatrix}[B_b]\\ [B_k]\\ [B_s]\end{bmatrix}\{d\}_e = \sum_{j=1}^{4}\left(\begin{bmatrix}[B_b]_j\\ [B_k]_j\\ [B_s]_j\end{bmatrix}\{d_j\}_e\right) \tag{10}$$

where $[B_b]_j = \begin{bmatrix}\partial_x & 0 & 0 & 0 & 0\\ 0 & \partial_y & 0 & 0 & 0\\ \partial_y & \partial_x & 0 & 0 & 0\end{bmatrix}N_j$, $[B_k]_j = \begin{bmatrix}0 & 0 & 0 & -\partial_x & 0\\ 0 & 0 & 0 & 0 & -\partial_y\\ 0 & 0 & 0 & -\partial_y & -\partial_x\end{bmatrix}N_j$, $[B_s]_j = \begin{bmatrix}0 & 0 & \partial_x & -1 & 0\\ 0 & 0 & \partial_y & 0 & -1\end{bmatrix}N_j$

and $\partial_x = \partial/\partial x$, $\partial_y = \partial/\partial y$.

Using Hamilton's principle, the governing equation of the laminated plate subject to mechanical loads is expressed as

$$\int_0^{t0}(\delta T - \delta U + \delta W)dt = 0 \tag{11}$$

where U is the strain energy, T is the kinetic energy and W is the work done by the mechanical forces of the laminated composite plate. Analytic expressions of U, T and W are given in the Appendix.

The global form of the final governing equation is then expressed as

$$[M]\{\ddot{d}\} + [K]\{d\} = \{F_m\} \tag{12}$$

where $[M]$, $[K]$, $\{d\}$ and $\{F_m\}$ are global mass matrix, global linear stiffness matrix, global displacement and force vectors, respectively. The generalized governing Eq. (12) can be employed to study the free vibration by dropping the force term as:

$$[K]\{d\} = \lambda[M]\{d\} \tag{13}$$

with the eigenvalue $\lambda = \omega^2$ where ω is the frequency of natural vibrations. Eq. (13) is solved within the framework of the finite element method using Cholesky factorization [51]. This method can be adopted since the stiffness matrix $[K]$ is symmetric and the mass matrix $[M]$ is symmetric positive-definite. The solution of the eigenvalue problem is implemented within MATLAB [52,53].

3. Effective material properties using micromechanics equations

The laminate under consideration is a three-phase graphene and fibre reinforced polymer nanocomposite. The concept of the three-phase material relies on the need to enhance its structural response by adding a small quantity of nano-reinforcement (graphene nanoplatelets in the present study), and improving its mechanical properties by doing so. First, particles of the nano-reinforcement are distributed into the matrix, resulting in a nano-reinforced, isotropic matrix. Then, the nano-reinforced matrix is further reinforced with fibres.

The effective material properties of the nano-reinforced matrix are derived in this article using the Halpin-Tsai model and the rule of mixtures. This micromechanical homogenization approach is widely adopted in published research to capture the effective response of graphene reinforced laminates, see for example [54-57].

For the calculation of the effective properties of the three-phase fibre/graphene reinforced matrix, a second set of micromechanics equations is adopted in this article. This set of equations is traditionally used to derive the effective material properties of a fibre reinforced matrix involving two-phase fibre reinforced composites [11]. This concept of using micromechanical homogenization schemes for three-phase laminates, initially adopted for two-phase fibre reinforced composites, has been elaborated in several publications. For instance, micromechanics equations adopted in [58] for a two-phase fibre reinforced composite, are also used in [40] to derive the effective material properties of three-phase fibre/graphene reinforced matrix. The same concept of using micromechanics approaches for three-phase composites, which had initially been adopted for two-phase composites, has also been implemented in a number of publications involving three-phase CNT/fibre reinforced laminates [41,49].

Elastic constants in this article are computed from the applicable micromechanical equations. First, the effective material properties of the graphene reinforced matrix are computed using the micromechanical equations applicable to uniformly distributed GPLs. Next step involves the computation of the material properties of the three-phase graphene/fibre reinforced composite using the applicable micromechanics equations.

3.1. Graphene reinforced matrix

In this section, Young's and shear moduli, Poisson's ratio and density of graphene reinforced matrix are computed using the micromechanical equations presented in [54,59-61]. In the equations, subscripts *GPL*, *M* and *GM* denote graphene nanoplatelets (*GPL*), the matrix (*M*) and the graphene reinforced matrix (*GM*). Young's modulus of the GPLs reinforced matrix is given by

$$E_{GM} = \left(\frac{3}{8}\frac{1+\xi_L\eta_L V_{GPL}}{1-\eta_L V_{GPL}} + \frac{5}{8}\frac{1+\xi_w\eta_w V_{GPL}}{1-\eta_w V_{GPL}}\right)\times E_M \tag{14}$$

where V_{GPL} denotes the volume content of GPLs. Parameters ξ_L and ξ_w are given in Eq. (15) in terms of the length (l_{GPL}), the width (w_{GPL}) and the thickness (h_{GPL}) of GPLs:

$$\xi_L = 2\frac{l_{GPL}}{h_{GPL}}, \xi_w = 2\frac{w_{GPL}}{h_{GPL}} \tag{15}$$

Symbols η_L and η_w in Eq. (14) are calculated next in terms of Young's moduli E_{GPL} of the graphene nanoplatelets and E_M of the matrix as

$$\eta_L = \frac{(E_{GPL}/E_M)-1}{(E_{GPL}/E_M)+\xi_L}, \eta_w = \frac{(E_{GPL}/E_M)-1}{(E_{GPL}/E_M)+\xi_w} \tag{16}$$

The volume content of graphene nanoplatelets can be computed in terms of its weight fraction W_{GPL} as

$$V_{GPL} = \frac{W_{GPL}}{W_{GPL} + (\rho_{GPL}/\rho_M)(1-W_{GPL})} \tag{17}$$

where ρ_{GPL} and ρ_M represent the mass densities of graphene nanoplatelets and the polymer matrix, respectively. Poisson's ratio, shear modulus and the density of the graphene reinforced matrix are given by

$$v_{GM} = v_{GPL}V_{GPL} + v_M(1-V_{GPL}) \tag{18}$$

$$G_{GM} = \frac{E_{GM}}{2(1+v_{GM})} \tag{19}$$

$$\rho_{GM} = \rho_{GPL}V_{GPL} + \rho_M(1-V_{GPL}) \tag{20}$$

3.2. Graphene and fibre reinforced matrix

Fibre reinforcement of the graphene reinforced matrix improves the properties of the composite further. The fibres employed for this purpose are unidirectional and continuous. Young's moduli, shear modulus, Poisson's ratio and density of the graphene/fibre reinforced nanocomposite are computed via micromechanical relations given in [11]:

$$E_{11} = E_{F11}V_F + E_{GM}(1-V_F) \tag{21}$$

$$E_{22} = E_{GM}\left(\frac{E_{F22} + E_{GM} + (E_{F22} - E_{GM})V_F}{E_{F22} + E_{GM} - (E_{F22} - E_{GM})V_F}\right) \tag{22}$$

$$G_{12} = G_{13} = G_{GM}\left(\frac{G_{F12} + G_{GM} + (G_{F12} - G_{GM})V_F}{G_{F12} + G_{GM} - (G_{F12} - G_{GM})V_F}\right) \tag{23}$$

$$G_{23} = \frac{E_{22}}{2(1 + v_{23})} \tag{24}$$

$$v_{12} = v_{F12}V_F + v_{GM}(1 - V_F) \tag{25}$$

$$v_{23} = v_{F12}V_F + v_{GM}(1 - V_F)\left(\frac{1 + v_{GM} + v_{12}E_{GM}/E_{11}}{1 - v_{GM}^2 + v_{12}v_{GM}E_{GM}/E_{11}}\right) \tag{26}$$

$$\rho = \rho_F V_F + \rho_{GM}(1 - V_F) \tag{27}$$

Subscripts *GM* and *F* refer to graphene reinforced matrix and fibres, respectively. The fibre volume content is represented by V_F and the density of fibres by ρ_F.

4. Optimal design problem

The design objective is the maximization of the fundamental frequency under different boundary conditions and employing a number of design parameters. Design parameters include the distributions of GPLs and fibres across the thickness, layer thicknesses and the fibre orientations. The constraints imposed on the optimization include the total weight of GPLs, total volume content of fibres as well as the weight content of GPLs and the volume content of fibres in individual layers.

The first two optimization problems involve laminates with uniform layer thicknesses with the distributions of GPLs (Problem 1) and GPLs plus fibres (Problem 2) taken as non-uniform across the thickness and their distributions across the thickness are to be determined optimally. The next optimization problem involves laminates with non-uniform layer thicknesses in addition to having non-uniform distributions of GPLs and fibres (Problem 3). In the final optimization problem (Problem 4), the fibre orientations are also specified as design variables in addition to the previous three design variables. As such Problem 4 has four design variables, namely, GPL and fibre distributions, layer thicknesses and fibre orientations.

Dimensions of the composite laminate are given by a in the x-direction and b in the y-direction as shown in Fig. 1. The total laminate thickness is D and the number of layers is N. In the first two optimization problems, thickness of each layer is specified as constant and equal to h with $Nh = D$. In the third and fourth optimization problems, the thicknesses h_i of layers are taken as design variables leading to laminates with non-uniform layer thicknesses with $\sum_{i=1}^{N} h_i = D$. The fibre and graphene volume contents of each layer are denoted as V_{Fi} and V_{GPLi} , respectively.

4.1. Formulation for laminates with uniform layer thicknesses (Problems 1 and 2)

The volume of fibres in each layer is given by $Vol_{Fi} = abhV_{Fi}$ and the total volume of fibres in the laminate by $Vol_{FT} = \sum_{i=1}^{N} Vol_{Fi} = abh\sum_{i=1}^{N} V_{Fi}$ for a laminate with N layers. The volume of the laminated plate is given by $Vol_{plate} = abD$. The maximum amount (volume) of fibres available for the laminate is specified as $Vol_{Fmax} = abDV_{Fmax}$ where V_{Fmax} is the maximum fibre volume content of the laminate. Based on these definitions, the design constraints for the total fibre volume are given by

$$Vol_{FT} \leqslant Vol_{Fmax} \Rightarrow abh\sum_{i=1}^{N} V_{Fi} \leqslant abDV_{Fmax} \Rightarrow \frac{h}{D}\sum_{i=1}^{N} V_{Fi} \leqslant V_{Fmax} \tag{28}$$

In the specific case of a composite laminate with 8 layers which is studied in the numerical results sections, Eq. (28) becomes:

$$\frac{h}{8h}\sum_{i=1}^{8} V_{Fi} \leqslant V_{Fmax} \Rightarrow \frac{1}{8}\sum_{i=1}^{8} V_{Fi} \leqslant V_{Fmax} \tag{29}$$

A similar formulation is adopted for the constraint on the overall weight of graphene nanoplatelets and for an 8-layered laminate, the constraint is given as

$$\frac{1}{8}\sum_{i=1}^{8} W_{GPLi} \leqslant W_{GPLmax} \tag{30}$$

In Eq. (30), W_{GPLi} and W_{GPLmax} denote the weight of graphene nanoplatelets for the i^{th} layer and the maximum graphene weight for the laminate, respectively. With the design constraints defined as above, the optimization problem for an 8-layered laminate can be stated as follows:

$$\max \ Fundamental \ Frequency \ f(V_F, W_{GPL}, \theta) = \omega \tag{31a}$$

$$subject \ to \ \frac{1}{8}\sum_{i=1}^{8} V_{Fi} \leqslant V_{Fmax} \tag{31b}$$

$$\frac{1}{8}\sum_{i=1}^{8} W_{GPLi} \leqslant W_{GPLmax} \tag{31c}$$

$$W_{GPLi} \geqslant 0 \tag{31d}$$

$$d_1 \leqslant V_{Fi} \leqslant d_2 \tag{31e}$$

$$-90^o \leq Fibre \ angle \ \theta \leq 90^o \tag{31f}$$

Eq. (31d) states that graphene weight of each layer must be greater than or equal to zero and Eq. (31e) imposes lower and upper limits d_1 and d_2 on the fibre volume content for each layer. As shown in Eqs. (31), each layer represents a three-phase material since the contents of graphene and fibre reinforcement are greater than zero. If for a layer, the case of zero graphene content arises (case of equality in Eq. (31d)), then the composite becomes two-phase. However, this is determined by the optimization algorithm since the code is set up for three-phase composites. Practically, some zero graphene layers arise in the middle of the laminate as observed in the results sections.

In order to assess the effectiveness of an optimal design, that is, the increase in the fundamental frequency as compared to a benchmark, a design efficiency factor is introduced. It is defined as the ratio of the maximum fundamental frequency ω_{max} of the optimally designed laminate and a reference frequency ω_0. The reference frequency corresponds to a laminate with uniformly distributed graphene and fibres across the thickness of the laminate with the efficiency factor for an 8-layered laminate defined as

$$\eta = \frac{\omega_{max}(V_F, W_{GPL}, \theta)}{\omega_0(V_i = \frac{V_{fmax}}{8}, W_{GPLi} = \frac{W_{GPLmax}}{8}, i = 1, 2, ..., 8)} \tag{32}$$

4.2. Formulation for non-uniform layer thicknesses (Problems 3 and 4)

For a laminate with non-uniform layer thicknesses, i.e., each layer having a different thickness, the layer thicknesses h_i become design variables to be determined optimally subject to the total thickness constraint $\sum_{i=1}^{N} \frac{h_i}{D} = 1$. The volume of fibres in each layer is given by $Vol_{Fi} = abh_iV_{Fi}$ and the total volume of fibres in the laminate by $Vol_{FT} = \sum_{i=1}^{N} Vol_{Fi} = ab\sum_{i=1}^{N} h_iV_{Fi}$ for a laminate with N layers. Design constraint on the total fibre volume content Vol_{FT} is given by

$$Vol_{FT} \leqslant Vol_{Fmax} \Rightarrow ab\sum_{i=1}^{N} h_iV_{Fi} \leqslant abDV_{Fmax} \Rightarrow \frac{1}{D}\sum_{i=1}^{N} h_iV_{Fi} \leqslant V_{Fmax} \tag{33}$$

A similar constraint applies to the total weight of graphene platelets and is given by

$$\frac{1}{D}\sum_{i=1}^{N} h_i W_{GPLi} \leqslant W_{GPLmax} \tag{34}$$

In the numerical results sections, optimization of an 8-layered laminate is studied. For this specific case, the optimal design problem can be stated as follows:

$$\text{max fundamental frequency } f\left(V_F, W_{GPL}, \frac{h_i}{D}, \theta i\right) = \omega \tag{35a}$$

$$\text{subject to } \frac{1}{D}\sum_{i=1}^{8} h_i V_{Fi} \leqslant V_{Fmax} \tag{35b}$$

$$\frac{1}{D}\sum_{i=1}^{8} h_i W_{GPLi} \leqslant W_{GPLmax} \tag{35c}$$

$$W_{GPL} \geq 0 \tag{35d}$$

$$d_1 \leq V_F \leq d_2 \tag{35e}$$

$$-90^o \leq \text{Fibre angles } \theta i \leq 90^o \tag{35f}$$

For this case, the design efficiency factor is defined as

$$\eta = \frac{\omega_{max}(V_F, W_{GPL}, \frac{hi}{D}, \theta)}{\omega_0(V_i = \frac{V_{fmax}}{8}, W_{GPLi} = \frac{W_{GPLmax}}{8}, h_i = \frac{D}{8}, i = 1, 2, ..., 8)} \tag{36}$$

where the denominator corresponds to a laminate with uniform graphene and fibre distributions as well as having uniform layer thicknesses.

4.3. Solution of the optimization problem

Numerical solutions of the optimization problems are obtained by a Sequential Quadratic Programming algorithm (SQP). This is an effective optimization method which generates steps by solving quadratic subproblems for nonlinearly constrained problems [62-64]. In particular, an approximation of the Hessian of the Lagrangian function is considered at each major iteration using a quasi-Newton updating method. This is then used to generate a Quadratic Programming sub-problem the solution of which is used to define a search direction. This scheme is briefly presented below. The optimization problem with nonlinear equality and inequality constraints is given by [62]:

$$\min f(x)$$

$$\textit{subject to } c_i(x) = 0, i \in E \tag{37}$$

$$c_i(x) \geq 0, i \in I$$

The problem is then linearized into:

$$\min_p f_k + \nabla f_k^T p + \frac{1}{2} p^T \nabla_{xx}^2 L_k p$$

$$\textit{subject to } \nabla c_i(x_k)^T p + c_i(x_k) = 0, i \in E \tag{38}$$

$$\nabla c_i(x_k)^T p + c_i(x_k) \geq 0, i \in I$$

The solution of the problem formulated above is implemented within MATLAB [52,53]. It is noted that since the MATLAB algorithms mentioned above are originally defined for minimization, the objective functions presented in Eqs. (31) and (35) are modified as follows:

$$min\ Fundamental\ Frequency\ f(V_F, W_{GPL},\ \theta) = -\omega.$$

The fundamental frequency is calculated by solving the eigenvalue problem. This solution is implemented within the optimization algorithm aiming to maximize the fundamental frequency as defined in the optimization formulation, considering the constraints presented in sections 4.1 and 4.2. In particular, the finite element model for the composite laminate is included in the optimization algorithm. The classical steps of the finite element method are implemented, the mass and the stiffness of the structure are determined and the eigenvalue problem is solved, resulting in the computation of the fundamental eigenfrequency. Then, optimization is implemented until the optimal solution satisfying the constraints is obtained.

5. Verification of the numerical approach

In the numerical results sections, the non-dimensional form of the fundamental frequency ω, namely, Ω is used which is given by

$$\Omega = \omega D\sqrt{\frac{\rho_M}{E_M}} \tag{39}$$

Verification of the method of solution implemented in the present study is done by comparing the present results with the results available in the literature and also with the results obtained by using a commercial software package. In the computations, the material properties given in Table 1 are used. For the dimensions of the GPLs, the following values are used: $l_{\text{GPL}} = 2.5$ μm, $w_{\text{GPL}} = 1.5$ μm, $h_{\text{GPL}} = 1.5$ nm. The graphene weight content is specified as $W_{GPL} = 1\%$. First, the natural frequencies obtained by the present method are compared in Table 2 with the results available in the literature, for the case of a GPL reinforced laminate. Results are given using the non-dimensionalized frequency defined in Eq. (39). The same non-dimensional frequency is used for numerical results presented in this work. Comparisons are given for the case of an isotropic plate (zero graphene and fibre content), as well as for the case of a graphene reinforced plate (with zero fibre content). As shown in Table 2, for both cases, a close agreement between the published research and the present model is observed.

Frequencies of the same composite laminate have been computed using ABAQUS commercial finite element analysis package and compared with the results obtained by the present method of solution. Four node shell elements and a 10x10 mesh have been used in the ABAQUS implementation. Then, several cases were examined as shown in Table 3 involving laminates with different number of layers and fibre angles as well as different boundary conditions. In all these cases, glass fibres are used as reinforcement with fibre content set to 50% for each layer. Results indicate a good agreement between the natural frequencies obtained by the model developed in this article and using the commercial software.

For further validation of the proposed model, the optimal fundamental frequency obtained by the proposed approach is compared with a number of discrete simulations conducted using the commercial software package. A two-layer hybrid laminate finite element model is developed and several simulations are conducted, adopting different stacking sequences. As shown in Table 4, both the proposed approach and the commercial software result in the same optimal stacking sequences as well as giving a very close value for the optimal fundamental frequency.

Table 1
Material properties of GPLs, matrix, carbon and glass fibres.

Material	E_{11}(GPa)	E_{22} (GPa)	G_{12} (GPa)	ν_{12}	Density (kg/m^3)
GPL	1010	1010	$E_{11}/(2(1+\nu))$	0.186	1060
Matrix	3	3	$E_{11}/(2(1+\nu))$	0.34	1200
Carbon fibres	263	19	27.60	0.20	1750
Glass fibres	72.4	72.4	$E_{11}/(2(1+\nu))$	0.20	2400

Table 2
Comparison of non-dimensional frequencies Ω of simply supported (SSSS) square plates reinforced by GPLs with the thickness/length ratio of $D/a = 0.1$

Pattern	Method	Mode 1	2
Isotropic plate (zero graphene and fibre content)	Present/Mesh 5x5	0.0610	0.1611
	Present/Mesh 10x10	0.0590	0.1441
	Present/Mesh 15x15	0.0587	0.1413
	Ref. [65]	0.0584	0.1391
	Ref. [27]	0.0584	0.1390
Uniformly distributed GPLs with $W_{GPL} = 1\%$	Present/Mesh 5x5	0.1267	0.3352
	Present/Mesh 10x10	0.1228	0.2999
	Present/Mesh 15x15	0.1221	0.2941
	Ref. [65]	0.1216	0.2895
	Ref. [27]	0.1216	0.2895

Table 3
Comparison of non-dimensionalized frequencies Ω of GPLs/glass fibre square plate with thickness/length ratio of $D/a = 0.1$, $W_{GPL} = 1\%$ and fibre volume content is 50%

Boundary conditions	Pattern	Stacking sequence	Method	Mode 1	2
SSSS	1 layer	[44]	Present	0.1579	0.3647
			Commercial software	0.1555	0.3601
	3 layers	[0/90/0]	Present	0.1500	0.3498
			Commercial software	0.1483	0.3454
	8 layers	$[0/30/45/90]_s$	Present	0.1530	0.3565
			Commercial software	0.1511	0.3520
CCCC	8 layers	$[0/30/45/90]_s$	Present	0.2639	0.4937
			Commercial software	0.2611	0.4885
SCSC	8 layers	$[0/30/45/90]_s$	Present	0.2226	0.3891
			Commercial software	0.2204	0.3844

6. Analysis of the effects of reinforcements on frequencies

Before presenting the results for the optimal design problems, some preliminary simulations are conducted with the GPLs and fibres distributed uniformly across the layers, i.e., all layers having the same volume content of the reinforcements. The objective of this exercise is to assess the effect of different graphene and/or fibre contents on the fundamental frequency and to study the trends as reinforcements increase. This study is conducted to observe the behaviour of three-phase composites which may have some unusual trends in terms of the effect of different reinforcements on frequencies. For this purpose, uniform glass or carbon fibre contents of 30% or 60% are specified for each layer. The results of this exercise are shown in Figs. 2 and 3 for different boundary conditions. In Fig. 2 results for an anti-symmetric stacking sequence and in Fig. 3 for a symmetric stacking sequence are given.

It can be observed from Figs. 2 and 3 that as the graphene weight increases beyond a certain limit, a lower percentage of fibres (30%) results in a higher frequency as compared to the higher percentage of fibres (60%) for both glass and carbon fibres. This cross-over point for glass fibres is approximately 3% of graphene weight and for carbon fibres approximately 6% of graphene weight. A physical explanation for this behaviour can be presented, by noting that the contribution of the Young's modulus of the graphene reinforced matrix E_{GM} (Eq. (14)) to E_{11} (Eq. (21)) decreases, as the fibre content V_F increases, due to the second term of Eq. (21) decreasing as V_F increases. Since the graphene reinforced matrix has a high elastic modulus E_{GM}, decrease in the contribution of E_{GM} to E_{11} affects the natural frequency negatively once V_F becomes too high. The reason for the cross-over point being higher in the case of carbon fibres is due to the high value of Young's modulus of carbon fibres which compensate the decrease in the contribution of E_{GM} as fibre content increases.

This observation indicates that the optimal distribution of graphene and the fibres along the thickness of the laminate needs to be taken into account for an efficient design since a simplified consideration, e.g., of uniform distribution of the graphene reinforcement across the thickness may lead to diminishing returns. Also the results indicate that a higher fibre content does not lead to higher frequencies at higher graphene contents since increasing the fibre content has the effect of reducing the frequency if the graphene content exceeds a certain threshold. It is observed that this threshold value is higher for carbon fibre reinforced

Table 4
Comparison of non-dimensional frequencies Ω with those obtained from the commercial software package for a GPLs/glass fibre SSSS square plate with thickness/length ratio $D/a = 0.1$, $W_{GPL} = 1\%$ and fibre volume content 50%.

Commercial software discrete simulations			Proposed optimization code	
Case	Stacking sequence	Non-dimensionalized frequency	Optimal stacking sequence	Optimal non-dimensionalized frequency
1	[0/0]	0.1483	**[45/45]**	**0.1579**
2	[30/0]	0.1505		
3	[45/0]	0.1510		
4	[60/0]	0.1496		
5	[90/0]	0.1464		
6	[0/30]	0.1505		
7	[30/30]	0.1537		
8	[45/30]	0.1543		
9	[60/30]	0.1528		
10	[90/30]	0.1496		
11	[0/45]	0.1510		
12	[30/45]	0.1543		
13	**[45/45]**	**0.1555**		
14	[60/45]	0.1543		
15	[90/45]	0.1510		
16	[0/60]	0.1496		
17	[30/60]	0.1528		
18	[45/60]	0.1543		
19	[60/60]	0.1537		
20	[90/60]	0.1505		
21	[0/90]	0.1464		
22	[30/90]	0.1496		
23	[45/90]	0.1510		
24	[60/90]	0.1505		
25	[90/90]	0.1483		

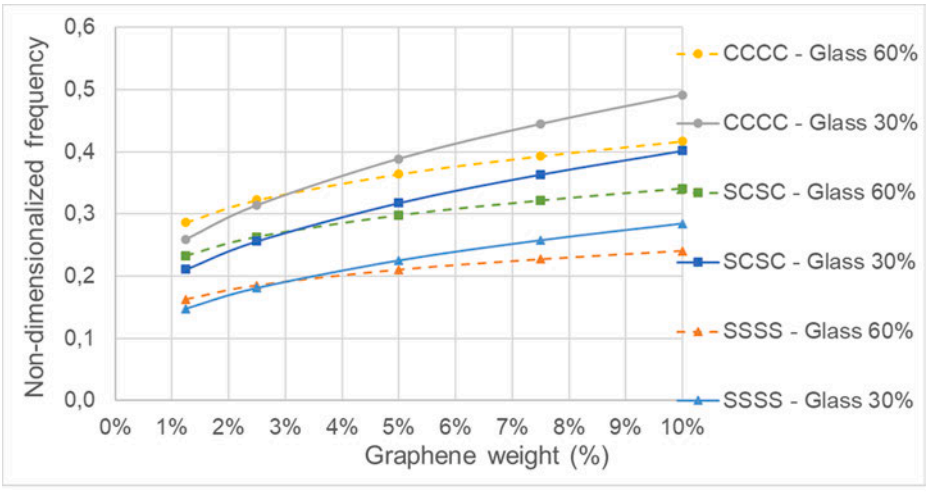

(a)

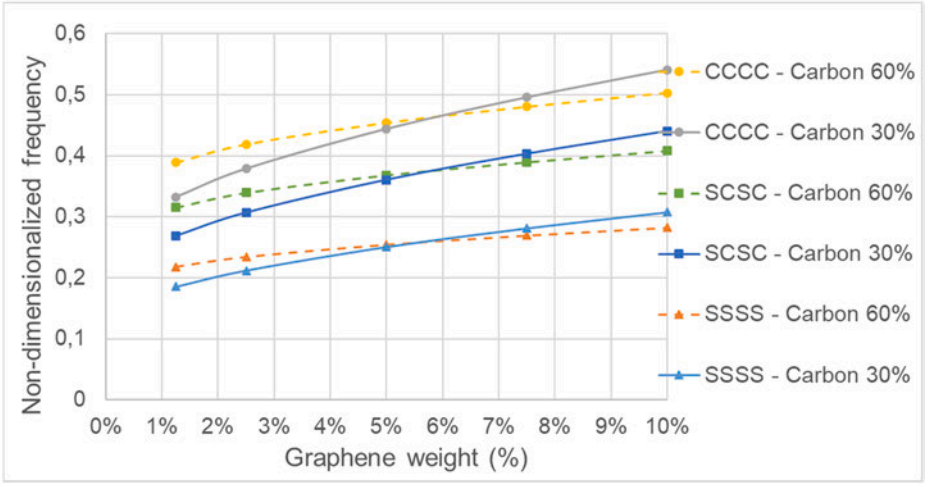

(b)

Fig. 2. Non-dimensional frequencies Ω of 8-layered laminates with uniform graphene and fibre distributions in layers and anti-symmetric stacking sequence $[0/90/0/90]_{\text{anti-s}}$ with $D/a = 0.1$, $a/b = 1$ for a) glass fibres, b) carbon fibres.

laminates as compared to glass fibre reinforced laminates. This effect is due to the higher stiffness of the carbon fibres. It is observed that the two different stacking sequences shown in Figs. 2 and 3, namely, cross-ply anti-symmetric and symmetric, result in similar behaviours.

7. Optimal design results

Optimization results obtained by the maximization of the fundamental frequency are given in this section. Results are presented for three different boundary conditions, namely, simply supported (SSSS), clamped (CCCC) and simply supported and clamped in opposite edges (SCSC). The simulations are conducted for eight-layered laminates and the design variables are the graphene weight and the fibre volume contents of layers, the layer thicknesses, the fibre angles as well as combinations of these variables. The layer thickness ratio is defined as the thickness of the layer over the total thickness of the laminate, i.e., h/D. The ratio of the total thickness of the laminate over the length of one edge is given by D/a and the aspect ratio by a/b.

7.1. Graphene content as the design variable

Next, the design problem for the optimal distribution of GPLs across the thickness is studied with the graphene weight percentages of layers being the only design variables of the problem. This leads to an optimal laminate with the graphene distributed non-uniformly and optimally across the thickness. The design constraint is the maximum GPL weight fraction for the overall laminate, denoted as W_{GPLmax} which is set to 1.25%, i.e., $W_{GPLmax} \leqslant 0.0125$. In Table 5, results for optimal graphene content of each layer, maximum frequencies and design efficiency factors are given. The reference frequency Ω_0 corresponds to a laminate with uniform graphene weight equal to 1.25% in all layers.

Table 5 shows that the outer layers of the laminate have a higher percentage of graphene as compared to the inner layers for optimum design. Since the first eigenmode corresponds to a bending deflection, the (top and bottom) outer layers of the plate influence the response to a higher extend as compared to the middle layers due to the increased contribution of the outer layers to laminate stiffness as compared to the inner layers. Therefore, the optimization algorithm assigns a higher content of reinforcement in the outer layers and less or even zero content of reinforcement in the middle layers, in order to maximize the natural frequency. The same trend is also observed in the majority of the results presented in this article.

For most of the cases shown in Table 5, only the two outer layers (out of the eight layers) get an increased amount of graphene while the

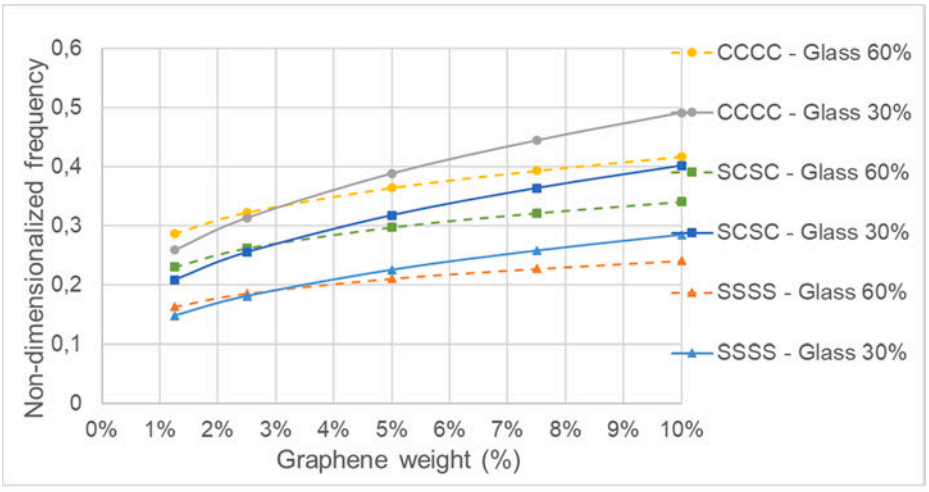

(a)

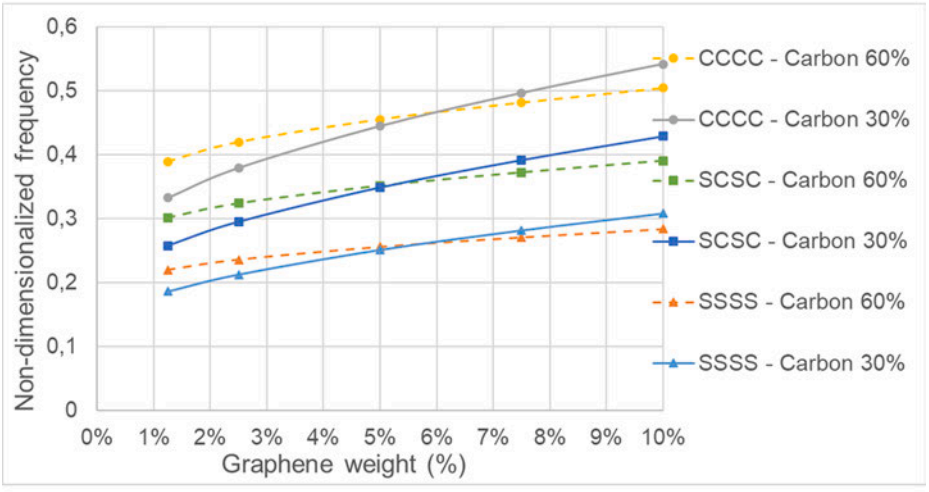

(b)

Fig. 3. Non-dimensional frequencies Ω of 8-layered laminates with uniform graphene and fibre distributions in layers and symmetrical stacking sequence $[90/0/90/0]_s$ with $D/a = 0.1$, $a/b = 1$ for a) glass fibres, b) carbon fibres.

Table 5
Maximum fundamental frequencies Ω of 8-layered laminates with W_{GPLi} (graphene weight content of i^{th} layer) as the design variables subject to $W_{GPLi} \geq 0$ and $W_{GPLmax} = 1.25\%$ with $D/a = 0.1$, $a/b = 1$ and SSSS boundary conditions

Stacking sequence	BCs	Fibre contents	Optimal W_{GPL} per layer	Ω	$\eta = \frac{\Omega_{max}}{\Omega_0}$
$[0/90/0/90]_{anti\text{-}s}$	**SSSS**	**Glass 30%**	$[0.048 / 0.0022 / 0 / 0]_s$	0.1766	1.196
		Glass 60%	$[0.036 / 0.014 / 0.0002 / 0]_s$	0.1774	1.091
		Carbon 30%	$[0.047 / 0.003 / 0 / 0]_s$	0.2054	1.108
		Carbon 60%	$[0.033 / 0.013 / 0.004 / 0]_s$	0.2254	1.033
$[90/0/90/0]_s$	**SSSS**	**Glass 30%**	$[0.049 / 0.0017 / 0 / 0]_s$	0.1767	1.196
		Glass 60%	$[0.036 / 0.014 / 0.0001 / 0]_s$	0.1774	1.090
		Carbon 30%	$[0.047 / 0.003 / 0 / 0]_s$	0.2068	1.108
		Carbon 60%	$[0.034 / 0.012 / 0.004 / 0]_s$	0.2275	1.034

middle layers are kept to a small or zero amount of graphene.

The highest increase in the fundamental frequency with respect to the reference frequency is 19.6% corresponding to the laminate with 30% glass fibres for the symmetric and anti-symmetric cases as indicated by the design efficiency index shown in the last column of Table 5. In the case of 30% fibre content (glass or carbon), increase in the frequency is approximately twice or more compared to the case of 60% fibre content. This indicates that in the present case of uniformly distributed fibres across the thickness, a more efficient design is achieved with lower fibre volume contents. As mentioned in section 6, this is attributed to the fact that the increase in the fibre content V_F leads to a decrease in the contribution of E_{GM} to E_{11} as can be observed from Eq. (21).

Moreover, the increase in the frequency (design efficiency) is higher for glass fibres than for carbon fibres. Also Table 5 indicates that symmetric and anti-symmetric stacking sequences have not produced significantly different results.

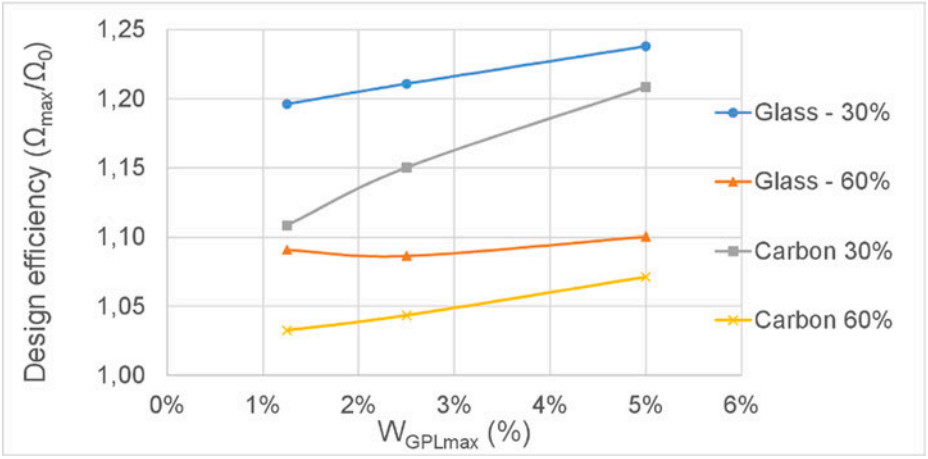

Fig. 4. Design efficiency vs W_{GPLmax} for different fibres and fibre contents with SSSS boundary conditions and $[0/90/0/90]_{anti\text{-}s}$ laminates.

Table 6
Maximum fundamental frequencies Ω of 8-layered laminates with two design variables: graphene and fibre contents (W_{GPLi}, V_{Fi}) of layers subject to $W_{GPLi} \geqslant 0$, $0.1 \leqslant V_{Fi} \leqslant 0.6$, $W_{GPLmax} = 1.25\%$, $V_{Fmax} = 30\%$ with $D/a = 0.1$, $a/b = 1$ and stacking sequence $[0/90/0/90]_{anti\text{-}s}$

BCs	Fibres	Optimal W_{GPL}	Optimal V_F	Ω	$\eta = \frac{\Omega_{max}}{\Omega_0}$
SSSS	**Glass**	$[0.035 / 0.015 / 0 / 0]_s$	$[0.6 / 0.4 / 0.1 / 0.1 /]_s$	0.1864	1.262
	Carbon	$[0.042 / 0.008 / 0 / 0]_s$	$[0.4 / 0.6 / 0.1 / 0.1 /]_s$	0.2209	1.192
CCCC	**Glass**	$[0.032 / 0.018 / 0 / 0]_s$	$[0.6 / 0.4 / 0.1 / 0.1]_s$	0.3113	1.202
	Carbon	$[0.027 / 0.014 / 0.009 / 0]_s$	$[0.48 / 0.52 / 0.1 / 0.1]_s$	0.3709	1.117
SCSC	**Glass**	$[0.033 / 0.018 / 0 / 0]_s$	$[0.6 / 0.4 / 0.1 / 0.1]_s$	0.2566	1.216
	Carbon	$[0.039 / 0.011 / 0 / 0]_s$	$[0.4 / 0.6 / 0.1 / 0.1]_s$	0.3045	1.132

To investigate the effect of increasing the allowable graphene weight for the overall laminate (W_{GPLmax}) on the design efficiency, three different values of W_{GPLmax}, equal to 1.25%, 2.5% and 5%, have been studied as shown in Fig. 4. The fibre volume contents across the thickness were kept uniform as before.

Fig. 4 indicates that increasing the total graphene weight is more efficient when a lower fibre content is used. For glass fibres with 60% fibre content, increasing the maximum graphene weight has almost no effect on the design efficiency. Results show that when a uniform fibre distribution is adopted, non-uniform distribution of graphene across the thickness leads to higher frequencies. The corresponding design efficiency factor becomes higher when lower fibre volume contents are used. An increase in the fibre content or use of carbon instead of glass result in increased frequency. However, this leads to lower design efficiency.

7.2. Graphene and fibre contents as design variables

Next, optimal designs with two sets of design variables are considered, namely, the optimal distributions of GPLs and fibres across the thickness. The results are shown in Table 6. The maximum graphene content for the overall laminate W_{GPLmax} is set to 1.25% and the maximum fibre volume content V_{Fmax} to 30%. The reference frequency Ω_0 to compute the design efficiency corresponds to a uniform graphene content of 1.25% and a uniform fibre content of 30% for all layers.

In most cases, as shown in Table 6, a higher graphene content is allocated to the two outer layers while zero graphene weight is allocated to the middle layers. For carbon fibres and CCCC boundary conditions, the top and bottom three layers have higher graphene content while only two middle layers have zero graphene content. Concerning the optimal fibre content, all boundary conditions result in higher fibre content in the two outer layers with the middle layers having the minimum fibre content as dictated by the constraint on minimum fibre content. Similar to the discussion presented in section 7.1, the optimization algorithm assigns a higher reinforcement content to the outer layers due to these layers affecting the structural response of the laminate more than the middle layers.

In the case of carbon fibres, it seems that values of fibre volume contents for the outer layers depend on the type of the boundary conditions. Design efficiency is observed to be the highest for glass fibres and SSSS boundary conditions (26.2%), followed by SCSC (21.6%) and CCCC (20.2%). For carbon fibres, highest efficiencies are obtained for SSSS (19.2%), followed by SCSC (13.2%) and CCCC (11.7%). Thus, as the boundary conditions become more stiff (from SSSS to CCCC), less space is left for improvement of the natural frequency, which results in the decrease of the design efficiency. Comparing Tables 5 and 6, it is observed that design efficiency index in Table 6 indicates an increase of 26.2% for glass fibres and 19.2% for carbon fibres for SSSS boundary conditions. The corresponding increases for the case of uniform fibre distributions shown in Table 5 are 19.6% and 10.8%, respectively, indicating that optimal non-uniform fibre distribution results in significantly increased frequencies for both glass and carbon fibres. It is noted that in both cases the same amount of total fibre content for the laminate is specified.

Therefore, this increase in the design efficiency in the case of non-uniform fibre (and graphene) distributions is due to the fact that optimization distributes the fibre reinforcement optimally by assigning a higher fibre content in the outer layers and a lower fibre content in the middle layers as compared to the case of a uniform fibre distribution presented in Table 5.

To investigate the sensitivity of the frequency to design parameters, contour plots with respect to graphene and fibre contents are drawn as shown in Fig. 5 for SSSS boundary conditions. In Fig. 5, the two horizontal axes indicate the variation of the graphene weight and fibre

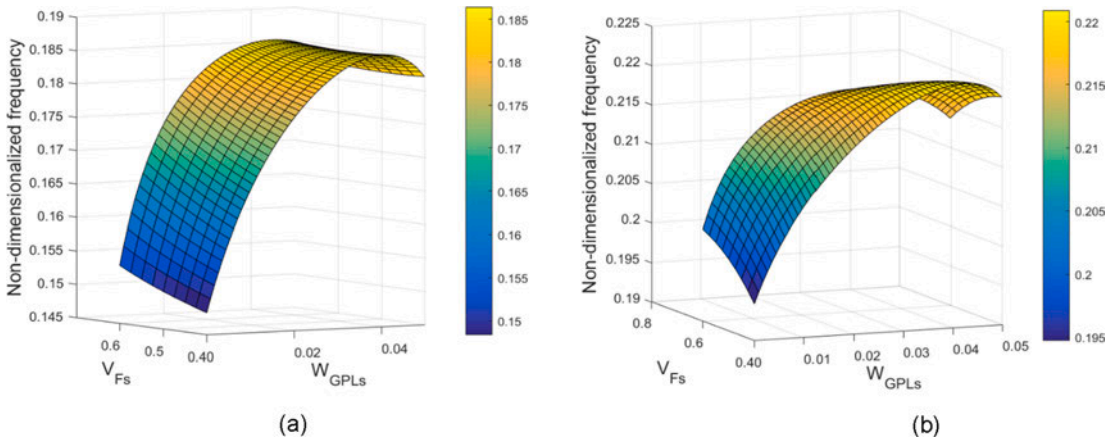

Fig. 5. Contour plots of frequency for SSSS boundary conditions with varying graphene weight and fibre volume contents of the surface layers for a) glass and b) carbon fibres.

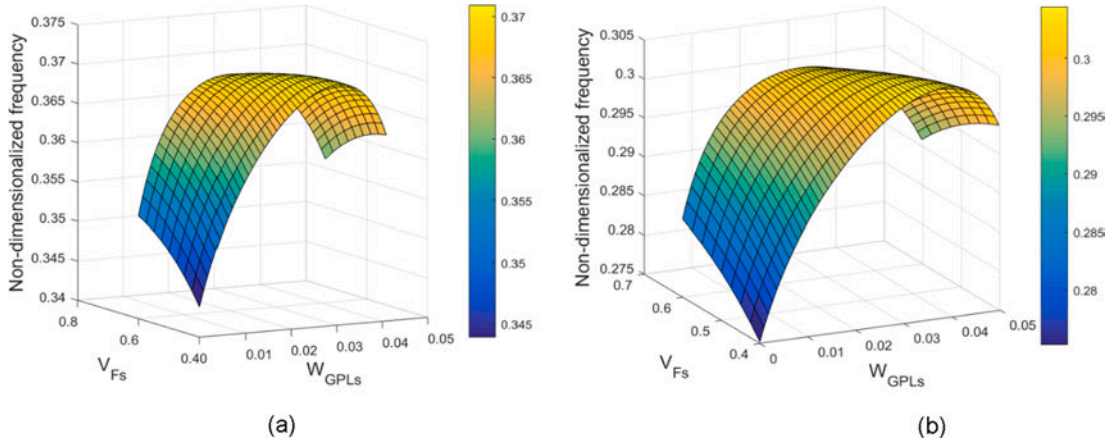

Fig. 6. Contour plots of the frequency for carbon fibre reinforced laminates with varying graphene weight and fibre volume contents of the outer layers for a) CCCC and b) SCSC boundary conditions.

Table 7
Maximum fundamental frequencies Ω of 8-layered laminates with zero graphene content and design variables as the fibre contents V_{Fi} of layers subject to $0.1 \leqslant V_{Fi} \leqslant 0.6$, $V_{Fmax} = 30\%$ with $D/a = 0.1$, $a/b = 1$ and stacking sequence $[0/90/0/90]_{\text{anti-s}}$

BCs		Optimal V_F	Ω	$\eta = \frac{\Omega_{max}}{\Omega_0}$	$\eta_2 = \frac{\Omega_{max}}{\Omega_{02}}$
SSSS	**Glass**	$[0.6 / 0.4 / 0.1 / 0.1]_s$	0.1079	0.731	1.202
	Carbon	$[0.57 / 0.43 / 0.1 / 0.1]_s$	0.1611	0.869	1.167
CCCC	**Glass**	$[0.6 / 0.4 / 0.1 / 0.1]_s$	0.1883	0.727	1.165
	Carbon	$[0.6 / 0.4 / 0.1 / 0.1]_s$	0.2508	0.755	1.113
SCSC	**Glass**	$[0.6 / 0.4 / 0.1 / 0.1]_s$	0.1533	0.727	1.173
	Carbon	$[0.6 / 0.4 / 0.1 / 0.1]_s$	0.2103	0.782	1.127

volume contents of the outer (surface) layers of the 8-layered laminate. The values of the graphene and fibre contents of the intermediate layers (layers 2 to 7) are taken from the optimization results shown in Table 6.

Both Fig. 5a and 5b indicate that there is an optimal graphene weight for the outer layer which maximizes the frequency. Exceeding this optimal value of the graphene weight leads to a decrease in the frequency. In the case of glass fibres (Fig. 5a), the maximum frequency is not sensitive to the change in the fibre volume content. However, for carbon fibres (Fig. 5b), when the graphene content is high, the lower fibre content results in higher frequency and increasing the fibre content results in lower frequency.

For glass fibres and CCCC or SCSC boundary conditions, similar patterns for the contour plots were observed. For carbon fibres and CCCC boundary conditions, the contour plot shown in Fig. 6a indicates that frequency is quite sensitive to change in the graphene weight around the maximum frequency as compared to SSSS boundary conditions (Fig. 5b). This becomes more pronounced for higher fibre volume contents and for the (more stiff) CCCC boundary conditions, followed by the SCSC boundary conditions (Fig. 6b).

To further investigate the contribution of graphene on maximizing the frequency, additional simulations with zero graphene weight have been performed. Two design efficiency factors are calculated for this case: a) $\eta = \frac{\Omega_{max}}{\Omega_0}$ where Ω_{max} is the optimal frequency and Ω_0 the reference frequency obtained for non-zero, uniform graphene weight

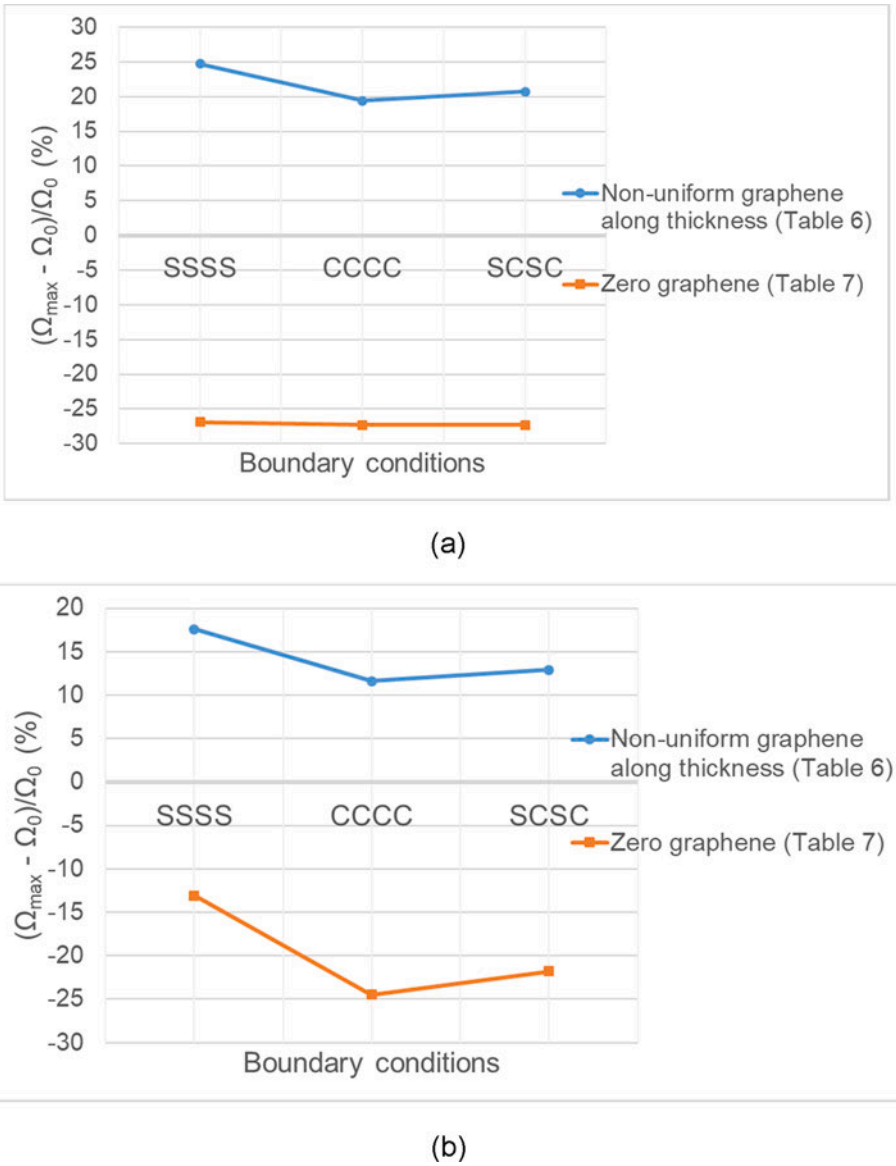

Fig. 7. Comparison between the maximum and the reference frequencies for three boundary conditions and a) glass, b) carbon fibres.

equal to 1.25% for all the layers of the laminate and b) $\eta_2 = \frac{\Omega_{max}}{\Omega_{02}}$ where the reference frequency Ω_{02} is obtained for zero graphene weight. The design efficiency factor η_2 shown in Table 7 indicates a significant increase of the fundamental frequency when the fibres are distributed optimally among the layers as compared to the frequency of a laminate with uniformly distributed fibres. The increase is observed to be greater in the case of glass fibre reinforced laminates as compared to the carbon fibre reinforced ones. When the efficiency factor η is examined in Table 7, it is observed that a significant reduction in the maximum frequency occurs in the absence of graphene reinforcement noting that the reference frequency Ω_0 refers to a laminate with uniformly distributed graphene of 1.25% volume content. The highest reduction in the frequency is observed in the case of glass fibres and CCCC and SCSC boundary conditions and it is equal to (1–0.727)/100 = 27.3%.

A more holistic insight on the positive contribution of the non-uniform distribution of graphene across the laminate thickness can be obtained by comparing the design efficiency factors in Table 6 (non-zero, non-uniform graphene distribution along thickness) and the factor η of Table 7 (zero graphene). Both factors are calculated using the same reference frequency Ω_0 which corresponds to uniform graphene distribution with a weight content of 1.25% for all layers. For glass fibres and CCCC boundary conditions, Table 6 indicates an increase of 20.2% of the maximum frequency with respect to the reference frequency. For the same case (glass fibres and CCCC), the reduction in the fundamental frequency with respect to the reference frequency Ω_0 obtained from Table 7 (1–0.727)/100 = 27.3%), a total increase equal to 20.2% + 27.3% = 47.5% of the optimal fundamental frequency with non-uniform graphene distribution arises, in comparison to zero graphene usage. Significant improvements in the vibration response also arise when the proposed non-uniform graphene distribution shown in Table 6 is used for all the cases presented in Tables 6 and 7.

To better represent the aforementioned improvement of the vibration behaviour of the composite laminate when a non-uniform graphene distribution is adopted, Fig. 7 represents the $(\Omega_{max}\text{-}\Omega_0)/\Omega_0$ (%) vs boundary conditions diagrams, obtained from Tables 6 and 7. The top line in each diagram represents the increase of the maximum frequency for the non-uniform graphene distribution shown in Table 6 with respect to the reference frequency (non-zero, uniform graphene) for glass and carbon fibres. The bottom line shows the corresponding percentage, representing the decrease of the maximum frequency obtained for zero graphene with respect to the reference frequency (non-zero, uniform graphene). The figure indicates that a significant increase of the

Table 8
Maximum fundamental frequencies Ω of 8-layered laminates with three design variables subject to $W_{GPLi} \geqslant 0$, $0.1 \leqslant V_{Fi} \leqslant 0.6$, $0.01 \leqslant h_i/D \leqslant 0.15$, $W_{GPLmax} = 1.25\%$, $V_{Fmax} = 30\%$ with $D/a = 0.1$, $a/b = 1$ and SSSS boundary conditions.

Stacking sequence	Fibres	Optimal W_{GPL}	Optimal V_F	h_i/D	Ω	$\eta = \frac{\Omega_{max}}{\Omega_0}$
$[0/90/0/90]_{anti\text{-}s}$	**Glass**	$[0.042/0.021/0/0]_s$	$[0.6/0.6/0.1/0.1]_s$	$[0.095/0.105/0.15/0.15]_s$	0.1892	1.281
	Carbon	$[0.041/0.02/0.003/0]_s$	$[0.6/0.6/0.1/0.1]_s$	$[0.08/0.12/0.15/0.15]_s$	0.2244	1.211
$[90/0/90/0]_s$	**Glass**	$[0.043/0.021/0/0]_s$	$[0.6/0.6/0.1/0.1]_s$	$[0.094/0.106/0.15/0.15]_s$	0.1892	1.280
	Carbon	$[0.043/0.021/0.003/0]_s$	$[0.6/0.6/0.1/0.1]_s$	$[0.07/0.13/0.15/0.15]_s$	0.2244	1.203

Table 9
Maximum fundamental frequencies Ω of 8-layered laminates with three design variables subject to $W_{GPLi} \geqslant 0$, $0.1 \leqslant V_{Fi} \leqslant 0.6$, $0.01 \leqslant h_i/D \leqslant 0.15$, $W_{GPLmax} = 1.25\%$. $V_{Fmax} = 30\%$ with $D/a = 0.1$, $a/b = 1$ and CCCC boundary conditions.

Stacking sequence	Fibres	Optimal W_{GPL}	Optimal V_F	h_i/D	Ω	$\eta = \frac{\Omega_{max}}{\Omega_0}$
$[0/90/0/90]_{anti\text{-}s}$	**Glass**	$[0.041/0.023/0/0]_s$	$[0.6/0.6/0.1/0.1]_s$	$[0.09/0.11/0.15/0.15]_s$	0,3146	1.214
	Carbon	$[0.019/0.014/0.021/0]_s$	$[0.6/0.6/0.1/0.1]_s$	$[0.08/0.12/0.15/0.15]_s$	0.3802	1.145
$[90/0/90/0]_s$	**Glass**	$[0.041/0.023/0/0]_s$	$[0.6/0.6/0.1/0.1]_s$	$[0.09/0.11/0.15/0.15]_s$	0,3146	1.214
	Carbon	$[0.103/0.008/0/0]_s$	$[0.1/0.6/0.27/0.1]_s$	$[0.05/0.15/0.15/0.15]_s$	0.3794	1.141

Table 10
Maximum fundamental frequencies Ω of 8-layered laminates with three design variables subject to $W_{GPLi} \geqslant 0$, $0.1 \leqslant V_{Fi} \leqslant 0.6$, $0.01 \leqslant h_i/D \leqslant 0.15$, $W_{GPLmax} = 1.25\%$, $V_{Fmax} = 30\%$ with $D/a = 0.1$, $a/b = 1$ and SCSC boundary conditions.

Stacking sequence	Fibres	Optimal W_{GPL}	Optimal V_F	Optimal h_i/D	Ω	$\eta = \frac{\Omega_{max}}{\Omega_0}$
$[0/90/0/90]_{anti\text{-}s}$	**Glass**	$[0.041/0.023/0/0]_s$	$[0.6/0.6/0.1/0.1]_s$	$[0.09/0.11/0.15/0.15]_s$	0.2595	1.230
	Carbon	$[0.109/0.006/0/0]_s$	$[0.1/0.6/0.27/0.1]_s$	$[0.05/0.15/0.15/0.15]_s$	0.3082	1.146
$[90/0/90/0]_s$	**Glass**	$[0.057/0.014/0/0]_s$	$[0.45/0.6/0.1/0.1]_s$	$[0.07/0.15/0.13/0.15]_s$	0.2614	1.254
	Carbon	$[0.093/0.011/0/0]_s$	$[0.1/0.6/0.27/0.1]_s$	$[0.05/0.15/0.15/0.15]_s$	0.3282	1.272

fundamental frequency corresponding to the non-uniform graphene distribution is observed for all cases as compared to zero graphene content. For glass fibres, this increase may reach 51% (SSSS) and is not less than 46% (CCCC). For carbon fibres the maximum increase is 36% (CCCC) and the minimum 30% (SSSS).

7.3. Graphene and fibre contents and layer thicknesses as design variables

Next, in addition to the two design variables of graphene and fibre contents studied so far, another design variable, namely, the layer thicknesses are included as design variables. This leads to optimal design for maximum frequency with three design variables. The results of the optimization with these design variables are shown in Tables 8, 9 and 10 corresponding to the three boundary conditions of SSSS, CCCC and SCSC, respectively.

Comparison between the results presented in Tables 8-10 (including non-uniform layer thicknesses) and Table 6 (with uniform layer thicknesses) indicates that the efficiency factor increases with the addition of layer thicknesses to design variables as expected. The minimum increase is 1.2% (CCCC-glass fibres) and the maximum increase is 2.8% (CCCC-carbon fibres). In the majority of the cases, the layers close to laminate surface receive a higher graphene content with an increase in the thicknesses of the middle layers. Thus, the optimal designs correspond to a reduced thickness in the surface layers which have increased graphene content compared to the cases of uniform layer thicknesses as observed in Table 6.

Moreover, for SCSC boundary conditions and carbon fibres, the symmetric stacking sequence results in significantly higher efficiency factor as compared to the anti-symmetric case. For the other boundary conditions, both stacking sequences result in similar efficiency factors.

7.4. Graphene and fibre contents, layer thicknesses and fibre orientations as design variables

In view of the importance of fibre orientations in the design of composite laminates, fibre angles are now introduced as the fourth set of design variables in addition to graphene and fibre contents and layer thicknesses. This leads to an optimal design problem with four design variables.

Results of this optimization problem are shown in Table 11. It is observed that the optimal designs for different boundary conditions result in different stacking sequences as expected. Similar to the previous cases, higher graphene weights are allocated to outer layers. Comparison between the results presented in Tables 8-10 (cross-ply laminates) indicates a further increase of the fundamental frequency for SSSS and SCSC boundary conditions. This increase is quite significant for SSSS boundary conditions (+7.8% for glass and + 18.4% for carbon fibres) and for SCSC-carbon fibres (+10.8%). It is noted that the design efficiency factors shown in Table 11 are calculated for a reference frequency obtained by using the anti-symmetric, cross-ply stacking sequence, and therefore efficiency comparisons between Table 11 and Tables 8-10 are based on this stacking sequence. For CCCC boundary conditions no increase of the design efficiency is observed, indicating that the cross-ply stacking sequence used in Table 9 results in the optimal vibration response.

A final investigation is conducted by assessing the effect of the variation of the fibre angles of the two outer layers on the fundamental frequency and the corresponding sensitivities. The reason the top two outer layers are chosen for this purpose is because the outer layers contribute most to the stiffness of the laminate. This work is done by means of contour plots of the frequencies with respect to fibre orientations. In the contour plots shown in Figs. 8-10, the problem parameters

Table 11
Maximum fundamental frequencies Ω of 8-layered laminates with four design variables subject to $W_{GPLi} \geqslant 0$, $0.1 \leqslant V_{Fi} \leqslant 0.6$, $0.01 \leqslant h_i/D \leqslant 0.15$, $-90^\circ \leqslant \theta_i \leqslant 90^\circ$, $W_{GPLmax} = 1.25\%$, $V_{Fmax} = 30\%$ with $D/a = 0.1$, $a/b = 1$.

Boundary conditions	Fibres	Optimal W_{GPL}	Optimal V_F	h_i/D	θ_i	Ω	$\eta = \frac{\Omega_{max}}{\Omega_0}$
SSSS	**Glass**	$[0.110/0.005/0/0]_s$	$[0.10/0.60/0.27/0.10]_s$	$[0.05/0.15/0.15/0.15]_s$	$[45/-45/45/45]_s$	0.2006	1.359
	Carbon	$[0.119/0.003/0/0]_s$	$[0.10/0.60/0.27/0.10]_s$	$[0.05/0.15/0.15/0.15]_s$	$[45/-45/45/45]_s$	0.2586	1.395
CCCC	**Glass**	$[0.041/0.023/0/0]_s$	$[0.6/0.6/0.1/0.1]_s$	$[0.09/0.11/0.15/0.15]_s$	$[0/90/0/90]_s$	0.3146	1.214
	Carbon	$[0.019/0.014/0.021/0]_s$	$[0.6/0.6/0.1/0.1]_s$	$[0.07/0.13/0.15/0.15]_s$	$[0/90/0/90]_s$	0.3802	1.145
SCSC	**Glass**	$[0.057/0.015/0/0]_s$	$[0.46/0.6/0.1/0.1]_s$	$[0.07/0.15/0.15/0.13]_s$	$[0/0/0/0]_s$	0.2625	1.244
	Carbon	$[0.087/0.012/0.001/0]_s$	$[0.10/0.60/0.27/0.10]_s$	$[0.05/0.15/0.15/0.15]_s$	$[0/0/0/0]_s$	0.3372	1.254

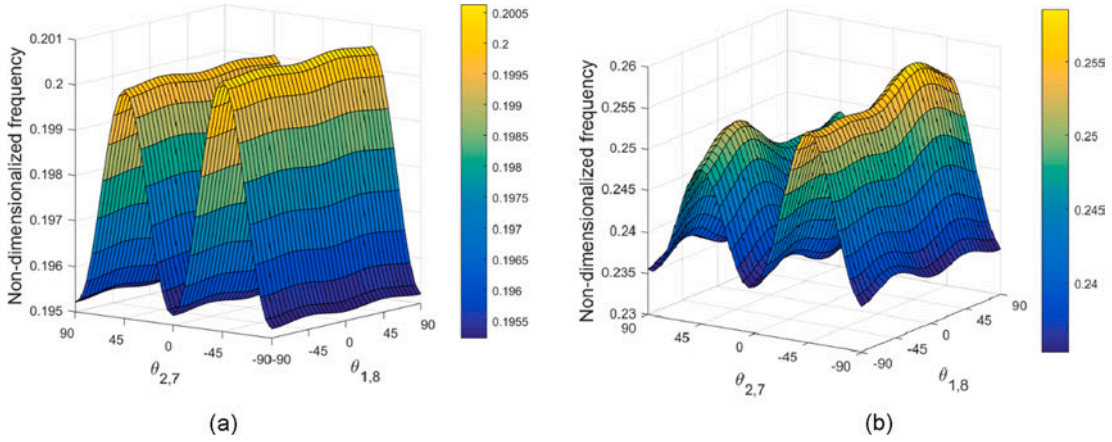

Fig 8. Contour plots of the frequency with respect to the fibres angles of the two outer layers for SSSS boundary conditions, a) glass fibres, b) carbon fibres.

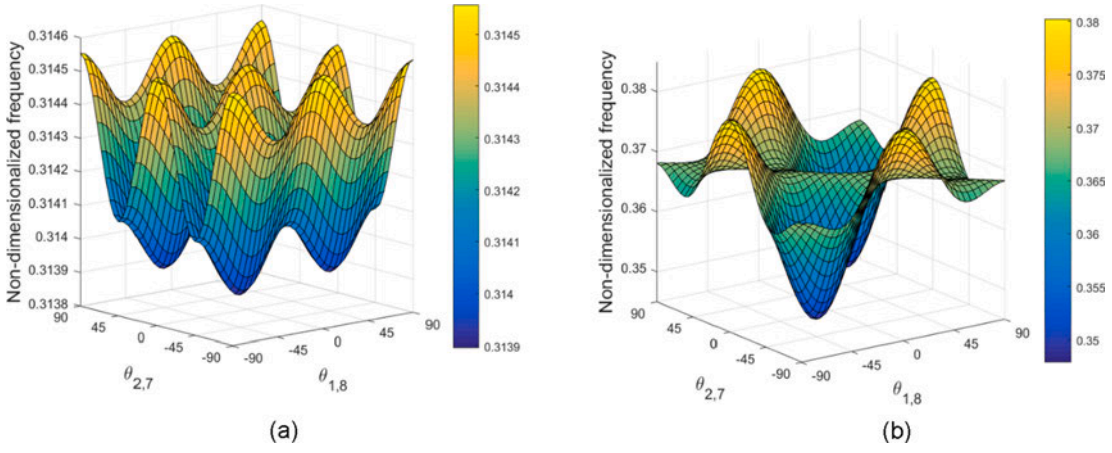

Fig 9. Contour plots of the frequency with respect to the fibres angles of the two outer layers for CCCC boundary conditions, a) glass fibres, b) carbon fibres.

have been assigned their optimal values presented in Table 11 in all layers except the top two outer layers. Thus, the only parameters which vary in these plots are the fibre angles of the outer layers, that is, θ_1 and θ_8 of the top and bottom layers, and θ_2 and θ_7 of the second outer layers.

Comparisons between the optimal solutions presented in Table 11 and Figs. 8-10 confirms the optimization solution and the corresponding angles $\theta_{1,8}$ and $\theta_{2,7}$ in every case. It is also observed that different boundary conditions result in different shapes of the contour plots as expected. Thus CCCC boundary conditions lead to multiple optimal points. For SSSS and SCSC boundary conditions, a single optimal point is observed and this point is more prominent in the case of carbon fibre reinforced laminates. This leads to the observation that when glass fibres are used for reinforcement, the difference between the minimum and the maximum values of the frequency is relatively small as compared to the case of carbon fibres.

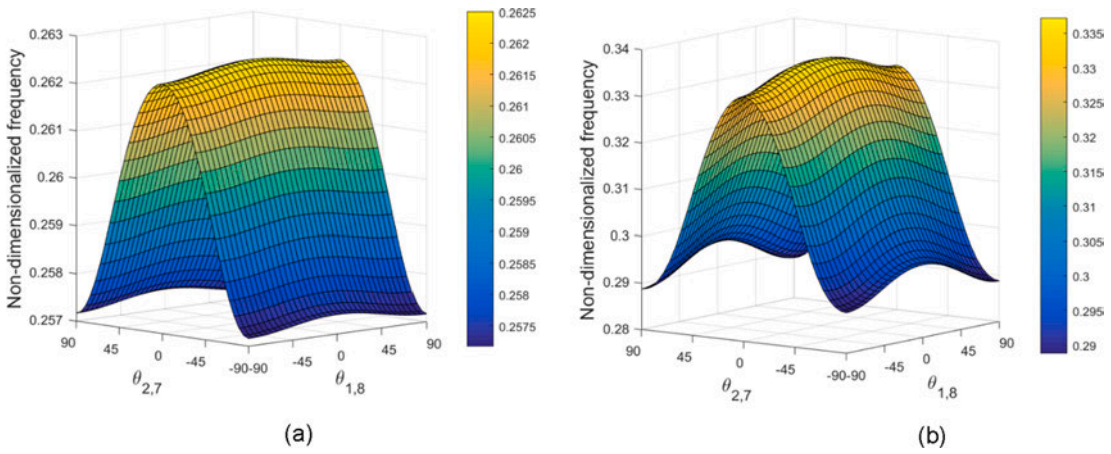

Fig 10. Contour plot of the frequency with respect to the fibres angles of the two outer layers for SCSC boundary conditions, a) glass fibres, b) carbon fibres.

8. Conclusions

Optimal design and analysis of a hybrid graphene/fibre reinforced composite laminate for maximum fundamental frequency was the subject of the present study. The composite material is defined as a three-phase nanocomposite consisting of graphene nanoplatelets, fibres and polymer matrix. The main objective was the study of the vibration response and optimization of this multiscale laminate combining a nano-scale reinforcement (graphene) within the traditional fibre reinforced matrix and the effect of the graphene content on the maximum frequency. To achieve a cost-effective design, the optimal distributions of the constituent materials along the thickness of the structure as well as optimal layer thicknesses are investigated to maximize the fundamental frequency.

For the implementation of the optimization scheme, a Sequential Quadratic Programming algorithm (SQP) was adopted. The natural vibration problem is solved within the framework of the finite element method using the First Order Shear Deformation plate theory (FSDT). Three different boundary conditions, namely, SSSS, CCCC and SCSC are investigated to assess their effect on the optimal designs. Effective properties of three-phase composite are obtained from micromechanics equations applicable to graphene and fibre reinforced polymers. The numerical results are given for symmetric and anti-symmetric 8-layered laminates.

Among the main findings of the study is the optimal distributions of graphene and fibre reinforcements along the thickness of the laminate. It is observed that a non-uniform distribution of graphene platelets, with higher graphene contents in the surface layers and lower or zero graphene contents in the middle layers, results in the optimal distribution of the graphene. When the fibre volume contents are also included as design variables, a similar pattern of optimal fibre distribution is observed, that is, higher fibre contents in the outer layers and the less fibre content in the middle layers.

A design efficiency factor is introduced which is defined as the ratio of the fundamental frequency of the optimally designed laminate over a reference frequency based on uniform distributions of the reinforcements and uniform layer thicknesses. This provides a quantitative measurement of the positive effect of the non-uniformly distributed reinforcements leading to optimal designs. When the layer thicknesses and the fibre angles are also included as design variables of the optimization problem, the design efficiency factors indicate a further increase in the fundamental frequency as expected.

Some specific conclusions are presented below:

a) Increasing graphene weight is more effective in improving the fundamental frequencies for lower fibre volume contents (Figs. 2 and 3).
b) When the graphene contents of layers are the only design variables of the optimization problem and a uniform fibre distribution along the thickness is adopted, a higher graphene content results in the outer layers as expected. The highest increase of the fundamental frequency with respect to the reference frequency is 19.6%. This corresponds to a symmetric cross-ply laminate with glass fibres of 30% volume content. The corresponding increase when 30% of carbon fibres is used is 10.8%. This is due to the fact that glass fibres have lower stiffness and graphene becomes more effective in improving the maximum frequency while carbon fibres have higher stiffness and addition of graphene is, relatively speaking, not as efficient as it was in the case of glass fibres.
c) For the case of optimal distribution of graphene (same as case b), the increase in the fundamental frequency when fibre volume content is 60% (instead of 30% as in case b), is half in the case of glass fibre reinforcement and one third for carbon fibre reinforcement. This indicates that the graphene reinforcement is more efficient at lower fibre contents.
d) It was observed that a higher design efficiency factor was obtained when glass instead of carbon fibres are used. This is attributed to the lower stiffness of glass fibres which results in higher contribution of graphene platelets to the fundamental frequency.
e) When both graphene and fibre reinforcements are specified as design variables, a non-uniform distribution along the thickness arises for both reinforcements. The optimal non-uniform fibre distributions result in significantly increased frequencies in comparison to uniform fibre distributions.
f) The highest increase of the fundamental frequency with respect to the reference frequency is 26.2% in the case of SSSS boundary conditions. CCCC boundary conditions result in the lowest increase in the design efficiency. This can be attributed to the fact that for CCCC boundary conditions, the fundamental frequencies are already relatively high compared to the case of SSSS boundary conditions.
g) When zero and non-zero graphene reinforcements are compared, results indicate that a large increase in the fundamental frequency is observed relative to case with zero graphene content compared to the case of non-uniformly distributed graphene. This increase reaches 51% in the case of additional reinforcements with glass fibre and 36% with carbon fibres.
h) When the layer thicknesses are specified as further design variables (in addition to graphene and fibre volume contents), a relatively small increase in the design efficiency factor is observed which is 1.2% for CCCC-glass fibres and 2.8% for CCCC-carbon fibres.
i) For the case of three design variables involving graphene and fibre contents of layers and the layer thicknesses, the fundamental frequency is 28.1% higher compared to the reference frequency in the case of glass fibre reinforced laminates with SSSS boundary

conditions compared to 26.2% for the case of uniform layer thickness (two sets of design variables). The corresponding increase is 19.6% in the case of uniform layer thicknesses and uniform fibre contents with the graphene contents of layers being the only design variables.

j) When the fibre angles are also included as the design variables in addition to the previous set of three design variables (graphene and fibre contents and thicknesses of layers), a significant increase in the design efficiency factor is observed. These increases are 7.8% for GFRP and 18.4% for CFRP laminates with SSSS boundary conditions. and 10.8% for CFRP laminates with SCSC boundary conditions.

k) For this case (four sets of design variables) and SSSS boundary conditions, the increase of the fundamental frequency with respect to the reference frequency reaches 35.9% for GFRP and 39.5% for CFRP laminates.

Future research on three-phase nanocomposites is to include the investigation of functionally graded nanomaterials where the graphene weight varies along the thickness of the laminate which may be a pre-defined distribution or an optimally determined continuous distribution. In addition, a non-constant graphene distribution in each layer may also result in an improved design and a cost-effective use of the expensive graphene reinforcement. Finally, more advanced theories and bounds for the micromechanical formulations presented in literature [66,67], can be adopted and compared for three-phase composites.

CRediT authorship contribution statement

Y. Jeawon: Formal analysis, Investigation, Writing - original draft. **G.A. Drosopoulos:** Conceptualization, Supervision, Validation, Writing - review & editing. **G. Foutsitzi:** Methodology, Software, Data curation. **G.E. Stavroulakis:** Methodology, Software, Data curation. **S. Adali:** Methodology, Resources, Writing - review & editing.

Declaration of Competing Interest

The authors declared that there is no conflict of interest.

Appendix

1. Strain energy

The strain energy of the laminated composite plate is expressed as

$$U=\frac{1}{2}\int_{V_e}\left(\{\varepsilon_{b0}\}^T\left[\overline{Q_b}\right]\{\varepsilon_{b0}\}+\{\varepsilon_{b0}\}^T z\left[\overline{Q_b}\right]\{\kappa\}+\{\kappa\}^T z\left[\overline{Q_b}\right]\{\varepsilon_{b0}\}+\{\kappa\}^T z^2\left[\overline{Q_b}\right]\{\kappa\}+\{\varepsilon_{s0}\}^T\left[\overline{Q_s}\right]\{\varepsilon_{s0}\}\right)dV=$$

$$=\frac{1}{2}\int_{V_e}\left\{\begin{matrix}\{\varepsilon_{b0}\}\\ \{\kappa\}\\ \{\varepsilon_{s0}\}\end{matrix}\right\}^T\left[\begin{matrix}\left[\overline{Q_b}\right] & z\left[\overline{Q_b}\right] & 0\\ z\left[\overline{Q_b}\right] & z^2\left[\overline{Q_b}\right] & 0\\ 0 & 0 & \left[\overline{Q_s}\right]\end{matrix}\right]\left\{\begin{matrix}\{\varepsilon_{b0}\}\\ \{\kappa\}\\ \{\varepsilon_{s0}\}\end{matrix}\right\}dV=\frac{1}{2}\int_{V_e}\{\bar{\varepsilon}\}^T[C(z)]\{\bar{\varepsilon}\}dV \tag{A1}$$

where V_e is the volume of an element. Substituting for $\{\varepsilon_{b0}\}$, $\{\kappa\}$ and $\{\varepsilon_{s0}\}$ in the above equation, U can be written as

$$U=\frac{1}{2}\{d\}_e^T[K]_e\{d\}_e \tag{A2}$$

where

$$[K]_e=\sum_{k=1}^{N}\left[\int_{V_k}[B]^T[C(z)]_k[B]dV_k\right] \tag{A3}$$

In equation (A3) V_k is the volume of the k^{th} layer, N is the number of lamina, $[C]$ is the elasticity tensor and $[B]$ is the strain – displacement matrix.

2. Kinetic energy

The kinetic energy of the composite plate is expressed as

$$T=\frac{1}{2}\sum_{k=1}^{N}\left(\int_{V_k}\rho_k\left[\left\{\dot{u}_1\right\}^2+\left\{\dot{u}_2\right\}^2+\left\{\dot{u}_3\right\}^2\right]dV_k\right), \tag{A4}$$

where ρ_k is the density of the k^{th} layer. Substituting the displacements relations of Eq. (1), Eq. (A4) becomes

$$T=\frac{1}{2}\sum_{k=1}^{N}\left(\int_{V_k}\rho_k\left[\dot{u}^2+2z\dot{u}\dot{\varphi}_x+\dot{v}^2+2z\dot{v}\dot{\varphi}_y+\dot{w}^2+z^2\dot{\varphi}_x^2+z^2\dot{\varphi}_y^2\right]dV_k\right)=\frac{1}{2}\sum_{k=1}^{N}\int_{V_k}\left\{\begin{matrix}u\\ v\\ w\\ \varphi_x\\ \varphi_y\end{matrix}\right\}^T\rho_k\left[\begin{matrix}1 & 0 & 0 & -z & 0\\ 0 & 1 & 0 & 0 & -z\\ 0 & 0 & 1 & 0 & 0\\ -z & 0 & 0 & z^2 & 0\\ 0 & -z & 0 & 0 & z^2\end{matrix}\right]\left\{\begin{matrix}u\\ v\\ w\\ \varphi_x\\ \varphi_y\end{matrix}\right\}dV_k$$

$$=\sum_{k=1}^{N}\frac{1}{2}\int_{V_k}\left\{\dot{\bar{u}}\right\}^T[I(z)]_k\left\{\dot{\bar{u}}\right\}dV_k \tag{A5}$$

Equation (A5) then becomes:

$$T=\frac{1}{2}\left\{\dot{d}\right\}^T[M]_e\left\{\dot{d}\right\} \tag{A6}$$

where

$$[M]_e = \int_{A_e} \sum_{k=1}^{N} \int_{z_{k-1}}^{z_k} [N]^T [I(z)]_k [N] dz dA \tag{A7}$$

where A_e is the area of the element and z_{k-1}, z_k are the z coordinates of the laminate corresponding to the bottom and top surface of the k^{th} layer.

3. Work done by the mechanical forces

The work done by the mechanical forces is given by

$$W = \{\overline{u}\}^T \{f_c\} + \int_{S_1} \{\overline{u}\}^T \{f_s^{(i)}\} dS + \int_V \{\overline{u}\}^T \{f_v\} dV = \{d\}_e^T [N]^T \{f_c\} + \{d\}_e^T \int_{S_1} [N]^T \{f_s^{(i)}\} dS + \{d\}_e^T \int_V [N]^T \{f_v\} dV \equiv \{d\}_e^T \{F_m\}_e \tag{A8}$$

In Equation (A8), $\{f_c\}$ denotes the concentrated forces and $\{f_s\}$, $\{f_v\}$ denote the surface and volume forces, respectively. S_1 is the surface area, V is the volume and $\{F_m\}_e$ is the vector of the applied mechanical forces on an element.

References

[1] Ebrahimi F (Ed.). Nanocomposites - New Trends and Developments. Intech, Rijeka, Croatia, 2012.
[2] Reddy B. (Ed.). Advances in Diverse Industrial Applications of Nanocomposites. Intech, Rijeka, Croatia, 2011.
[3] Gao F. (Ed.). Advances in polymer nanocomposites - Types and applications. Woodhead Publishing Limited, Cambridge, UK, 2012.
[4] Mittal V. (Ed.). Polymer-Graphene Nanocomposites. The Royal Society of Chemistry 2012, Cambridge, UK.
[5] Zhao S, Zhao Z, Yang Z, Ke L, Kitipornchai S, Yang J. Functionally graded graphene reinforced composite structures: A review. Eng Struct 2020;210:110339.
[6] Mohan VB, Lau K, Hui D, Bhattacharyya D. Graphene-based materials and their composites: A review on production, applications and product limitations. Compos Part B: Eng 2018;1421:200–20.
[7] Tairidis GK, Foutsitzi G, Stavroulakis GE. Optimal design of smart composites. In Demetriou IC, Pardalos PM, editors. Approximation and Optimization. Algorithms, Complexity and Applications. Springer, Cham, 2019.
[8] Narita Y. Layerwise optimization for the maximum fundamental frequency of laminated composite plates. J Sound Vib 2003;263(5):1005–16.
[9] Liu Q. Exact sensitivity analysis of stresses and lightweight design of Timoshenko composite beams. Compos Struct 2016;143:272–86.
[10] Kuo S-Y. Thermal buckling, vibration and flutter of composite laminates containing two non-uniformly distributed fibers. J Aeronautics Astronautics Aviation 2016;48 (3):173–82.
[11] Vo-Duy T, Ho-Huu V, Do-Thi TD, Dang-Trung H, Nguyen-Thoi T. A global numerical approach for lightweight design optimization of laminated composite plates subjected to frequency constraints. Compos Struct 2017;159:646–55.
[12] Shi G, Araby S, Gibson CT, Meng Q, Zhu S, Ma J. Graphene platelets and their polymer composites: fabrication, structure, properties and applications. Adv Funct Mater 2018;28(19):1–44.
[13] Cataldi P, Athanassiou A, Bayer I. Graphene nanoplatelets-based advanced materials and recent progress in sustainable applications. Appl Sci 2018;8(9):1–35.
[14] Ray SC. Applications of Graphene and Graphene-Oxide Based Nanomaterials. Oxford, UK: Elsevier; 2015.
[15] Lee C, Wei X, Kysar JW, Hone J. Measurement of the elastic properties and intrinsic strength of monolayer graphene. Science 2008;321(5887):385–8.
[16] Rafiee MA, Rafiee J, Wang Z, Song H, Yu Z-Z, Koratkar N. Enhanced mechanical properties of nanocomposites at low graphene content. ACS Nano 2009;3(12): 3884–90.
[17] Tang LC, Wan YJ, Yan D, Pei YB, Zhao L, Li YB, et al. The effect of graphene dispersion on the mechanical properties of graphene/epoxy composites. Carbon 2013;60:16–27.
[18] Young RJ, Liu M, Kinloch IA, Li S, Zhao X, Vallés C, et al. The mechanics of reinforcement of polymers by graphene nanoplatelets. Compos Sci Technol 2018; 154:110–6.
[19] Thai CH, Ferreira AJM, Tran TD, Phung-Van P. Free vibration, buckling and bending analyses of multilayer functionally graded graphene nanoplatelets reinforced composite plates using the NURBS formulation. Compos Struct 2019; 220:749–59.
[20] Mohamad N, Yaakub J, Ab Maulod HE, Jeefferie AR, Yuhazri MY, Lau KT, et al. Vibrational damping behaviors of graphene nanoplatelets reinforced NR/EPDM nanocomposites. J Mech Eng Sci 2017;11:3274–87.
[21] Duffy KJ, Adali S. Optimal fibre orientation of antisymmetric hybrid laminates for maximum fundamental frequency and frequency separation. J Sound Vib 1991;146 (2):181–90.
[22] An H, Chen S, Huang H. Multi-objective optimal design of hybrid composite laminates for minimum cost and maximum fundamental frequency and frequency gaps. Compos Struct 2019;209:268–76.
[23] Pashmforoush F. Statistical analysis on free vibration behavior of functionally graded nanocomposite plates reinforced by graphene platelets. Compos Struct 2019;213:14–24.
[24] Feng C, Kitipornchai S, Yang J. Nonlinear free vibration of functionally graded polymer composite beams reinforced with graphene nanoplatelets (GPLs). Eng Struct 2017;140:110–9.
[25] Rout M, Hota SS, Karmakar A. Thermoelastic free vibration response of graphene reinforced laminated composite shells. Eng Struct 2019;178:179–90.
[26] Reddy RMR, Karunasena W, Lokuge W. Free vibration of functionally graded-GPL reinforced composite plates with different boundary conditions. Aerosp Sci Technol 2018;78:147–56.
[27] Guo H, Cao S, Yang T, Chen Y. Vibration of laminated composite quadrilateral plates reinforced with graphene nanoplatelets using the element-free IMLS-Ritz method. Int J Mech Sci 2018;142:610–21.
[28] Gholami R, Ansari R. Nonlinear harmonically excited vibration of third-order shear deformable functionally graded graphene platelet-reinforced composite rectangular plates. Eng Struct 2018;156:197–209.
[29] Xu Z, Huang Q. Vibro-acoustic analysis of functionally graded graphene-reinforced nanocomposite laminated plates under thermal-mechanical loads. Eng Struct 2019; 186:345–55.
[30] Kiani Y. Isogeometric large amplitude free vibration of graphene reinforced laminated plates in thermal environment using NURBS formulation. Comput Methods Appl Mech Eng 2018;332:86–101.
[31] Fazzolari FA. Elastic buckling and vibration analysis of FG polymer composite plates embedding graphene nanoplatelet reinforcements in thermal environment. Mech Adv Mater Struct 2019. https://doi.org/10.1080/15376494.2019.1567886.
[32] Saidi AR, Bahaadini R, Majidi-Mozafari K. On vibration and stability analysis of porous plates reinforced by graphene platelets under aerodynamical loading. Compos Part B: Eng 2019;164:778–99.
[33] Bekyarova E, Thostenson ET, Yu A, Kim H, Gao J, Tang J, et al. Multiscale carbon nanotube-carbon fiber reinforcement for advanced epoxy composites. Langmuir 2007;23:3970–4.
[34] Papageorgiou DG, Li Z, Liu M, Kinloch IA, Young RJ. Mechanisms of mechanical reinforcement by graphene and carbon nanotubes in polymer nanocomposites. Nanoscale 2020;12:2228–67.
[35] Yang X, Wang Z, Xu M, Zhao R, Liu X. Dramatic mechanical and thermal increments of thermoplastic composites by multi-scale synergetic reinforcement: Carbon fiber and graphene nanoplatelets. Mater Des 2013;44:74–80.
[36] Hadden CM, Klimek-McDonald DR, Pineda EJ, King JA, Reichanadter AM, Miskioglu I, et al. Mechanical properties of graphene, nanoplatelet/carbon fiber/ epoxy hybrid composites: Multiscale modeling and experiments. Carbon 2015;95: 100–12.
[37] Aluko O, Gowtham S, Odegard GM. Multiscale modeling and analysis of graphene nanoplatelet/carbon fiber/epoxy hybrid composite. Compos Part B: Eng 2017;131: 82–90.
[38] Imran KA, Shivakumar KN. Graphene-modified carbon/epoxy nanocomposites: Electrical, thermal and mechanical properties. J Compos Mater 2019;53(1): 93–106.
[39] Al Mahmud H, Radue MS, Chinkanjanarot S, Pisani WA, Gowtham S, Odegard GM. Multiscale modeling of carbon fiber-graphene nanoplatelet-epoxy hybrid composites using a reactive force field. Compos Part B: Eng 2019;172:628–35.
[40] Rafiee M, Nitzsche F, Labrosse MR. Modeling and mechanical analysis of multiscale fiber-reinforced graphene composites: Nonlinear bending, thermal post-buckling and large amplitude. Int J Non Linear Mech 2018;103:104–12.
[41] Gholami R, Ansari R, Gholami Y. Numerical study on the nonlinear resonant dynamics of carbon nanotube/fiber/polymer multiscale laminated composite rectangular plates with various boundary conditions. Aerosp Sci Technol 2018;78: 118–29.
[42] Ebrahimi F, Dabbagh A. Vibration analysis of multi-scale hybrid nanocomposite plates based on a Halpin-Tsai homogenization model. Compos Part B: Eng 2019; 173:106955.
[43] Radebe IS, Drosopoulos GA, Adali S. Buckling of non-uniformly distributed graphene and fibre reinforced multiscale angle-ply laminates. Meccanica 2019;54: 2263–79.
[44] An H, Chen S, Huang H. Maximization of fundamental frequency and buckling load for the optimal stacking sequence design of laminated composite structures. Proc Institution of Mechanical Engineers, Part L: J Materials: Design Appl 2018. 146442071876502.
[45] Kayikci R, Sonmez FO. Design of composite laminates for optimum frequency response. J Sound Vib 2012;331(8):1759–76.

[46] Apalak MK, Karaboga D, Akay B. The Artificial Bee Colony algorithm in layer optimization for the maximum fundamental frequency of symmetrical laminated composite plates. Eng Optim 2014;46(3):420–37.
[47] Sadr MH, Ghashochi BH. Optimization of laminated composite plates for maximum fundamental frequency using Elitist-Genetic algorithm and finite strip method. J Global Optim 2011;54(4):707–28.
[48] Kamarian S, Shakeri M, Karimi B, Pourasghar A. Free vibration analysis and design optimization of nanocomposite-laminated beams using various higher order beam theories and imperialist competitive algorithm. Polym Compos 2015;37(8): 2442–51.
[49] Kamarian S, Shakeri M, Yas MH. Natural frequency analysis and optimal design of CNT/fiber/polymer hybrid composites plates using Mori-Tanaka approach, GDQ technique, and firefly algorithm. Polym Compos 2016;39(5):1433–46.
[50] Reddy JN. Mechanics of Laminated Composite Plates and Shells. 2nd ed. CRC Press; 2004.
[51] Higham NJ. Cholesky factorization. In: Padua D, (editor). Encyclopedia of Parallel Computing. Springer, 2011 Boston, MA.
[52] MATLAB. (2016). version 9.0.0.341360 (R2016a). Natick, Massachusetts: The MathWorks Inc.
[53] Gill PE, Murray W, Wright MH. Numerical Linear Algebra and Optimization. Addison Wesley; 1991.
[54] Huang Y, Yang Z, Liu A, Fu J. Nonlinear buckling analysis of functionally graded graphene reinforced composite shallow arches with elastic rotational constraints under uniform radial load. Mater 2018;11(6):910.
[55] Yang J, Chen D, Kitipornchai S. Buckling and free vibration analyses of functionally graded graphene reinforced porous nanocomposite plates based on Chebyshev-Ritz method. Compos Struct 2018;193:281–94.
[56] Chen D, Yang J, Kitipornchai S. Nonlinear vibration and postbuckling of functionally graded graphene reinforced porous nanocomposite beams. Compos Science Tech 2017;142:235–45.
[57] Yang J, Wu H, Kitipornchai S. Buckling and postbuckling of functionally graded multilayer graphene platelet-reinforced composite beams. Compos Struct 2017; 161:111–8.
[58] Shen H-S. A comparison of buckling and postbuckling behavior of FGM plates with piezoelectric fiber reinforced composite actuators. Compos Struct 2009;91:375–84.
[59] Song M, Yang J, Kitipornchai S, Zhu W. Buckling and postbuckling of biaxially compressed functionally graded multilayer graphene nanoplatelet-reinforced polymer composite plates. Int J Mech Sci 2017;131–132:345–55.
[60] Wang Y, Feng C, Zhao Z, Yang J. Eigenvalue buckling of functionally graded cylindrical shells reinforced with graphene platelets (GPL). Compos Struct 2018; 202:38–46.
[61] Wang Y, Feng C, Zhao Z, Yang J. Buckling of graphene platelet reinforced composite cylindrical shell with cutout. International Journal of Structural Stability and Dynamics 2018;18(03):1850040:1-17.
[62] Nocedal J, Wright SJ. Numerical Optimization. Springer Series in Operations Research and Financial Engineering. Springer; 2006.
[63] Zabinsky ZB. Optimal design of composite structures. In: Floudas CA, Pardalos PM, editors. Encyclopedia of Optimization. Kluwer Academic Publishers; 2001. p. 153–60.
[64] Papalambros PY, Wilde DJ. Principles of Optimal Design. Modeling and Computation: Cambridge University Press; 2017.
[65] Song M, Kitipornchai S, Yang J. Free and forced vibrations of functionally graded polymer composite plates reinforced with graphene nanoplatelets. Compos Struct 2017;159:579–88.
[66] Kanaun SK, Jeulin D. Elastic properties of hybrid composites by the effective field approach. J Mech Phy Solids 2001;49:2339–67.
[67] Genin GM, Birman V. Micromechanics and structural response of functionally graded, particulate-matrix, fiber-reinforced composites. Int J Solids Struct 2009;46 (10):2136–50.

Chapter 5: Optimization of Graphene/Fibre Reinforced Cantilever Skew Laminates for Maximum Fundamental Frequency via Non-Uniform Distribution of Reinforcements

Thin-Walled Structures 189 (2023) 110903

Contents lists available at ScienceDirect

Thin-Walled Structures

journal homepage: www.elsevier.com/locate/tws

Full length article

Optimization of graphene/fibre reinforced cantilever skew laminates for maximum fundamental frequency via non-uniform distribution of reinforcements

Y. Jeawon [a], G.A. Drosopoulos [b,a,*], G. Foutsitzi [c], G.E. Stavroulakis [d], S. Adali [e]

[a] Discipline of Civil Engineering, University of KwaZulu-Natal, Durban, South Africa
[b] Discipline of Civil Engineering, University of Central Lancashire, Preston, UK
[c] Department of Informatics and Telecommunications, University of Ioannina, Ioannina, Greece
[d] School of Production Engineering and Management, Technical University of Crete, Chania, Greece
[e] Discipline of Mechanical Engineering, University of KwaZulu-Natal, Durban, South Africa

ARTICLE INFO

Keywords:
Optimal design
Graphene reinforcement
Vibration
Finite element analysis
Skew cantilever laminates

ABSTRACT

Three-phase graphene/fibre-reinforced cantilever skew laminates are optimized with the design objective of maximizing the fundamental frequency. Four optimal design problems are formulated involving one, two, three, and four design variables: graphene content, fibre content, layer thicknesses, and the fibre orientations. Optimization is implemented using a Sequential Quadratic Programming optimization algorithm within finite element analysis. It is observed that optimizing the graphene and fibre contents across the thickness leads to increased fundamental frequency. A trend is observed for the frequency of skew laminates to increase but for their design efficiency to decrease compared to rectangular laminates.

1. Introduction

The use of laminated rectangular and skew plates as structural components has increased due to their significant advantages. These include high strength/weight and high stiffness/weight ratios compared to conventional materials. Composite plates, used as lightweight components, are often exposed to severe vibrations. In this case, a critical issue is to avoid resonance when the natural frequency of the laminate coincides with the excitation frequency. Avoiding resonance becomes particularly important in aerospace applications due to weight limitations. One of the methods adopted to resolve this issue is to design a laminate such that its fundamental frequency is higher than the excitation frequency. This approach leads to an optimal design problem with the objective of maximizing the fundamental frequency for a given weight of the laminate.

One of the recently introduced technologies to produce lightweight composites is to use nanoscale reinforcements which have high stiffness–weight ratios compared to traditional fibre reinforcements. Currently, carbon nanotubes (CNTs) and graphene nanoplatelets (GPLs) are among the most widely used nanomaterials introduced as reinforcements. Due to their excellent mechanical properties, a small amount of nano reinforcement can substantially improve the mechanical properties and the vibration response of the laminates.

Several studies on skew plates' vibration response have been reported in the literature. Vibrations of skew laminates with cut-outs were studied in [1], and the vibrations of laminated skew plates with and without cut-outs in [2]. Vibrations of skew cantilever plates with stiffeners were studied in [3] to observe the differences in the frequencies compared to rectangular plates. Results indicated that cantilever skew plates provide improved flexural rigidity as compared to rectangular plates. Vibrations of laminated cantilever trapezoidal plates were the subject of the study in [4]. In [5,6], free vibrations of skew laminates were studied, and it was observed that as the skew angle increases, the natural frequency also increases. In [7], an investigation of the free vibrations of skew plates indicated an increase of the fundamental frequency with increasing skew angle, aspect ratio and width to thickness ratio. In [8], vibrations of laminated skew plates were studied, and it was observed that the frequency increases with increasing skew angle.

Several studies focused on the response of graphene or carbon nanotube-reinforced laminates known as two-phase nanocomposites. Vibrations of functionally graded and carbon nanotube reinforced skew laminates were studied in [9–12]. The effects of nanotube content on the frequencies of skew laminates were investigated in [13], and the impact of carbon nanotube waviness and agglomeration on the vibrations of skew laminates in [14]. The vibration response of skew plates with varying stiffness was studied in [15], and it was observed that an increase in the skew angle increased the fundamental frequency confirming the previous results.

* Corresponding author at: Discipline of Civil Engineering, University of Central Lancashire, Preston, UK.
E-mail address: gdrosopoulos@uclan.ac.uk (G.A. Drosopoulos).

https://doi.org/10.1016/j.tws.2023.110903
Received 24 February 2023; Received in revised form 18 May 2023; Accepted 23 May 2023
Available online 23 June 2023

Several studies involved the vibrations of functionally graded graphene nanoplatelet-reinforced two-phase composites. The studies [16–19] observed that a small increase in the graphene content increased the fundamental frequency substantially. Functionally graded graphene-reinforced plates subject to thermal and mechanical loads were investigated in [20]. This study also indicated that adding a small amount of graphene leads to a considerably higher fundamental frequency.

Several investigations studied the optimal design of skew laminates. Optimization of skew laminates to maximize the frequency was the subject of the paper [21], with the study based on the first-order shear deformation theory. It was observed that as the skew angle increased, the optimal fibre orientations increased and for large enough skew angles, the influence of the fibre orientations became insignificant. Fundamental frequencies of symmetric and anti-symmetric skew laminates were maximized in [22] by determining the optimal stacking sequence. Genetic algorithms, particle swarm optimization and cuckoo search methods were used in [23] to maximize the fundamental frequency of skew plates.

The vibrations of graphene-reinforced skew plates on point supports were studied in [24]. The nonlinear vibration response of graphene-reinforced beams was studied in [25] and it was observed that the non-uniform distribution of graphene across thickness yielded better results as compared to the uniform distribution of graphene. The effect of graphene nanoplatelets on a polymer composite was studied in [26] and it was noted that a proper alignment of the nanoplatelets significantly improved the mechanical response compared to randomly orientated GPLs.

Recently, the mechanical response of three-phase composites using GPLs or CNTs and with glass or carbon fibre reinforcements in a polymer matrix has been investigated. These studies aim to balance the benefits of nanoscale reinforcements to achieve lower weight and higher stiffness with the increased cost of using nano materials. An investigation on the optimization of three-phase graphene/fibre-reinforced rectangular laminates with the objective of maximizing the fundamental frequency was presented in [27]. Design variables used in this study were the graphene content, the fibre content, the layer thicknesses and the fibre orientations and the numerical results were given only for the simply supported and clamped boundary conditions. Results highlighted the improvement of the design efficiency by introducing optimal non-uniform distributions of graphene and fibre reinforcements across the laminate thickness. The vibration response of three-phase, graphene/carbon fibre-reinforced laminates was studied in [28], emphasizing the contribution of graphene reinforcement to increase the fundamental frequency. In [29], the influence of using graphene reinforcement in addition to carbon or glass fibres on the buckling response of angle-ply laminates was evaluated. Results indicated that an increase in the graphene content led to substantially higher buckling loads.

Based on the literature study and according to authors' best knowledge, no research has been conducted on optimizing the fundamental frequency of three-phase graphene/fibre-reinforced skew cantilever laminates. The present article involves the optimal designs of three-phase, skew cantilever laminates using four design parameters. Both graphene nanoplatelets and glass or carbon fibres are used as reinforcements leading to three-phase laminates. Design variables include the graphene and fibre contents of layers, the thickness of each layer and the fibre orientations. The overall scheme is implemented in MATLAB using finite element analysis. A design efficiency factor is introduced to provide a quantitative criterion to compare and assess the results of different optimal designs and the effectiveness of the design parameters. The vibration response and the design efficiency of three-phase skew and rectangular plates are also evaluated for comparison purposes.

Sections 2 and 3 of the article provide basic constitutive equations and the finite element formulation adopted in this work. The effective material properties using micromechanics equations are given in Section 4. Section 5 presents the optimal design problems, formulated for an increasing number of design variables. The verification of the proposed scheme by comparison with published literature and commercial finite element software is provided in Section 6. Sections 7 and 8 present the investigation's results, discussions, and conclusions.

2. Basic equations

The geometry of the skew plate under consideration is shown in Fig. 1. The length, width and thickness of the plate are defined as a, b and D in the x, y and z directions, respectively. Clamped boundary conditions are imposed on one side of the skew plate with a length equal to b (Fig. 1). The remaining three edges have free boundary conditions. The laminate consists of N layers with θ_k denoting the angle between the principal material direction and the coordinate x of the kth lamina. The mid-plane of the laminate coincides with the xy plane as shown in Fig. 1. The skew angle of the laminate is denoted by α. The coordinates of the bottom and top of the kth layer are denoted as $z = z_k$ and $z = z_{k+1}$ in the thickness direction.

2.1. Kinematics

The kinematics of the composite plate are formulated using the first-order shear deformation theory (FSDT) with the displacement field defined as:

$$u_1(x,y,z,t) = u(x,y,t) - z\varphi_x(x,y,t) \tag{1a}$$

$$u_2(x,y,z,t) = v(x,y,t) - z\varphi_y(x,y,t) \tag{1b}$$

$$u_3(x,y,z,t) = w(x,y,t) \tag{1c}$$

where $\{u\} = \{u_1, u_2, u_3\}^T$ is the displacement vector and $\{\bar{u}\} = \{u, v, w, \varphi_x, \varphi_y\}^T$ indicates the vector of generalized displacements in terms of the three mid-plane displacements and the normal rotations about the x and y-axes. The strain vector is given by:

$$\{\varepsilon\} = \nabla_S \{\bar{u}\} \tag{2}$$

where $\{\varepsilon\} = \{\varepsilon_{xx}, \varepsilon_{yy}, \gamma_{xy}, \gamma_{yz}, \gamma_{xz}\}^T$ and ∇_S is defined as

$$\nabla_S = \begin{bmatrix} \partial/\partial x & 0 & 0 & -z\partial/\partial x & 0 \\ 0 & \partial/\partial y & 0 & 0 & -z\partial/\partial y \\ \partial/\partial y & \partial/\partial x & 0 & -z\partial/\partial y & -z\partial/\partial x \\ 0 & 0 & \partial/\partial y & 0 & -1 \\ 0 & 0 & \partial/\partial x & -1 & 0 \end{bmatrix} \tag{3}$$

2.2. Constitutive equations

The constitutive equation of the kth lamina is expressed as:

$$\{\sigma\}_k = [Q]_k \{\varepsilon\} \tag{4}$$

where $\{\sigma\}$ is the stress vector and $[Q]$ is the elastic stiffness matrix. Under plane-stress conditions, the non-zero components $Q_{ij}^{(k)}$ of the elastic stiffness matrix for an orthotropic material are given by [30]:

$$Q_{11}^{(k)} = \frac{E_1^{(k)}}{\left(1 - v_{12}^{(k)} v_{21}^{(k)}\right)}, \quad Q_{12}^{(k)} = \frac{v_{12}^{(k)} E_2^{(k)}}{\left(1 - v_{12}^{(k)} v_{21}^{(k)}\right)} = Q_{21}^{(k)},$$

$$Q_{22}^{(k)} = \frac{E_2^{(k)}}{(1 - v_{12}^{(k)} v_{21}^{(k)})},$$

$$Q_{66}^{(k)} = G_{12}^{(k)}, \quad Q_{44}^{(k)} = k_s G_{23}^{(k)}, \quad Q_{55}^{(k)} = k_s G_{13}^{(k)} \tag{5}$$

In the above equations, $E_1^{(k)}$, $E_2^{(k)}$ are the longitudinal and transverse moduli, $v_{12}^{(k)}, v_{21}^{(k)}$ denote the Poisson's ratios, $G_{12}^{(k)}, G_{23}^{(k)}, G_{13}^{(k)}$ denote the shear moduli of the kth layer and k_s is the shear correction factor taken as 5/6. The elastic coefficient $Q_{ij}^{(k)}$ in the material coordinates

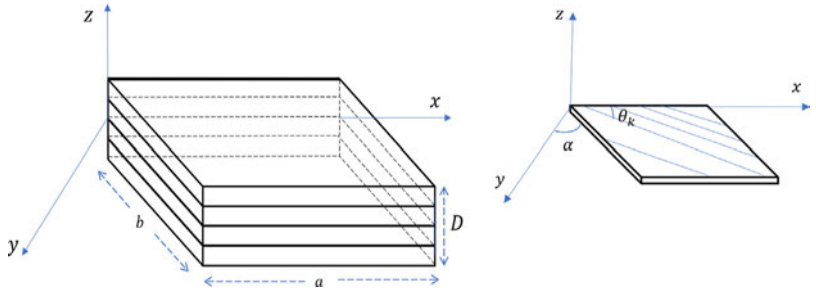

Fig. 1. Geometry of the laminated skew plate.

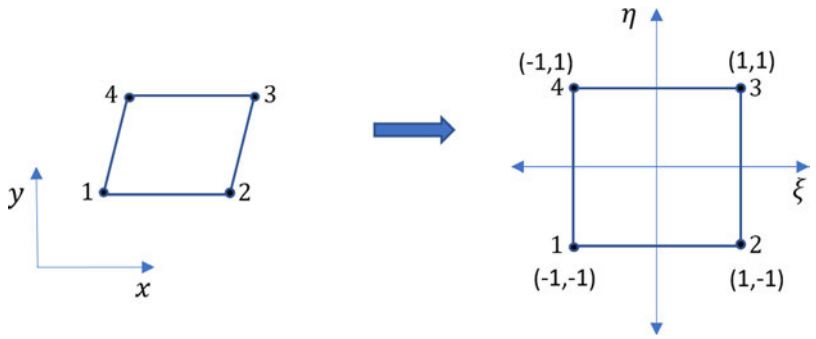

Fig. 2. Transformation of an isoparametric element from Cartesian (global) coordinates to natural (local) coordinates.

can be transformed into the coefficients $\overline{Q}_{ij}^{(k)}$ referred to the laminate coordinate system (x, y, z) using the relation:

$$\left[\overline{Q}\right]_{(k)} = \left([L]^T [Q] [L]\right)_{(k)} \tag{6}$$

where $[L(\theta_k)]$ is a transformation matrix and θ_k is the fibre orientation of the kth lamina as shown in Fig. 1 [30].

3. Finite element formulation

To solve the vibration problem, the finite element method is used. For skew plates, the borders of the elements are not parallel to the global axes of the plate as shown in Fig. 2. In the present study, isoparametric elements are utilized due to their capacity to simulate an arbitrary geometry accurately. The skew plate is discretized using four-noded isoparametric quadrilateral elements with five degrees of freedom (DOF) per node. Using these elements, the global coordinates x and y are related to the natural coordinates ξ and η as follows:

$$x(\xi,\eta) = \sum_{j=1}^{4} N_j(\xi,\eta)\, x_j, \quad y(\xi,\eta) = \sum_{j=1}^{4} N_j(\xi,\eta)\, y_j \tag{7}$$

where the Lagrange interpolation functions N_j are given by

$$N_j(\xi,\eta) = \frac{1}{4}\left(1+\xi_j\xi\right)\left(1+\eta_j\eta\right) \tag{8}$$

In Eq. (8), x_j, y_j are the coordinates of the node j in the cartesian (physical) domain and ξ_j, η_j are the coordinates of the node j in the natural (computational) domain as shown in Fig. 2. The same interpolation functions are used to define the generalized displacement vector within an element as

$$\begin{aligned}\left\{\overline{u}(x,y,t)\right\} \equiv \left\{u, v, w, \varphi_x, \varphi_y\right\}^T &= \sum_{j=1}^{4}\left(N_j(\xi,\eta)\,[I]_{5\times5}\left\{d_j(t)\right\}_e\right)\\ &= \left[N_u\right]\{d(t)\}_e\end{aligned} \tag{9}$$

where $\left\{d_j\right\}_e = \left\{u_j, v_j, w_j, \varphi_{xj}, \varphi_{yj}\right\}^T$ is the nodal displacement vector at the jth node of the element e and $[I]_{5\times5}$ denotes the 5×5 identity matrix.

Substituting Eq. (9) into (2) gives:

$$\{\varepsilon(x,y,t)\} = \nabla_S\left([H]\left[N_u\right]\{d\}_e\right) = [B]\{d\}_e \tag{10}$$

where $[B]$ is the strain–nodal displacement matrix.

3.1. Governing equations

The equations governing the dynamic response and the variationally consistent boundary conditions of the composite plate shown in Fig. 1, are derived using Hamilton's principle

$$\int_{t_1}^{t_2} (\delta T - \delta U + \delta W)\, dt = 0 \tag{11}$$

where T is the kinetic energy, U is the strain energy and W is the work done by external forces. At the initial and final times t_1 and t_2, the first variations vanish. The energy terms in Eq. (11) are defined as follows:

$$\begin{aligned}T &= \frac{1}{2}\int_V \rho\{\dot{u}\}^T\{\dot{u}\}\, dV = \frac{1}{2}\sum_{k=1}^{N}\int_A\int_{z_{k-1}}^{z_k}\rho_k\{\dot{u}\}^T\{\dot{u}\}\, dz dA\\ U &= \frac{1}{2}\int_V \{\sigma\}^T\{\varepsilon\}\, dV = \sum_{k=1}^{N}\int_A\int_{z_{k-1}}^{z_k}\{\sigma\}_k^T\{\varepsilon\}\, dz dA,\\ W &= \{u\}^T\{f_c\} + \int_{S_1}\{u\}^T\{f_s\}\, dS + \int_V\{u\}^T\{f_v\}\, dV\end{aligned} \tag{12}$$

where N is the number of layers, V_k is the volume and ρ_k is the density of the kth layer. V and S_1 denote the volume and the surface area of the plate, respectively. $\{f_c\}$ denotes the concentrated forces and $\{f_S\}$, $\{f_V\}$ denote the surface and volume forces, respectively. Finally, a dot over a variable represents a time derivative.

Using the displacements relations (1), the strain displacement relations (2) and the constitutive relations (4), the Hamilton's principle (11) can be written as:

$$\begin{aligned}&\int_{t_1}^{t_2}\left\{\sum_{k=1}^{N}\left(\int_A\int_{z_{k-1}}^{z_k}\{\delta\varepsilon\}^T\left[\overline{Q}\right]_k\{\varepsilon\}dz dA - \int_A\int_{z_{k-1}}^{z_k}\{\delta\dot{u}\}^T\rho_k\{\dot{u}\}dz dA\right)\right.\\ &\left. - \left(\{\delta u\}^T\{f_c\} + \int_A\{\delta u\}^T\{f_s\}\, dA + \int_V\{\delta u\}^T\{f_V\}\, dV\right)\right\} dt = 0\end{aligned} \tag{13}$$

Next, the displacements given by Eq. (9) and the strain–nodal displacement relations (10) are substituted in (13) to discretize the variational expression (13). Assembly of the discretized equation for the total number of elements is then implemented and the global mass matrix, stiffness matrix, as well as the displacement and force vectors are derived. The equations of motion of the system can be expressed as follows [27]

$$[M]\{\ddot{d}\} + [K]\{d\} = \{F_m\} \tag{14}$$

where $[M]$, $[K]$, $\{d\}$ and $\{F_m\}$ are the global mass matrix, the global linear stiffness matrix, the global displacement vector and the force vector, respectively. It is noted that the essential boundary conditions are enforced by imposing prescribed values at the corresponding DOF of the discretized domain. Then, in the system of equations of motion, the lines and columns of the prescribed degrees of freedom, as well as the lines of the force vector are eliminated.

3.2. Eigenvalue problem

By setting the force term to zero, and assuming that the plate undergoes a harmonic motion $d = d_0 e^{-i\omega t}$, the generalized governing equation (14) can be used to solve the free vibration problem for the laminated skew plate. In this case, Eq. (14) can be expressed as:

$$[K]\{d_0\} = \lambda [M]\{d_0\} \tag{15}$$

where eigenvalue $\lambda = \omega^2$ and ω is the frequency of natural vibrations. To obtain the numerical solution of the problem, a MATLAB code is developed based on the finite element formulation of the problem. It is noted that the selective integration technique is adopted for the calculation of the stiffness matrix in order to avoid shear locking effect. The present finite element formulation can now be used to solve optimization problems and maximize the fundamental frequency of skew laminates.

4. Effective material properties

The skew plate is a three-phase multiscale laminate reinforced with graphene nanoplatelets and glass or carbon fibres. Effective material properties of the nanocomposite are determined using the Halpin–Tsai model and the rule of mixtures as detailed in [31,32]. First, micromechanical equations are used to determine the effective properties of the (two-phase) graphene-reinforced matrix. Next, using the effective properties of the graphene-reinforced matrix, the properties of the three-phase nanocomposite are computed based on the micromechanical relations given in [33]. It is noted that the present approach of first determining the properties of the two-phase composite and then calculating the overall properties of the three-phase graphene/fibre-reinforced composite, has also been adopted in a number of studies. For example, the micromechanics equations used in [34] for a two-phase fibre-reinforced composite were also applied in [35] to calculate the effective material properties of a three-phase graphene/fibre-reinforced matrix. This approach can also be observed in [36,37].

4.1. Effective material properties of the graphene-reinforced matrix

The effective material properties of graphene-reinforced matrix are determined using the micromechanics equations given in [31,38–40]. Subscripts *GPL*, *M* and *GM* refer to graphene nanoplatelets, the matrix and the graphene-reinforced matrix, respectively. The effective Young's modulus of the graphene-reinforced matrix is calculated using the relation:

$$E_{GM} = \left(\frac{3}{8}\frac{1+\xi_L\eta_L V_{GPL}}{1-\eta_L V_{GPL}} + \frac{5}{8}\frac{1+\xi_w\eta_w V_{GPL}}{1-\eta_w V_{GPL}}\right) E_M \tag{16}$$

where V_{GPL} is the volume of graphene nanoplatelets and E_M is Young's modulus of the matrix. In Eq. (16), ξ_{L} and ξ_w are given by:

$$\xi_{\mathrm{L}} = 2\frac{l_{GPL}}{h_{GPL}}, \qquad \xi_{\mathrm{w}} = 2\frac{w_{GPL}}{h_{GPL}} \tag{17}$$

where l_{GPL} is the length, w_{GPL} is the width and h_{GPL} is the thickness of the graphene nanoplatelets. The values for η_L and η_w used in Eq. (16) can be determined from the following expressions:

$$\eta_L = \frac{(E_{GPL}/E_M) - 1}{(E_{GPL}/E_M) + \xi_{\mathrm{L}}}, \qquad \eta_w = \frac{(E_{GPL}/E_M) - 1}{(E_{GPL}/E_M) + \xi_w} \tag{18}$$

where E_{GPL} is the Young's modulus of graphene nanoplatelets and E_M is the Young's modulus of the matrix. The volume V_{GPL} of the graphene nanoplatelets can be calculated from the Eq. (19):

$$V_{GPL} = \frac{W_{GPL}}{W_{GPL} + (\rho_{GPL}/\rho_M)(1 - W_{GPL})} \tag{19}$$

where W_{GPL} is the weight fraction of graphene nanoplatelets. The effective shear modulus, Poisson's ratio and density for the graphene-reinforced matrix are given by:

$$G_{GM} = \frac{E_{GM}}{2(1+\upsilon_{GM})} \tag{20a}$$

$$\upsilon_{GM} = \upsilon_{GPL}V_{GPL} + \upsilon_M(1 - V_{GPL}) \tag{20b}$$

$$\rho_{GM} = \rho_{GPL}V_{GPL} + \rho_M(1 - V_{GPL}) \tag{20c}$$

where ρ_{GPL} and ρ_M represent the mass densities of the graphene nanoplatelets and of the polymer matrix, respectively.

4.2. Effective material properties of the graphene and fibre-reinforced matrix

The effective material properties of the three-phase nanocomposite are determined using the following equations [29,33]:

$$E_{11} = E_{F11}V_F + E_{GM}(1 - V_F) \tag{21}$$

$$E_{22} = E_{GM}\left(\frac{E_{F22} + E_{GM} + (E_{F22} - E_{GM})V_F}{E_{F22} + E_{GM} - (E_{F22} - E_{GM})V_F}\right) \tag{22}$$

$$G_{12} = G_{13} = G_{GM}\left(\frac{G_{F12} + G_{GM} + (G_{F12} - G_{GM})V_F}{G_{F12} + G_{GM} - (G_{F12} - G_{GM})V_F}\right) \tag{23}$$

$$G_{23} = \frac{E_{22}}{2(1+\upsilon_{23})} \tag{24}$$

$$\upsilon_{12} = \upsilon_{F12}V_F + \upsilon_{GM}(1 - V_F) \tag{25}$$

$$\upsilon_{23} = \upsilon_{F12}V_F + \upsilon_{GM}(1 - V_F)\left(\frac{1 + \upsilon_{GM} + \frac{\upsilon_{12}E_{GM}}{E_{11}}}{1 - \upsilon_{GM}^2 + \frac{\upsilon_{12}\upsilon_{GM}E_{GM}}{E_{11}}}\right) \tag{26}$$

$$\rho = \rho_F V_F + \rho_{GM}(1 - V_F) \tag{27}$$

In Eqs. (21)–(27), the subscripts F and GM refer to fibres and graphene-reinforced matrix, respectively. V_F and ρ_F denote the fibre volume content and the density, respectively.

5. Optimal design problems

The present study aims to maximize the fundamental frequencies of 45° skew graphene/fibre-reinforced laminates. The design variables are defined as the GPLs and fibre contents of laminate, the layer thicknesses and the fibre orientations. These are among the design variables that crucially affect the mechanical response of laminates, and they are key parameters in industrial applications. A sequence of optimization problems is formulated with the number of design variables increasing from one set to four sets of design variables. This approach makes it possible to evaluate the effectiveness of each set of design variables as compared to one another.

In the first optimization problem, the graphene contents of layers are specified as the design variables taking the layer thicknesses uniform and fibre contents of layers constant. In this case, GPLs are distributed non-uniformly across the thickness. In the second optimization problem, two design variables are specified, namely, the GPLs and fibre contents of each layer, leading to laminates with non-uniformly

distributed reinforcements. In the third design problem, three design variables are the graphene and fibre contents as well as the layer thicknesses leading to laminates with non-uniform layer thicknesses. The last problem involves four design variables, namely, the graphene and the fibre contents, the thickness and the fibre orientation of each layer. As it will become apparent in the numerical results, the chosen order of adding variables leads to a gradual increase of the fundamental frequency, for increasing number of design variables. It is noted that different order of adding variables could also be adopted within the same numerical framework. In such a case, the vibration response may provide additional results, noticing though, that for the case that all design variables are considered (e.g., the four design variables of this article), the same results with the present investigation would be expected. This task is left for future investigation.

The layer thicknesses are denoted by h_k and the number of layers by N. The layer thicknesses are kept constant in the first two optimization problems and the total thickness of the laminate is $Nh = D$.

In the third and fourth optimization problems layer thicknesses h_k are non-uniform and the total laminate thickness is given by $\sum_{k=1}^{N} h_k = D$. The GPL and fibre contents of the kth layer are denoted by V_{GPLk} and V_{Fk}, respectively.

5.1. Optimization problems with one and two design variables

In the first two optimization problems, the layer thicknesses are taken as uniform. Design variables are the GPLs content (Problem 1) and the GPLs and fibre contents (Problem 2). The volume of fibres (Vol_{Fk}) in the kth layer is given by $Vol_{Fk} = abhV_{Fk}$ where h is the layer thickness and V_{Fk} is the fibre volume content of the kth layer. The total volume of fibres in the laminate is then given by summing up the fibre volumes and is given by $Vol_{FT} = \sum_{k=1}^{N} Vol_{Fk} = abh\sum_{k=1}^{N} V_{Fk}$. The maximum fibre volume for the laminate is given by $Vol_{Fmax} = abDV_{Fmax}$ with V_{Fmax} denoting the maximum fibre volume content. The design constraint on the total fibre volume can be expressed as:

$$Vol_{FT} \le Vol_{Fmax} \Rightarrow abh\sum_{k=1}^{N} V_{Fk} \le abDV_{Fmax} \tag{28}$$

Inequality (28) implies that $\frac{h}{D}\sum_{k=1}^{N} V_{Fk} \le V_{Fmax}$. In the present study, the results are given for laminates with 8 layers and in this case, the inequality (28) can be expressed as:

$$\frac{1}{8}\sum_{k=1}^{8} V_{Fk} \le V_{Fmax} \tag{29}$$

Similarly, the constraint on the weight of GPLs can be expressed as:

$$\frac{1}{8}\sum_{k=1}^{8} W_{GPLk} \le W_{GPLmax} \tag{30}$$

where W_{GPLmax} is the total weight of GPLs reinforcement and W_{GPLk} is the weight of GPLs in the kth layer. The optimization problem can be stated as follows:

Maximize the fundamental frequency $\omega\left(V_F, W_{GPL}\right)$ (31a)

subject to the constraints

$$\frac{1}{8}\sum_{k=1}^{8} V_{Fk} \le V_{Fmax} \tag{31b}$$

$$\frac{1}{8}\sum_{k=1}^{8} W_{GPLk} \le W_{GPLmax} \tag{31c}$$

$$W_{GPLk} \ge 0 \tag{31d}$$

$$d_1 \le V_{Fk} \le d_2 \tag{31e}$$

Inequalities (31b) and (31c) are the constraints on the maximum fibre and GPLs contents, respectively. Inequality (31e) limits the minimum and maximum fibre volume content of layers. In the present study, the lower fibre limit is specified as $d_1 = 10\%$ and the upper fibre limit as $d_2 = 60\%$.

An important consideration for optimal design problems is the definition of a criterion that can be used to assess the improvement achieved by optimization as compared to non-optimal designs. Furthermore, the criterion can also be used to compare and assess the contributions of different design parameters for improving the objective function. In the present study, non-optimal solutions correspond to the solutions obtained for laminates with uniform GPLs and fibre distributions across the thickness, that is, $W_{GPLk} = \left(\frac{W_{GPLmax}}{N}\right)$ and $V_{Fk} = \left(\frac{V_{Fmax}}{N}\right)$, for $k = 1$ to N. In order to assess the effectiveness of optimal solutions, a design efficiency factor is introduced. It is defined as the ratio of the maximum fundamental frequency ω_{MAX} corresponding to the optimal design and the frequency ω_0 of the laminate with uniform properties. As such, ω_0 can be described as the reference frequency. In the present case, the reference frequency corresponds to the frequency of a laminate with uniformly distributed graphene and fibre contents across the laminate thickness. Thus, the design efficiency factor is given by:

$$\eta = \frac{\omega_{MAX}\left(V_{Fk}, W_{GPLk}\right)}{\omega_0(V_k, W_k)} \tag{32}$$

where the fibre content V_k and the graphene content W_k of the kth layer of the reference laminate are given by:

$$V_k = \frac{V_{Fmax}}{8}, \quad W_k = \frac{W_{GPLmax}}{8} \quad \text{for } k = 1, 2 \ldots, 8 \tag{33}$$

with V_{Fk} and W_{GPLk} in Eq. (32) determined optimally. For the calculation of the reference frequency ω_0 shown in Eq. (32), a uniform thickness is considered for all layers and a symmetric stacking sequence $[90/0/90/0]_s$ is adopted.

5.2. Optimization problems with three and four design variables

Optimization problems with three and four design variables and non-uniform layer thicknesses are formulated next. In this case, in addition to the contents of fibres and GPLs in each layer, the layer thicknesses and the fibre angles are also determined optimally. For these design problems, non-uniform layer thickness of the kth layer is denoted as h_k and the fibre volume as $Vol_{Fk} = abh_kV_{Fk}$. The total fibre volume of the laminate is $Vol_{FT} = \sum_{k=1}^{N} Vol_{Fk} = ab\sum_{k=1}^{N} h_kV_{Fk}$. The constraint on the total volume of fibres is defined as:

$$Vol_{FT} \le Vol_{Fmax} \Rightarrow ab\sum_{k=1}^{N} h_kV_{Fk} \le abDV_{Fmax} \tag{34}$$

which leads to the constraint:

$$\frac{1}{D}\sum_{k=1}^{N} h_kV_{Fk} \le V_{Fmax} \tag{35}$$

Similarly, the constraint on the total graphene weight is

$$\frac{1}{D}\sum_{k=1}^{N} h_kW_{GPLk} \le W_{GPLmax} \tag{36}$$

Layer thicknesses are subject to the constraint:

$$\sum_{k=1}^{N} \frac{h_k}{D} = 1 \tag{37}$$

For an 8-layered laminate, the optimal design problem with four design variables can be expressed as:

Maximize the fundamental frequency $\omega\left(V_{Fk}, W_{GPLk}, \frac{h_k}{D}, \theta_k\right)$ (38a)

subject to:

$$\frac{1}{D}\sum_{k=1}^{8} h_k V_{Fk} \le V_{Fmax} \tag{38b}$$

$$\frac{1}{D}\sum_{k=1}^{8} h_k W_{GPLk} \le W_{GPLmax} \tag{38c}$$

$$W_{GPLk} \ge 0 \tag{38d}$$

$$d_1 \le V_{Fk} \le d_2 \tag{38e}$$

$$-90^\circ \le \theta_k \le 90^\circ \tag{38f}$$

$$\sum_{k=1}^{8} \frac{h_k}{D} = 1 \tag{38g}$$

The inequality (38f) limits the fibre orientation of the kth layer, θ_k. The design efficiency factor for this case, which involves four design variables, is given by:

$$\eta = \frac{\omega_{MAX}\left(V_{Fk}, W_{GPLk}, \frac{h_k}{D}, \theta_k\right)}{\omega_0(V_k, W_k, \frac{h}{D}, \theta_0)} \tag{39}$$

with V_{Fk}, W_{GPLk}, h_k/D and θ_k to be determined optimally. For the calculation of the reference frequency ω_0 shown in Eq. (39), V_k and W_k are given by Eq. (33), a uniform thickness is considered for all layers and a symmetric stacking sequence $[90/0/90/0]_s$ is adopted.

5.3. Optimization algorithm

For the numerical solution of the optimal design problems, Sequential Quadratic Programming Algorithm (SQP) is implemented. SQP generates a sequence of steps by solving quadratic sub-problems for nonlinearly constrained problems [41–43]. At each iteration, the algorithm calculates an approximation of the Hessian of the Lagrangian function using a quasi-Newton updating method which searches for zero values, local maxima and local minima of the function. This is then adopted to create a Quadratic Programming sub-problem with the solution used to define a search direction. More details for the SQP algorithm can be found in [41]. The solution is implemented using MATLAB [44].

6. Verification of the optimization code

The finite element formulation and the optimization scheme are verified using the results available in the literature and ABAQUS commercial finite element software. First, the frequencies obtained in the present work are compared with skew plate frequencies available in the literature. The first four eigenfrequencies calculated by the proposed finite element formulation are compared with the frequencies given in [8], using skew angles of $\alpha = 30^\circ$ and $\alpha = 45^\circ$ for SSSS and CCCC boundary conditions. Material and geometric properties are $E_{11}/E_{22} = 40, G_{12} = G_{13} = 0.6E_2, G_{23} = 0.5E_2, \nu_{12} = \nu_{13} = \nu_{23} = 0.25, a/D = 10$ [8]. The non-dimensional frequency is given by $\Omega = (\omega a^2/\pi^2 D)\sqrt{\rho/E_2}$. The results are presented in Tables 1 and 2, for two stacking sequences of $\alpha = 30^\circ$ and $\alpha = 45^\circ$. The comparison indicates that frequencies obtained by the present approach are close to those in [8].

To further verify the results in the present article, frequencies are compared with those given in [45] for different skew angles. Material and geometric properties are taken as $E_{11}/E_{22} = 40, G_{12} = 0.6E_2, G_{13} = G_{23} = 0.5E_2, \nu_{12} = \nu_{13} = \nu_{23} = 0.25, a/D = 10$ [45].

Results presented in Tables 3 and 4 indicate that the frequencies obtained by the present approach and the ones given in [45] are quite close.

A further comparison is given between the frequencies obtained by the present approach and the ones given in [46] for cantilever skew plates. The material properties are taken as $E_{11} = E_{22}, G_{12} = E_{11}/(2(1+\upsilon))$, $G_{13} = G_{23} = G_{12}$, with $E_{11} = 71.02$ GPa, $\upsilon = 0.333$. In Table 5, the results of the comparison are presented for different aspect and length-to-thickness ratios. It is observed that the frequencies of the two approaches are quite close for different skew angles.

To verify the overall optimization scheme, a model of the two-layered skew cantilever laminate with uniformly distributed graphene nanoplatelets, fibre reinforcements and layer thicknesses is developed using commercial finite element software. A 10 × 14 mesh size is used and shell elements are adopted. The skew angle for this case is specified as 45°. To compare with the optimization results, a different stacking sequence is adopted at each finite element simulation and the corresponding frequency is computed. Subsequently, an optimization problem is formulated and solved using the proposed optimization method with fibre angles specified as the only design variables. This process aims to compare the optimal frequency and fibre orientations obtained from the optimization with the maximum frequency and the corresponding stacking sequence calculated using the commercial finite element software.

Table 1
Fundamental frequencies $\Omega = (\omega a^2/\pi^2 D)\sqrt{\rho/E_2}$ of 5-layered skew laminates with stacking sequence [90/0/90/0/90], $a/D = 10$, $a/b = 1$.

Skew angle	Mode	SSSS		CCCC	
		Present work (mesh 12 × 12)	Ref. [8]	Present work (mesh 12 × 12)	Ref. [8]
30	1	2.0848	2.0911	2.8388	2.8003
	2	3.6112	3.5138	4.1801	4.0576
	3	4.7697	4.7002	5.1229	5.0306
	4	5.0427	4.8869	5.4646	5.3010
45	1	2.8410	2.8829	3.5274	3.4745
	2	4.3390	4.2841	4.8950	4.7408
	3	5.8240	5.5876	6.1907	5.9583
	4	6.2147	6.1920	6.5084	6.3817

Table 2
Fundamental frequencies $\Omega = (\omega a^2/\pi^2 D)\sqrt{\rho/E_2}$ of 5-layered skew laminates with stacking sequence [45/−45/45/−45/45], $a/D = 10$, $a/b = 1$.

Skew angle	Mode	SSSS		CCCC	
		Present work (mesh 12 × 12)	Ref. [8]	Present work (mesh 12 × 12)	Ref. [8]
30	1	2.1039	2.0018	2.7137	2.6641
	2	3.7737	3.6276	4.2492	4.1408
	3	4.4619	4.2875	4.8365	4.7411
	4	5.281	5.0723	5.6414	5.5027
45	1	2.5616	2.4796	3.4126	3.3529
	2	4.4007	4.2221	4.9539	4.8122
	3	5.7859	5.5867	6.1886	6.0713
	4	5.8596	5.6013	6.3145	6.1108

Table 3
Fundamental frequency $\Omega = (\omega a^2/\pi^2 D)\sqrt{\rho/E_2}$ of 5-layered skew laminates with stacking sequence [90/0/90/0/90], $a/D = 10$, $a/b = 1$.

Skew angle	SSSS		CCCC	
	Present work (mesh 12 × 12)	Ref. [45]	Present work (mesh 12 × 12)	Ref. [45]
15	1.6892	1.6874	2.4323	2.4750
30	2.0348	2.0884	2.7327	2.7922
45	2.7525	2.8932	3.3793	3.4739

Table 4
Fundamental frequency $\Omega = (\omega a^2/\pi^2 D)\sqrt{\rho/E_2}$ of 4-layered skew laminates with stacking sequence [45/−45/45/−45], $a/D = 10$, $a/b = 1$.

Skew angle	SSSS		CCCC	
	Present work (mesh 12 × 12)	Ref. [45]	Present work (mesh 12 × 12)	Ref. [45]
15	1.9653	1.9366	2.3752	2.4007
30	2.1482	2.1196	2.7024	2.7418
45	2.6237	2.6752	3.3759	3.4434

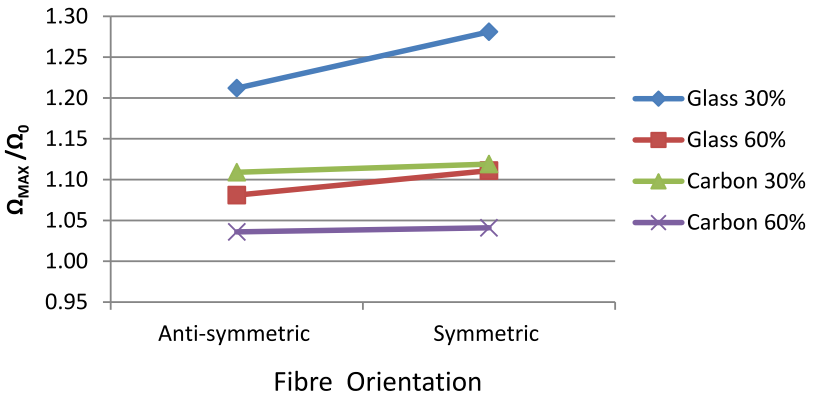

Fig. 3. Design efficiencies of anti-symmetric and symmetric laminates with GPLs content as the single design variable.

Table 5
Fundamental frequencies (Hz) of cantilever thin skew plates.

Skew angle	Aspect ratio a/b	Length-to-thickness ratio a/D	Mode	CFFF	
				Present work (mesh 15 × 15)	Ref. [46]
15	2.80	143	1	42.240	42.1970
			2	235.200	234.280
			3	278.146	275.620
			4	704.614	690.730
30	2.43	138.5	1	47.5120	47.441
			2	234.410	233.320
			3	330.610	327.060
			4	687.360	675.860
45	1.89	138	1	53.631	53.450
			2	223.690	222.400
			3	394.000	387.980
			4	629.730	618.940
60	1.35	138.5	1	65.400	64.688
			2	235.650	233.410
			3	462.590	452.010
			4	677.100	657.240

Table 6
Properties of constituent materials.

Material	E_{11} (GPa)	E_{22} (GPa)	G_{12} (GPa)	υ_{12}	Density (kg/m^3)
GPLs	1010	1010	$E_{11}/2(1+\nu)$	0.186	1060
Matrix	3	3	$E_{11}/2(1+\nu)$	0.34	1200
Carbon fibres	263	19	27.60	0.20	1750
Glass fibres	72.4	72.4	$E_{11}/2(1+\nu)$	0.20	2400

A non-dimensional fundamental frequency Ω is defined and used for the present results, as well as in the subsequent sections of the article:

$$\Omega = \omega D\sqrt{\frac{\rho_M}{E_M}} \tag{40}$$

with ρ_M and E_M representing the density and the Young's modulus of the matrix. The material properties used in the numerical results are given in Table 6. Dimensions of GPLs used in the present and subsequent sections are $l_{GPL} = 2.5$ μm, $w_{GPL} = 1.5$ μm, and $h_{GPL} = 1.5$ nm. The weight of GPLs is specified as 1% and the fibre volume content as 50%. The results of this comparison are given in Table 7.

Results obtained using the commercial software package show that the stacking sequence $[0°, 0°]$ produces the maximum frequency which is equal to 0.00364. The present optimization scheme gives a maximum frequency of 0.0037 with fibre orientations of $[-0.28°, 0.28°]$. Thus, both the solution produced by the commercial finite element software and the one obtained by the proposed MATLAB optimization code lead to almost identical results for the optimal frequency and the fibre orientations.

7. Results and discussions

7.1. Optimization using the graphene content as the single design variable

In the present case, GPLs distribution across the thickness is the only design variable. Layer thicknesses and fibre distributions are defined as uniform with the results given for symmetric and anti-symmetric laminates. Numerical results are given for the fibre volume contents of 30% and 60% in Table 8. The frequency of the optimal laminates is indicated in non-dimensional form in Eq. (40) as Ω. The non-dimensional frequency Ω_0 of the reference laminate is determined by substituting ω_0 as defined at the end of Section 5.1, into the Eq. (40). Design efficiency for this case is given by $\eta = \frac{\Omega}{\Omega_0}$ which is the same as the one defined in Section 5.1 by Eq. (32).

Table 8 indicates that the distribution of the GPLs across the thickness tends to be higher in the outer layers with the inner layers having zero GPLs content. This is due to the outer layers contributing more to the laminate stiffness as compared to the middle layers. It is noted that a significant increase in the fundamental frequency is observed with the GPLs distributed optimally as compared to the laminates with uniformly distributed GPLs. A maximum increase of 28.1% is observed for the symmetric laminates having a glass fibre content of 30%. The corresponding increase for the anti-symmetric laminates is 21.2%. Concerning the laminates with 30% carbon fibre content, the fundamental frequency increases by 11.9% for the symmetric and 10.9% for the anti-symmetric cases. In the case of laminates with 60% glass or carbon fibre contents, a lower percent of increase in the frequency is observed. The increase in the fundamental frequency of laminates with optimal GPLs distributions is shown in Fig. 3.

Table 7
Comparison of the optimal non-dimensional frequencies Ω with those obtained from the commercial finite element software for GPLs/glass fibre skew plates with $D/a = 0.03$, $W_{GPL} = 0.01$, $V_F = 0.50$, $a/b = 0.71$ and skew angle $\alpha = 45°$.

Solution obtained by the commercial finite element software			Solution obtained by the proposed optimization code	
Case	Stacking sequence	Non-dimensional frequency	Optimal stacking sequence	Optimal non-dimensional frequency
1	**[0,0]**	**0.00364**	[−0.28, 0.28]	0.0037
2	[30,0]	0.00356		
3	[45,0]	0.00336		
4	[60,0]	0.00332		
5	[90,0]	0.00333		
6	[0,30]	0.00344		
7	[30,30]	0.00328		
8	[45,30]	0.00320		
9	[60,30]	0.00317		
10	[90,30]	0.00318		
11	[0,45]	0.00336		
12	[30,45]	0.00320		
13	[45,45]	0.00313		
14	[60,45]	0.00310		
15	[90,45]	0.00311		
16	[0,60]	0.00332		
17	[30,60]	0.00317		
18	[45,60]	0.00310		
19	[60,60]	0.00306		
20	[90,60]	0.00307		
21	[0,90]	0.00333		
22	[30,90]	0.00318		
23	[45,90]	0.00311		
24	[60,90]	0.00307		
25	[90,90]	0.00309		

Table 8
Optimal fundamental frequencies of an 8-layered cantilever skew laminates having the design variable W_{GPL} with $W_{GPLmax} = 0.0125$, $D/a = 0.03$, $h/D = 0.125$, $a/b = 0.71$ and skew angle $\alpha = 45°$.

Stacking sequence	Fibre content	Optimal W_{GPL} per layer	Ω	Ω_0	$\eta = \frac{\Omega}{\Omega_0}$
$[90/0/90/0]_{\text{anti-s}}$	Glass 30%	$[0.050/0.0/0.0/0.0]_{\text{anti-s}}$	0.0040	0.0033	1.212
	Glass 60%	$[0.039/0.011/0.0/0.0]_{\text{anti-s}}$	0.0040	0.0037	1.081
	Carbon 30%	$[0.050/0.0/0.0/0.0]_{\text{anti-s}}$	0.0051	0.0046	1.109
	Carbon 60%	$[0.041/0.009/0.0/0.0]_{\text{anti-s}}$	0.0057	0.0055	1.036
$[90/0/90/0]_{\text{s}}$	Glass 30%	$[0.050/0.0/0.0/0.0]_{\text{s}}$	0.0041	0.0032	1.281
	Glass 60%	$[0.048/0.002/0.001/0.0]_{\text{s}}$	0.0040	0.0036	1.111
	Carbon 30%	$[0.050/0.0/0.0/0.0]_{\text{s}}$	0.0047	0.0042	1.119
	Carbon 60%	$[0.041/0.009/0.001/0.0]_{\text{s}}$	0.0051	0.0049	1.041

The highest fundamental frequency is obtained for the anti-symmetric case for laminates with a 60% carbon fibre content as shown in Table 8. An increase of 42.5% in the frequency is observed for this case as compared to the frequency of the graphene and glass fibre-reinforced anti-symmetric laminates with 60% fibre content. Table 8 indicates that graphene–glass fibre-reinforced laminates with 30% and 60% fibre contents have the same frequency for the anti-symmetric case. For the symmetric case, laminates with 30% glass fibre content have a slightly higher frequency than those with 60% glass fibre content. Thus, higher glass fibre content has a minor effect on the fundamental frequency for cross-ply laminates.

The design efficiencies of the graphene–glass fibre-reinforced laminates with optimal GPL distribution across the thickness are investigated in Fig. 4. Glass fibre reinforcement is uniformly distributed with a 30% fibre content. Results are given for symmetric and anti-symmetric laminates. It is observed that the effect of the stacking sequence on the design efficiency depends on the type of stacking sequence with anti-symmetric laminates having higher design efficiencies up to $[50/40/50/40]_{\text{anti-s}}$ stacking sequence. Symmetric laminates have higher design efficiencies for the stacking sequences $[75/30/75/30]_{\text{s}}$ and $[90/0/90/0]_{\text{s}}$ indicating that design efficiencies depend on the type of laminate.

Maximum fundamental frequencies are plotted against GPLs weight contents in Fig. 5 for the symmetric stacking sequences and in Fig. 6 for the anti-symmetric stacking sequences. The design variable in Figs. 5 and 6 is the optimal distribution of GPLs across the thickness with fibres distributed uniformly. Results are given up to a graphene weight of 10% to observe the effect of high graphene content on the frequency and determine the cross-over points.

Fig. 5 shows that the frequencies of the symmetric graphene–glass fibre-reinforced laminates are higher for 60% fibre content up to a value of about 1% graphene content. Afterwards, laminates with 30% fibre content have higher frequencies than those with 60% glass fibre content. A similar trend is observed for the anti-symmetric graphene–glass fibre laminates as shown in Fig. 6.

In the case of carbon fibre-reinforced laminates, the same phenomenon is observed for both the symmetric and the anti-symmetric cases but for a higher graphene weight of about 3%. These results indicate that higher fibre content exceeding a certain value (cross-over points) leads to diminishing returns and not cost-effective designs for skew laminates. In the case of 60% fibre reinforcements, a significant drop is observed in the slope of the curves as shown in Figs. 5 and 6 after the cross-over points which highlights this comment.

7.2. Optimization using GPLs and fibre distributions as design variables

The next optimization problem introduces two design variables, namely the GPLs and the fibre contents. Layer thicknesses are specified as uniform and the results are shown in Table 9.

Table 9 indicates that optimization leads to higher GPL and fibre contents in the outer layers as expected. Similar to the previous case of optimization using only the GPL distribution as the design variable,

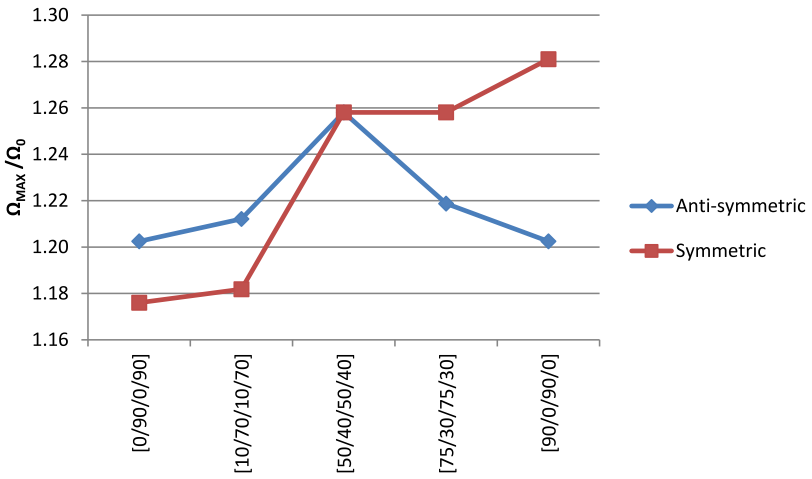

Fig. 4. Design efficiencies for anti-symmetric and symmetric laminates with GPLs content as the single design variable and 30% uniform glass fibre distribution.

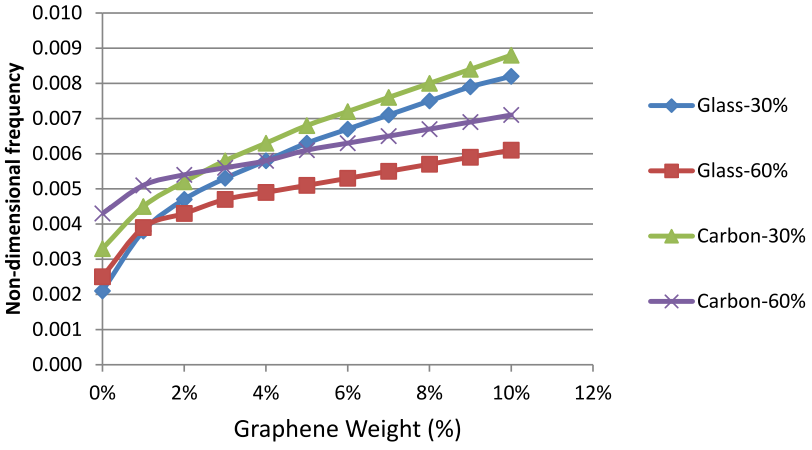

Fig. 5. Fundamental frequency vs. GPLs content for laminates with symmetric stacking sequence $[90/0/90/0]_s$, $D/a = 0.03$, $h/D = 0.125$, $a/b = 0.71$ and skew angle $\alpha = 45°$.

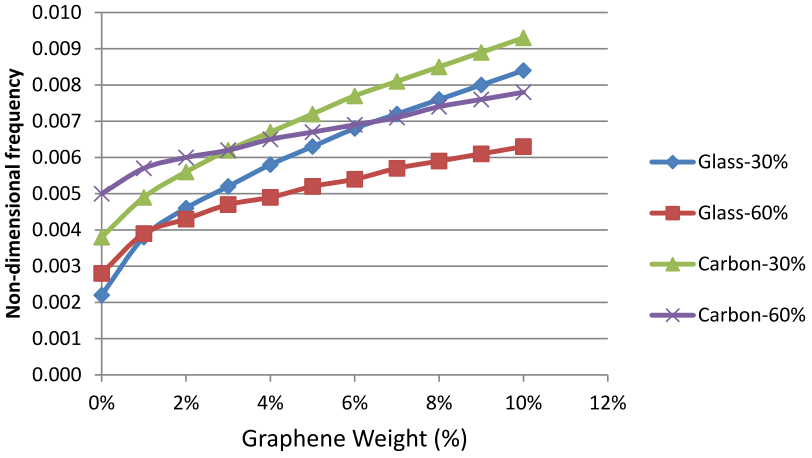

Fig. 6. Fundamental frequency vs. GPLs content for laminates with anti-symmetric stacking sequence $[90/0/90/0]_{anti\text{-}s}$, $D/a = 0.03$, $h/D = 0.125$, $a/b = 0.71$ and skew angle $\alpha = 45°$.

glass fibre reinforcement leads to higher design efficiencies as compared to the carbon fibre reinforcement. For the symmetric laminates, design efficiency is 34% and for the anti-symmetric laminates 27% in the case of glass fibre reinforcements. Both these values are higher as compared to carbon fibre-reinforced laminates as shown in Table 9. Compared to carbon fibres, lower material properties in the case of glass fibres, resulting in a lower laminate stiffness, leads to GPL reinforcements being more effective for graphene–glass fibre laminates. It is noted that this result applies to design efficiencies, and not the maximum frequencies which are higher in the case of carbon fibre reinforcements as expected.

A comparison between Tables 8 and 9 indicates the effect of increasing the number of design variables on the fundamental frequency. With carbon fibre reinforcement, frequency increases by 9.8% for anti-symmetric and by 17% for symmetric stacking sequence. In the case of glass fibre reinforcement, the corresponding frequency increase is

Table 9
Fundamental frequencies of 8-layered laminates with two design variables, namely, GPLs and fibre distributions across the thickness with $W_{GPLmax} = 0.0125$, $V_{Fmax} = 0.30$, $D/a = 0.03$, $h/D = 0.125$, $a/b = 0.71$ and skew angle $\alpha = 45°$.

Stacking sequence	Fibres	Optimal W_{GPL} per layer	Optimal V_F per layer	Ω	Ω_0	$\eta = \frac{\Omega}{\Omega_0}$
$[90/0/90/0]_{anti\text{-}s}$	Glass	$[0.037/0.013/0.0/0.0]_{anti\text{-}s}$	$[0.60/0.40/0.10/0.10]_{anti\text{-}s}$	0.0042	0.0033	1.273
	Carbon	$[0.047/0.004/0.0/0.0]_{anti\text{-}s}$	$[0.43/0.57/0.10/0.10]_{anti\text{-}s}$	0.0056	0.0046	1.217
$[90/0/90/0]_s$	Glass	$[0.050/0.0/0.0/0.0]_s$	$[0.40/0.60/0.10/0.10]_s$	0.0043	0.0032	1.344
	Carbon	$[0.050/0.0/0.0/0.0]_s$	$[0.10/0.60/0.40/0.10]_s$	0.0055	0.0042	1.310

Table 10
Fundamental frequency of an 8-layered skew laminate with zero graphene content and the single design variable V_F subject to $V_{Fmax} = 0.30$ with $D/a = 0.03$, $h/D = 0.125$, $a/b = 0.71$ and skew angle $\alpha = 45°$.

Stacking sequence	Fibres	Optimal V_F per layer	Ω	Ω_{02}	$\eta_2 = \frac{\Omega}{\Omega_{02}}$	$\eta = \frac{\Omega}{\Omega_0}$
$[90/0/90/0]_{anti\text{-}s}$	Glass	$[0.60/0.40/0.10/0.10]_{anti\text{-}s}$	0.0027	0.0022	1.227	0.818
	Carbon	$[0.54/0.46/0.10/0.10]_{anti\text{-}s}$	0.0046	0.0038	1.211	1.000
$[90/0/90/0]_s$	Glass	$[0.40/0.60/0.10/0.10]_s$	0.0025	0.0021	1.190	0.781
	Carbon	$[0.10/0.60/0.40/0.10]_s$	0.0043	0.0033	1.303	1.024

5% for anti-symmetric and 4.9% for symmetric stacking sequences. These results indicate that a cost-effective design can be achieved using less fibre reinforcement if both graphene and fibres are distributed optimally across the thickness.

To assess the effect of GPLs reinforcement on optimal design, graphene content is set to zero and optimization is performed using the fibre reinforcement as the only design variable. The results are given in Table 10 for both anti-symmetric and symmetric cases.

Two design efficiencies are shown in Table 10, namely, $\eta_2 = \frac{\Omega}{\Omega_{02}}$, and $\eta = \frac{\Omega}{\Omega_0}$. The design efficiency η_2 is computed as the ratio of the maximum frequency Ω and the reference frequency Ω_{02} corresponding to a laminate with zero graphene content. This index can be used to evaluate the increase in the fundamental frequency of the laminate with non-uniform (optimal) fibre distribution only as compared to the frequency of the reference laminate with uniform fibre distribution across the thickness. In addition, η is calculated using the reference frequency Ω_0, which corresponds to the frequency of a laminate with uniform graphene content of 1.25% per layer. This index will be used to compare the efficiencies of the optimal two-phase fibre-reinforced composite laminates (only fibre reinforcement, Table 10) and the efficiencies of the optimal three-phase graphene/fibre-reinforced laminates (Table 9).

Noting the values η_2 of the design efficiency, it is observed that a significant increase of η_2 from 19% to 30% is observed for the two-phase fibre-reinforced laminate with optimal (non-uniform) fibre distribution across the laminate thickness as compared to the frequency corresponding to the laminate with uniform fibre distribution.

To investigate the impact of introducing graphene reinforcement on the frequency, a comparison of the results presented in Table 10 (zero graphene, optimal distribution of fibres) and Table 9 (optimal distribution of both graphene and fibres) is made. For the anti-symmetric laminate with non-zero graphene and glass fibre reinforcement, a design efficiency of 1.273 is obtained in Table 9, indicating an increase of 27.3% of the frequency as compared to the reference plate. For the same fibre type and orientation, but for zero graphene content (Table 10), the design efficiency η is 0.818 which indicates a decrease of $1.000 - 0.818 = 0.182$ or 18.2% in the fundamental frequency as compared to the reference frequency. For this case, the overall increase of the fundamental frequency of the laminate with non-zero graphene content is equal to 27.3%+18.2%=45.5% as shown in Table 11 in comparison to the laminate with zero graphene. This is a substantial improvement of the frequency which is due to adding a small graphene content as reinforcement.

As shown in Table 11, an even higher increase of 56.3% is obtained for the symmetric glass fibre/graphene-reinforced laminate. For anti-symmetric and symmetric carbon fibre/graphene-reinforced laminates, the increases of the fundamental frequency are equal to 21.7% and 28.6%, respectively, as compared to the frequencies of the optimal two-phase fibre-reinforced laminates.

7.3. Optimization with three and four design variables and non-uniform layer thicknesses

Next, non-uniform layer thicknesses and fibre angles are introduced as additional design variables, leading to optimization with three and four design variables. These are graphene and fibre contents, the layer thicknesses and the fibre angles. Results with three design variables and predefined stacking sequences are given in Table 12.

Table 12 indicates that higher graphene and fibre reinforcements are assigned to outer layers as expected. Furthermore, two outer layers have lower thicknesses as compared to the inner layers for the anti-symmetric laminates. In the case of symmetric laminates, only the surface layer has a lower thickness with the other layers having the same thicknesses. The increase in the fundamental frequency, as compared to the reference frequency, is 30.3% and 23.9% for the anti-symmetric case with glass and carbon fibre reinforcements, respectively. For the symmetric laminate, the increases are 46.9% and 54.8%, and thus, significantly higher than the anti-symmetric case. A comparison with the laminates with uniform layer thicknesses (Table 9), indicates that in the case of non-uniform layer thicknesses (Table 12), an increase in the fundamental frequency, with respect to the reference frequency, occurs. For the anti-symmetric case, this is equal to 3% and 2.2% for glass and carbon fibre reinforcements. For the symmetric laminates with non-uniform layer thicknesses, the increase in the fundamental frequency is 12.5% and 23.8% for glass and carbon fibre reinforcements, respectively.

The fourth optimization problem involves GPLs and fibre contents, layer thicknesses and fibre angles as the design parameters, with the results shown in Table 13.

The increase in the fundamental frequency (compared to reference frequency) of anti-symmetric laminates is 45.5% for glass fibre and 52.2% for carbon fibre reinforcements. For the symmetric laminate, the increase is 46.9% for glass fibre and 64.3% for carbon fibre reinforcements. The same increase was observed for the symmetric laminates with glass fibre reinforcement and predefined stacking sequence, as shown in Table 12. Therefore, the stacking sequence $[90/0/90/0]_s$, which was used in Table 12, is the optimal one.

In the case of laminates with four design variables (Table 13) involving glass and carbon fibres (anti-symmetric laminate) and carbon fibres (symmetric laminate), the increases in the fundamental frequencies (comparing to reference frequency) are higher by 15.2%, 28.3%, and 9.5% as compared to the case with three design variables (Table 12).

The improvement in the frequencies is due to including the fibre angles in the optimization process. It is noted that for both anti-symmetric and symmetric cases, higher frequency and higher design efficiency are observed for carbon fibre-reinforced laminates as compared to the glass fibre-reinforced ones.

Table 11
Comparison between the maximum and the reference frequencies for the results shown in Table 9 (non-zero, optimal graphene/fibre distribution) and Table 10 (zero graphene, optimal fibre distribution).

	Stacking sequence	Fibre type	Maximum frequency Ω	Reference frequency Ω_0	$\eta = \frac{\Omega}{\Omega_0}$	$\frac{\Omega-\Omega_0}{\Omega_0}$ (%)
Optimal graphene distribution	$[90/0/90/0]_{anti\text{-}s}$	Glass	0.0042	0.0033	1.273	27.30%
		Carbon	0.0056	0.0046	1.217	21.70%
	$[90/0/90/0]_s$	Glass	0.0043	0.0032	1.344	34.40%
		Carbon	0.0055	0.0042	1.310	31.00%
Zero graphene	$[90/0/90/0]_{anti\text{-}s}$	Glass	0.0027	0.0033	0.818	−18.20%
		Carbon	0.0046	0.0046	1.000	0
	$[90/0/90/0]_s$	Glass	0.0025	0.0032	0.781	−21.90%
		Carbon	0.0043	0.0042	1.024	2.40%

Table 12
Fundamental frequencies of 8-layered skew laminates with three design variables (GPLs and fibre contents, thickness ratios) and with $W_{GPLmax} = 0.0125$, $V_{Fmax} = 0.30$, $D/a = 0.03$, $a/b = 0.71$ and skew angle $\alpha = 45°$.

Stacking sequence	Fibres	Optimal W_{GPL} per layer	Optimal V_F per layer	h/D	Ω	Ω_0	$\eta = \frac{\Omega}{\Omega_0}$
$[90/0/90/0]_{anti\text{-}s}$	Glass	$[0.046/0.019/0.0/0.0]_{anti\text{-}s}$	$[0.60/0.60/0.10/0.10]_{anti\text{-}s}$	$[0.09/0.11/0.15/0.15]_{anti\text{-}s}$	0.0043	0.0033	1.303
	Carbon	$[0.054/0.016/0.0/0.0]_{anti\text{-}s}$	$[0.60/0.60/0.10/0.10]_{anti\text{-}s}$	$[0.08/0.12/0.15/0.15]_{anti\text{-}s}$	0.0057	0.0046	1.239
$[90/0/90/0]_s$	Glass	$[0.127/0.0/0.0/0.0]_s$	$[0.10/0.60/0.27/0.10]_s$	$[0.05/0.15/0.15/0.15]_s$	0.0047	0.0032	1.469
	Carbon	$[0.127/0.0/0.0/0.0]_s$	$[0.10/0.60/0.27/0.10]_s$	$[0.05/0.15/0.15/0.15]_s$	0.0065	0.0042	1.548

Table 13
Fundamental frequencies of 8-layered skew laminates with four design variables (GPLs and fibre contents, thickness ratios, fibre angles) and with $W_{GPLmax} = 0.0125$, $V_{Fmax} = 0.30$, $D/a = 0.03$, $a/b = 0.71$ and skew angle $\alpha = 45°$.

Fibres	Optimal W_{GPL} per layer	Optimal V_F per layer	h/D	Optimal fibre angles	Ω	Ω_0	$\eta = \frac{\Omega}{\Omega_0}$
Glass	$[0.141/0.0/0.0/0.0]_{anti\text{-}s}$	$[0.10/0.60/0.27/0.10]_{anti\text{-}s}$	$[0.05/0.15/0.15/0.15]_{anti\text{-}s}$	$[45/-8/-8/29]_{anti\text{-}s}$	0.0048	0.0033	1.455
Carbon	$[0.141/0.0/0.0/0.0]_{anti\text{-}s}$	$[0.10/0.60/0.27/0.10]_{anti\text{-}s}$	$[0.05/0.15/0.15/0.15]_{anti\text{-}s}$	$[-9/-5/-6/-25]_{anti\text{-}s}$	0.0070	0.0046	1.522
Glass	$[0.127/0.0/0.0/0.0]_s$	$[0.10/0.60/0.27/0.10]_s$	$[0.05/0.15/0.15/0.15]_s$	$[90/0/90/0]_s$	0.0047	0.0032	1.469
Carbon	$[0.027/0.045/0.0/0.0]_s$	$[0.60/0.10/0.27/0.10]_s$	$[0.15/0.05/0.15/0.15]_s$	$[-6/50/-18/88]_s$	0.0069	0.0042	1.643

Table 14
Fundamental frequencies of 8-layered skew ($a/b = 0.71$) and rectangular ($a/b = 1$) laminates with the design variable W_{GPL} and with $W_{GPLmax} = 0.0125$, $D/a = 0.03$, $h/D = 0.125$.

Symmetric fibre orientation $[90°/0°/90°/0°]_s$						
Fibre type	Laminate type	W_{GPL}	Ω	Increase (%)	Ω_0	$\eta = \frac{\Omega}{\Omega_0}$
Glass 30%	Rectangular (0°)	$[0.057/0.0/0.0/0.0]_s$	0.0031	–	0.0024	1.292
	45° Skew	$[0.050/0/0/0]_s$	0.0041	32%	0.0032	1.281
Carbon 30%	Rectangular (0°)	$[0.057/0.0/0.0/0.0]_s$	0.0036	–	0.0032	1.125
	45° Skew	$[0.05/0/0/0]_s$	0.0047	31%	0.0042	1.119

Table 15
Fundamental frequencies of 8-layered skew ($a/b = 0.71$) and rectangular ($a/b = 1$) laminates with two design variables (GPLs and fibre contents) and with $W_{GPLmax} = 0.0125$, $V_{Fmax} = 0.30$, with $D/a = 0.03$, $h/D = 0.125$.

Symmetric fibre orientation $[90°/0°/90°/0°]_s$							
Fibre type	Laminate type	W_{GPL}	V_F	Ω	Increase (%)	Ω_0	$\eta = \frac{\Omega}{\Omega_0}$
Glass	Rectangular (0°)	$[0.0565/0.0/0.0/0.0]_s$	$[0.4/0.6/0.1/0.1]_s$	0.0033	–	0.0024	1.375
	45° Skew	$[0.050/0.0/0.0/0.0]_s$	$[0.4/0.6/0.1/0.1]_s$	0.0043	30%	0.0032	1.344
Carbon	Rectangular (0°)	$[0.0565/0.0/0.0/0.0]_s$	$[0.1/0.6/0.1/0.4]_s$	0.0045	–	0.0032	1.406
	45° Skew	$[0.050/0.0/0.0/0.0]_s$	$[0.1/0.6/0.4/0.1]_s$	0.0055	22%	0.0042	1.310

7.4. Comparison of the optimal designs of rectangular and skew laminates

In this section a comparison of the frequencies of the skew and rectangular plates is presented with both plates being cantilevers. Results are given for one, two, three and four design variables. The fundamental frequencies for these cases are shown in Tables 14 to 17 with the number of design variables increasing from one to four.

Results indicate that the fundamental frequencies of the skew laminates are higher than those of the rectangular laminates for both glass and carbon fibre reinforcements. As observed in Tables 14 to 17, increases are 32%, 30%, 31% and 47% for laminates with glass fibre reinforcement with the increasing number of variables. In the case of carbon fibre reinforcement, the increases in the fundamental frequencies of the skew laminates as compared to the rectangular laminates are 31%, 22%, 18% and 17% for laminates with one, two, three and four design variables, respectively. These results agree with the results given in the Refs. [5–8] where it was noted that the increase of the skew angle increases the fundamental frequency.

Even though the fundamental frequencies of skew plates are higher, their design efficiencies are lower compared to the rectangular plates as shown in Tables 14–17. However, in the case of the skew plate with glass fibre reinforcement and with four design variables, design efficiency is higher than the rectangular plate as shown in Table 17. Since higher design efficiencies are derived for most of the rectangular plates as compared to the skew plates, the fundamental frequency increases are higher for the rectangular plates as compared to the skew plates. Thus, optimal, non-uniform graphene and fibre distributions along the thickness is more effective for rectangular plates. The highest design efficiency is obtained for the rectangular plate with four design variables and carbon fibre reinforcement which is 1.844 (Table 17).

Table 16
Fundamental frequencies of 8-layered skew ($a/b = 0.71$) and rectangular ($a/b = 1$) laminates with three design variables (GPLs and fibre contents, layer thickness ratios) and with $W_{GPLmax} = 0.0125$, $V_{Fmax} = 0.30$, $D/a = 0.03$.

Symmetric fibre orientation $[90°/0°/90°/0°]_s$								
Fibre type	Laminate type	W_{GPL}	V_F	h/D	Ω	Increase (%)	Ω_0	$\eta = \frac{\Omega}{\Omega_0}$
Glass	Rectangular (0°)	$[0.14/0.0/0.0/0.0]_s$	$[0.1/0.6/0.1/0.27]_s$	$[0.05/0.15/0.15/0.15]_s$	0.0036	–	0.0024	1.500
	45° Skew	$[0.13/0.0/0.0/0.0]_s$	$[0.10/0.60/0.27/0.10]_s$	$[0.05/0.15/0.15/0.15]_s$	0.0047	31%	0.0032	1.469
Carbon	Rectangular (0°)	$[0.14/0.0/0.0/0.0]_s$	$[0.1/0.6/0.1/0.27]_s$	$[0.05/0.15/0.15/0.15]_s$	0.0055	–	0.0032	1.719
	45° Skew	$[0.13/0.0/0.0/0.0]_s$	$[0.10/0.60/0.27/0.10]_s$	$[0.05/0.15/0.15/0.15]_s$	0.0065	18%	0.0042	1.548

Table 17
Fundamental frequencies of 8-layered skew ($a/b = 0.71$) and rectangular ($a/b = 1$) laminates with four design variables (GPLs and fibre contents, thickness ratios, fibre angles) and with $W_{GPLmax} = 0.0125$, $V_{Fmax} = 0.30$, $D/a = 0.03$.

Fibre type	Laminate type	W_{GPL}	V_F	h/D	θ	Ω	Increase (%)	Ω_0	$\eta = \frac{\Omega}{\Omega_0}$
Glass	Rectangular (0°)	$[0.037/0.0303/0.0/0.0]_s$	$[0.6/0.6/0.1/0.1]_s$	$[0.15/0.05/0.15/0.15]_s$	$[5/51/-20/88]_s$	0.0032	–	0.0024	1.333
	45° Skew	$[0.127/0.0/0.0/0.0]_s$	$[0.1/0.6/0.27/0.1]_s$	$[0.05/0.15/0.15/0.15]_s$	$[90/0/90/0]_s$	0.0047	47%	0.0032	1.469
Carbon	Rectangular (0°)	$[0.01/0.111/0.0/0.0]_s$	$[0.6/0.1/0.27/0.1]_s$	$[0.15/0.05/0.15/0.15]_s$	$[3/50/0/88]_s$	0.0059	–	0.0032	1.844
	45° Skew	$[0.027/0.045/0.0/0.0]_s$	$[0.6/0.1/0.27/0.1]_s$	$[0.15/0.05/0.15/0.15]_s$	$[-6/50/-18/88]_s$	0.0069	17%	0.0042	1.643

8. Conclusions

In the present study, maximizing the fundamental frequencies of graphene/fibre-reinforced cantilever skew laminates is studied. Design parameters include the distributions of the graphene and fibres across the laminate thickness, layer thicknesses and the fibre angles. To assess the effectiveness of different design variables in maximizing the fundamental frequency, the number of design variables is increased in steps. The effective material properties are calculated using micromechanics relations and the numerical solutions are obtained using finite element analysis based on the first-order shear deformation theory. For the implementation of the optimization scheme, a Sequential Quadratic Programming algorithm (SQP) is adopted.

Results indicate that the optimal, non-uniform distributions of the graphene and the fibres lead to higher contents in the outer layers and lower or zero reinforcement in the inner layers. This result is expected and is due to the outer layers contributing more to the stiffness of the laminates. In the case of the graphene being the only reinforcement in the optimization, diminishing returns were observed when the graphene content exceeds a certain limit and the design becomes less cost-effective.

When both graphene and fibre contents along the thickness are adopted as the two design variables and the upper limit on total fibre content is specified as 30%, a higher frequency is obtained as compared to the case with 60% uniform fibre content. Thus, the skew laminates can be designed cost effectively using lower fibre volume contents by distributing the fibres and the graphene across the thickness optimally.

Comparisons are given for the optimal designs of three-phase graphene/fibre-reinforced laminates (the present design) and the traditional two-phase laminates reinforced with fibres only. Results indicate a substantial increase in the fundamental frequency for the three-phase laminates as compared to the two-phase laminates. This increase is higher for glass fibre reinforcement (more than 45%) but is also very significant for carbon fibre reinforcement (more than 20%).

To provide a quantitative criterion for evaluating the results, a design efficiency factor is defined and calculated for each optimal design. Using this factor, optimal design results can be compared and the design efficiencies of different reinforcements can be assessed. The design efficiency increases when the number of design variables increases as expected and the highest design efficiency corresponds to the case with four design variables.

Finally, results for the optimal designs of rectangular and 45° skew plates are compared. It is shown that although the maximum fundamental frequency is higher for the 45° skew laminates, the design efficiency decreases compared to the rectangular laminates for most cases. The differences in the design efficiencies of these two laminate types depend on the number of design variables used in the optimization.

CRediT authorship contribution statement

Y. Jeawon: Writing – original draft, Visualization, Investigation, Formal analysis. **G.A. Drosopoulos:** Writing – review & editing, Supervision, Resources, Methodology, Data curation, Conceptualization. **G. Foutsitzi:** Validation, Software, Methodology, Data curation. **G.E. Stavroulakis:** Writing – review & editing, Resources, Data curation. **S. Adali:** Writing – review & editing, Methodology, Conceptualization.

Declaration of competing interest

The authors declare that they have no known competing financial interests or personal relationships that could have appeared to influence the work reported in this paper.

Data availability

Data will be made available on request

Acknowledgements

The research reported in this paper was supported by research grants from the University of KwaZulu-Natal (UKZN), South Africa and from National Research Foundation (NRF) of South Africa. The authors gratefully acknowledge the supports provided by UKZN, South Africa and NRF, UK.

References

[1] K.D. Rao, K.S. Babu, Modal analysis of thin FRP skew symmetric angle-ply laminate with circular cut-out, Int. J. Eng. Res. Technol. 1 (2012) 1–5.
[2] A. Mandal, C. Ray, S. Haldar, Free vibration analysis of laminated composite skew plates with cut-out, Arch. Appl. Mech. 87 (9) (2017) 1511–1523.
[3] W.H. Liu, W.C. Chen, Vibration analysis of skew cantilever plates with stiffeners, J. Sound Vib. 159 (1) (1992) 1–11.
[4] K. Hosokawa, J. Xie, T. Sakata, Free vibration analysis of cantilevered laminated trapezoidal plates, Sci. Eng. Compos. Mater. 8 (1999) 1–10.
[5] S. Chikkol Venkateshappa, Y.J. Suresh, W.P. Prema Kumar, Free flexural vibration studies on skew plates, Int. J. Aerosp. Lightweight Struct. 2 (2013) 405–420.
[6] A.K. Garg, R.K. Khare, T. Kant, Free vibration of skew fiber reinforced composite and sandwich laminates using a shear deformable finite element model, J. Sandw. Struct. Mater. 8 (1) (2006) 33–53.
[7] F. Gburi, L. Alansari, M. Kadhom, A. Al-Saffar, Free vibration of skew isotropic plate using ANSYS, J. Mech. Eng. Res. Dev. 43 (2020) 472–486.
[8] M. Gürses, Ö. Civalek, A.K. Korkmaz, H. Ersoy, Free vibration analysis of symmetric laminated skew plates by discrete singular convolution technique based on first-order shear deformation theory, Internat. J. Numer. Methods Engrg. 79 (3) (2009) 290–313.

[9] Y. Kiani, Free vibration of FG-CNT reinforced composite skew plates, Aerosp. Sci. Technol. 58 (2016) 178–188.
[10] C. Ömer, A. Mehmet, Free vibration and buckling analyses of CNT reinforced laminated non-rectangular plates by discrete singular convolution method, Eng. Comput. 38 (Suppl 1) (2022) S489–S521.
[11] E. García-Macías, R. Castro-Triguero, E. Saavedra Flores, M. Friswell, R. Gallego, Static and free vibration analysis of functionally graded carbon nanotube reinforced skew plates, Compos. Struct. 140 (2016) 473–490.
[12] L.W. Zhang, On the study of the effect of in-plane forces on the frequency parameters of CNT-reinforced composite skew plates, Compos. Struct. 160 (2017) 824–837.
[13] L. Zhang, Z. Lei, K. Liew, Vibration characteristic of moderately thick functionally graded carbon nanotube reinforced composite skew plates, Compos. Struct. 122 (2015) 172–183.
[14] E. García-Macías, R. Castro-Triguero, Coupled effect of CNT waviness and agglomeration: A case study of vibrational analysis of CNT/polymer skew plates, Compos. Struct. 193 (2018) 87–102.
[15] T. Farsadi, D. Asadi, H. Kurtaran, Fundamental frequency optimization of variable stiffness composite skew plates, Acta Mech. 232 (2020) 555–573.
[16] C.H. Thai, A.J.M. Ferreira, T.D. Tran, P. Phung-Van, Free vibration, buckling and bending analyses of multilayer functionally graded graphene nanoplatelets reinforced composite plates using the NURBS formulation, Compos. Struct. 220 (2019) 749–759.
[17] M. Song, S. Kitipornchai, J. Yang, Free and forced vibrations of functionally graded polymer composite plates reinforced with graphene nanoplatelets, Compos. Struct. 159 (2017) 579–588.
[18] F. Pashmforoush, Statistical analysis on free vibration behavior of functionally graded nanocomposite plates reinforced by graphene platelets, Compos. Struct. 213 (2019) 14–24.
[19] A. Shahrjerdi, S. Yavari, Free vibration analysis of functionally graded graphene-reinforced nanocomposite beams with temperature-dependent properties, J. Braz. Soc. Mech. Sci. Eng. 40 (2018) 25.
[20] Z. Xu, Q. Huang, Vibro-acoustic analysis of functionally graded graphene-reinforced nanocomposite laminated plates under thermal-mechanical loads, Eng. Struct. 186 (2019) 345–355.
[21] U. Topal, Ü. Uzman, Frequency optimization of laminated skew plates, Mater. Des. 30 (2009) 3180–3185.
[22] K. Kalita, P. Dey, S. Haldar, Robust genetically-optimized skew laminates, Proc. Inst. Mech. Eng. C J. Mech. Eng. Sci. 233 (1) (2018) 146–159.
[23] K. Kalita, Dey P., S. Haldar, X. Gao, Optimizing frequencies of skew composite laminates with metaheuristic algorithms, Eng. Comput. 36 (2020) 741–761.
[24] Y. Kiani, K. Kamil Zur, Free vibrations of graphene platelet reinforced composite skew plates resting on point supports, Thin-Walled Struct. 176 (2022) 109363.
[25] C. Feng, S. Kitipornchai, J. Yang, Nonlinear free vibration of functionally graded polymer composite beams reinforced with graphene nanoplatelets (GPLs), Eng. Struct. 140 (2017) 110–119.
[26] R.J. Young, M. Liu, I.A. Kinloch, S. Li, X. Zhao, C. Vallés, D.G. Papageorgiou, The mechanics of reinforcement of polymers by graphene nanoplatelets, Compos. Sci. Technol. 154 (2018) 110–116.
[27] Y. Jeawon, G.A. Drosopoulos, G. Foutsitzi, G.E. Stavroulakis, S. Adali, Optimization and analysis of frequencies of multi-scale graphene/fibre reinforced nanocomposite laminates with non-uniform distributions of reinforcements, Eng. Struct. 228 (2020) 111525.
[28] S.K. Georgantzinos, G.I. Giannopoulos, S.I. Markolefas, Vibration analysis of carbon fibre-graphene-reinforced hybrid polymer composites using finite element techniques, Materials 13 (2020) 4225.
[29] I.S. Radebe, G.A. Drosopoulos, S. Adali, Buckling of non-uniformly distributed graphene and fibre reinforced multiscale angle-ply laminates, Meccanica 54 (14) (2019) 1–17.
[30] JN. Reddy, Mechanics of Laminated Composite Plates and Shells, second ed., 2004, p. CRC Press.
[31] Y. Huang, Z. Yang, A. Liu, J. Fu, Nonlinear buckling analysis of functionally graded graphene reinforced composite shallow arches with elastic rotational constraints under uniform radial load, Materials 11 (6) (2018) 910.
[32] J. Yang, H. Wu, S. Kitipornchai, Buckling and post-buckling of functionally graded multilayer graphene platelet-reinforced composite beams, Compos. Struct. 161 (2017) 111–118.
[33] T. Vo-Duy, V. Ho-Huu, T.D. Do-Thi, H. Dang-Trung, T. Nguyen-Thoi, A global numerical approach for lightweight design optimization of laminated composite plates subjected to frequency constraints, Compos. Struct. 159 (2017) 646–655.
[34] H.-S. Shen, A comparison of buckling and post-buckling behavior of FGM plates with piezoelectric fibre reinforced composite actuators, Compos. Struct. 91 (2009) 375–384.
[35] M. Rafiee, F. Nitzsche, M.R. Labrosse, Modeling and mechanical analysis of multiscale fibre reinforced graphene composites: Nonlinear bending, thermal post-buckling and large amplitude, Int. J. Non-Linear Mech. 103 (2018) 104–112.
[36] R. Gholami, R. Ansari, Y. Gholami, Numerical study on the nonlinear resonant dynamics of carbon nanotube/fibre/polymer multiscale laminated composite rectangular plates with various boundary conditions, Aerosp. Sci. Technol. 78 (2018) 118–129.
[37] S. Kamarian, M. Shakeri, M.H. Yas, Natural frequency analysis and optimal design of CNT/fibre/polymer hybrid composites plates using Mori–Tanaka approach, GDQ technique, and firefly algorithm, Polym. Compos. 9 (5) (2016) 1433–1446.
[38] M. Song, J. Yang, S. Kitipornchai, W. Zhu, Buckling and postbuckling of biaxially compressed functionally graded multilayer graphene nanoplatelet-reinforced polymer composite plates, Int. J. Mech. Sci. 131–132 (2017) 345–355.
[39] Y. Wang, C. Feng, Z. Zhao, J. Yang, Eigenvalue buckling of functionally graded cylindrical shells reinforced with graphene platelets (GPL), Compos. Struct. 202 (2018) 38–46.
[40] Y. Wang, C. Feng, Z. Zhao, J. Yang, Buckling of graphene platelet reinforced composite cylindrical shell with cutout, Int. J. Struct. Stab. Dyn. 18 (03) (2018) 1850040.
[41] J. Nocedal, S.J. Wright, Numerical Optimization, in: Springer Series in Operations Research and Financial Engineering, 2006.
[42] Z.B. Zabinsky, Optimal design of composite structures, in: C.A. Floudas, P.M. Pardalos (Eds.), Encyclopaedia of Optimization, Kluwer Academic Publishers, 2001, pp. 153–160.
[43] P.Y. Papalambros, D.J. Wilde, Principles of Optimal Design, in: Modelling and Computation, Cambridge University Press, 2017.
[44] MATLAB, Version 9.0.0.341360 (R2016a), The MathWorks Inc, Natick, Massachusetts, 2016.
[45] AK. Garg, RK. Khare, T. Kant, Free vibration of skew fiber-reinforced composite and sandwich laminates using a shear deformable finite element model, J. Sandw. Struct. Mater. 8 (1) (2006) 33–53.
[46] O.G. McGee, Natural vibrations of shear deformable cantilevered skew thick plates, J. Sound Vib. 176 (3) (1994) 351–376.

Chapter 6: Fundamental Frequency Analysis of Functionally Graded Graphene-reinforced Rectangular Composite Plates

Yajur Jeawon[a], Georgia Foutsitzi[b], Georgios A. Drosopoulos[c,a]*

[a] Discipline of Civil Engineering, University of KwaZulu-Natal, Durban, South Africa

[b] Department of Informatics and Telecommunications, University of Ioannina, Ioannina, Greece

[c] Discipline of Civil Engineering, University of Central Lancashire, Preston, UK

** Corresponding author (gdrosopoulos@uclan.ac.uk)*

Abstract

This article adopts a functionally graded (FG) distribution of the reinforcement in the thickness direction to determine the fundamental frequency of graphene and fibre-reinforced laminate plates. The work aims to investigate distributions of reinforcement which lead to maximum frequencies for the laminate. Four types of non-uniform distributions are applied to graphene nanoplatelets (GPLs) or fibre reinforcement, investigating the influence of adopting FG distribution for the two reinforcement types. A layerwise functionally graded distribution is also introduced, by considering different distribution type per layer of the laminate. The problem is solved using finite element analysis and first-order shear deformation theory. Different FG distributions, boundary conditions, fibre orientations, and volume contents for graphene and fibre reinforcements are among the many parameters that are tested. It can be seen that as the volume content of fibres increases, uniform graphene reinforcement leads to higher frequencies compared to non-uniform FG graphene distributions. For low fibre content, with values less than 5% (glass) and 7.8% (carbon), a non-uniform FG distribution of graphene (Type X) results in the highest frequencies. Layerwise FG distribution of graphene nanoplatelets (GPLs) are seen to increases fundamental frequencies by approximately 2% compared to non-layerwise FG graphene distribution.

Keywords: Functionally graded laminates, Graphene-fibre reinforcement, Maximum fundamental frequency, Finite Element Analysis, Simply supported laminates, Layerwise functionally graded laminates

1. Introduction

The benefits of using composite laminates in several structural applications have increased over the years, due to their excellent mechanical characteristics including superior strength and reduced material weight [1]. To further improve the structural response of composite materials, nanomaterials of advanced properties are adopted as reinforcement, resulting in the design of reinforced nanocomposite laminates [2]. Common nanoreinforcement materials such as graphene nanoplatelets, carbon nano-fibres and carbon nanotubes are used to improve the mechanical properties and structural response of nanocomposites [3]. Thus, nanocomposites have been adopted across many different industries in the engineering field for various applications including automobiles, electromagnetic shielding, aircrafts and gas pipelines [4, 5]. An estimation of the material properties of nanocomposite structures is provided in [6].

Graphene nanoplatelets (GPLs) as a nanoreinforcement material in laminate composites have gained significant recognition because of their superior mechanical qualities. Research results indicate that the adding minimal amounts of graphene nanoplatelets (GPLs) into the matrix of a composite laminate can significantly improve its thermal, electrical and mechanical characteristics [7]. These superior properties of the nanoreinforcement material can be considered in the design to produce lightweight composite laminates with increased structural tolerances and performance output. Research has been conducted to verify the significant improvement of the graphene-reinforced nanocomposite laminate's properties [7]. One such study was conducted by Rafiee et al. [8], indicating that the benefits in strength and stiffness of adding 1% weight content of carbon nanotubes can also be achieved by adding only 0.1% of graphene weight fraction.

Composite laminates are widely used in ship building, machinery robot arms, aircrafts and other applications as structural components that undergo severe vibrations. To avoid resonance and improve in this sense the vibration response, laminates are designed to work in a higher fundamental frequency [9]. Multiple studies have been presented, highlighting a variety of methods used to improve the natural frequencies of nanocomposite plates. In [10] natural frequencies of skew laminates that contain stiffeners were investigated. The natural frequency of the laminate was found to improve as the skew angle increased. Biswas et al. [11]

presented results related to the fundamental frequency of composites with various cutouts and boundary conditions considered as design variables. According to the outputs of the investigation, higher fundamental frequencies were produced for clamped boundary conditions than for cantilever conditions [11]. Increasing the length-to-width ratio for a nanocomposite multilayer organic solar cell resulted in improved fundamental frequencies [12]. Brethee et al. [13] analysed symmetric and anti-symmetric laminated composite plates with a central cutout in terms of free vibration. Comparison between anti-symmetric and symmetric fibre orientations provided that anti-symmetric fibre orientation produced a higher non-dimensional fundamental frequency over a symmetric orientation [13].

The free vibration characteristics of laminated composite plates, subjected to various constraints, with and without cut-outs, were investigated in [14]. Results showed that improved fundamental frequency and stiffness were derived, when the number of layers is increased. Farsadi et al. in [15], studied the impact of various boundary conditions and fibre angles and found these to influence the natural frequencies of the composite. In [16] Farshi et al. investigated optimal fundamental frequencies via a layer wise approach. Studies provided in [17, 18] indicated that an increase in the fundamental frequency is seen when more layers are added to the laminate composite. In [18] it was also observed that the outer layers are more effective on the bending and frequency response of the composite. Pingulkar et al. provided in [19] that the orientation and hybridization of the material in the outer layers had a far greater effect on the natural frequency than the fibre volume fraction and change in the matrix material.

Numerous numerical studies take into account the quantity of nanocomposite reinforcement and assess its impact on the laminate's vibration response. The volume percentage and distribution of nanoreinforcement, the number and arrangement of layers, and the laminate's shape are some of the variables that affect the natural frequencies of CNT-reinforced composite laminates [20]. Ebrahimi et al. investigated multi-scale carbon nanotube (CNT)/glass fibre reinforced nanocomposite laminated plates and found that the natural frequency is amplified when the content of CNTs and/or glass fibre reinforcement is increased [21]. CNTs were used in [22] to enhance the vibrational response of nanocomposite beams. The study showed that the high elasticity modulus of the carbon nanotube reinforcement contributed to superior fundamental frequency and stiffness values of the plate.

According to [23], the flexural modulus and fracture toughness improved by 14% and 28%, respectively, when the weight of graphene nanoparticles increased by 0.5%, when trying to fabricate graphene-reinforced nanocomposites with enhanced fracture toughness. Adding a small content of graphene reinforcement resulted in improved deflections and natural frequencies, according to an investigation presented in [24]. In [25] it was found that when graphene volume content increased, the natural frequency improved for graphene/fibre reinforced hybrid polymer composites and a greater increase in the natural frequency was experienced by the plate with clamped boundary conditions than the one that was simply supported. Three composite plates were analysed in terms of their natural frequency in [26], considering carbon fibre reinforcement, graphene, and hybrid carbon fibre/graphene reinforcement. Results indicated that the graphene reinforcement enhanced the natural frequency, with the hybrid plate having the optimal fundamental frequency among the three plates.

A study involving fundamental frequency optimization of a 3-phase graphene/fibre reinforced composite laminate is presented in [27]. Findings showed that adding graphene nanoplatelets (GPLs) to the composite laminate increased the fundamental frequency and that the distribution in the outer layers was the most influential for the vibration response [27]. In [28] it was found that for graphene-reinforced composites with functionally graded reinforcement, the functionally graded distribution pattern, clamped boundary conditions, the graphene volume fraction and the thickness ratio had a notable effect on natural frequencies. Notable gains in flexural rigidity, shear, and mass inertia were achieved, by increasing the graphene content in thick plates in [29]. These improvements were then translated into improved fundamental frequencies. The natural frequencies of “functionally graded porous truncated conical shells” reinforced with GPLs were investigated in [30] to determine impact due to porosity and GPLs distributions. Superior reinforcing effects are evident when GPLs with large surface area and GPL nanofillers are added to the composite, resulting in improved fundamental frequencies [30]. A free vibration analysis was performed in [31] on porous cylindrical, graphene-reinforced, functionally graded panels. It was observed that raising the panel's GPL mass fraction, aspect ratio, length-to-thickness ratio and length-to-radius ratio, resulted in an increase in the fundamental frequency. In [32] it is found that the vibration response of laminated curved beams strengthened with graphene reinforcement is improved, with increasing GPL content.

The idea of composite laminates with functionally graded reinforcement has emerged as an intriguing and distinctive approach. Composites consisting of two or more constituent materials, with contents that are continuously or discreetly varied, and with the aim of optimizing the composites' mechanical response, are known as functionally graded materials [33]. To efficiently assign reinforcement contents to critical zones of laminates and produce higher fundamental frequencies, functionally graded nanocomposites can be utilized by distributing the reinforcement in a pattern, on each layer of the laminate [34].

In a study of carbon nanotube-reinforced composites using functionally graded reinforcement types presented in [35], the composite's bending, buckling, and vibration response was highly dependent on the volume rate change of the carbon nanotube. An investigation was conducted in [36] to determine if the natural frequency of a skew composite plate is affected by carbon nanotube distribution and volume proportion. The plate's fundamental frequency was found to be superior with increasing carbon nanotube content and that the natural frequencies were stronger for the FG-X reinforcement pattern than the uniform distribution for a 2-phase composite. In [37], the difference in fundamental frequencies for different functionally graded graphene distributions and a uniform distribution pattern was investigated. For the simply supported boundary condition, the largest fundamental frequencies were produced by the FG-X distribution and then the uniform distribution for the graphene-reinforced composite. It is noted that in the outer surface layers the FG-X distribution, has higher GPL content than the middle layers. In [38], the vibration properties of graphene-reinforced magnetic nanocomposite beams with multiple layers were examined for five distinct FG distributions. The findings demonstrated that adding small contents of graphene causes the natural vibration frequencies to improve, and that the highest fundamental frequencies were produced for the FG-X distribution when compared to other distributions.

In [39] it was found that the volume fractions and material arrangements significantly affect the magnitude of the natural frequencies of functionally graded laminates. In [40] the effects on the fundamental frequency in terms of altering the plate thickness and functionally graded distributions were investigated. Results indicated that a 1% increase in the GPL content improved the fundamental frequency from 121% for a thick plate to 149% for a thin plate for a simply supported plate. The investigation also concluded that it is more efficient to allocate zero GPLs in the middle layers and

higher GPL contents at the outer layers. According to [41] for functionally graded carbon nanotube reinforced composite plates (CNTRC), the boundary conditions, the width to thickness ratio, the volume fraction of reinforcement, aspect ratio and the distribution pattern of reinforcement are among the factors that have a significant impact on the mechanical behaviour.

The influence on the natural frequency of a functionally graded graphene-reinforced composite laminate cylindrical panel was investigated in [42]. Four distribution patterns were applied to the composite, namely, FG-O , FG-V, UD and FG-X, among which, the FG-O and FG-X were found to produce the lowest and highest natural frequencies, respectively. In [43], layerwise distributions of functionally graded GPLs were examined. The analysis revealed that increasing the percentage of GPLs content by a small amount and using GPLs with a square-shaped, which involve a lower amount graphene layers and concentrate on dispersion in the outer surfaces, significantly improved the composite's natural frequency. The free vibration of FG graphene-reinforced composite cylindrical panels with multiple layers was investigated in [44], under four distribution patterns. It was shown that the maximum natural frequency was produced by the FG-X pattern, leading also to the most enhanced vibration response, when the graphene content was increased [44]. The type of distribution is an extremely important factor for influencing the fundamental frequency. In [45] it was highlighted that a large improvement in the fundamental frequency was observed, when GPLs are introduced in the top and bottom layers of the composite laminate. In [46] the effect of using functionally graded graphene reinforcement on a composite sandwich beam was examined. In this instance the maximum fundamental frequency was produced by the FG-V distribution type, followed by the FG-X type. It was also found that increasing the GPL length and width increased the fundamental frequency [46].

This article explores the use of functionally graded reinforcement distributions for a 3-phase graphene/fibre reinforced composite laminate to enhance the vibration response. Five functionally graded distribution patterns are studied, within finite element analysis adopting a first-order shear deformation theory namely, Type 'O', Type 'A', Uniform, Type 'V', and Type 'X'. Among the goals of the article, is to explore how the contents for each of the two reinforcement types (fibres and graphene nanoplatelets) influence the vibration response, for each distribution pattern. In addition, numerical tests on the composite laminate's vibration response

are conducted, for functionally graded fibre and GPL reinforcement distribution. The article also proposes a layerwise functionally graded distribution of the reinforcements, aiming to investigate the impact on natural frequencies, of adopting a different pattern of reinforcement distribution per layer. As far as the Author is aware, only limited studies are found in existing literature regarding the above concepts and in this sense, the innovation and impact of this study are highlighted.
To achieve a cost-effective design, resulting in maximum natural frequencies, a number of variables, including the fibre volume content and distribution type, the fibre type and stacking sequence, boundary conditions, and layerwise functionally graded distributions, are numerically tested, for different FG distribution patterns and reinforcement contents.

2. Formulation of the finite element model

The proposed research investigates the vibrational response of a graphene-reinforced nanocomposite plate subjected to functionally graded distributions of reinforcement with respect to the fundamental frequency achieved with various constraints applied. The composite is investigated for a 2-phase configuration consisting of graphene nanocomposites dispersed into the matrix of the composite and a 3-phase structure which, in addition, includes fibre reinforcement. The composite plate is defined by a length a and a width b located along the x- and y-axes and D which represents the plate thickness along the z-axis. The z-axis is normal to the plate where the plate's midplane and the xy-plane coincide. The plate is oriented with the coordinates of the principal material for the k^{th} lamina having an angle of θ_k to the x-axis and comprises of N layers. $z = z_k$ and $z = z_{k-1}$ represent the k^{th} lamina's top and bottom layers. Figure 1 presents a visual representation of the plate geometry.

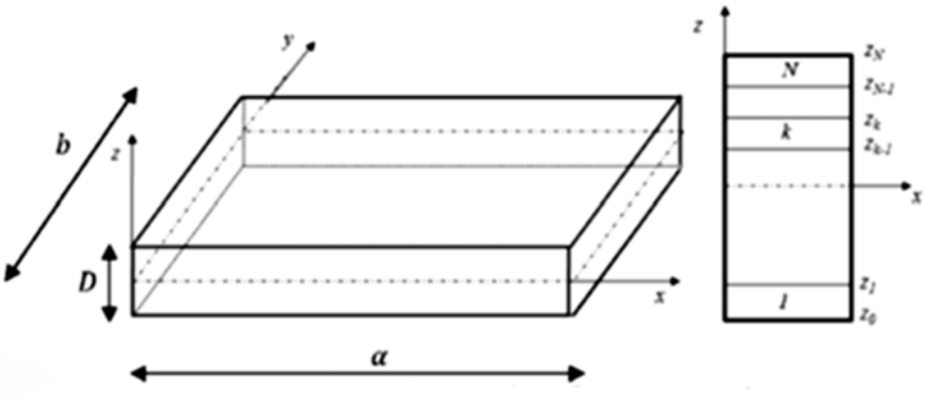

Figure 1: Laminated plate geometry

2.1 Displacement and strains

The first-order shear deformation theory (FSDT) is used to formulate the composite plate displacement field as follows:

$$\begin{aligned} u_1(x,y,z,t) &= u(x,y,t) - z\varphi_x(x,y,t) \\ u_2(x,y,z,t) &= v(x,y,t) - z\varphi_y(x,y,t) \quad or\ \{u\} = [H]\{\bar{u}\} \\ u_3(x,y,z,t) &= w(x,y,t) \end{aligned} \tag{1}$$

where the displacements along the (x, y, z) coordinates, the normal rotations about the *x* and *y*-axes and the point displacements on the mid-plane of the panel are given by u_1, u_2, u_3 , φ_x, φ_y and (u, v, w), respectively. The strain equations are given as:

$$\{\varepsilon\} = \nabla_S\{\bar{u}\} \tag{2}$$

where $\{\varepsilon\} = \{\varepsilon_{xx}, \varepsilon_{yy}, \gamma_{xy}, \gamma_{yz}, \gamma_{xz}\}^T$, $\{\bar{u}\} = \{u, v, w, \varphi_x, \varphi_y\}^T$ and

$$\nabla_S = \begin{bmatrix} \partial/\partial x & 0 & 0 & -z\,\partial/\partial x & 0 \\ 0 & \partial/\partial y & 0 & 0 & -z\,\partial/\partial y \\ \partial/\partial y & \partial/\partial x & 0 & -z\,\partial/\partial y & -z\,\partial/\partial x \\ 0 & 0 & \partial/\partial y & 0 & -1 \\ 0 & 0 & \partial/\partial x & -1 & 0 \end{bmatrix} \tag{3}$$

2.2 Constitutive equations

Eq. (4) represents the k^{th} lamina constitutive relationship as:

$$\{\sigma\}_k = [Q]_k\{\varepsilon\} \tag{4}$$

where the stress vector and elastic stiffness matrix is defined as $\{\sigma\}$ and [Q] respectively. The nonzero components $\mathrm{Q}_{\mathrm{ij}}^{(\mathrm{k})}$ of the elastic stiffness matrix , under plane-stress assumptions and for an orthotropic material are given by [48]:

$$Q_{11}^{(k)} = \frac{E_1^{(k)}}{\left(1 - v_{12}^{(k)} v_{21}^{(k)}\right)}, \quad Q_{12}^{(k)} = \frac{{v_{12}}^{(k)} E_2^{(k)}}{\left(1 - v_{12}^{(k)} v_{21}^{(k)}\right)} = Q_{21}^{(k)}, \quad Q_{22}^{(k)} = \frac{E_2^{(k)}}{(1 - v_{12}^{(k)} v_{21}^{(k)})},$$

$$Q_{66}^{(k)} = G_{12}^{(k)}, \quad Q_{44}^{(k)} = k_s G_{23}^{(k)}, \quad Q_{55}^{(k)} = k_s G_{13}^{(k)} \tag{5}$$

In the above equations, the longitudinal and transverse moduli are represented by $E_1^{(k)}$, $E_2^{(k)}$. The Poisson's Ratio is given by $v_{12}^{(k)}, v_{21}^{(k)}$ and the Shear moduli of the k^{th} layer is $G_{12}^{(k)}, G_{23}^{(k)}, G_{13}^{(k)}$. The shear correction factor, k_s , is assigned a value of $\frac{5}{6}$.

To obtain coefficients $\bar{Q}_{ij}^{(k)}$ represented on the laminate coordinate system(x, y, z), Eq. (6) is used to transform the elastic coefficient $Q_{ij}^{(k)}$, represented in the material coordinates for the k^{th} lamina:

$$\left[\overline{Q}\right]_{(k)} = ([L]^T[Q][L])_{(k)} \tag{6}$$

where $[L(\theta_k)]$ and θ_k *are symbols used to represent* a transformation matrix and the fibre orientation of the k^{th} lamina, respectively as shown in Figure 11.

2.3 Discrete System Equations

A solution to the vibration problem for the laminated plate can be found by using the finite element method, and dynamic equations of motion. This research utilizes a

four-noded isoparametric quadrilateral Lagrangian element to accurately define the laminated plate with each node on the plate containing five degrees of freedom. Eq. (7) defines the generalized displacement vector:

$$\{\overline{u}(x,y,t)\} \equiv \{u,v,w,\varphi_x,\varphi_y\}^T = [N_u]\{d\}_e = \sum_{j=1}^{4}\left(N_j[I]_{5x5}\{d_j\}_e\right) \tag{7}$$

Where the 5x5 identity matrix is $[\mathrm{I}]_{5\mathrm{x}5}$, the Lagrangian shape functions are represented by N_j and the nodal displacement vector is $\{d_j\}_e = \{u_j, v_j, w_j, \varphi_{xj}, \varphi_{yj}\}^T$ for the j^{th} node of the element e. Eq. (8) is formed when Eq. (7) is substituted into Eq. (2):

$$\{\varepsilon(x,y,t)\} = \nabla_S([H][N_u]\{d\}_e) = [B]\{d\}_e \tag{8}$$

where the strain-nodal displacement matrix is $[B]$. In order to determine the dynamic equations of the laminate plate, the Hamilton's principle is applied and the relationship is given by:

$$\int_{t_1}^{t_2}\left\{\sum_{k=1}^{N}\left(\int_A\int_{z_{k-1}}^{z_k}\{\delta\varepsilon\}^T[\bar{Q}]_k\{\varepsilon\}\,dzdA - \int_A\int_{z_{k-1}}^{z_k}\{\delta\dot{u}\}^T\rho_k\{\dot{u}\}dzdA\right)\right.$$

$$\left.-\left(\{\delta u\}^T\{f_c\} + \int_A\{\delta u\}^T\{f_s\}dA + \int_{V_e}\{\delta u\}^T\{f_V\}dV\right)\right\}dt = 0 \tag{9}$$

where the volume and area of the element, e, are V_e and A_e respectively. The density of the k^{th} layer is ρ_k. Additionally, $[\bar{Q}]_k$ represents the elastic stiffness matrix provided in Eq. (4). In Eq. (9), $\{f_V\}$ and $\{f_s\}$, denote the volume and surface forces, respectively and the concentrated forces are denoted by $\{f_c\}$.

The elementary governing equations of motion for each element can be derived by substituting the discretization of mechanical displacements (7), the displacements relations (1) and the strain-nodal displacement relation (8) into Hamilton's principle Eq. (9). The governing equations of motion for the global system can be formulated by assembling the obtained discretized equations for the total number of elements by

using the standard procedure of the finite element method and can be expressed as follows [27]:

$$[M]\{\ddot{d}\} + [K]\{d\} = \{F_m\} \tag{10}$$

where $\{F_m\}, [K], [M]$ *and* $\{d\}$ are the global force vector, the global linear stiffness matrix, global mass matrix and the global displacement vector, respectively. Eq. (10) can be used to analyse the free vibration by eliminating the force term to give:

$$[K]\{d\} = \lambda[M]\{d\} \tag{11}$$

where $\lambda = \omega^2$is the eigenvalue and the natural vibration frequency is represented by ω. The finite element model previously presented is implemented via MATLAB model codes to study the free vibration response of rectangular laminated composite plates for various design parameters. Notice that, a selective integration technique is applied when calculating the stiffness matrix to mitigate against shear locking effects.

3. Overall effective material properties of the composite

The composite being investigated is a 3-phase polymer nanocomposite plate where graphene nanoplatelets (GPLs) are utilized as a nano-reinforcement to enhance its structural response and mechanical properties. In order to achieve a 3-phase composite, a nanoreinforced, isotropic matrix is produced by dispersing nanoreinforcement particles into the matrix. Fibre reinforcement is then added to the nanoreinforced matrix. The Halpin-Tsai model and rule of mixtures [49,50] which is commonly applied in published papers to effectively calculate the effective material properties of a 2-phase matrix reinforced with graphene was used to obtain the effective material properties of the composite. The process involves first determining the effective material properties of the 2-phase graphene-reinforced matrix by using micromechanical equations and thereafter by applying the same equations, 3-phase nanocomposite properties can be calculated [51]. This approach has been used in a number of studies such as in [52], to determine a 2-phase laminate's effective

properties and then used in [53] to determine a 3-phase laminate's effective properties.

3.1 Calculation of the effective material properties of a graphene-reinforced matrix

Micromechanics equations used in [49,54-56] were adopted and applied to a graphene-reinforced matrix to determine the effective material properties. The subscripts for the matrix, graphene nanoplatelets (GPLs) and the graphene-reinforced matrix were assigned as M, GPL and GM respectively. The following equation was used to derive the Young's Modulus of the graphene-reinforced matrix:

$$E_{GM} = \left(\frac{3}{8}\frac{1+\xi_L\eta_L V_{GPL}}{1-\eta_L V_{GPL}} + \frac{5}{8}\frac{1+\xi_w\eta_w V_{GPL}}{1-\eta_w V_{GPL}}\right) \times E_M \tag{12}$$

The Young's modulus of the matrix and the volume of graphene nanoplatelets (GPLs) are represented as E_M and V_{GPL}, respectively. By using the values for graphene nanoplatelet length ($\mathrm{l_{GPL}}$), width (w_{GPL}) and thickness ($\mathrm{h_{GPL}}$), the parameters ξ_L and ξ_w can be calculated in the equations:

$$\xi_\mathrm{L} = 2\frac{\mathrm{l_{GPL}}}{\mathrm{h_{GPL}}}, \qquad \xi_\mathrm{w} = 2\frac{\mathrm{w_{GPL}}}{\mathrm{h_{GPL}}} \tag{13}$$

Using Eq. (14) where $\mathrm{E_M}$ and $\mathrm{E_{GPL}}$ are the Young's moduli for the matrix and graphene nanoplatelets, the values for η_L and η_w can be derived:

$$\eta_\mathrm{L} = \frac{(\mathrm{E_{GPL}/E_M})-1}{(\mathrm{E_{GPL}/E_M})+\xi_\mathrm{L}}, \qquad \eta_\mathrm{w} = \frac{(\mathrm{E_{GPL}/E_M})-1}{(\mathrm{E_{GPL}/E_M})+\xi_\mathrm{w}} \tag{14}$$

Eq. (15) can be used to calculate $\mathrm{V_{GPL}}$ using the graphene nanoplatelets (GPLs) weight fraction $\mathrm{W_{GPL}}$:

$$\mathrm{V_{GPL}} = \frac{\mathrm{W_{GPL}}}{\mathrm{W_{GPL}}+(\rho_\mathrm{GPL}/\rho_\mathrm{M})(1-\mathrm{W_{GPL}})} \tag{15}$$

The Poisson's ratio, effective Shear modulus and matrix density for the graphene-reinforced matrix are given by the following equations:

$$G_{GM} = \frac{E_{GM}}{2(1+v_{GM})} \quad (16)$$

$$v_{GM} = v_{GPL}V_{GPL} + v_M(1 - V_{GPL}) \quad (17)$$

$$\rho_{GM} = \rho_{GPL}V_{GPL} + \rho_M(1 - V_{GPL}) \quad (18)$$

where ρ_M and ρ_{GPL} symbolize mass density of the polymer matrix and the graphene nanoplatelets.

3.2 Effective material properties of the 3-phase graphene and fibre reinforced matrix

The equations below represent the effective material properties for a 3-phase graphene/fibre reinforced matrix [51,54,55,57]:

$$E_{11} = E_{F1}\ V_F + E_{GM}(1 - V_F) \quad (19)$$

$$E_{22} = E_{GM}\ \left(\frac{E_{F22}+E_{GM}+(E_{F2}\ -E_{GM})V_F}{E_{F22}+E_{GM}-(E_{F22}-\ E_{GM})V_F}\right) \quad (20)$$

$$G_{12} = G_{13} \quad (21)$$

$$G_{12} = G_{GM}\ \left(\frac{G_{F12}+G_{GM}+(G_{F12}-G_{GM})V_F}{G_{F1}\ +G_{GM}-(G_{F12}-\ G_{GM})V_F}\right) \quad (22)$$

$$G_{23} = \frac{E_{22}}{2(1+V_{23})} \quad (23)$$

$$v_{12} = v_{F12}V_F + v_{GM}(1 - V_F) \quad (24)$$

$$v_{23} = v_{F12}V_F + v_{GM}(1 - V_F)\left(\frac{1+v_{GM}+v_{12}E_{GM}/E_{11}}{1-v^2{}_{GM}+v_{12}v_{GM}E_{GM}/E_{11}}\right) \quad (25)$$

$$\rho = \rho_F V_F + \ \rho_{GM}(1 - V_F) \quad (26)$$

The subscript GM and F denote the graphene-reinforced matrix and fibre, respectively. ρ_F and V_F are used to represent the fibre density and fibre volume, respectively.

3.3 Functionally graded distribution of reinforcement

In the present work, the fibre volume content $V_F^{(k)}$ or the volume content of graphene nanoplatelets (GPLs) $V_{GPL}^{(k)}$ of each layer are assumed to be distributed functionally through the thickness direction of each ply as:

$$V_F^{(k)} = V_F^* f^{(k)}(\bar{z}), \qquad V_{GPL}^{(k)} = V_{GPL}^* f^{(k)}(\bar{z}) \tag{27}$$

where V_F^* and V_{GPL}^* are the total fibre and GPLs volumes, respectively. Figure 2 shows the functionally graded distribution types which are tested in this study.

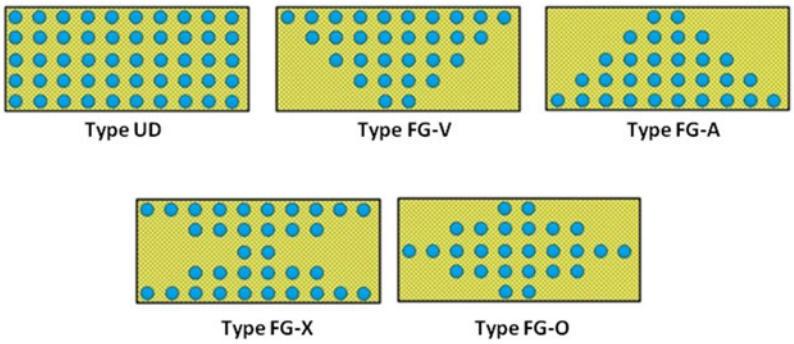

Figure 2: Functionally graded distribution patterns for each ply of the laminate ([58]) (CC BY 4.0 DEED)

The function $f^{(k)}(\bar{z})$ in Eq. (27) determines the type of the fibre and GPL arrangement the thickness direction of each layer (i.e. of each ply of the laminate), and is determined by:

$$f^{(k)}(z) = \begin{cases} 1, & UD - Uniform \\ 1 + \bar{z}, & FG - \text{Type 'V'} \\ 2(1 - \bar{z}), & FG - \text{Type 'O'} \\ 2\bar{z}, & FG - \text{Type 'X'} \\ 1 - \bar{z}, & FG - \text{Type 'A'} \end{cases} \tag{28}$$

Since the fibre and GPL distribution can be applied in each ply separately (layerwise), each layer can be defined with the mid-plane of the layer coinciding with the origin of the local coordinate system. Thus, the variable $\bar{z}$ in the above equations represents the orthogonal component of the defined local system of the k^{th} layer and it is given by $\bar{z} = [2z - (z_{k+1} + z_k)]/(z_{k+1} - z_k)$.

Due to relations (28), the material properties $\bar{Q}_{ij}^{(k)}$ are functions of the transverse coordinate z. Therefore, the function 'integral' embedded in MATLAB has been employed to calculate the integrals with respect to z.

4. Verification of the optimization code

The proposed finite element analysis scheme for the evaluation of the natural frequencies of functionally graded, 3-phase, laminates reinforced with graphene and

fibre, is implemented in Matlab. To verify the proposed scheme, comparison of the results obtained from this study to results derived from published research presented in [59] takes place. The model used for the verification is a five-layered, rectangular laminate with SSSS or SCSC boundary conditions. The laminate consists of carbon nanotube (CNT) reinforcement which has been applied in terms of Uniform, Type 'A', and Type 'X' functionally graded distributions. The CNT volume content is obtained considering Eq. (27), that is in this case, $V_{CNT}^{(k)} = V_{CNT}^{*} f^{(k)}(\bar{z})$.

The analysis is implemented using a 10 x 10 mesh size with shell elements. Results are produced a non-dimensional fundamental frequency Ω form, defined by:

$$\Omega = \omega D \sqrt{\frac{\rho_M}{E_M}} \tag{29}$$

In Eq. (29), ρ_M and E_M represent the matrix density and Young's modulus. D is the laminate thickness. In the verification analysis $V_{CNT}^{*} = 0.11$ is equal to 0.11.

Table 1: Verification of the fundamental frequency for a 5-layered simply supported (SSSS) rectangular laminate with (0/90/0/90/0) fibre orientation and $V_{CNT}^{*} = 0.11$ subject to thickness over length ratio $D/a = 0.1$ and aspect ratio $a/b = 1$.

		Distribution Type		
Verification Source	Mode	Uniform	Type 'A'	Type 'X'
DSC-Shannon's Delta Kernel [59]	1	14.2952	14.2243	14.4170
	2	19.4565	19.4051	19.4805
	3	19.4590	19.3875	19.4811
	4	27.1007	26.9832	27.3274
	5	38.3273	29.8078	31.0052
DSC-Lagrange Delta Kernel [59]	1	14.3007	14.2271	14.4189
	2	19.4594	19.4068	19.4916
	3	19.4612	19.3904	19.4873
	4	27.1023	26.9863	27.3317
	5	38.3291	29.8103	31.0115
Present Study	1	14.24281	14.20288	14.35139
	2	19.50747	19.55746	19.55748
	3	19.50747	19.55746	19.55748
	4	27.86508	27.77468	28.11309
	5	39.4968	32.53359	32.65229

Table 2: Verification of the fundamental frequency for a 5-layered simply supported and clamped (SCSC) rectangular laminate with (0/90/0/90/0) fibre orientation and $V_{CNT}^{*} = 0.11$ *subject to thickness over length ratio D/a=0.1 and aspect ratio a/b=1.*

		Distribution Type		
Verification Source	Mode	Uniform	Type 'A'	Type 'X'
DSC-Shannon's Delta Kernel [59]	1	17.3918	17.3640	17.8205
	2	20.1052	19.8932	20.1768
	3	30.0584	29.7346	30.1614
	4	32.9473	30.9571	33.9174
	5	39.7681	38.6854	40.0546
DSC-Lagrange Delta Kernel [59]	1	17.3934	17.3669	17.8312
	2	20.1087	19.8957	20.1805
	3	30.0612	29.7360	30.1683
	4	32.9501	30.9595	33.9220
	5	39.7713	38.6889	40.0614
Present Study	1	17.74844	17.74191	17.84505
	2	19.50747	19.55746	19.55748
	3	29.63102	29.55694	29.87145
	4	33.69359	33.73472	33.81878
	5	39.49685	39.59798	39.5981

The results from Table 1 and 2 show that the fundamental frequency produced correlates with the results obtained from previously published articles for the boundary condition SSSS and SCSC. Therefore, the proposed numerical scheme will be used in the next sections to evaluate the vibration response of 3-phase, graphene/fibre reinforced, and functionally graded laminates.

The frequencies for the first two eigenmodes show a close correlation between the present study and that of published articles with the percentage difference being within 0.15% to 0.78% for Table 1 and 0% to 3% for Table 2 (SCSC) for each distribution type. The fundamental frequency is mainly investigated in this research within the suggested optimization concept and for this reason, those differences are acceptable. Some higher differences that appear for higher natural modes, could be

reduced if a denser mesh was adopted. However, this would increase the computational cost for the majority of subsequent simulations.

5. Results and Discussion

3-phase, graphene/fibre reinforced, functionally graded laminates are evaluated in this section in terms of their vibration response. The dimensions of the graphene nanoplatelets (GPLs) in the subsequent analysis were taken equal to $l_{GPL} = 2.5\,\mu m$, $w_{GPL} = 1.5\,\mu m$, and $h_{GPL} = 1.5\,nm$. An eight-layered laminate is considered, with thickness-to-length ratio D/a=0.03, different boundary conditions, including simply supported (SSSS), cantilever (CFFF), clamped (CCCC), as well as alternating clamped and simply supported (SCSC) and aspect ratio a/b = 1.

Fibre orientations included anti-symmetric stacking sequence, $[0/90/0/90]_{anti\text{-}s}$ but more stacking sequences were tested. The functionally graded distributions provided in relations (27) and (28) are adopted. Results are provided in terms of non-dimensional frequency as shown in Eq. (29).

5.1 3-phase graphene/fibre reinforced laminate with functionally graded graphene reinforcement

In this section, vibration response of 3-phase graphene/fibre reinforced laminates is examined, by using functionally graded distribution for the graphene nanoplatelets (GPLs) reinforcement. The distribution types provided in Figure 2 are adopted and parameters like the boundary conditions, the V_{GPL}^{*} content and the stacking sequence are tested.

Table 3 shows the results regarding the effect of different laminate boundary conditions. The simulation has been conducted for the following four boundary conditions: clamped on all four edges (CCCC), simply supported (SSSS), cantilever (CFFF) and clamped on two edges and simply supported on two edges (SCSC).

It is first noticed that Uniform distribution results in higher natural frequencies than the other distribution types, for the four boundary conditions. This differentiates with the results derived in [59] and presented in Tables 1, 2, where Type X distribution leads to highest natural frequencies. This difference in the optimal distribution type is attributed to the contribution of the fibre reinforcement, in this paper, as compared to zero fibre reinforcement in [59]. This matter, of identifying the distribution type which leads to highest natural frequencies, is further investigated in the subsequent part of this article.

The SSSS boundary conditions resulted in the Uniform distribution of graphene producing the largest fundamental frequency of 0.2383 and 0.2166 for carbon and

glass fibres, resulting in an improvement of the frequency equal to 10% for carbon fibres.

The CFFF boundary conditions also resulted in the highest fundamental frequency for Uniform distribution of graphene. The maximum natural frequencies produced by glass and carbon fibres are 0.0388 and 0.0471, respectively. It can be seen that with carbon fibres three distribution types performed best and produced the same maximum frequency, namely, the Uniform distribution, Type 'X' and Type A'.

Under clamped conditions (CCCC), the maximum value produced for the fundamental frequency is again the one derived from Uniform distribution type for both fibre types with a frequency value of 0.4220 and 0.3740 for carbon and glass fibres, indicating an increase of 12.83% for carbon fibres.

Similar to previous cases, SCSC boundary conditions resulted in maximum fundamental frequencies for the Uniform distribution, with values equal 0.3428 and to 0.3058 for carbon and glass fibres, respectively.

When the results are compared, it is evident that the fundamental frequency values are significantly different in magnitude for every boundary condition. The lowest fundamental frequencies are produced for CFFF boundary conditions. The fundamental frequencies obtained by CFFF with glass fibres are approximately 5 times lower than SSSS, 8 times lower than SCSC and 10 times smaller than CCCC boundary conditions. The fundamental frequencies derived by CFFF with carbon fibres are approximately 5 times lower than SSSS, 7 times lower than SCSC and 9 times lower than CCCC.

Table 3: Fundamental frequency for an 8-layered laminate with anti-symmetric fibre orientation ($[0/90/0/90]_{anti\text{-}s}$) under various boundary conditions subject to constant $V_{GPL}^{*} = 0.05$, $V_F = 0.3$ and $D/a = 0.03$

Boundary Condition	Fibre type	Distribution Type	Ω
Simply Supported (SSSS)	Glass	Uniform	0.2166
		Type 'X'	0.2131
		Type 'V'	0.2123
		Type 'O'	0.2120
		Type 'A'	0.2123
	Carbon	Uniform	0.2383
		Type 'X'	0.2363
		Type 'V'	0.2357
		Type 'O'	0.2354
		Type 'A'	0.2357
Cantilever (CFFF)	Glass	Uniform	0.0388
		Type 'X'	0.0384
		Type 'V'	0.0382
		Type 'O'	0.0382
		Type 'A'	0.0383
	Carbon	Uniform	0.0471
		Type 'X'	0.0471
		Type 'V'	0.0469
		Type 'O'	0.0469
		Type 'A'	0.0471
Clamped (CCCC)	Glass	Uniform	0.3740
		Type 'X'	0.3688
		Type 'V'	0.3676
		Type 'O'	0.3672
		Type 'A'	0.3676
	Carbon	Uniform	0.4220
		Type 'X'	0.4195
		Type 'V'	0.4187
		Type 'O'	0.4183
		Type 'A'	0.4187
Simply supported and clamped (SCSC)	Glass	Uniform	0.3058
		Type 'X'	0.3014
		Type 'V'	0.3002
		Type 'O'	0.3000
		Type 'A'	0.3005
	Carbon	Uniform	0.3428
		Type 'X'	0.3406
		Type 'V'	0.3395
		Type 'O'	0.3395
		Type 'A'	0.3402

Table 4: Fundamental frequency for an 8-layered simply supported rectangular laminate with varying symmetric fibre orientations subject to constant $V_{GPL}^{*} = 0.05$, $V_F = 0.3$ and $\mathrm{D/a} = 0.03$.

Stacking sequence	Fibre type	Distribution Type	Ω
$[90/0/90/0]_s$	Glass	Uniform	0.2166
		Type 'X'	0.2132
		Type 'V'	0.2123
		Type 'O'	0.2120
		Type 'A'	0.2123
	Carbon	Uniform	0.2391
		Type 'X'	0.2372
		Type 'V'	0.2366
		Type 'O'	0.2363
		Type 'A'	0.2366
$[45/45/45/45]_s$	Glass	Uniform	0.2171
		Type 'X'	0.2147
		Type 'V'	0.2139
		Type 'O'	0.2136
		Type 'A'	0.2139
	Carbon	Uniform	0.2479
		Type 'X'	0.2471
		Type 'V'	0.2465
		Type 'O'	0.2462
		Type 'A'	0.2465
$[0/30/45/60]_s$	Glass	Uniform	0.2167
		Type 'X'	0.2137
		Type 'V'	0.2129
		Type 'O'	0.2126
		Type 'A'	0.2129
	Carbon	Uniform	0.2444
		Type 'X'	0.2430
		Type 'V'	0.2424
		Type 'O'	0.2421
		Type 'A'	0.2424
$[30/30/30/30]_s$	Glass	Uniform	0.2169
		Type 'X'	0.2143
		Type 'V'	0.2135
		Type 'O'	0.2132
		Type 'A'	0.2135
	Carbon	Uniform	0.2456
		Type 'X'	0.2445
		Type 'V'	0.2438
		Type 'O'	0.2436
		Type 'A'	0.2438

Table 4 continued

Stacking sequence	Fibre type	Distribution Type	Ω
$[60/60/60/60]_s$	Glass	Uniform	0.2169
		Type 'X'	0.2143
		Type 'V'	0.2135
		Type 'O'	0.2132
		Type 'A'	0.2135
	Carbon	Uniform	0.2456
		Type 'X'	0.2445
		Type 'V'	0.2438
		Type 'O'	0.2436
		Type 'A'	0.2438
$[90/90/90/90]_s$	Glass	Uniform	0.2166
		Type 'X'	0.2132
		Type 'V'	0.2123
		Type 'O'	0.2120
		Type 'A'	0.2123
	Carbon	Uniform	0.2391
		Type 'X'	0.2372
		Type 'V'	0.2365
		Type 'O'	0.2363
		Type 'A'	0.2365

In Table 4 the fundamental frequency change is investigated for various stacking sequences. in Table 4 and similar to previous results, the Uniform distribution leads to higher fundamental frequencies for the stacking sequences that are tested. In particular, the highest fundamental frequencies were observed for the Uniform distribution type, with carbon fibres providing a maximum frequency higher by 14.29% compared to glass fibres.

The lowest frequency for carbon fibres, was equal to 0.2363 and was obtained for a Type 'O' distribution with 90° fibres in every layer, as well as with $[90/0/90/0]_s$ fibre orientation in the laminate. An increase in the frequency equal to 4.91% is observed from Type 'O' to Uniform distribution.

For the simulations with glass fibres and fibre angles equal to 30° and 60° in every layer, the highest frequency (0.2169) was obtained from the Uniform distribution and the lowest (0.2120) from the distribution Type 'O'. The increase in frequency from Type 'O' to Uniform is 2.31%.

In Table 4, a comparison is made between the different stacking sequences; observation shows a uniform fibre angle of 45° provided the highest fundamental

frequencies. The lowest frequency values are produced for uniform fibre angles of 30°.

Table 5: Fundamental frequency for an 8-layered simply supported rectangular laminate with anti-symmetric fibre orientation ([0/90/0/90]$_{anti\text{-}s}$) and varying V_{GPL}^{*} subject to constant $V_F = 0.3$ with $D/a = 0.03$.

Fibre type	Distribution Type	Ω	% difference with previous V_{GPL}^{*}
$V_{GPL}^{*} = 0.005$			
Glass	Uniform	0.1139	-
	Type 'X'	0.1137	-
	Type 'V'	0.1135	-
	Type 'O'	0.1134	-
	Type 'A'	0.1135	-
Carbon	Uniform	0.1559	-
	Type 'X'	0.1555	-
	Type 'V'	0.1554	-
	Type 'O'	0.1554	-
	Type 'A'	0.1554	-
$V_{GPL}^{*} = 0.01$			
Glass	Uniform	0.1333	17%
	Type 'X'	0.1326	17%
	Type 'V'	0.1322	16%
	Type 'O'	0.1321	16%
	Type 'A'	0.1322	16%
Carbon	Uniform	0.1705	9%
	Type 'X'	0.1698	9%
	Type 'V'	0.1696	9%
	Type 'O'	0.1695	9%
	Type 'A'	0.1696	9%
$V_{GPL}^{*} = 0.02$			
Glass	Uniform	0.1620	22%
	Type 'X'	0.1603	21%
	Type 'V'	0.1598	21%
	Type 'O'	0.1596	21%
	Type 'A'	0.1598	21%
Carbon	Uniform	0.1926	13%
	Type 'X'	0.1913	13%
	Type 'V'	0.1909	13%
	Type 'O'	0.1907	13%
	Type 'A'	0.1909	13%

Table 5 continued

$V_{GPL}^{*} = 0.05$			
Glass	Uniform	0.217	34%
	Type ‘X’	0.213	33%
	Type ‘V’	0.212	33%
	Type ‘O’	0.212	33%
	Type ‘A’	0.212	33%
Carbon	Uniform	0.238	24%
	Type ‘X’	0.236	24%
	Type ‘V’	0.236	23%
	Type ‘O’	0.235	23%
	Type ‘A’	0.236	23%
$V_{GPL}^{*} = 0.1$			
Glass	Uniform	0.274	26%
	Type ‘X’	0.270	27%
	Type ‘V’	0.269	27%
	Type ‘O’	0.268	27%
	Type ‘A’	0.269	27%
Carbon	Uniform	0.292	23%
	Type ‘X’	0.291	23%
	Type ‘V’	0.290	23%
	Type ‘O’	0.289	23%
	Type ‘A’	0.290	23%
$V_{GPL}^{*} = 0.15$			
Glass	Uniform	0.316	16%
	Type ‘X’	0.314	16%
	Type ‘V’	0.312	16%
	Type ‘O’	0.312	16%
	Type ‘A’	0.312	16%
Carbon	Uniform	0.336	15%
	Type ‘X’	0.335	15%
	Type ‘V’	0.334	15%
	Type ‘O’	0.333	15%
	Type ‘A’	0.334	15%
$V_{GPL}^{*} = 0.2$			
Glass	Uniform	0.353	12%
	Type ‘X’	0.351	12%
	Type ‘V’	0.349	12%
	Type ‘O’	0.349	12%
	Type ‘A’	0.349	12%
Carbon	Uniform	0.374	11%
	Type ‘X’	0.374	12%
	Type ‘V’	0.372	12%
	Type ‘O’	0.372	12%
	Type ‘A’	0.372	12%

By varying the volume content of graphene (V_{GPL}^{*}) from 0.005 to 0.2, the effect on the natural frequency is tested and the results recorded in Table 5. The analysis was implemented for seven volume content values of 0.005, 0.01, 0.02, 0.05, 0.1, 0.15 and 0.2. Increasing the quantity of V_{GPL}^{*} causes the resultant non-dimensional fundamental frequencies to improve. The same result is observed for both glass and carbon fibre types. Each analysis also shows that the non-dimensional frequency is higher when using carbon fibres than glass fibres with an increase of approximately 10% to 11% from glass to carbon fibres.

The percentage increase in the fundamental frequencies for higher quantity of V_{GPL}^{*} has been recorded in Table 5. The results indicated that an increase in the V_{GPL}^{*} amount from 0.005 to 0.01 resulted in enhancement of the frequency of approximately 9% for carbon fibres and 16% to 17% for glass fibres. The increase in V_{GPL}^{*} from 0.01 to 0.02 caused a frequency increase of 13% and 21% for carbon and glass fibres, respectively. The next increase in V_{GPL}^{*} from 0.02 to 0.05 produced a frequency increase equal to 33% for glass and approximately 23% to 24% for carbon fibres.

Increasing the value of V_{GPL}^{*} from 0.05 to 0.1 caused the frequency to improve by approximately 23% and 27% for carbon and glass fibres, respectively. The increase in the V_{GPL}^{*} content from 0.1 to 0.15 resulted in approximately a 15% and 16% increase in the frequency for carbon and glass fibres respectively. Finally, the increase in the V_{GPL}^{*} content from 0.15 to 0.2 improved the frequency by approximately 12% for both fibre types.

These descriptions lead to the conclusion that from $V_{GPL}^{*} = 0.005$ to $V_{GPL}^{*} = 0.05$, the fundamental frequencies increase with a higher rate, as compared to those obtained for $V_{GPL}^{*} = 0.1$ and higher. This means that raising the volume content of graphene in the laminate will present a diminishing return for V_{GPL}^{*} higher than 0.05.

It is also observed that the laminates utilizing a Uniform distribution of graphene nanoplatelets (GPLs) lead to the highest fundamental frequencies. For a given V_{GPL}^{*} content, the variance in the fundamental frequency obtained from each distribution type is very low.

Table 6: Fundamental frequency for an 8-layered simply supported rectangular laminate with anti-symmetric fibre orientation ([0/90/0/90]$_{anti\text{-}s}$) and varying V_F subject to constant $V_{GPL}^{*} = 0.05$ with $D/a = 0.03$.

Fibre type	Distribution Type	Ω
$V_F = 0.02$		
Glass	Uniform	0.2331
	Type 'X'	0.2336
	Type 'V'	0.2323
	Type 'O'	0.2320
	Type 'A'	0.2323
Carbon	Uniform	0.2344
	Type 'X'	0.2350
	Type 'V'	0.2337
	Type 'O'	0.2334
	Type 'A'	0.2337
$V_F = 0.05$		
Glass	Uniform	0.2309
	Type 'X'	0.2309
	Type 'V'	0.2296
	Type 'O'	0.2294
	Type 'A'	0.2296
Carbon	Uniform	0.2343
	Type 'X'`	0.2346
	Type 'V'	0.2334
	Type 'O'	0.2331
	Type 'A'	0.2334
$V_F = 0.078$		
Glass	Uniform	0.2290
	Type 'X'	0.2285
	Type 'V'	0.2273
	Type 'O'	0.2270
	Type 'A'	0.2273
Carbon	Uniform	0.2344
	Type 'X'	0.2344
	Type 'V'	0.2332
	Type 'O'	0.2329
	Type 'A'	0.2332

Table 6 continued

$V_F = 0.1$		
Glass	Uniform	0.2275
	Type ‘X’	0.2267
	Type ‘V’	0.2255
	Type ‘O’	0.2252
	Type ‘A’	0.2255
Carbon	Uniform	0.2345
	Type ‘X’	0.2343
	Type ‘V’	0.2333
	Type ‘O’	0.2329
	Type ‘A’	0.2333
$V_F = 0.3$		
Glass	Uniform	0.2166
	Type ‘X’	0.2131
	Type ‘V’	0.2123
	Type ‘O’	0.2120
	Type ‘A’	0.2123
Carbon	Uniform	0.2383
	Type ‘X’	0.2363
	Type ‘V’	0.2357
	Type ‘O’	0.2354
	Type ‘A’	0.2357
$V_F = 0.5$		
Glass	Uniform	0.2087
	Type ‘X’	0.2038
	Type ‘V’	0.2032
	Type ‘O’	0.2030
	Type ‘A’	0.2032
Carbon	Uniform	0.2433
	Type ‘X’	0.2405
	Type ‘V’	0.2401
	Type ‘O’	0.2399
	Type ‘A’	0.2401
$V_F = 0.6$		
Glass	Uniform	0.2057
	Type ‘X’	0.2005
	Type ‘V’	0.2000
	Type ‘O’	0.1998
	Type ‘A’	0.2000
Carbon	Uniform	0.2460
	Type ‘X’	0.2429
	Type ‘V’	0.2426
	Type ‘O’	0.2425
	Type ‘A’	0.2426

To further research the effect of fibre reinforcement on the kind of functionally graded graphene distribution that produces the highest frequencies, the fibre volume content is considered as variable in Table 6. In particular, $\mathrm{V_F}$ is assigned different volume contents ranging from 2% to 60% and V_{GPL}^{*} is functionally graded distributed in the laminate at a constant value of 0.05.

It is observed in Table 6 that for increasing fibre content, and as the fibre content remains lower than 0.05 (glass fibres) and 0.078 (carbon fibres), the Type 'X' distribution produces the highest fundamental frequency in comparison to the remaining distribution types. This differentiates with the results derived for fibre volume content equal to 30% provided in Table 3, where the Uniform distribution leaded to highest frequencies.

It is also observed that when the volume content of glass fibre reinforcement increases, the non-dimensional frequency decreases. The decrease was higher for fibre content between 30% and 50%. The decrease in this case is 4% whereas the decrease in the natural frequency from 50% to 60% fibre content is 1%.

On the other hand, increasing the quantity of carbon fibre reinforcement resulted in an increase in the frequencies of 2% and 1% for $V_F = 0.5$ and $V_F = 0.6$, respectively. The largest observed fundamental frequency for carbon fibre reinforcement is 0.2460 for $V_F = 0.6$ and graphene reinforcement with a Uniform distribution.

To further investigate the influence of the fibre volume content on the optimal distribution type, figures 3 and 4 below provide the variation of the fundamental frequencies for increasing fibre content, for both Uniform and Type X distributions.

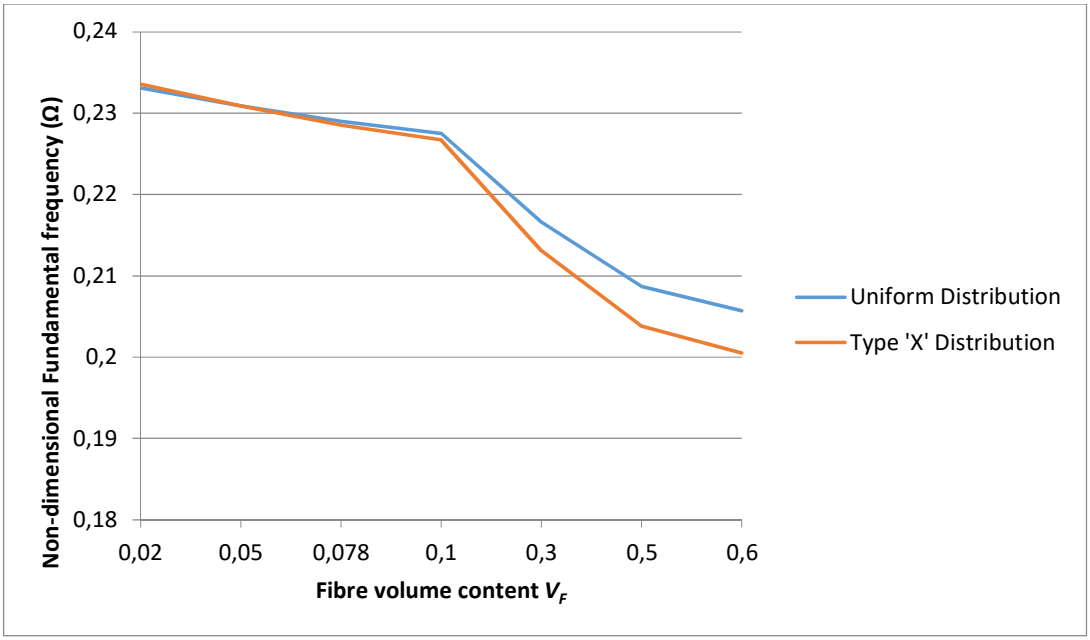

Figure 3: Fundamental frequency for various glass fibre (V_F) content using Uniform and Type 'X' distribution and V^*_{GPL}=0.05

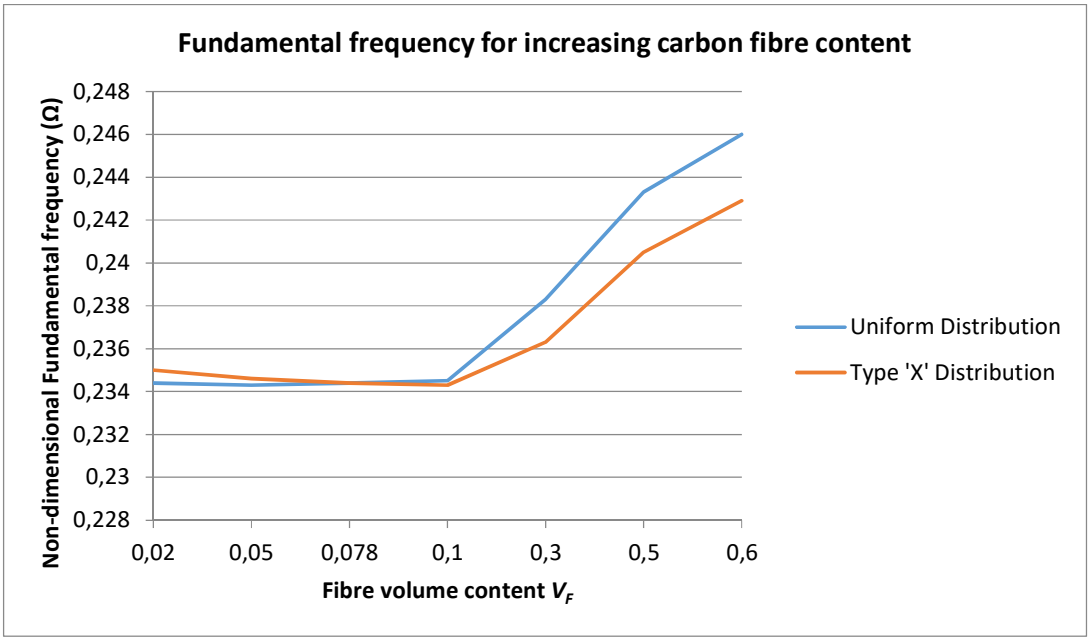

Figure 4: Fundamental frequency for various carbon fibre (V_F) content using Uniform and Type 'X' distribution and V^*_{GPL}=0.05

It is observed in figure 3 for glass fibres, that at the lowest fibre content, the Type 'X' distribution is slightly higher than the Uniform distribution in terms of magnitude of the fundamental frequency. Type 'X' leads to higher frequencies up to the value

$V_F = 0.05$ while for higher fibre volume content, Uniform distribution results in higher frequencies.

A similar comment is made by observing figure 4 for carbon fibres. Thus, for lower fibre content, Type 'X' distribution leads to higher frequencies, up to fibre content equal to 0.078. For higher fibre content values, the Uniform distribution resulted in larger frequencies.

It is concluded that in the laminate with less fibre content, the Type 'X' functionally graded distribution of graphene nanoplatelets (GPLs) results in higher fundamental frequencies as compared to Uniform distribution. As the fibre content increases, fibre reinforcement becomes dominant, indicating that the non-uninform, functionally graded graphene distribution does not offer any further increase in the fundamental frequency.

5.2 2-phase graphene-reinforced functionally graded laminate (zero fibre reinforcement)

A number of simulations are conducted with zero fibre reinforcement to evaluate the influence of fibre and graphene reinforcements on the vibration response. Then, comparison between the maximum frequencies and functionally graded distribution types can be made, for the 2-phase graphene-reinforced and 3-phase graphene and fibre-reinforced laminates.

The results for the fundamental frequencies for different boundary conditions, zero fibre content and different functionally graded graphene distributions, with $V_{GPL}^{*} = 0.05$ are shown in Table 7. Results indicate that for each boundary condition, the Type 'X' distribution produced the highest fundamental frequencies. In addition, clamped boundary conditions (CCCC) led to the highest frequencies.

The lowest fundamental frequencies were produced by the cantilever boundary conditions, for which the frequencies generated were approximately 10 times lower than those obtained from the clamped condition.

Table 7: Fundamental frequency for an 8-layered laminate under various boundary conditions subject to constant $V_{GPL}^{*} = 0.05$ *and* $V_F = 0$.

Boundary Condition	Distribution Type	Ω
Simply Supported (SSSS)	Uniform	0.2347
	Type 'X'	0.2355
	Type 'V'	0.2342
	Type 'O'	0.2339
	Type 'A'	0.2342
Cantilever (CFFF)	Uniform	0.0417
	Type 'X'	0.0419
	Type 'V'	0.0417
	Type 'O'	0.0416
	Type 'A'	0.0417
Clamped (CCCC)	Uniform	0.4037
	Type 'X'	0.4051
	Type 'V'	0.4031
	Type 'O'	0.4026
	Type 'A'	0.4031
Simply supported and clamped (SCSC)	Uniform	0.3304
	Type 'X'	0.3315
	Type 'V'	0.3298
	Type 'O'	0.3295
	Type 'A'	0.3298

Table 8: Fundamental frequency for an 8-layered simply supported rectangular laminate subject to varying V_{GPL}^{*}, $V_F = 0$ and $D/a = 0.03$.

Distribution Type	Ω	% increase
$V_{GPL}^{*} = 0.005$		
Uniform	0.0928	-
Type 'X'	0.0930	-
Type 'V'	0.0927	-
Type 'O'	0.0926	-
Type 'A'	0.0927	-
$V_{GPL} = 0.01$		
Uniform	0.1172	26.34
Type 'X'	0.1176	26.41
Type 'V'	0.1171	26.28
Type 'O'	0.1169	26.27
Type 'A'	0.1171	26.28
$V_{GPL}^{*} = 0.02$		
Uniform	0.1550	32.23
Type 'X'	0.1555	32.29
Type 'V'	0.1548	32.18
Type 'O'	0.1545	32.18
Type 'A'	0.1548	32.18
$V_{GPL}^{*} = 0.05$		
Uniform	0.2347	51.37
Type 'X'	0.2355	51.44
Type 'V'	0.2342	51.34
Type 'O'	0.2339	51.35
Type 'A'	0.2342	51.34
$V_{GPL}^{*} = 0.1$		
Uniform	0.3277	39.64
Type 'X'	0.3290	39.70
Type 'V'	0.3271	39.67
Type 'O'	0.3267	39.67
Type 'A'	0.3271	39.67
$V_{GPL}^{*} = 0.15$		
Uniform	0.4006	22.25
Type 'X'	0.4024	22.30
Type 'V'	0.4000	22.29
Type 'O'	0.3995	22.29
Type 'A'	0.4000	22.29
$V_{GPL}^{*} = 0.2$		
Uniform	0.4630	15.58
Type 'X'	0.4654	15.64
Type 'V'	0.4626	15.64
Type 'O'	0.4620	15.64
Type 'A'	0.4626	15.64

In Table 8 increasing values of the V^*_{GPL} content and zero fibre reinforcement are considered, and the frequencies are determined for each distribution type. Results indicate that an increase in the V^*_{GPL} content increases the value of the fundamental frequencies. As shown in Table 8, increasing the quantity of V^*_{GPL}results in higher frequencies but the as the V^*_{GPL} value increased the percentage increase diminished. In particular, for V^*_{GPL} content up to 0.05, higher increases of the frequencies are obtained, as compared to those derived for higher V^*_{GPL} values, where the increase rate gradually decreases. Similar results can be seen for the 3-phase graphene and fibre reinforced laminate as given in the descriptions provided for Table 8.

Figures 5 and 6 graphically illustrate the difference in the magnitude of the fundamental frequencies derived for 0% and 30% glass and carbon fibres, respectively, and increasing V^*_{GPL} content. It is noted that functionally graded graphene content is used, and anti-symmetric fibre orientation ($[0/90/0/90]_{anti\text{-}s}$) is applied for non-zero fibre content.

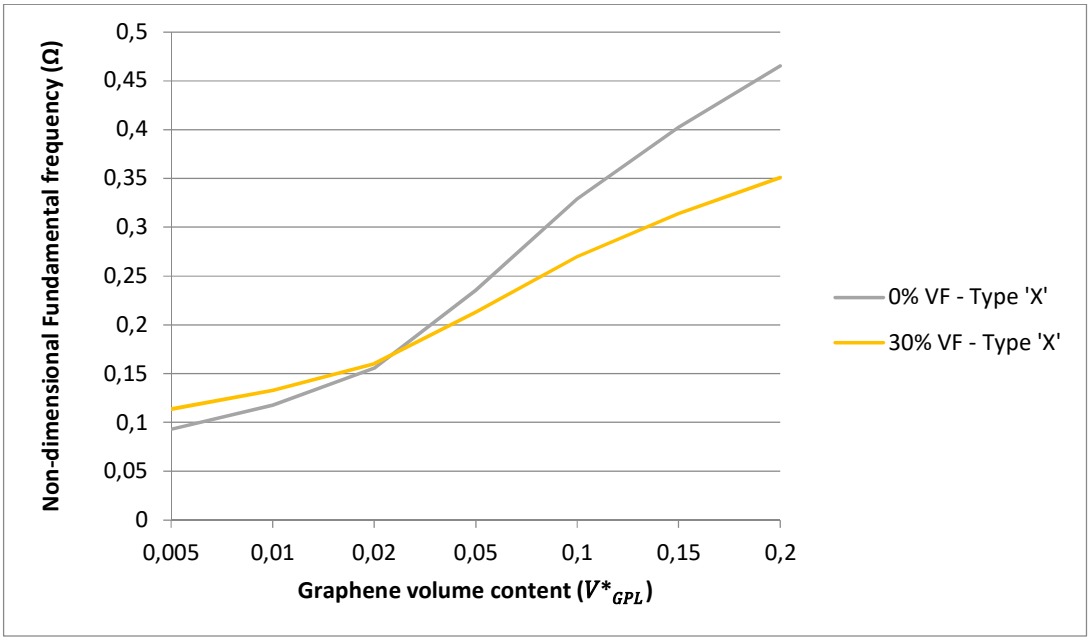

Figure 5: Comparison of the fundamental frequency produced for V_F= 0 and V_F= 0.3 (anti-symmetric glass fibres)

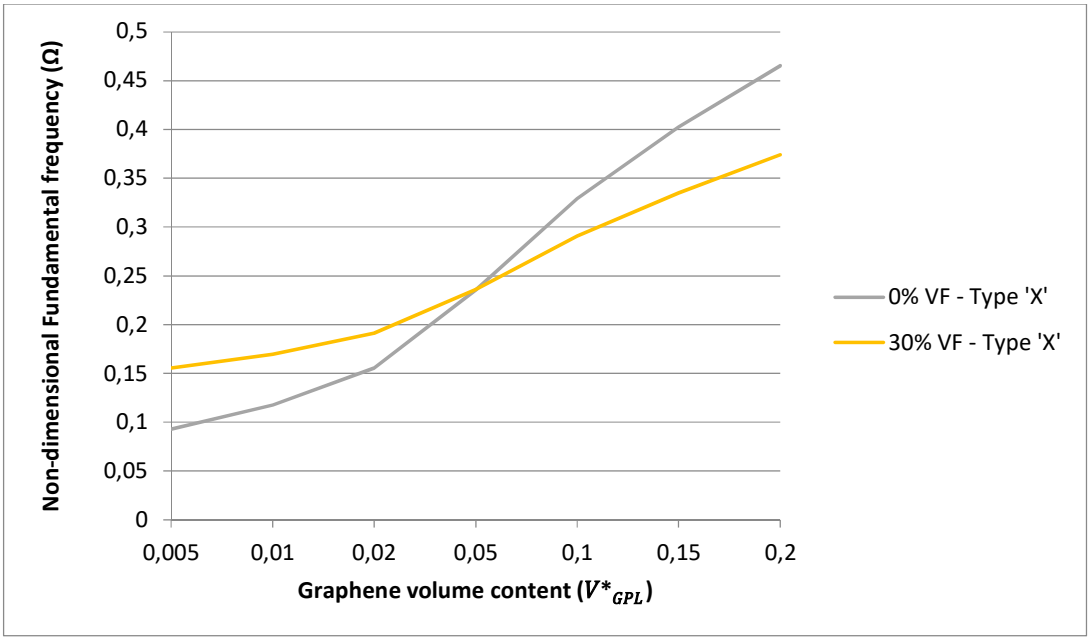

Figure 6: Comparison of the fundamental frequency produced between V_F= 0 and V_F= 0.3 (anti-symmetric carbon fibres)

It is observed that for both fibre types, the 30% fibre content leads to higher fundamental frequencies than the laminate with zero fibre reinforcement, until certain graphene content values are reached. For higher graphene content values, the laminate with zero fibre reinforcement leads to higher fundamental frequencies than the laminate with 30% fibre content. For glass fibres, the cross-over point after which the laminates with zero fibre reinforcement lead to higher frequencies, is approximately equal to V^*_{GPL} = 0.022 and for carbon fibres to V^*_{GPL} = 0.05.

Thus, as the graphene content V^*_{GPL} increases beyond those cross-over points, the 2-phase functionally graded graphene-reinforced laminate results in an improved vibration response compared to the 3-phase graphene/fibre reinforced laminate. It is observed that for glass fibres, this occurs for low graphene content, just above 2%, while for carbon fibres this occurs for higher graphene content (5%).

This output is confirmed by comparing the results shown in Table 3 (graphene/fibre reinforced laminate) and Table 7 (graphene-reinforced laminate with zero fibre reinforcement), both obtained for V^*_{GPL} = 0.05. Thus, frequencies provided by zero fibre reinforcement (Table 7) are higher than those obtained for glass fibre reinforcement (Table 3) for every functionally graded distribution. For carbon fibres (Table 3), frequencies are slightly higher than those given in Table 7 (zero

reinforcement). Finally, it is noted that uniform distribution led to similar diagrams as those provide in Figure 5 and 6.

5.3 Layerwise functionally graded laminates

In this section layerwise functionally graded laminates are investigated in the sense that each layer is assigned a different functionally graded distribution for the graphene nanoplatelet reinforcement. In addition, a brief study is conducted on functionally graded fibre distribution, with uniform graphene reinforcement.
In Table 9, different functionally graded graphene distribution types are assigned per layer and a number of combinations are tested.

Table 9: Fundamental frequency for a simply supported rectangular laminate subject to a layerwise variation in the functionally graded graphene distribution pattern with $V_{GPL}^{*} = 0.05$ *and* $V_F = 0.3$ *with anti-symmetric fibre orientation.*

Fibre type	Layerwise Distribution	Ω
Glass	[A/A/A/A/X/X/X/X]	0.2172
	[A/A/A/A/V/V/V/V]	0.2212
	[A/A/A/A/O/O/O/O]	0.2166
	[X/X/X/X/V/V/V/V]	0.2172
	[X/X/X/X/O/O/O/O]	0.2126
	[X/X/X/X/A/A/A/A]	0.2083
	[V/V/V/V/X/X/X/X]	0.2083
	[V/V/V/V/O/O/O/O]	0.2077
	[V/V/V/V/A/A/A/A]	0.2034
	[O/O/O/O/X/X/X/X]	0.2126
	[O/O/O/O/V/V/V/V]	0.2166
	[O/O/O/O/A/A/A/A]	0.2077
Carbon	[A/A/A/A/X/X/X/X]	0.2398
	[A/A/A/A/V/V/V/V]	0.2432
	[A/A/A/A/O/O/O/O]	0.2393
	[X/X/X/X/V/V/V/V]	0.2398
	[X/X/X/X/O/O/O/O]	0.2359
	[X/X/X/X/A/A/A/A]	0.2323
	[V/V/V/V/X/X/X/X]	0.2323
	[V/V/V/V/O/O/O/O]	0.2318
	[V/V/V/V/A/A/A/A]	0.2282
	[O/O/O/O/X/X/X/X]	0.2359
	[O/O/O/O/V/V/V/V]	0.2393
	[O/O/O/O/A/A/A/A]	0.2318

*Type ‘A’ – A; Type ‘X’ – X; Type ‘O’ – O; Type ‘V’ – V

For glass fibres, the distribution Type ‘A’ at the first four layers and Type ‘V’ at the last four layers ([A/A/A/A/V/V/V/V]) resulted in the highest frequency, of 0.2212. It can also be seen that the Type ‘X’ distribution is best combined with the Type ‘V’ distribution, resulting in a frequency of 0.2172. The Type ‘V’ distribution produced the highest frequency of 0.2083 when combined with Type ‘X’. Lastly, the Type ‘O’ distribution is best combined with the Type ‘V’ and produces a frequency of 0.2166.

For carbon fibres the highest frequency is also obtained from [A/A/A/A/V/V/V/V] distribution and is equal to 0.2432. In addition, Type ‘X’ and Type ’V’ distributions lead to a frequency of 0.2398; Type ‘V’ and Type ’X’ to a frequency of 0.2323 and Type ‘O’ combined with Type ‘V’ to a frequency value of 0.2393. The maximum

frequency obtained using carbon fibres is 10% higher than the maximum frequency derived using glass fibres.

A comparison is conducted between the maximum frequency produced by the layerwise distribution and the one provided by the same functionally graded distribution type for each layer, as shown in Table 33. The Uniform distribution type in Table 3 led to the maximum fundamental frequency, 0.2383, for carbon and 0.2166, for glass fibres, respectively. When comparing the glass fibre reinforced laminate, the layerwise distribution [A/A/A/A/V/V/V/V] resulted in a frequency of 0.2212 which is 2.12% higher than the laminate with the Uniform distribution of Table 3.

For the carbon fibres, the layerwise distribution of [A/A/A/A/V/V/V/V] provided the highest fundamental frequency of 0.2432, which is 2.06% higher than the carbon fibre composite using Uniform distribution for every layer (Table 4). This result indicates that a laminate with optimized functionally graded distributions per layer can achieve even higher fundamental frequencies than a composite with the same distribution for each layer.

Next, a first effort in this article is made to change the concept for the functionally graded reinforcement, and to consider functionally graded distribution for the fibre reinforcement. The purpose of this effort is to identify potential benefits of using functionally graded fibres in the thickness direction.

In Table 10 the vibration response of functionally graded fibre reinforcement is presented, for the distribution types adopted in previous sections. Graphene content is uniform along the laminate thickness.

Table 10: Fundamental frequency for a simply supported rectangular laminate with anti-symmetric fibre orientation subject to constant $V_{GPL} = 0.05$ and functionally graded fibres with $V_F^* = 0.3$

Fibre type	Distribution Type	Ω	% increase from
Glass	Uniform	0.2166	0.00%
	Type 'X'	0.2169	1.78%
	Type 'V'	0.2168	2.12%
	Type 'O'	0.2167	2.22%
	Type 'A'	0.2168	2.12%
Carbon	Uniform	0.2383	0.00%
	Type 'X'	0.2395	1.35%
	Type 'V'	0.2393	1.53%
	Type 'O'	0.2391	1.57%
	Type 'A'	0.2393	1.53%

Results indicate that the Type 'X' distribution leads to larger fundamental frequencies for both carbon and glass fibres. In addition, all distribution types shown in Table 10, excluding the Uniform type, result in higher frequencies than those given in Table 3 for uniform fibre reinforcement and functionally graded graphene nanoplatelets. Percentages of the increase in frequencies shown in Table 10, as compared to Table 3, are provided in the last column of Table 10. An observation of the results shows that the maximum increase is 2.22%, for Type 'O' distribution.

The effort of evaluating functionally graded fibres is extended in another investigation, where a layerwise variation in the functionally graded fibres and uniform graphene content are considered.

Table 11: Fundamental frequency for a simply supported rectangular laminate subject to a layerwise variation in the functionally graded fibre distribution with $V_{GPL} = 0.050$, $V_F^* = 0.3$ and anti-symmetric fibre orientation.

Fibre type	Layerwise	Ω
Glass	[A/A/A/A/X/X/X/X]	0.2175
	[A/A/A/A/V/V/V/V]	0.2181
	[A/A/A/A/O/O/O/O]	0.2174
	[X/X/X/X/V/V/V/V]	0.2175
	[X/X/X/X/O/O/O/O]	0.2168
	[X/X/X/X/A/A/A/A]	0.2162
	[V/V/V/V/X/X/X/X]	0.2162
	[V/V/V/V/O/O/O/O]	0.2161
	[V/V/V/V/A/A/A/A]	0.2155
	[O/O/O/O/X/X/X/X]	0.2168
	[O/O/O/O/V/V/V/V]	0.2174
	[O/O/O/O/A/A/A/A]	0.2161
Carbon	[A/A/A/A/X/X/X/X]	0.2408
	[A/A/A/A/V/V/V/V]	0.2421
	[A/A/A/A/O/O/O/O]	0.2406
	[X/X/X/X/V/V/V/V]	0.2408
	[X/X/X/X/O/O/O/O]	0.2393
	[X/X/X/X/A/A/A/A]	0.2380
	[V/V/V/V/X/X/X/X]	0.2380
	[V/V/V/V/O/O/O/O]	0.2378
	[V/V/V/V/A/A/A/A]	0.2365
	[O/O/O/O/X/X/X/X]	0.2393
	[O/O/O/O/V/V/V/V]	0.2406
	[O/O/O/O/A/A/A/A]	0.2378

Table 11 shows the results for a composite laminate subject to a layerwise variation in the functionally graded fibres and a constant value of $V_{GPL} = 0.05$. Analysis of the results for the glass fibre distribution indicates that the highest fundamental frequency of 0.2181 is obtained for a combination of Type 'A' and Type 'V' distributions. The carbon fibre distribution provides the highest fundamental frequency of 0.2421 for a combination of Type 'A' and Type 'V' which is the same as the glass fibre distribution. For the same layerwise distributions, there is an increase in the value of the fundamental frequency for a change from glass to carbon fibres of 11%.

Comparison between Tables 9 (layerwise, functionally graded graphene reinforcement) and 11 (layerwise functionally graded fibre reinforcement) indicates that except the case of the highest frequency, which is obtained for

[A/A/A/A/V/V/V/V], in every other combination the functionally graded fibre reinforcement leads to higher frequencies than those obtained by the corresponding functionally graded graphene reinforcement.

The highest frequency obtained for layerwise functionally graded fibre reinforcement (Table 11) is slightly higher than the one derived from non-layerwise functionally graded fibre reinforcement (Table 10). For glass fibres, the highest frequency from the layerwise fibre distribution is 0.5% higher than the one from the non-layerwise distribution, while for carbon fibres, the layerwise distribution results in 1% higher frequency compared to the non-layerwise distribution.

6. Conclusion

The present study investigates 3-phase graphene/fibre reinforced nanocomposite laminates with functionally graded reinforcement along the thickness in terms of the vibration response. First order shear deformation theory and a finite element analysis formulation are applied to determine the natural frequencies for different types of functionally graded distributions. The model proposed in this research is able to capture functionally graded distributions for either the fibre or the graphene nanoplatelets (GPLs) reinforcement. In addition, the numerical scheme can implement layerwise functionally graded reinforcement. Micromechanics equations are used to obtain the effective material properties of the laminate. Within the given framework, a rectangular, 8-layered laminate was tested for stacking sequences, different boundary conditions fibre volumes and types, graphene volume content, and functionally graded distribution patterns.

For functionally graded graphene nanoplatelets (GPLs) distribution, it is evident that for V_{GPL}^{*} larger than 5%, improvement rate of the fundamental frequencies diminishes, as compared to V_{GPL}^{*} values lower than 5%, leading to diminishing returns. In terms of the optimal functionally graded distribution, it is determined that as the volume content of fibres rise, the uniform graphene reinforcement leads to higher frequencies, indicating that the fibre content dominates the response and the functionally graded graphene distributions do not increase the frequencies. However, for low fibre content, with values less than 5% (glass) and 7.8% (carbon), the Type X distribution of functionally graded graphene results in the highest frequencies.

The study also highlights the efficiency of using fibres to enhance the vibration response of the functionally graded graphene-reinforced laminate. Observations show the level of V_{GPL}^{*} content determines whether adding fibre reinforcement contributes towards higher fundamental frequencies. For V_{GPL}^{*} higher than 2.2% and 5% for glass and carbon fibres, respectively, zero fibre reinforcement leads to higher frequencies than 30% fibres content. Thus, it is more efficient for this graphene content, not to use fibre reinforcement.

In a relevant comment, it can be seen that for V_{GPL}^{*}=5%, elevating the fibre content results in decreasing frequencies for glass fibres. Therefore, for this V_{GPL}^{*} content, using glass fibres does not contribute to cost-effective design. For carbon fibres, frequencies decrease up to a fibre content (about 10%) while for higher fibre content, frequencies increase.

When a layerwise functionally graded distribution is considered for graphene nanoplatelets, results indicate an increase approximately equal to 2% compared to non-layerwise functionally graded distribution. Finally, layerwise functionally graded distributions for graphene or fibre reinforcements, result in the [A/A/A/A/V/V/V/V] distribution, as the one providing the highest fundamental frequency.

The study can be extended by introducing in-plane functionally graded materials. Optimization procedures and machine learning methods can also be adopted, in order to provide the optimal vibration response, within a data-driven framework. These are left for future investigation.

Declarations

Competing Interests: The writers have disclosed no relevant non-financial or financial interests.

References

1. G. Drosopoulos, G. Stavroulakis, Non-linear mechanics for composite heterogeneous structures, CRC Press, Taylor & Francis, 2022.
2. V. Monfared, S.Ramakrishna, A.Alizadehetal., A systematic study on composite materials in civil engineering, Ain Shams Engineering Journal, 1 (2023) 2090-4479.
3. A. Negi, G. Bhardwaj, J. S. Saini, K. Khanna, & R. K. Godara, Analysis of CNT reinforced polymer nanocomposite plate in the presence of discontinuities using XFEM, Theoretical and Applied Fracture Mechanics, 103 (2019) 102292.
4. F. Tornabene, N. Fantuzzi, M. Bacciocchi, Linear static response of nanocomposite plates and shells reinforced by agglomerated carbon nanotubes, Composites Part B: Engineering, 115, (2017) 449–476.
5. T. Hassan, A. Salam, A. Khan, S. U. Khan, H. Khanzada, M. Wasim, I. S. Kim, Functional nanocomposites and their potential applications: A review, Journal of Polymer Research, 28 (2021) 36.
6. M. Brcic, M. Canadija, J. Brnic, J., Estimation of material properties of nanocomposite structures, Meccanica, 48(9), (2013) 2209–2220.
7. M. Song, S. Kitipornchai, J. Yang, Free and forced vibrations of functionally graded polymer composite plates reinforced with graphene nanoplatelets, Composite Structures, 159, (2017) 579–588.
8. M. A. Rafiee, J. Rafiee, Z. Wang, H. Song, Z. Yu, N. Koratkar, Enhanced Mechanical Properties of Nanocomposites at Low Graphene Content. ACS Nano, 3(12), (2009) 3884–3890.
9. M. Sayed, A. Mousa, Vibration, Stability, and Resonance of Angle-Ply Composite Laminated Rectangular Thin Plate under Multiexcitations, Mathematical Problems in Engineering, 2013, (2013) 1–26.
10. W. H. Liu, W. C. Chen, Vibration analysis of skew cantilever plates with stiffeners, Journal of Sound and Vibration, 159(1), (1992) 1–11.
11. S. Biswas, B. R. Lokavarapu, Fundamental frequencies of composite rectangular plates with different cut-outs, Materials Today: Proceedings, 2023, ISSN 2214-7853.
12. Y. Zou, Y. Kiani, Vibrations of Nonlocal Polymer-GPL Plates at Nanoscale: Application of a Quasi-3D Plate Model, Mathematics, 11, (2023) 4109.

13. K. Brethee, Free vibration analysis of a symmetric and anti-symmetric laminated composite plates with a cutout at the center, Al-Qadisiya Journal For Engineering Sciences Vol 2, (2009) 324-334.
14. L. Sinha, D. Das, A. N. Nayak, S. S. Kumar, Experimental and numerical study on free vibration characteristics of laminated composite plate with/without cut-out, Composite Structures, 256, (2020) 1-54.
15. T. Farsadi, D. Asadi, H. Kurtaran, Fundamental frequency optimization of variable stiffness composite skew plates, Acta Mechanica, 232, (2021) 555-573.
16. B. Farshi, R. Rabiei, Optimum design of composite laminates for frequency constraints, Composite Structures, 81(4), (2007) 587–597.
17. B. Wang, F. Zhao, Z. Zhao, K. Xu, Influence factors on natural frequencies of composite materials, Frontiers of Mechanical Engineering, 15(4), (2020) 571–584.
18. M. K. Apalak, M. Yildirim, R. Ekici, Layer optimisation for maximum fundamental frequency of laminated composite plates for different edge conditions, Composites Science and Technology, 68(2), (2008) 537-550.
19. P. Pingulkar, B. Suresha, Free Vibration Analysis of Laminated Composite Plates Using Finite Element Method, Polymers and Polymer Composites, 24(7), (2016) 529–538.
20. M. Avey, F. Kadioglu, S. Ahmetolan, Mathematical modeling and solution of nonlinear vibration problem of laminated plates with CNT originating layers interacting with two-parameter elastic foundation, J Braz. Soc. Mech. Sci. Eng, 45, (2023) 185.
21. F. Ebrahimi, A. Enferadi, A. Dabbagh, Wave Dispersion Behaviors of Multi-Scale CNT/Glass Fiber/Polymer Nanocomposite Laminated Plates, Polymers , 14, (2022) 5448.
22. M. Hocaoğlu, H. Karagülle, Effect of carbon nanotube reinforcement on the natural frequencies and damping ratios of nanocomposite beams, Materials Research Express, 7, (2020) 025021.
23. Z. Feng, Y. Li, C. Xin, D. Tang, W. Xiong, H. Zhang, Fabrication of Graphene-Reinforced Nanocomposites with Improved Fracture Toughness in Net Shape for Complex 3D Structures via Digital Light Processing, C, 5(2), (2019) 25.
24. M. Rafiee, F. Nitzsche, M.R. Labrosse, Modeling and mechanical analysis of multiscale fiber-reinforced graphene composites: Nonlinear bending, thermal

post-buckling and large amplitude, International Journal of Non-Linear Mechanics, 103, (2018) 104-112.

25. S. K. Georgantzinos, G. I. Giannopoulos, S. I. Markolefas, Vibration Analysis of Carbon Fiber-Graphene-Reinforced Hybrid Polymer Composites Using Finite Element Techniques, Materials, 13(19), (2020) 4225.
26. M. S. Koppanati, M. N. Rani, K. Bhaskar, Free Vibration Analysis of Graphene Reinforced Laminated Composite Plates using Experimental Modal Testing, Mechanics of Advanced Composite Structures, 10(2), (2023) 363-374.
27. Y. Jeawon, G. A. Drosopoulos, G. Foutsitzi, G. E. Stavroulakis, S. Adali, Optimization and analysis of frequencies of multi-scale graphene/fibre reinforced nanocomposite laminates with non-uniform distributions of reinforcements, Engineering Structures, 228, (2021) 111525.
28. F. Pashmforoush, Natural frequency prediction of functionally graded graphene-reinforced nanocomposite plates using ensemble learning and support vector machine models, Proceedings of the Institution of Mechanical Engineers, Part C: Journal of Mechanical Engineering Science, 237(4), (2023) 782-798.
29. A. Alnujaie , M. Alshahrani, W. S. Ibrahim, Y. Yasin, Z. S. Obaid, I. J. Alhani, M. H. Khaddour, S. K. Hadrawi, Y. Riyahi, M. H. Ghazwani, Dynamic analysis of thick plates reinforced with agglomerated GNPs, Heliyon, 9(9), (2023) 18379.
30. R. Bahaadini, A. R. Saidi, Z. Arabjamaloei, A. Ghanbari-Nejad-Parizi, Vibration Analysis of Functionally Graded Graphene Reinforced Porous Nanocomposite Shell, International Journal of Applied Mechanics, 11(7), (2019) 1950068
31. M. Moghaddasi, Y. Kiani, Free and forced vibrations of graphene platelets reinforced composite laminated arches subjected to moving load, Meccanica, 57, (2022) 1105–1124.
32. J-R. Cho, Free Vibration Analysis of Functionally Graded Porous Cylindrical Panels Reinforced with Graphene Platelets, Nanomaterials, 13, (2023) 1441.
33. S. S. Ahankari, K. K. Kar, Functionally Graded Composites: Processing and Applications, Composite Materials, (2016) 119–168.
34. C. H. Thai, A. J. M. Ferreira, T. D. Tran, P. Phung-Van, Free vibration, buckling and bending analyses of multilayer functionally graded graphene nanoplatelets (GPLs) reinforced composite plates using the NURBS formulation, Composite Structures, 220, (2019) 749-759.

35. Y. Zhou, X. Zhang, Natural frequency analysis of functionally graded material beams with axially varying stochastic properties. Applied Mathematical Modelling, 67, (2019) 85–100.
36. Y. Kiani, Free vibration of FG-CNT reinforced composite skew plates. Aerospace Science and Technology, 58, (2016) 178–188.
37. F. Pashmforoush, Statistical analysis on free vibration behavior of functionally graded nanocomposite plates reinforced by graphene platelets, Composite Structures, 213, (2019) 14-24.
38. D. Liu, Free Vibration of Functionally Graded Graphene Platelets Reinforced Magnetic Nanocomposite Beams Resting on Elastic Foundation, Nanomaterials, 10(11), (2020) 2193.
39. C. T. Loy, K. Y. Lam, J. N. Reddy, Vibration of functionally graded cylindrical shells. International Journal of Mechanical Sciences, 41(3), (1999) 309–324.
40. R. Reddy, W. Karunasena, W. Lokuge, Free vibration of functionally graded-GPL reinforced composite plates with different boundary conditions, Aerospace Science and Technology, 78, (2018) 147–156.
41. J-R. Cho, A. Young-Ju , Investigation of Mechanical Behaviors of Functionally Graded CNT-Reinforced Composite Plates, Polymers, 14(13), (2022) 2664.
42. M. Babaei, F. Kiarasi, M. S. Tehrani, A. Hamzei, E. Mohtarami, K. Asemi, Three dimensional free vibration analysis of functionally graded graphene reinforced composite laminated cylindrical panel, Proceedings of the Institution of Mechanical Engineers, Part L: Journal of Materials: Design and Applications, 236(8), (2022) 1501-1514.
43. M. S. Tayebi, S. J. Salami, M. Tavakolian, Free vibration analysis of functionally graded composite rectangular plates reinforced with graphene nanoplatelets (GPLs) using full layerwise finite element method, Proceedings of the Institution of Mechanical Engineers, Part C: Journal of Mechanical Engineering Science, 0(0), (2023).
44. Y. Zhou, Y. Zhang, B. N. Chirukam, J. Li, C. Lu, M. Babaei, K. Asemi, Free Vibration Analyses of Stiffened Functionally Graded Graphene-Reinforced Composite Multilayer Cylindrical Panel, Mathematics, 11(17), (2023) 3662.
45. M. Tam, Z. Yang, S. Zhao, J. Yang, Vibration and Buckling Characteristics of Functionally Graded Graphene Nanoplatelets Reinforced Composite Beams with Open Edge Cracks, Materials, 12(9), (2019) 1412.

46. M. M. Kheirikhah, M. Ghiasvand, S. Gohari, Free Vibration Analysis of Composite Sandwich Beams Reinforced by Functionally Graded Graphene Nanoplatelets, Mechanics of Composite Materials, 59, (2023).
47. I. Mishra, S. K. Sahu, Modal Analysis of Woven Fiber Composite Plates with Different Boundary Conditions, International Journal of Structural Stability and Dynamics, 15(01), (2015) 1540001.
48. JN. Reddy, Mechanics of Laminated Composite Plates and Shells, second ed., 2004, p. CRC Press.
49. Y. Huang, Z. Yang, A. Liu, J. Fu, Nonlinear buckling analysis of functionally graded graphene reinforced composite shallow arches with elastic rotational constraints under uniform radial load, Materials, 11 (6), (2018) 910.
50. J. Yang, H. Wu, S. Kitipornchai, Buckling and post-buckling of functionally graded multilayer graphene platelet-reinforced composite beams, Composite Structures, 161, (2017) 111–118.
51. T. Vo-Duy, V. Ho-Huu, T.D. Do-Thi, H. Dang-Trung, T. Nguyen-Thoi, A global numerical approach for lightweight design optimization of laminated composite plates subjected to frequency constraints, Composite Structures, 159 (2017) 646–655.
52. H.-S. Shen, A comparison of buckling and post-buckling behavior of FGM plates with piezoelectric fibre reinforced composite actuators, Compos. Struct., 91, (2009) 375–384.
53. M. Rafiee, F. Nitzsche, M.R. Labrosse, Modeling and mechanical analysis of multiscale fibre reinforced graphene composites: Nonlinear bending, thermal post-buckling and large amplitude, Int. J. Non-Linear Mech., 103, (2018) 104–112.
54. M. Song, J. Yang, S. Kitipornchai, W. Zhu, Buckling and postbuckling of biaxially compressed functionally graded multilayer graphene nanoplatelet-reinforced polymer composite plates, International Journal of Mechanical Sciences, 131-132, (2017) 345–355.
55. Y. Wang, C. Feng, Z. Zhao, J. Yang, Eigenvalue buckling of functionally graded cylindrical shells reinforced with graphene platelets (GPL), Composite Structures, 202, (2017) 38-46.

56. Y. Wang, C. Feng, Z. Zhao, J. Yang, Buckling of Graphene Platelet Reinforced Composite Cylindrical Shell with Cutout, International Journal of Structural Stability and Dynamics, 18(03), (2018) 1850040.
57. I. S. Radebe, G. A. Drosopoulos, S. Adali, Buckling of non-uniformly distributed graphene and fibre reinforced multiscale angle-ply laminates, Meccanica, 54, (2019) 2263-2279.
58. Z. Shi, X. Yao, F. Pang, Q. Wang, An exact solution for the free-vibration analysis of functionally graded carbon-nanotube-reinforced composite beams with arbitrary boundary conditions, Scientific Reports, 7(1), (2017) 12909.
59. Ö. Civalek, S. Dastjerdi, B. Akgöz, Buckling and free vibrations of CNT-reinforced cross-ply laminated composite plates, Mechanics Based Design of Structures and Machines, 50(6), (2020) 1914-1931.

Chapter 7: Conclusion

This chapter provides a summary and conclusion of the major research findings that are derived from the analyses conducted in Chapters 5 through 6 as well as recommendations for expanding the research for future work. More detailed conclusions for the research can be found at the end of Chapter 5 to 6.

7.1 Conclusions

The current study proposed optimization schemes, implemented using finite element analysis to optimize and maximize a graphene-reinforced nanocomposite plate's vibrational response. In order to enhance the nanocomposite's vibrational capacity and prevent resonance, the vibration was maximized and quantified in terms of fundamental frequency. In addition, a scheme for the evaluation of the vibration response of functionally graded nanocomposite laminates was provided in the thesis.

In Chapter 4, the proposed methodology involved the use of micromechanical equations and first order shear deformation theory (FSDT) to formulate a 3-phase graphene/fibre reinforced nanocomposite, derive the effective material properties and apply an optimization scheme in MATLAB. The micromechanical equations are applied to first formulate the graphene-reinforced matrix and then to derive the properties of the 3-phase graphene/fibre reinforced matrix. The vibration analysis is calculated using four-noded Mindlin plate elements and optimization scheme applied via a Sequential Quadratic Programming algorithm. The optimization scheme introduces various design variables that are modified to measure the resultant effect on the fundamental frequency. A design efficiency rating was calculated by dividing the optimized fundamental frequency by the frequency from uniform distributions of reinforcement. Using the design efficiency rating, different nanocomposite design scenarios are compared.

In the study optimal distributions of graphene and fibre reinforcement were determined along the laminate thickness. The optimal distribution of graphene was found to be non-uniformly distributed in the surface layers of the laminate with zero or minimum distribution in the middle layers. A similar observation is made when fibre reinforcement is introduced.

The design efficiency rating indicated an increase in the fundamental frequency when the layer thickness and fibre angles are introduced as additional design variables to the graphene and fibre content. Additionally, graphene reinforcement was found to be more efficient when the fibre reinforced volume was lower. A non-uniform distribution of graphene and fibre reinforcement along the thickness was found to produce superior fundamental frequencies than that produced by uniform distributions. Clamped (CCCC) boundary conditions resulted in fundamental frequency values which are relatively high compared to simply supported (SSSS) but SSSS boundary conditions showed a higher increase in the design frequency than CCCC boundary condition.

In Chapter 5, the optimization scheme is extended to graphene/fibre reinforced cantilever skew laminates. Isoparametric elements are used to analyse a skew plate due to their accuracy for simulating arbitrary geometry. Micromechanical equations are applied to obtain effective material properties for a 3-phase graphene/fibre reinforced skew cantilever laminate plate. Thereafter, the skew plate is represented using four-noded isoparametric quadrilateral elements with five degrees of freedom per node. A Sequential Quadratic Programming algorithm is used to apply the optimization scheme to the skew cantilever laminate plate.

The design optimization for the skew laminate included parameters such as graphene and fibre content and distribution across the thickness, layer thicknesses and fibre angles. Design variables are implemented in sequence starting with one variable and culminating in a four variable design. The first variable assigned is graphene content, followed by fibre content, layer thickness and finally fibre angle. The optimal distribution of graphene and fibres is again higher distributions in the surface layers and minimal to zero in the middle layer due to the outer layer contributing more to the overall laminate stiffness. The effectiveness of increasing quantities of graphene decreases after a certain limit where the design becomes inefficiency from a cost perspective. A cost effective design can be achieved with lower quantities of fibre added to the graphene-reinforced composite due to results showing a higher fundamental frequency for 30% fibre content than 60% added to the graphene-reinforced skew composite.

The fundamental frequency of a 3-phase composite reinforced with graphene and fibres is significantly higher than that of a 2-phase composite reinforced solely with fibres. For every simulation, a design efficiency factor is computed, and the findings indicate that the efficiency factor rises with the number of design variables. The optimal designs for the 45° skew plate was compared to the rectangular plate where the results show the fundamental frequency of the skew plate to be superior to the rectangular plate but the design efficiency of the skew plate is smaller than the rectangular plate.

Lastly, a study is conducted to investigate the effects of functionally graded reinforcement along the thickness of a rectangular laminated composite plate. In this study micromechanical equations and four-noded isoparametric quadrilateral elements with five degrees of freedom per node were used to calculate the vibration response of the composite plate, aiming to maximize the fundamental frequency. To achieve this, five functionally graded distribution patterns are applied via the reinforcement materials (graphene and fibre) in the composite. Those functionally graded distributions are applied via a function which transforms the graphene and fibre content into functionally graded graphene and fibre pattern distributions. The distribution patterns included in the study is Uniform, Type ‘X’, Type ‘V’ Type ‘O’ and Type ‘A’. Functionally graded graphene distributions show a diminishing effect in improving the fundamental frequency above a 5% graphene content limit. Results show that when fibres are introduced into the composite the uniform distribution produces the larger fundamental frequencies indicating that fibre content dominates the frequency response and functionally graded graphene becomes less effective in increasing the frequency response. However, when the fibre content is low the Type ‘X’ functionally graded graphene distribution produces the largest fundamental frequency.

The study investigates the efficiency in using fibres to reinforce the vibration response of the functionally graded graphene-reinforced laminate. Results indicate that certain limits of graphene content are more effective with zero fibre content. A layerwise functionally graded distribution is also investigated to determine the

effectiveness in improving the fundamental frequency. The results show that a layerwise distribution slightly improved the observed fundamental frequency.

The overall results of this research indicate some key aspects of the nanocomposite design. The addition of graphene nanoparticles as reinforcement into the polymer matrix of the composite has a positive effect in increasing the magnitude of the fundamental frequency. Increasing the number of design variables ultimately resulted in a more refined and optimally reinforced composite laminate with larger fundamental frequencies and improved design efficiencies. Depending on the amount of fibre reinforcement, the type of functionally graded distribution can be changed to optimize the nanocomposite and increase the fundamental frequency. Skew composites resulted in larger fundamental frequencies but reduced design efficiencies compared to square composite laminates. The result is a plethora of design variables and composite characteristics that can be used to increase the fundamental frequency and optimize the 3-phase graphene/fibre reinforced nanocomposite.

The vibrational analysis model presented not only agrees with previously published research which serves as a verification model for future research but also provides extensive data relating to a variety of solutions to optimize and maximize the vibrational response and fundamental frequency in order to avoid resonance and improve and advance industry applications. The proposed methodology can be extended to include different reinforcement materials making the model a diverse and powerful tool. This data can then be extrapolated and introduced in the design of various industry applications such as airplane wings or lightweight structures which become subject to intense vibrations. Stronger and lighter materials can lead to a more robust, safe and cost effective design. The conducted investigation can also be applied to the aerospace and automotive industry, the energy sector and others.

As with any research methodologies, the limitations to the study must be presented to form a holistic analysis. In this regard one important limitation of the work presented in this thesis is the inability to make an in depth comparison of the results with experimental data from previous research. The lack of experimental data

available contributes to this limitation where correlation with such data would attribute to forming a complete and closed end analysis.
The processing computational efficiency of the computer used to run the analysis was able to accommodate the complexity of laminate in the thesis. In case more advanced laminates are simulated in relevant future applications, for instance models of greater dimensions, more complex geometry, or more layers, more powerful processing equipment will be needed. Simulation in computer clusters or parallel processing capabilities may also be involved for those cases.

7.2 Recommendations for future research

A comprehensive numerical framework is provided in this thesis to investigate the vibration response of graphene-reinforced nanocomposite plates.

The methodology of the numerical evaluation of functionally graded laminates can be extended to incorporate in-plane functionally graded material concepts. In this sense, a more holistic representation of functionally graded distributions will be achieved, considering distribution patterns in-plane and along the thickness. In another step, optimization can be introduced, to evaluate optimal design variables in functionally graded distributions. The aim will be to determine the optimal functionally graded distribution, along the plane and the thickness of the laminates.
All the presented work can be integrated into artificial intelligence, adopting machine learning techniques. There are several parameters which crucial influence the vibration response of the laminates. Traditional and modern machine learning tools can therefore be adopted, to provide a prediction of the influence of those parameters on the vibration response. To train the machine learning tools, data can be numerically generated, from the codes which have been developed for this thesis. By doing this, fast predictions of the vibration response, with limited computational cost may be achieved.

It is apparent that there is limited experimental research available regarding the vibration analysis of graphene reinforced nanocomposite plates, as such it is recommended that future research regarding this topic be done in terms of experimental analysis to provide data that can be used to compare the theoretical

results and the experimental results and ultimately reinforce the concepts and theories used for theoretical analysis.

The results in this thesis led to improved responses using the chosen gradient optimization scheme as provided in detail in the thesis. Indeed, other local optimal points cannot be excluded with the adopted scheme. However, the obtained response indicates clear improvements in terms of maximizing the natural frequencies, as indicated for instance by the increase in the design efficiency factor that is introduced in the thesis. In this framework, the adoption of the gradient optimization scheme in the thesis is justified. The introduction of advanced global optimization schemes could provide a further insight in the investigated topics. It is, therefore, recommended that a global optimization algorithm can be investigated in future research to add to the results of this thesis and compare the optimal distributions of graphene and fibre reinforcement in each case.

Also, relevant numerical analysis can be conducted in the framework of modern data-driven approaches. The concept in this case is to replace to some extent, the finite element simulation by introducing appropriate machine learning tools. Data numerically derived can be used to train machine learning algorithms that will then be used to predict the response of nanocomposite laminates. A more advanced application in this field is the development of digital twins of the nanocomposite laminate structures that interact and predict the mechanical response of the real structures. These concepts are left for future implementation.

In this research the optimisation of the fundamental frequency (first eigenmode) was the focus and intent where various parameters were tested to determine the effect of the fundamental frequency and the specifications that lead to optimised results. There are numerous modes that follow the first eigenmode which can be studied and optimised to further reduce the occurrence of resonance, as seen in [1], where the optimisation involved various modes and the gaps between modes to distance the possibility of resonance occurring. To do this for all modes or even a significant amount of modes would take an extensive amount of time and processing power. Further studies can be built on this research to investigate the sensitivity of the eigenmodes to the constraints analysed and investigate additional mode values and mode gaps to optimise the composite to a higher degree and refine the optimisation activity.

Authorship Contribution Statement

25 June 2024

25 May 2024

The following statement details the contributions of each author on the following articles/chapters and refers to the examination committee of the PhD thesis of the first co-author, Mr. Y. Jeawon. The purpose of this document is to provide evidence for the contribution of Mr. Y. Jeawon on the conducted research and support his PhD thesis. This document will be submitted to the research office of UKZN (South Africa). There is no other suggested usage for this document once submitted to UKZN.

> Y. Jeawon, G.A. Drosopoulos, G. Foutsitzi, G.E. Stavroulakis, S. Adali, Optimization and analysis of frequencies of multi-scale graphene/fibre reinforced nanocomposite laminates with non-uniform distributions of reinforcements, Eng.Struct, 228, (2021) 111525.
>
> Y. Jeawon, G.A. Drosopoulos, G. Foutsitzi, G.E. Stavroulakis, S. Adali, Optimization of graphene/fibre reinforced cantilever skew laminates for maximum fundamental frequency via non-uniform distribution of reinforcements, Thin-Walled Structures, 189, (2023) 110903.
>
> Y. Jeawon, G.A. Drosopoulos, G. Foutsitzi, Fundamental frequency analysis of functionally graded graphene-reinforced rectangular composite plates, (Article has been submitted for publication and is currently under review.)

- Y. Jeawon : Developed the data and analysis of the optimization using the finite element analysis Matlab codes, conducted the simulations for all analyses and produced the first draft for each paper inclusive of all results, discussions and conclusion.
- G. A. Drosopoulos : Supervised Y. Jeawon, provided instructions where necessary and assisted in the revision of the articles .
- G. Foutsitzi : Provided the initial version of the core finite element code in MATLAB.

- G.E. Stavroulakis : Provided insight and experience to guide the research direction and assisted in revision of the articles.

- S. Adali : Assisted in the overall discussions, provided guidance and revision of the articles.